A study of three-dimensional effects in end-stage boundary layer transition.

Ph.D. Thesis

Thomas James Marshall
Department of Mathematics
University College London

2004

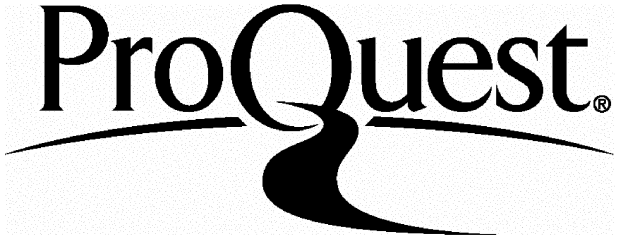

Abstract

A theoretical study into the three-dimensional effects at the end-stages of transition of laminar flow to fully turbulent flow in a boundary layer is presented. Various theoretical approaches have been broadly successful in capturing and explaining the early stages of the entry of three-dimensionality but a description of the late stages eludes satisfactory theoretical description. The particular aspect of this that we concentrate on here is the inclusion of three-dimensional effects which are vital for the generation of so-called "Omega" (Ω) vortices. These herald the last stages of transition and the subsequent interactions between them and the fluid closer to the wall causes rapid transition to turbulence.

Asymptotic methods are used to derive a system of nonlinear integro-differential equations, which extends previous work to three-dimensions. In particular they describe the capture of fluid in spanwise vortices of finite spanwise extent centred about a critical layer. The behaviour of these derived equations is studied. An analytical study of the critical layer equations gives a condition for the existence of a non-zero critical layer jump term. An expression for the spanwise critical layer jump term is found but it involves a triple repeated integral and a computational study is required to make further progress. The feedback of the developing vortices onto the flow is found to be particularly strong, emphasizing the importance of the entrance of three-dimensionality earlier in the flow development. This leads to the breakdown of the proposed theory and new scalings are needed. An explanation for this strong feedback is presented. However further analytic progress is made through a consideration of a relatively weak interaction between the critical layer and the bulk of the flow. This is analogous to delaying the feedback mechanism and we study the behaviour of recirculating flow within a vortex by considering two active timescales.

Contents

1 Introduction **9**

1.1 Experimental and Computational Research 11

1.1.1 K-type transition 13

1.2 Theoretical Approach 17

1.3 Description of Later Chapters 19

2 The Three-Dimensional Critical Layer **21**

2.1 Derivation of Equations 23

2.1.1 Expected Vortex Shapes 37

2.2 An expression for the jump term 40

2.3 Approximations for the Jump Term 52

2.3.1 The jump is zero for a linear pressure forcing 52

2.3.2 Short-Scale 3D Perturbations 55

2.3.3 The Case of two different Slopes 57

2.4 Properties of the Flow Leaving the Critical Layer 66

2.5 Numerical Method 72

2.5.1 Plots of the critical layer solution 85

2.6 The Jump Term for large negative X 103

2.6.1 Analysis for large χ 103

2.6.2 The Interaction Upstream 107

2.7 Conclusions 114

3 Three-Dimensional Vortex Development **116**

3.1 Derivation and Solution of the equations 119

3.2 Behaviour for $\phi \sim 1$ 139

3.3 The Jump Term at X_R and X_L 142

3.4 Analysis at vortex generation 145

3.5 Numerical Method 153

3.6 Results 163

3.7 Conclusions 185

4 Final Comments **188**

4.1 Acknowledgements 192

List of Figures

2.1 The Li *et al.* (1998) triple-deck setup. 26

2.2 P and P_X for $T = -1, ..., 1$. 38

2.3 The Changes in Order of Integration of the First Integral. 49

2.4 The Changes in Order of Integration of the Second Integral. 49

2.5 The Pressure Distribution. 57

2.6 The Characteristic trajectories. 58

2.7 The Characteristic Trajectory for $\chi > 0$. 60

2.8 Scalings for the jet. 70

2.9 Grids for numerical method. 79

2.10 Initial pressure distribution plotted for all z. 86

2.11 Initial streamwise derivative of the pressure plotted for all z. 86

2.12 Initial spanwise derivative of the pressure. 87

2.13 The two-dimensional jump term at the first time step. 88

2.14 The two-dimensional vorticity at the first time step on a (χ, Y) grid. . 89

2.15 The two-dimensional vorticity at the first time step on a (X, Y) grid. 89

2.16 The spanwise velocity on a χ, Y grid at the first time step for a fixed $z = 0.2$. 91

2.17 The spanwise vorticity on a χ, Y grid at the first time step for a fixed $z = 0.2$. 96

2.18 The spanwise vorticity on a χ, Y grid at the first time step for a fixed $z = 0.2$ showing problem with large χ. 96

2.19 The spanwise velocity on a X, Y grid at the first time step for a fixed $z = 0.2$. 97

2.20 The spanwise derivative of the spanwise velocity on a X, Y grid at the first time step for a fixed $z = 0.2$. 97

2.21 The spanwise vorticity on a X, Y grid at the first time step for a fixed $z = 0.2$. 98

2.22 The χ derivative of the spanwise vorticity at the first time step on a X, Y grid for a fixed $z = 0.2$. 98

2.23 The spanwise velocity on a z, Y grid at the first time step with the streamwise point fixed ($X = 1.8$). 99

2.24 The spanwise derivative of the spanwise velocity on a z, Y grid at the first time step with the streamwise point fixed ($X = 1.8$). 99

2.25 The spanwise vorticity on a z, Y grid at the first time step with the streamwise point fixed ($X = 1.8$). 100

2.26 J_X^L for $z = 0.2$. 101

2.27 $J_X^L + (O(L^{-1})$ term of $J_X^a)$ for $z = 0.2$. 101

2.28 $J_X^L + (O(L^{-1})$ and $O(L^{-3})$ terms of $J_X^a)$ for $z = 0.2$. 102

2.29 $J_X^L + (O(L^{-1}), O(L^{-3})$ and $O(L^{-5})$ terms of $J_X^a)$ for $z = 0.2$. 102

2.30 The setup for large χ. 111

2.31 A Characteristic with large value of χ. 112

3.1 The triple-deck structure for small μ. 123

3.2 The Vortex Structure. 129

3.3 The local pressure. 129

3.4 P at first vortex step for $\xi = 0$. 157

3.5 P_X at first vortex step for $\xi = 0$. 157

3.6 The Vortex in Normalised Coordinates. 160

3.7 z^* plotted against time for $\xi = 0$. 168

3.8 Area of the vortex plotted against time for $\xi = 0$. 168

3.9 $\triangle\chi$ plotted against time for $\xi = 0$. 169

3.10 $\triangle\chi$ plotted against ξ for selected time steps. 169

3.11 χ_{min} and χ_{max} plotted against ξ for $T = -0.405$. 170

3.12 χ_{min} and χ_{max} plotted against ξ for $T = -0.355$. 170

3.13 P_T at $T = -0.355$. 171

3.14 X_L, X_{min} and X_R plotted against ξ for $T = -0.405$. 172

3.15 X_L, X_{min} and X_R plotted against ξ for $T = -0.355$. 172

3.16 Area at $T = -0.405$. 173

3.17 A_ξ at $T = -0.405$. 173

3.18 A_ϕ at $T = -0.405$. 174

3.19 The spanwise velocity at $T = -0.405$. 174

3.20 The ξ derivative of the spanwise velocity at $T = -0.405$. 175

3.21 The ϕ derivative spanwise velocity at $T = -0.405$. 175

3.22 The spanwise vorticity at $T = -0.405$. 176

3.23 Surface plot of the jump term at $T = -0.405$. 177

3.24 Contour plot of the jump term at $T = -0.405$. 177

3.25 Area at $T = -0.355$. 178

3.26 A_ξ at $T = -0.355$. 178

3.27 A_ϕ at $T = -0.355$. 179

3.28 The spanwise velocity at $T = -0.355$. 179

3.29 The ξ derivative of the spanwise velocity at $T = -0.355$. 180

3.30 The ϕ derivative of the spanwise velocity at $T = -0.355$. 180

3.31 The spanwise vorticity at $T = -0.355$. 181

3.32 Surface plot of the jump term at $T = -0.355$. 182

3.33 Contour plot of the jump term at $T = -0.355$. 182

3.34 Surface plot of the jump term at $T = -0.305$. 183

3.35 Contour plot of the jump term at $T = -0.305$. 183

3.36 Surface plot of the jump term at $T = -0.265$. 184

3.37 Contour plot of the jump term at $T = -0.265$. 184

Chapter 1

Introduction

There are several motivations for the current work. The first concerns are the recent successes in theoretical research into certain two-dimensional aspects of the transition process in a planar boundary layer (eg. Li *et al.* 1998). Another motivation is the results from experimental (eg. Klebanoff *et al.* 1962, Bake *et al.* 2002*a*) and computational work (eg. Rist & Fasel 1995), which have shown that three-dimensional influences play a significant role in the transition process for a boundary layer. This thesis extends the work of Li *et al.* (1998) to three-dimensions in order to increase the realism of theoretical research into this prominent subject. The problem of understanding transition is far-reaching for several real-life situations such as optimising aircraft to reduce drag by delaying transition in the flow over a wing. Due to its importance transition has been studied extensively for many years; from the theoretical work of Tollmien and Schlichting in the 1920s being verified experimentally by Shubauer and Skramstad in 1943 to the substantial amount of work in progress today.

A full understanding of transition has not yet been achieved and there is still a large volume of research undertaken, forty years after the classic K-type transition process was identified in the experiments of Klebanoff *et al.* (1962). Since these early experiments several paths to turbulence have been identified including N-

type transition and indeed the exact route depends on a wide variety of factors such as geometry, disturbance amplitude and spectrum (and this ignores receptivity issues). The theoretical work undertaken here is based on the end-stages of K-type transition but it may provide some understanding for many other transition paths since recently Bake *et al.* (2000) have identified many common features, especially in the end-stages of the transition process. Several of these common features can be identified in other flow situations such as in pipe flow (Eliahou *et al.* 1998, Han *et al.* 2000) and channel flow (Sandham & Kleiser 1992).

Transition of laminar flow to fully turbulent flow, even in seemingly simple flows such as boundary layer flow over a flat plate, is a complicated phenomenon involving rapidly changing time and length scales. Experimental and computational studies of transition must be conducted very carefully so that the amplitude of the initial disturbances are small enough so that the features of the flow are clear. An example of problems caused by insufficient accuracy is the fact that even though Tollmien-Schlichting waves were predicted in 1929 (Tollmien 1929) their existence was not verified experimentally until 1943 (Shubauer & Skramstad 1943).

In the sections that follow a summary of the transition process is given. We concentrate on K-type transition, which was the first to be discovered (see Klebanoff *et al* 1962) but one which has proved to be extremely difficult to understand. For a fuller review of K-type transition see the reviews by Bowles (2000*a*) and Kachanov (1994).

1.1 Experimental and Computational Research

There has been a large amount of both experimental and computational research into transition including transition in boundary layers, closed channel flows and others. In his excellent review of the physical mechanisms involved with laminar boundary layer transition, Kachanov (1994) identifies three general aspects of the problem, which must be studied for a full understanding of transition. They are receptivity, linear stability and nonlinear breakdown.

In simple terms, receptivity can be thought of as the problem of how to disturb the basic flow within an experiment either physical or computational. It is a significant problem since different features are seen in the transition process depending on the form of the initial disturbance. For example, as noted by Kachanov (1994) and Shaikh (1997) turbulent spots seen towards the end of the transition process are not seen if the initial disturbance is periodic but are visible for so-called natural disturbances. For a review of the experimental research of receptivity see Nishioka & Morkovin (1986) and Kachanov (2000). Recent investigations by Bake *et al.* (2002*a*) have shown in both the Blasius boundary layer and boundary layers with a favourable streamwise pressure gradient, that boundary layers are more receptive to three-dimensional perturbations than two-dimensional perturbations. The work of Würz *et al.* (2003) agrees with this in that acoustic-roughness receptivity generates three-dimensional waves more effectively than two-dimensional waves.

The linear stability stage is described by linear hydrodynamic stability and it corresponds to the propagation of small-amplitude instability waves. Most of the initial research concentrated on the two-dimensional problem, probably influenced by Squire's theorem (see Drazin & Reid 1981), which states that the two-dimensional boundary layer is more unstable than its three-dimensional equivalent. Kachanov (1994) notes several properties of the linear stability stage found by Lin (1955) such as the results that a favourable streamwise pressure gradient stabilizes the boundary layer and that the presence of an inflection point in the velocity profile decreases

the stability of the boundary layer. In the Blasius boundary layer there is no inflection point, which implies that there is no Rayleigh (inflectional) instability but there still exists an instability, which relies on the viscosity. These are called the Tollmien-Schlichting instabilities. If we take a small perturbation to a solution of the Navier-Stokes equations then we can derive the Orr-Sommerfeld equation, which retains viscous terms in the Orr-Sommerfeld equation but neglects the viscous effects of the basic velocity profile's development (see Drazin & Reid 1981 for a review of the derivation). The perturbation waves are the Tollmien-Schlichting waves.

An important consideration of linear stability is the influence of nonparallel effects on the relative stability of the boundary layer. Theoretical work by Stewart & Smith (1987) showed that nonparallel effects can influence the three-dimensional stability of nonparallel flows. For a full review of experiments relating to the linear stability stage we direct the reader to the review of Fasel & Konzelmann (1990) in which they come to the significant conclusion that there is no universal condition of stability for real, nonparallel flows. Theoretical studies of the three-dimensional linear stability stage have also been carried out in which it has been shown that the three-dimensional flow exhibits different behaviour from that of a typical two-dimensional flow (see review by Saric *et al.* 2003). In the fully three-dimensional flow inflectional instability can be initiated by a crossflow and hence lead to different results. We do not consider any of these features here.

The nonlinear stage occurs when the amplitudes of the instability waves reach values of 1-2% of the free-stream velocity, which marks the nonlinear breakdown of the flow leading to randomisation and a final transition to turbulence (Kachanov 1994). One can go straight to the nonlinear stage if the amplitude of the disturbance is sufficiently large. This has proved to be a very challenging problem and still generates a huge amount of research. We now concentrate on providing a summary of the K-type route of transition.

1.1.1 K-type transition

K-type transition was first recognised by Klebanoff in the late 1950s (Klebanoff *et al.* 1962) and the main conclusion is the importance of spanwise disturbances within the transition process and hence that transition is a fully three-dimensional process. K-type transition is characterised by a downstream growth of a spanwise modulation of both mean flow and disturbance amplitude and the formation of peaks and troughs in the spanwise direction (Klebanoff *et al.* 1962). Spikes are also visible in the traces of the streamwise velocity profile. These are associated with but it seems not the cause of the strong shear layers seen in the flow. It has also been shown that these spikes are deterministic (Breuer *et al.* 1997, Bake *et al.* 2002*b*). We use the experimental setup and results of Klebanoff *et al.* (1962) as a framework for this summary of the K-type transition process.

In a low turbulence wind tunnel, the flow over a flat plate is artificially disturbed through, for example, a vibrating ribbon. If the amplitude of the disturbances is sufficiently small then two-dimensional Tollmien-Schlichting waves are seen to develop. These two-dimensional waves develop into growing three-dimensional structures by a secondary instability process. The secondary instability theory is reviewed by Herbert (1988) and it explains the deformation of the Tollmien-Schlichting waves into lambda vortices. Alternative theoretical approaches are due to wave-vortex interaction theory (Hall & Smith 1991). The downstream amplification of the spanwise disturbance modulation is caused by the interaction of the stationary and travelling disturbances forming streamwise vortices (Klebanoff *et al.* 1962; Kachanov 1994). This marks the end of the linear stability region described above. Healey (1995) shows agreement between the Orr-Sommerfeld results and experiments at the lower-branch of the neutral stability curve. The so-called neutral stability curve refers to a curve in a Reynolds number, disturbance wave frequency plane, where the Reynolds number in this case depends on the boundary layer thickness. The disturbances lying on the curve are neutral meaning they have a zero growth rate. The

lower and upper portions of the curve are known as the lower and upper branches respectively. For an introduction to the neutral stability curve and more details on the choice of Reynolds number see Bowles (2000*a*). Healey (1995) has shown that Tollmien-Schlichting waves have the character of lower branch disturbances even along the upper branch at transition Reynolds numbers and that, experimentally, lower-branch disturbances dominate.

These three-dimensional structures then develop non-linearly into lambda vortices. This non-linear stage is characterised by localised deviations from the linear pattern at isolated time instants, which grow in magnitude with downstream distance (Shaikh 1997). The lambda vortices themselves generate strong shear layers by the Stuart mechanism (Stuart 1965). In front of and to the sides of the lambda vortex fast moving fluid is pushed down towards the wall and so forming a shear layer separating it from slower moving fluid near the wall. Behind the vortex, fluid is moved away from the wall and vortex stretching results in a high shear away from the wall. See Sandham & Kleiser (1992) especially their figure 13. Williams *et al.* (1984) consider the formation of strong shear layers and they find that the vortex loop (or lambda vortex) exists near the critical layer and is identified by "a strong longitudinal component of vorticity where the transverse vorticity component is minimum." Williams *et al.* (1984) explain the formation of the high shear layer above the lambda vortex by arguing that fluid above the lambda vortex moves faster than the lambda vortex.

After the creation of strong shear layers associated with the lambda vortices then there is a rapid breakdown to short-scaled structures known as "spikes". These spikes are named after the spikes seen in velocity perturbation traces. They are associated with the omega vortices seen in the flow. There has been a large amount of research into the behaviour of the spikes. The early research proposed that these were random, stochastic features (Klebanoff *et al.* 1962). However it has since been shown, notably in experiments by Kachanov and co-workers in the 1980s that these spikes are deterministic, periodic structures (see Kachanov 1994 for a review and

Borodulin & Kachanov 1995). It has even been proposed that the spikes behave as solitons, and favourable comparisons of theory with experiments were found in Kachanov *et al.* (1993), where the Benjamin-Ono equation was used to generate theoretical soliton solutions. The relevance of these comparisons was questioned in the work of Moston *et al.* (2000), in which they found that a singularity is reached in the sublayer before the fully nonlinear stage is reached.

Breuer *et al* (1997) show the development of the disturbance after the shear layers have been established by looking at a wavepacket introduced into the flow. One characteristic of the results is the 'spikes' seen to form in the trace of velocity perturbation. One interesting feature of the spike is a 'kink' in the velocity perturbation as it changes from positive to negative, which could be caused by the growth of short-scale structures in the flow. Breuer *et al.* (1997) show that this 'kink' is a repeatable occurrence, confirming that this feature is not due to some instability mechanism. Borodulin & Kachanov (1990) show, as noted in Kachanov (1994), "that the highest intensity of random, turbulent fluctuations amplified at late stages of the K-breakdown is observed inside the boundary layer in the region that is closer to the high-shear layer than to the spikes." Again emphasising the repeatable nature of this stage of transition.

Rist & Fasel (1995) use direct numerical simulation to investigate the transition process and their results appear to agree very well with experiments. They use a spatial model for the flow. A spatial model is physically more realistic in that it allows both the base flow and the disturbance flow to develop in the downstream direction, thus providing a better model of laboratory experiments. It is well suited for simulations of controlled transition experiments and allows interactions between non-parallel and nonlinear effects. Conversely, in the temporal model the flow is assumed to be spatially periodic and the disturbance grows or decays in time dependent upon whether the base flow is unstable or stable respectively. It is also seen that different visualisation techniques in fact hide certain mechanisms thus showing that in an experiment it is very important to consider how the data is viewed.

The computational results of Rist & Fasel (1995) and the experimental results of Borodulin & Kachanov (1995) have shown that the 'spikes' exist at the centre of the ring-like vortex.

The spikes breakdown locally, showing the first signs of random motions through turbulent spots. These isolated patches of turbulence are called omega vortices and in Bake *et al.* (2000) ring-like vortices (i.e Ω-vortices) are seen snatching away from the tip of the lambda vortex. Bake *et al.* (2000) also consider the N-type breakdown and find that its downstream development is, qualitatively the same as that observed in K-type transition. A full understanding of the late stages of the transition process is not yet complete as much of the research has concentrated on the earlier stages. Meyer *et al.* (1999), Bake *et al.* (2002*b*), Meyer *et al.* (2003) and Rist (2003) have attempted to fill this gap with results that show the development of Ω-vortices and find the final breakdown process to be dominated by locally appearing vortical structures and shear layers.

The turbulent spots eventually grow to subsume the entire flow marking fully turbulent flow. The exact mechanisms involved are still not fully understood. A further understanding of the structures at the end stages could provide further insight into fully turbulent flow since several structures found in the transition process can be identified within turbulent flow (Robinson 1991).

1.2 Theoretical Approach

One approach into understanding the route of transition to turbulence on a flat plate is to take a small perturbation to a solution of the Navier-Stokes equations. As we have stated earlier this technique derives the Orr-Sommerfeld equation and the perturbation waves are termed the Tollmien-Schlichting waves. Lighthill gives a clear explanation of the structure and mechanism of a Tollmien-Schlichting mode and why viscosity is necessary for its growth in Rosenhead (1963). Tollmien-Schlichting waves do not rely on an inflection point for growth. This factor distinguishes them from other (inviscid) solutions of the Orr-Sommerfeld equation. The next step is to study these structures and their development into three-dimensional structures. One approach for high Reynolds' number flows, which has been successful is outlined below but for a fuller review, see Smith (1993).

The Tollmien-Schlichting waves are governed by the triple-deck equations (also called the interactive boundary layer equations). A full review of the triple-deck equations can be found in Smith (1982) and Sobey (2000). The boundary layer is considered in three sections; a viscous lower deck, where the no-slip condition is satisfied, a middle deck and an upper deck, which matches with the potential flow outside the boundary layer. This nonlinear stage corresponds to nonlinear Tollmien-Schlichting wave development, in the context of transition, given that the linearised system captures Tollmien-Schlichting waves (Smith 1979). The vortex-wave interaction theory captures the onset of three-dimensional spanwise perturbations (Smith & Walton 1989, Smith & Bowles 1992 and Stewart & Smith 1992). The strongly nonlinear triple-deck equations capture the generation of lambda vortices. Importantly for the work that follows, Smith (1988) identified a finite-time break-up of this interactive step corresponding to the step 1, which is summarised at the beginning of chapter 2. The break-up is associated with a shortening of the streamwise length scale with large values of the streamwise pressure gradients and strong shear layers. There is

also an associated mathematical constraint on the velocity profile,

$$\int_0^\infty \frac{1}{(U(y)-c)^2} dy = 0, \tag{1.1}$$

where c is the local phase speed, $U(y_c) = c$, $U''(y_c) = 0$ and y_c is the wall normal coordinate at the critical layer. This inflection point defines the critical layer, which as shown in Li *et al.* (1998), Bowles *et al.* (2003) and chapters 2, 3 of this thesis, is the significant region. The critical layer is the point at which the phase speed is equivalent to the streamwise velocity. Here the fluid is effectively moving with the wave and it is at this point that the flow is most sensitive to nonlinear and three-dimensional disturbances. Quantitative comparisons by Smith & Bowles (1992) show the theoretical constraint (1.1) to agree with the experiments of Nishioka *et al.* (1979) at the first spike.

The finite-time break-up of Smith (1988) suggests that still shorter time and length scales are required to understand the behaviour of the flow near the singularity. This is considered by Li *et al.* (1998). In the case of external boundary layer flows the perturbations satisfy a form of the Benjamin-Ono equation, which yields soliton solutions (Drazin 1983, Drazin & Johnson 1989).

The criterion for the winding up of a vortex is the onset of a pressure maximum/minimum in the scaled pressure variation (i.e. $p_X \to 0$). The shorter time scales associated with this are studied in Li *et al.* (1998), for the internal flow case and in Bowles (2000*b*) for the external flow scales. In the latter the shorter time scales are relevant only for trapped circulating fluid - a vortex. In the theoretical interpretation of experimental and computational results this criterion and (1.1) correspond to the formation of the 'first spike' in certain transition paths (Li *et al.* 1998).

1.3 Description of Later Chapters

In chapter 2 a theoretical approach describing the late-stages of transition as presented in Li *et al.* (1998) is extended to include the three-dimensional influence of vortex stretching. It commences with the derivation using asymptotic techniques of a system of nonlinear integro-differential equations, which describe this process. The spanwise terms are introduced at the critical layer which coincides with the inflection point in the streamwise velocity profile. It is a natural starting place for the introduction of three-dimensional influences into an established two-dimensional model. We find the three-dimensional equations in the critical layer to be, in normalised terms,

$$Yw_X - P_X w_Y = -P_z, \tag{1.2}$$

$$Y\tau_X - P_X \tau_Y = w_z, \tag{1.3}$$

$$J_X = \int_{-\infty}^{\infty} \tau_X dY, \tag{1.4}$$

with the pressure in the bulk of the flow satisfying,

$$a_1 P_T + a_2 P P_X = \frac{1}{\pi} \int_{-\infty}^{\infty} \frac{P_{ss}}{X - s} dX + \mu J_X. \tag{1.5}$$

The spanwise velocity within the critical layer is w, z is the spanwise variable, P is the pressure distribution and τ is the perturbation vorticity within the critical layer. a_1, a_2 and μ are constants. J_X describes the feedback of the critical layer (incipient vortex) dynamics on the pressure development. An expression for the spanwise critical layer term, J_X in terms of the spanwise and streamwise variable can be found but the expression for the three-dimensional part involves a triple repeated integral, which requires a computational approach. The integral in (1.5) is the Cauchy principal part of the singularity at $s = X$.

An approximate linear pressure distribution is applied to the system ($P_X \sim$ constant), where it is found that the spanwise effects are passive (i.e. the critical layer jump term does not feedback on the pressure displacement). A three-dimensional

short-scale analysis then follows, which shows that a non-constant derivative of the pressure is required for a non-zero spanwise critical layer interactive term.

A numerical approach is presented in 2.5, which investigates these equations. The results imply a growing jet of spanwise vorticity in the downstream streamwise direction but our analysis shows this integrates to zero. Numerical results and conclusions are presented, which show in the general case a surprisingly strong streamwise vorticity feeding back onto the flow. This causes the failure of the planned numerical approach and indeed reveals that the presumed three-dimensionality is too strong in general for (1.2) - (1.5) to be a well-posed system. The nature of the failure is thoroughly investigated. There are special cases in which the formulation is valid however. The chapter concludes with an analysis to show this predicted feature of the numerical scheme to be a true consequence of the governing derived equations. Finally we show that this strong feedback mechanism is controlled by considering unsteady influences active over slightly longer length scales. In conclusion the choice of spanwise scale is still too short and we conclude three-dimensional effects first enter over even longer spanwise scales.

In chapter 3 a continuation of the study of chapter 2 is taken by considering such increased spanwise scales leading to reduced values of the parameter μ, which corresponds to a delay in the feedback of the critical layer jump term until the generation of vortices in the flow. This study is an extension of Bowles (2000*b*) to three-dimensions. We begin with a derivation of the equations in three-dimensions, and we find that the area of a particle's streamwise orbit is fixed once captured inside the vortex. This realisation is crucial in allowing further analysis of the build up of vorticity within the trapped vortex through vortex stretching. An analysis of the behaviour for early vortices is then considered before a numerical solution is presented for the spanwise behaviour within the vortex.

Chapter 2

The Structure of the Three-Dimensional Critical Layer and its Consequences

Historically, experimental and computational research, ranging from the first identification of K-type transition in the experiments of Klebanoff *et al.* (1962) to the recent computations of Bake *et al.* (2002*a*) have highlighted the significance of three-dimensionality during the transition process. It is the three-dimensional mechanism that drives the route to transition through secondary instability leading to, in the end stages, the onset of lambda vortices and later omega vortices. Most theoretical work has concentrated on the two-dimensional problem and there have been notable successes with this approach such as those cited in the introduction. However the theoretical understanding of the end-stages of the fully three-dimensional transition process has proved a more elusive problem. We expect the spanwise influence to have a significant contribution and hence its study is an important theoretical problem. It is hoped that this work and the new features recognized will provide insight into the potential for further study of this important and challenging subject.

The recent theoretical work of Smith (1988) and Li *et al.* (1998), which studied the

end-stages of transition in the two-dimensional boundary-layer, has highlighted the importance of a critical layer in the flow solution. The work of Bowles *et al.* (2003) has shown that this approach outlines an accurate method of modelling the end-stages of transition. Hence, we use the research of Li *et al.* (1998) as a basis for the flow and extend for three-dimensions. This is achieved by introducing some small spanwise variation in the pressure, which is active inside the critical layer and it is found here that even with a small spanwise perturbation the three-dimensional terms become significant inside the critical layer, which drives a strong feedback onto the main flow. This feature introduces an unexpectedly strong feedback mechanism, which affects the whole theory.

2.1 Derivation of Equations

We introduce three-dimensional spanwise influences into the two-dimensional spike theory developed in Li *et al.* (1998) and Smith (1988). Here the flow is considered two-dimensional for the finite-time break-up (Smith 1988 and step 1 in Li *et al.* 1998) and three-dimensional effects are studied by considering a spanwise velocity introduced at the beginning of step 2, where normal pressure gradients enter, as time progresses from this break-up. A brief summary of step 1 is included as the results found are required as boundary and initial conditions for the study of the flow beyond the break-up. The full Navier-Stokes equations in a non-dimensional form, subject to suitable initial and boundary conditions, are,

$$\bar{u}_x + \bar{v}_y + \bar{w}_z = 0, \tag{2.1}$$

$$\bar{u}_t + \bar{u}\bar{u}_x + \bar{v}\bar{u}_y + \bar{w}\bar{u}_z = -\bar{p}_x + \epsilon^8\left(\bar{u}_{yy} + \bar{v}_{yy} + \bar{w}_{zz}\right), \tag{2.2}$$

$$\bar{v}_t + \bar{u}\bar{v}_x + \bar{v}\bar{v}_y + \bar{w}\bar{v}_z = -\bar{p}_y + \epsilon^8\left(\bar{u}_{yy} + \bar{v}_{yy} + \bar{w}_{zz}\right), \tag{2.3}$$

$$\bar{w}_t + \bar{u}\bar{w}_x + \bar{v}\bar{w}_y + \bar{w}\bar{w}_z = -\bar{p}_z + \epsilon^8\left(\bar{u}_{yy} + \bar{v}_{yy} + \bar{w}_{zz}\right). \tag{2.4}$$

As is customary, $(\bar{u}, \bar{v}, \bar{w})$ are the streamwise, normal and spanwise velocities respectively and (x, y, z) are the streamwise, normal and spanwise variables respectively. The pressure is given by $\bar{p}$ and $\epsilon = Re^{-1/8}$, where Re is the Reynolds number. We consider a large Reynolds number so that ϵ is small.

Summary of Step 1

Step 1 refers to the finite-time break-up in an unsteady interacting boundary layer and is also known as the nonlinear Tollmien-Schlichting stage as it captures the linear Tollmien-Schlichting waves in the linear region for triple-deck scales. The external incompressible triple-deck equations are used as the beginning of the following study. In this nonlinear Tollmien-Schlichting stage it is the viscous sublayer (lower deck)

that is important, where the flow solution has the expansion,

$$[\bar{u}, \bar{v}, \bar{p}] = [\epsilon u, \epsilon^3 v, \epsilon^2 p(x,t)] + ..., \tag{2.5}$$

$$[\bar{x}, \bar{y}, \bar{t}] = [\bar{x}_0 + \epsilon^3 x, \epsilon^5 y, \epsilon^2 t] + ..., \tag{2.6}$$

near $\bar{x} = \bar{x}_0$. Given these expansions the governing equations are,

$$u = \psi_y, \qquad \text{and,} \qquad v = -\psi_x, \tag{2.7}$$

$$u_t + uu_x + vu_y = -p_x(x,t) + u_{yy}. \tag{2.8}$$

subject to $u = \psi = 0$ at $y = 0$ and $u \sim y + A(x,t)$ as $y \to \infty$. The undisturbed flow corresponds to $u = y$, $v = 0$ and $A = 0$. The initial flow development can be provoked by perturbing these either linearly or nonlinearly. The pressure, p and the negative displacement, A are both unknown functions of x and t but they are linked by the following Cauchy-Hilbert relation in the subsonic case,

$$p(x,t) = \frac{1}{\pi} \int\!\!\!\!\!\!- _{-\infty}^{\infty} \frac{A_\chi(\chi,t)}{x-\chi} d\chi, \tag{2.9}$$

found from the potential flow properties holding in the upper deck.

A finite-time break-up is possible for this initial value problem (Smith 1988) and is expected to be achieved for arbitrary initial conditions. This is described as a moderate break-up, where for $\xi = O(1)$ the length scale,

$$x - x_0 = c(t - t_0) + (t - t_0)^{3/2}\xi, \tag{2.10}$$

contracts near the break-up position, $x = x_0$ at time, $t = t_0$ with the scaled solution,

$$[u, \psi, p] = [u_0(y), \psi_0(y), p_0] + (t_0 - t)^{1/2}[u_1(\xi, y), \psi_1(\xi, y), p_1(\xi)] + O(t_0 - t)^{3/4}. \tag{2.11}$$

A study of (2.7) and (2.8) following the analysis of Smith (1988) leads to the non-linear equation,

$$p_1 p_1' = \hat{b}(p_1 - 3\xi p_1'), \tag{2.12}$$

for $p_1(\xi)$, where $\hat{b}$ is a constant that depends on integrals of the initial streamwise velocity and its form is proved to be true in the general case in Li *et al.* (1998). 2.12 is a form of Burgers equation. In step 1 the critical layer jump term is zero (Smith 1988). This break-up marks the end of step 1 and introduces new physical properties locally, which are considered in step 2 of Li *et al.* (1998) for the two-dimensional case and here for the three-dimensional case.

The Introduction of Spanwise Influences into step 2

The introduction of three-dimensionality is achieved by including a spanwise variation in the pressure. The influence of increasing this variation is first felt on the governing pressure equation through the term describing the streamwise velocity jump at the critical level. This velocity is active in the critical layer, where it acts to intensify the spanwise influence of the vorticity. Thus a spanwise pressure variation drives a velocity, which intensifies the vorticity at the critical layer, leading to a variation in the jump term, which feeds back on the governing pressure equation. The main deck remains unchanged apart from the addition of a passive cross-flow velocity. Introducing the spanwise variation inside the critical layer is the natural choice since as shown in Li *et al.* (1998) the critical layer jump term plays a significant role in the understanding of the theoretical problem and it is within the critical layer that the flow is most sensitive to three-dimensional perturbations.

As with the step 2 case considered in Li *et al.* (1998) there are four main tiers to consider in the normal direction. The main flow, which is designated as region I in figure 2.1 and comprises the bulk of the flow and has size ϵ^5. The significant but thin critical layer (region II in figure 2.1) is located at the inflection point. It is here that the flow velocity is equal to the phase speed c. Li *et al.* (1998) show that there exists a critical layer with thickness of order $\epsilon^{11/2}$. They find that it is the vorticity at fourth order inside the critical layer that is responsible for the jump. We choose the three-dimensional scaling so that this vorticity has a spanwise variation and is

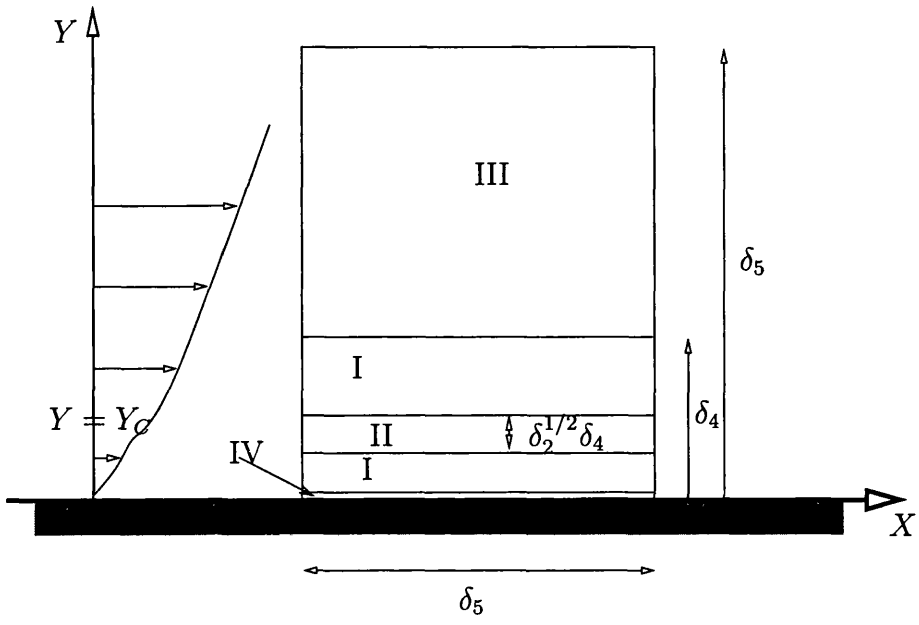

Figure 2.1: The Li *et al.* (1998) triple-deck setup.

affected by vortex stretching. The spanwise scalings are chosen by consideration of the continuity and momentum equations at fourth order inside the critical layer. A w is generated from $uw_X \sim -p_z$, which gives,

$$wz \sim \delta_1^2 \delta_2^{1/2} \delta_5, \tag{2.13}$$

with $(\delta_1, \delta_2, \delta_5)$ denoting $(\epsilon, \epsilon^{1/2}, \epsilon^{9/2})$. The inclusion of a three-dimensional influence in the continuity equation reflecting vortex stretching implies,

$$\frac{w}{z} \sim \frac{\delta_1 \delta_2^2}{\delta_5}, \tag{2.14}$$

Hence, $w \sim \delta_1 \delta_2^{5/4} = \epsilon^{13/8}$ inside the critical layer and $z \sim \delta_5 \delta_2^{-3/4} = \epsilon^{33/8}$. Since $w \sim \frac{1}{Y}$ as $Y \to \infty$ inside the critical layer we obtain the scaling for w in the bulk of the flow to be $w \sim \delta_1 \delta_2^{7/4} = \epsilon^{15/8}$. The third tier (III) lies outside the main tier and has a normal extent comparable with the streamwise X extent, of order $\delta_5 = \epsilon^{9/2}$. The third tier influences the flow through a Cauchy-Hilbert type integral, which will be derived in this section. There is also a viscous layer (IV) but it is shown

subsequently on page 34 that this has little effect in the current situation, leaving an inviscid flow locally.

We begin by considering the main tier, I in figure 2.1. The scalings follow from an order of magnitude argument based on the form of the moderate break-up described in Smith (1988) and in the summary of step 1. As $t \to t_0$ in (2.11) we obtain for $T = t_0 - t$,

$$\bar{u} \sim \epsilon T^{1/2}, \tag{2.15}$$

Continuity implies that we have a streamwise velocity of order $\epsilon^3 T^{-1}$. If we enforce $\bar{v}_y \to 0$ in the outer tier then by continuity in the outer tier a second order streamwise velocity term of order $\epsilon^3 T^{-1}$ is generated in the outer tier (the outer tier is a square region and so the streamwise and normal variables are the same size). This streamwise velocity will act as a boundary condition for the $\tilde{u}_2$ term defined below as $y \to \infty$ if $\epsilon T \sim \epsilon^3 T^{-1}$. Hence $T \sim \epsilon$.

The following expansions are equivalent to those presented in Li *et al.* (1998) but with the introduction of a spanwise variable and velocity. Here,

$$\bar{x} = \text{constant} + \delta_1\delta_3 cT + \delta_5 X, \qquad \bar{t} = \text{constant} + \delta_3 T, \tag{2.16}$$

where δ_3 denotes ϵ^3. The expansions for the first tier are,

$$\bar{u} = \delta_1[u_0(y) + \delta_2\tilde{u}(X,y,t) + \delta_2^2\tilde{u}_2(X,y,t) + ...], \tag{2.17}$$

$$\bar{v} = \delta_1\delta_4\delta_5^{-1}[\delta_2\tilde{v}(X,y,t) + \delta_2^2\tilde{v}_2(X,y,t) + ...], \tag{2.18}$$

$$\bar{p} = \delta_1^2[p_0 + \delta_2\tilde{p}(X,z,t) + \delta_2^2\tilde{p}_2(X,y,z,t) + ...], \tag{2.19}$$

$$\bar{w} = \delta_1\delta_2^{7/4}\tilde{w} + \dots, \tag{2.20}$$

for scaled X, y, T of $O(1)$ and $\bar{y} = \delta_4 y$, with δ_4 being ϵ^5.

On substitution of the expansions into the Navier-Stokes equations we obtain at first order,

$$\tilde{u}_X + \tilde{v}_y = 0, \tag{2.21}$$

$$(u_0 - c)\tilde{u}_X + \tilde{v}u_{0y} = -\tilde{p}_X, \tag{2.22}$$

and at second order,

$$\tilde{u}_{2X} + \tilde{v}_{2y} = 0, \tag{2.23}$$

$$(u_0 - c)\tilde{u}_{2X} + \tilde{v}_2 u_{0y} + [\tilde{u}_T + \tilde{u}\tilde{u}_X + \tilde{v}\tilde{u}_y] = -\tilde{p}_{2X}. \tag{2.24}$$

We include, for completeness the equation for the spanwise variable, $\tilde{w}$, although it is passive,

$$(u_0 - c)\tilde{w}_X = -\tilde{p}_z, \tag{2.25}$$

and hence,

$$\tilde{w} = \frac{B}{(u_0 - c)}, \qquad \text{where,} \qquad B_X = -\tilde{p}_z. \tag{2.26}$$

Now we can solve (2.22) to find, at leading order,

$$\tilde{v} = \tilde{p}_X(u_0(y) - c)\fint_0^y [u_0(\hat{y}) - c)]^{-2} d\hat{y}, \tag{2.27}$$

for an unknown pressure $\tilde{p}$, which is found at the second order. This satisfies the boundary condition, $\tilde{v}(0) = 0$. We introduce,

$$\Phi(y) = (u_0(y) - c)\fint_0^y [u_0(\hat{y}) - c)]^{-2} d\hat{y}, \tag{2.28}$$

so that,

$$\tilde{v} = \tilde{p}_X \Phi(y), \qquad \text{and,} \qquad \tilde{u} = -\tilde{p}\Phi'(y). \tag{2.29}$$

As $y \to \infty$ we impose the boundary condition $\tilde{v}_y = 0$, which suppresses the pressure displacement interaction in the usual triple deck mechanism by setting the pressure displacement to be constant at the first order. This condition is necessary since our length scales are short, which implies that A_χ in (2.9) is large. This generates a large pressure in (2.9), which is too large and this pressure will swamp the dynamics we are considering. However if we set the gradient in A equal to zero locally then no such pressure is generated. We impose the condition in this way as otherwise $\tilde{v} \to -yA_\chi$ as $y \to \infty$. If $\tilde{v}$ does not grow like y (i.e. $\tilde{v}_y = 0$) then this pressure is not generated. We also have that $u_0 \sim \lambda y$, as $y \to \infty$ and we shall consider the contribution for large y on page 35. The condition that $\tilde{v}_y = 0$ as $y \to \infty$ implies,

$$\int_0^\infty [u_0(y) - c)]^{-2} dy = 0, \tag{2.30}$$

which along with the onset of maxima and minima in the local pressure is the criteria for the occurrence of the winding up vortex, which we will study in chapter 3 (Smith 1988). Solving (2.24) for the second order terms leads to,

$$\begin{aligned} -(u_0(y) - c)^2 \frac{\partial}{\partial y}\left(\frac{\tilde{v}_2}{(u_0(y) - c)}\right) &= -\tilde{p}_{2X} - \tilde{u}_T - \tilde{u}\tilde{u}_X - \tilde{v}\tilde{u}_y, \qquad (2.31) \\ &= -\tilde{p}_{2X} + \tilde{p}_T \Phi'(y) - \tilde{p}\tilde{p}_X \left((\Phi'(y))^2 - \Phi(y)\Phi''(y)\right). \end{aligned}$$

Integration of the above equation implies,

$$\left[\frac{\tilde{v}_2}{(u_0(\hat{y}) - c)}\right]_0^y = \int_0^y \frac{\tilde{p}_{2X} - \tilde{p}_T \Phi'(\hat{y}) + \tilde{p}\tilde{p}_X \left((\Phi'(\hat{y}))^2 - \Phi(\hat{y})\Phi''(\hat{y})\right)}{(u_0(\hat{y}) - c)^2} d\hat{y} + \left[\frac{\tilde{v}_2}{(u_0(y) - c)}\right]_{y_c-}^{y_c+}. \tag{2.32}$$

The last term on the right hand side is the jump term, which is the jump in velocity across the discontinuity and can be calculated by consideration of the critical layer expressions, as will show shortly. Furthermore, we will show on page 35 that as $y \to \infty$,

$$\left[\frac{\tilde{v}_2}{(u_0(y) - c)}\right]_0^\infty = \frac{1}{\pi}\int_{-\infty}^\infty \frac{1}{X - s}\frac{\partial^2 \tilde{p}}{\partial s^2} ds. \tag{2.33}$$

Therefore taking $y \to \infty$ in (2.32) leads to,

$$\frac{1}{\pi} \fint_{-\infty}^{\infty} \frac{1}{X-s} \frac{\partial^2 \tilde{p}}{\partial s^2} ds = a_1 \tilde{p}_T + a_2 \tilde{p} \tilde{p}_X + j, \tag{2.34}$$

with j defined as the unknown jump contribution across the critical layer and,

$$a_1 = -\fint_0^{\infty} \frac{\Phi'(y)}{(u_0(y)-c)^2}\, dy, \qquad \text{and,} \qquad a_2 = \fint_0^{\infty} \frac{(\Phi'(y))^2 - \Phi(y)\Phi''(y)}{(u_0(y)-c)^2}\, dy. \tag{2.35}$$

The term in $\tilde{p}_{2X}$ does not appear in (2.34) as it is multiplied by $\fint_0^{\infty}(u_0(y)-c)^{-2}\, dy$, which is equal to zero. This, as with most of the derivation, apart from the extra spanwise influences in (2.25), is identical to the derivation found in Li *et al.* (1998). It is in the critical layer, the slender region near $y = y_c$ where $u_0(y_c) = c$, that the significant three-dimensional contribution is first felt and it is the analysis of this region that follows.

The Three-Dimensional Critical Layer

In the critical layer the streamwise and time scalings remain the same as region I but the wall normal extent is, as expected, much smaller. We will show that the y scales are now reduced by a factor $\delta_2^{1/2}$. We must first consider the solution in the main flow as the critical layer is approached. We achieve this by expanding u_0 locally around the critical layer. Before continuing with the critical layer solution we consider again the solutions for $\tilde{u}$ and $\tilde{v}$ in tier I and expand u_0 locally around the critical layer (i.e. where y is near y_c) such that,

$$u_0 - c = b_1(y-y_c) + b_3(y-y_c)^3 + \ldots. \tag{2.36}$$

There is no term in $(y-y_c)^2$ due to the inflexion point in u_0. The study of the solutions in tier I with this expansion will provide boundary conditions for the

critical layer solutions. In tier I we find,

$$\begin{aligned}\bar{u} &= \delta_1\Big\{c + b_1(y-y_c) + b_3(y-y_c)^3 + b_4(y-y_c)^4 + \\ &\quad \delta_2\left\{-a_{11} + 2a_{12}(y-y_c) - 3\alpha(y-y_c)^2\tilde{p}\right\} + \\ &\quad \delta_2^2\left\{-\frac{\beta}{b_1}\log|y-y_c| + \frac{\beta}{b_1} - 2c_{10}b_1^2(y-y_c)\right\} + \ldots\Big\}, \qquad (2.37)\end{aligned}$$

and,

$$\begin{aligned}\bar{v} &= \delta_1\delta_4\delta_5^{-1}\Big\{\delta_2\left\{\frac{-\tilde{p}_X}{b_1} + a_{11X}(y-y_c) - a_{12X}(y-y_c)^2 + \alpha(y-y_c)^3\right\} + \\ &\quad \delta_2^2\left\{\frac{-c_{10X}}{b_1^2} + \frac{\beta_X}{b_1}(y-y_c)\log|y-y_c| - \frac{c_{10X}}{b_1^2}(y-y_c)^2\right\} + \ldots\Big\}, \qquad (2.38)\end{aligned}$$

where $a_{10} = b_1^{-1}\tilde{p}$, $a_{11} = b_1 I_1\tilde{p}$, with $I_1 = \int_0^{y_c}[u_0(\hat{y}) - c)]^{-2}d\hat{y}$, $a_{12} = 3b_3b_1^{-2}\tilde{p}$, $c_{10X} = b_1^{-1}(\tilde{p}_{2X} + a_{11T} + a_{11} + a_{11}a_{11X} - 2a_{12}a_{10X})$, $\alpha = b_1^{-1}\left(b_3a_{11} - 2b_4a_{10}\right)$ and $\beta_X = 2a_{12T} - 2a_{11}a_{12X} + 3\alpha a_{10X}$.

The y scales are reduced by a factor $\delta_2^{1/2}$. The justification for this reduction in scales is given in Smith (1988) but essentially the scales are chosen, in the case of the moderate break-up considered here, to smooth out the logarithmic irregularity found in the critical layer. This is done by introducing nonlinear terms into the critical layer. We find the size of Y in the critical layer through fixing the balance,

$$(u_0 - c)\tilde{u}_X \sim \tilde{v}\tilde{u}_Y. \qquad (2.39)$$

As the critical layer is approached we have, $u_0 \sim (y - y_c)$ from matching the expansion in (2.37) with (2.17) and $\tilde{v} \sim \tilde{p}_X$ from matching the expansions in (2.38) with (2.18). If we let ϖ denote the critical layer thickness then,

$$\varpi^2 \sim \delta_2. \qquad (2.40)$$

As the critical layer is approached we write $(y - y_c) = \delta_2^{1/2}Y$ in (2.37) and (2.38), which gives the following matching conditions on the critical layer solutions,

$$\begin{aligned}\bar{u} &= \delta_1\Big\{c + \delta_2^{1/2}b_1Y - \delta_2 a_{11} + \delta_2^{3/2}\left(b_3Y^3 + 2a_{12}Y\right) + \\ &\quad \delta_2^2\left(b_4Y^4 - 3\alpha\tilde{p}Y - \frac{\beta_X}{b_1}\log|\delta_2^{1/2}|Y + \frac{\beta}{b_1}\right) + \ldots\Big\}, \qquad (2.41)\end{aligned}$$

and,

$$\bar{v} = \delta_1\delta_4\delta_5^{-1}\Big\{ -\delta_2\frac{\tilde{p}_X}{b_1} + \delta_2^{3/2}a_{11}Y - \delta_2^2\left(a_{12}Y^2 + \frac{c_{10X}}{b_1^2}\right) + \delta_2^{5/2}\left(\alpha Y^3 + \frac{\beta_X}{b_1}Y\log|\delta_2^{1/2}Y|\right) + \ldots\Big\}. \tag{2.42}$$

The expansions holding are reduced by a factor $\delta_2^{1/2}$ giving,

$$\bar{u} = \delta_1[c + \delta_2^{1/2}U_1 + \delta_2 U_2 + \delta_2^{3/2}U_3 + \delta_2^2 U_4 + ...], \tag{2.43}$$

$$\bar{v} = \delta_1\delta_4\delta_5^{-1}\delta_2^{1/2}[\delta_2^{1/2}V_1 + \delta_2 V_2 + ...], \tag{2.44}$$

$$\bar{p} = \delta_1^2[p_0 + \delta_2 P_1 + \delta_2^2 P_2 + \delta_2^{5/2}P_3...], \tag{2.45}$$

$$\bar{w} = \delta_1[\delta_2^{5/4}W_4 + \ldots], \tag{2.46}$$

with $\bar{y} = \delta_4(y_0 + \delta_2^{1/2}Y)$.

Substituting the expansions in the critical layer into the Navier-Stokes equations with our knowledge of the matching conditions allows us to solve the equations found through substituting (2.43) - (2.46) into the Navier-Stokes equations and then derive governing equations for the jump term. On substitution, we find,

$$U_1U_{1X} + V_1U_{1Y} = -P_{1X}, \tag{2.47}$$

$$U_{1T} + U_1U_{2X} + U_2U_{1X} + V_1U_{2Y} - V_2U_{1Y} = 0, \tag{2.48}$$

$$U_{2T} + U_1U_{3X} + U_2U_{2X} + U_3U_{1X} + V_1U_{3Y} + V_2U_{2Y} + V_3U_{1Y} = -P_{2X}, \tag{2.49}$$

$$U_{3T} + U_1U_{4X} + U_2U_{3X} + U_3U_{2X} + U_4U_{1X} + V_1U_{4Y} + V_2U_{3Y} + V_3U_{2Y} + V_4U_{1Y} = -P_{3X} + U_{1YY}. \tag{2.50}$$

Continuity implies, $U_{nX} = -V_{nY}$ for $n = 1, 2, 3$ and therefore we may write $U_n = \Psi_{nY}$ and $V_n = -\Psi_{nX}$ for $n = 1, 2, 3$. The extra spanwise terms do not show themselves above but do enter into the fourth equation (2.50) through continuity at this order namely,

$$U_{4X} + V_{4Y} + W_{4z} = 0. \tag{2.51}$$

We will find (2.50) to be significant in provoking the velocity jump that is of interest to us. The spanwise velocity is controlled by the spanwise momentum balance,

$$U_1 W_{4X} + V_1 W_{4Y} = -P_{1z}. \tag{2.52}$$

The normal momentum balance shows the normal pressure gradients to be zero for the first four terms in the expansion for pressure and hence they are equal to the pressures in the bulk of the flow, (i.e. $P_1 = \tilde{p}$, $P_2 = \tilde{p}_2(X,T)$, $P_3 = \tilde{p}_3(X,T)$). Matching with the bulk of the flow leads to the solutions of (2.47) - (2.49),

$$\Psi_1 = \frac{b_1 Y^2}{2} + b_1^{-1}\tilde{p},\ U_1 = b_1 Y,\ V_1 = -b_1^{-1}\tilde{p}_X,\ \Psi_2 = a_{11}(X,T)Y, \tag{2.53}$$

$$\Psi_3 = \frac{b_3 Y^4}{4} + a_{12}(X,T)Y^2 + c_{10}(X,T). \tag{2.54}$$

Finding the solution for (2.50) is more difficult but by taking its Y-derivative and using the spanwise continuity we derive,

$$b_1 Y U_{4XY} - b_1^{-1}\tilde{p}_X U_{4YY} - b_1 W_{4z} = 6Y^2 b_3 a_{11X} - 2a_{12T} - 2a_{11}a_{12X}. \tag{2.55}$$

From the analysis in tier I, U_4 can be written, for large Y as,

$$U_4 = b_4 Y^4 + 3a_{13}Y^2 + \Phi_{4Y}, \qquad \text{with,} \qquad \Phi_4 = \beta_X Y \ln|Y| + c_{11}Y. \tag{2.56}$$

If we now impose this matching condition on (2.55) and write the vorticity as, $\tau_4 = \Phi_{4YY}$ we find the equation for the vorticity inside the critical layer,

$$\begin{aligned} b_1 Y \tau_{4X} - b_1^{-1}\tilde{p}_X \tau_{4Y} &= -6b_1^{-3}\left(b_3 b_1 \tilde{p}_T - 2b_4 \tilde{p}\tilde{p}_X\right) + b_1 W_{4z}, \\ &= m(X,T) + b_1 W_{4z}. \end{aligned} \tag{2.57}$$

We are interested in the jump term, which is the jump in $\tilde{v}_{2y} = -\tilde{u}_{2X}$ in tier I. In the critical layer this matches with U_{4X} since,

$$\left[\frac{\tilde{v}_2}{(u_0(y)-c)}\right]_{Y_c-}^{Y_c+} = \left[\frac{\tilde{v}_2}{b_1 Y}\right]_{Y_c-}^{Y_c+} = -\frac{1}{b_1}\left[\tilde{u}_{2X}\right] = \frac{1}{b_1}U_{4X}, \tag{2.58}$$

and hence the jump term is given by,

$$j = b_1^{-1}\frac{\partial J}{\partial X}, \qquad \text{where,} \qquad J = \int_{-\infty}^{\infty} \tau_4 \, dY. \tag{2.59}$$

The equation for τ_4 is linear in τ_4. Therefore the three and two-dimensional parts can be considered separately and the solution will be the sum of the two solutions. The two-dimensional part will be considered in the next section in the same manner as Li *et al.* (1998) leaving an integral for J, which must be found numerically, whilst the three-dimensional part is more complicated due to the driving equation for W_4 and hence involves a triple repeated integral.

Near Wall Contribution

The viscous wall layer has no effect on the main pressure term, $\tilde{p}$. This is shown in Brotherton-Ratcliffe & Smith (1982) and Smith (1988) for the moderate break up case. In summary it is shown in Smith (1988) that a classical Stokes-Layer balance can be derived, such that,

$$-c\tilde{u}_{1X} = -\tilde{p}_X + \tilde{u}_{1\eta\eta}, \tag{2.60}$$

where $y = \epsilon^{3/4}\eta$ and subject to $\tilde{u}_1 = 0$ at $\eta = 0$ for no-slip at the wall and $\tilde{u}_{1X} \to c^{-1}\tilde{p}_X$ as $\eta \to \infty$ so that the solution merges with the main deck. Brotherton-Ratcliffe & Smith (1982) solve (2.60) using Fourier Transforms and they find that the viscous wall layer does affect the $\tilde{p}_2$ term but it has no influence on the main pressure term, $\tilde{p}$. The vertical displacement velocity near the wall is smaller than the second order term in (2.18). Physically this is due to the speed of the pressure distribution as it moves downstream being too great. As a result the interaction with the wall layer is weak and does not feedback onto the distribution to first order.

Contribution from $y \to \infty$

Tier (III) is the region outside tier (I) and has normal $\bar{y}$ extent of order δ_5, which is the same as the streamwise, $\bar{x}$ extent. Writing $\bar{y} = \delta_4 \hat{y}$ and considering the flow solution as a small perturbation of the shear flow, we expand for $\bar{u}$, $\bar{v}$ and $\bar{p}$,

$$\bar{u} = \delta_1 \left(\hat{y} + \delta_1 \hat{u} + \dots \right), \tag{2.61}$$

$$\bar{v} = \delta_2 \delta_4 \delta_5^{-1} \left(\delta_1 \hat{v} + \dots \right), \tag{2.62}$$

$$\bar{p} = \delta_1^2 \left(\delta_1 \hat{p} + \dots \right). \tag{2.63}$$

The contribution from $y \to \infty$ in tier (I) to be used in (2.32) is given by,

$$\left[\frac{\tilde{v}_2}{(u_0(y) - c)} \right]_0^\infty = \frac{\partial \hat{v}}{\partial \hat{y}} |_{\hat{y}=0}, \tag{2.64}$$

since here, as $\hat{y} \to 0$, $\frac{\partial \hat{v}}{\partial \hat{y}} \sim \delta_2 \delta_4 \delta_5^{-1} \delta_1 = \epsilon^{-5/2}$ and at the extreme normal position in tier (I), $\tilde{v}_{2y} \sim \delta_1 \delta_4 \delta_5^{-1} \delta_4^{-1} = \epsilon^{-5/2}$. To find $\hat{v}$ substitute into the Navier-Stokes equations,

$$\hat{y} \hat{u}_X + \hat{v} = -\hat{p}_X, \tag{2.65}$$

$$\hat{y} \hat{v}_X = -\hat{p}_y, \tag{2.66}$$

$$\hat{u}_X + \hat{v}_{\hat{y}} = 0. \tag{2.67}$$

Hence we obtain the Laplace's equation in two-dimensions for $\hat{v}$,

$$\frac{\partial^2 \hat{v}}{\partial \hat{y}^2} + \frac{\partial^2 \hat{v}}{\partial X^2} = 0, \tag{2.68}$$

with the boundary condition, $\hat{v} = -\hat{p}_X$ at $\hat{y} = 0$. Since $\hat{p}_{\hat{y}} = 0$ at $\hat{y} = 0$, we can assume a zero normal pressure gradient so that we can write $\hat{p} = \tilde{p}$. The solution of Laplace's equation is found by taking a Fourier transform and solving to find,

$$\left[\frac{\tilde{v}_2}{(u_0(y) - c)} \right]_0^\infty = \frac{\partial \hat{v}}{\partial \hat{y}} |_{\hat{y}=0} = \frac{1}{\pi} \int_{-\infty}^{\infty} \frac{1}{X - u} \frac{\partial^2 \tilde{p}}{\partial u^2} du, \tag{2.69}$$

a Cauchy-Hilbert integral of $\frac{\partial^2 \tilde{p}}{\partial u^2}$.

By substituting the results from tier (III) and the critical layer into the governing equation from the main tier we find,

$$a_1 \tilde{p}_T + a_2 \tilde{p} \tilde{p}_X = j + \frac{1}{\pi} \int\!\!\!\!\!\!- _{-\infty}^{\infty} \frac{1}{X-u} \frac{\partial^2 \tilde{p}}{\partial u^2} du, \tag{2.70}$$

for the scaled pressure $\tilde{p}(X,T)$. The governing equation is a Benjamin-Ono equation, which exhibits soliton behaviour if $j = 0$. For some boundary conditions it may be solved exactly.

Boundary and Initial Conditions

The boundary conditions on (2.70) are essentially,

$$\tilde{p} \propto |X|^{1/3} \text{ as } X \to \pm\infty, \tag{2.71}$$

for finite times as in Li *et al.* (1998). This boundary condition is chosen so that the pressure matches with the flow solution away from the position of the singularity found in Smith (1988) (step 1). It is also a solution of Burgers equation, thus confirming the consistency of the analysis with that of step 1 (and Smith 1988). The spanwise terms do not impact on the boundary conditions as they only influence within the critical layer and we assume $\tilde{p}_z \to 0$ as $X \to \pm\infty$. In our choice of three-dimensional pressure perturbations later, care will be taken to ensure consistency with these boundary conditions. It will be shown, unfortunately, that these boundary conditions have an unexpected effect on the jump term, which results in the collapse of the assumption of a infinitesimal jump term as $X \to \pm\infty$. The initial conditions are also unchanged from the two-dimensional Li *et al.* (1998) case. The initial conditions are chosen to match with (2.11) at the end of step 1 (summarised earlier and see Smith (1988)). Therefore,

$$\tilde{p} \sim |T|^{1/2} p_1(\zeta) \text{ as } T \to -\infty, \qquad \text{for} \qquad \zeta \equiv X/|T|^{3/2} \text{ of } O(1),$$

where p_1 is the second order term in the expansion of pressure in step 1 given in (2.11).

2.1.1 Expected Vortex Shapes

Before continuing with a study of the critical layer behaviour a brief description of the solutions to the governing Benjamin-Ono equation will be given, assuming the critical layer jump term to be zero. These results demonstrate the behaviour of the pressure as governed by the Benjamin-Ono equation so that we may acquire some understanding of the influence of the pressure. This will provide an insight into the global behaviour of the pressure. This section also demonstrates the model three-dimensional perturbation that is used throughout the thesis. The first paragraph considers the two-dimensional results, whilst the rest of the section studies the effect of a three-dimensional disturbance on the pressure.

The first plot in figure 2.2 shows the solution of,

$$\tilde{p}_T + \tilde{p}\tilde{p}_X = \frac{0.1}{\pi}\int_{-\infty}^{\infty} \frac{1}{X-u}\frac{\partial^2 \tilde{p}}{\partial u^2}du, \tag{2.72}$$

for $T = -1, \ldots, 1$. This is the normalised form of the modified Benjamin-Ono equation derived in (2.70) with $j = 0$. The constant multiplying the integral is chosen to be equal to 0.1 for the numerical plots given in figure 2.2 and this choice has no significant impact on the results. Here T is the computational time with $T = -1$ corresponding to the end of step 1 (Smith 1988) and $T = 1$ corresponds to $T \to \infty$. It is shown here and in the second plot of 2.2 that as time progresses there does exist an $X = X_c$ such that $P_X(X_c) = 0$, which corresponds to the existence of a vortex (Smith *et al.* 2000, Bowles 2000*b*, Bowles *et al.* 2003). At this point Li *et al.* (1998) predicts that the solutions for the two-dimensional jump term are not defined and hence the analysis for the two-dimensional case breaks down. In the manipulation of the derived equation as part of the numerical derivation in section 2.5 we will show that both the two-dimensional and the three-dimensional components of the vorticity are multiplied by $1/\tilde{p}_x$, which becomes infinite at X_c. The breakdown in the analysis leads to the approach given in chapter 3.

In the computational approach implemented in section 2.5 we impose a weak initial

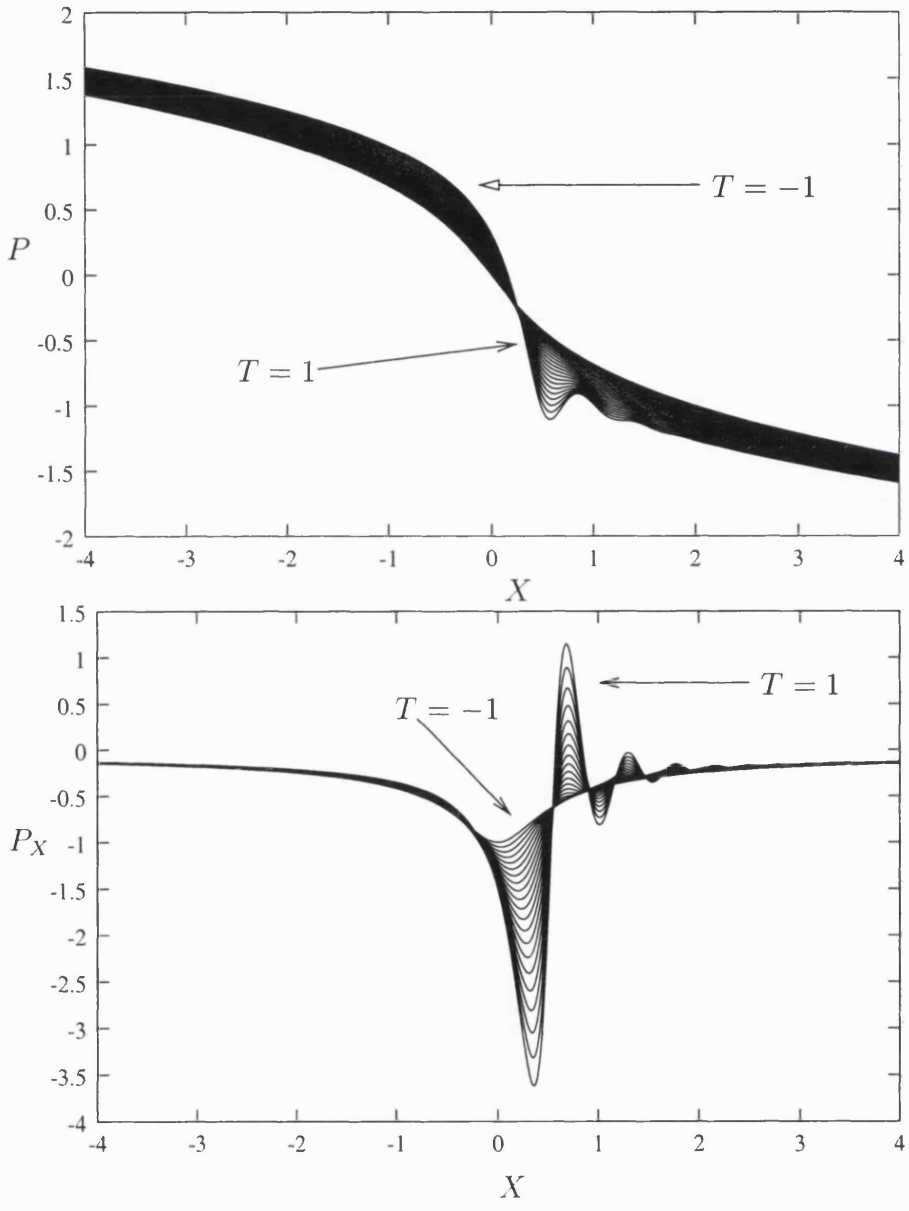

Figure 2.2: P and P_X for $T = -1, ..., 1$.

three-dimensional perturbation given by,

$$\tilde{p}(z, X, T_0) = \tilde{p}(X, T_0) + 0.1 X e^{-X^2} e^{-z^2}, \tag{2.73}$$

where T_0 is the time at the beginning of step 2. Another condition on the perturbation, which is derived at the end of section 2.2 is,

$$\int_{-\infty}^{\infty} \tilde{p}_z(z, X, T)\, dX = 0. \tag{2.74}$$

The perturbation (2.73) satisfies this condition. The condition is imposed as otherwise the jump term is larger than the other terms in the Benjamin-Ono equation and it will also be shown in section 2.2 that if the pressure satisfies the condition initially then it will always satisfy this condition. The plots in figures 2.10 and 2.11 on page 86 show the relative weakness of this initial disturbance but in the results later in the thesis we see that even this weak disturbance is sufficient to force a strong spanwise jump term.

2.2 An expression for the jump term

The analysis of this section considers an analytical study of the critical layer equations. The governing Benjamin-Ono equation (2.70) is similar to the governing equation in Li *et al.* (1998) and it may be solved using a congruous numerical method, which is briefly summarised in section 2.5. The numerical method is based on the numerical method derived by Li (1997). The motivations of this section are to derive expressions for the jump term, which can be used in the numerical approach for the governing pressure. We will show at the beginning of this section that for the two-dimensional case it is possible to derive a comparatively straightforward expression for the jump term. Unfortunately in the three-dimensional case, as we will show in this section, the jump term can only be expressed in terms of elliptic integrals, which are too complicated to be useful for the numerical method in 2.5.

A feature of the critical layer equation for the vorticity, τ is that it is linear in τ and hence its solution will be the sum of the three-dimensional and two-dimensional parts. Throughout the thesis, as in the derivation that follows and in particular the results in section 2.5.1, the differences in behaviour of the two-dimensional and three-dimensional parts are significant and therefore it is sensible to consider the two cases separately. We begin this section with the analysis for the two-dimensional jump term, which is the same as the derivation given in Li *et al.* (1998).

The Two-Dimensional Jump Term

We will begin our study of the critical layer jump term with the exclusively two-dimensional problem although it is not strictly two-dimensional since $\tilde{p}$ is a function of the spanwise variable and hence some spanwise influence does exist. We derive the expression found in Smith & Bodonyi (1987) and Li *et al.* (1998). In the two-dimensional case the system (2.57) - (2.59) reduces to,

$$b_1 Y \tau_{4X} - b_1^{-1} \tilde{p}_X \tau_{4Y} = m(X,T), \tag{2.75}$$

where $m(X,T) = -6b_1^{-3}\left(b_3 b_1 \tilde{p}_T - 2b_4 \tilde{p}\tilde{p}_X\right)$ and,

$$j = b_1^{-1}\frac{\partial J}{\partial X}, \qquad \text{and,} \qquad J = \fint_{-\infty}^{\infty} \tau_4 dY. \tag{2.76}$$

Using the method of characteristics reduces (2.75) to,

$$\frac{dX}{b_1 Y} = \frac{dY}{-b_1^{-1}\tilde{p}_X} = \frac{d\tau_4}{m(X,T)}. \tag{2.77}$$

This yields two equations,

$$\frac{1}{2}b_1 Y^2 + b_1^{-1}\tilde{p} = b_1^{-1}\chi \equiv \text{(constant)}, \qquad \text{and,} \qquad b_1 Y\frac{d\tau_4}{dX} = m(X,T). \tag{2.78}$$

Substituting for Y changes the variables from (X,Y) to (X,χ) and on a constant χ we have,

$$\frac{d\tau_4}{dX} = \frac{m(X,T)}{\sqrt{2}\sqrt{\chi-\tilde{p}}}\text{sgn}(Y). \tag{2.79}$$

Therefore,

$$\tau_4 = \int_{X_0}^{X} \frac{m(s,T)}{\sqrt{2}\sqrt{\chi-\tilde{p}}}\text{sgn}(Y)ds + \int_{X_0}^{\infty} \frac{m(s,T)}{\sqrt{2}\sqrt{\chi-\tilde{p}}}ds, \tag{2.80}$$

where the second term above is found from the condition that $\tau_4 = 0$ on an incoming streamline. We introduce $X_0(\chi)$ as the point where the characteristic intersects the Y-axis. We define the even part of τ_4 as τ_{4e}. The change of variable modifies (2.76) so that,

$$\begin{aligned} J = \fint_{-\infty}^{\infty} \tau_4 dY &= 2\fint_0^{\infty} \tau_{4e} dY, \\ &= \frac{2}{\sqrt{2}}\fint_{\tilde{p}(X,T)}^{\infty} b_1^{-1}\tau_{4e}\frac{d\chi}{\sqrt{\chi-\tilde{p}(X,T)}}. \end{aligned} \tag{2.81}$$

Hence,

$$J(X) = \fint_{\tilde{p}(X,T)}^{\infty} b_1^{-1}\int_{X_0(\chi)}^{\infty} \frac{m(s,T)}{\sqrt{\chi-\tilde{p}(s,T)}\sqrt{\chi-\tilde{p}(X,T)}}\,ds\,d\chi. \tag{2.82}$$

We change the order of integration with $\tilde{p}(X_0(\chi)) = \chi$ so that,

$$J(X) = b_1^{-1}\int_{-\infty}^{\infty}\fint_{\tilde{p}(s,T)}^{\infty} \frac{m(s,T)}{\sqrt{\chi-\tilde{p}(s,T)}\sqrt{\chi-\tilde{p}(X,T)}}\,d\chi\,ds, \tag{2.83}$$

$$= -b_1^{-1}\fint_{-\infty}^{\infty} m(s,T)\ln|\tilde{p}(X,T)-\tilde{p}(s,T)|\,ds. \tag{2.84}$$

Therefore,

$$J_X(X) = -b_1^{-1}\tilde{p}_X(X,T)\fint_{-\infty}^{\infty} \frac{m(s,T)}{\tilde{p}(X,T)-\tilde{p}(s,T)}\,ds. \tag{2.85}$$

We obtain on substitution into (2.70), utilizing the condition, proven in Li *et al.* (1998) that $\frac{a_1}{a_2} = \frac{-b_1 b_3}{4b_4}$ and putting $\mu = 6b_3 b_1^{-4}$,

$$a_1\tilde{p}_T + a_2\tilde{p}\tilde{p}_X = \mu\tilde{p}_X\fint_{-\infty}^{\infty} \frac{\left(\tilde{p}_T(s,T) + a_1^{-1}a_2(\tilde{p}\tilde{p}_s(s,T)\right)\,ds}{\tilde{p}(X,T)-\tilde{p}(s,T)} + \frac{1}{\pi}\int_{-\infty}^{\infty}\frac{1}{X-u}\frac{\partial^2\tilde{p}}{\partial u^2}du, \tag{2.86}$$

agreeing with Li *et al.* (1998) for their external case.

The Three-Dimensional Jump Term

Here an expression for the three-dimensional jump term is found. This is more difficult than the two-dimensional case as there is an extra equation forcing the vorticity, giving the following system of equations in the critical layer,

$$b_1 Y W_{4X} - b_1^{-1}\tilde{p}_X W_{4Y} = -\tilde{p}_z, \tag{2.87a}$$

$$b_1 Y \tau_{4X} - b_1^{-1}\tilde{p}_X \tau_{4Y} = b_1 W_{4z}, \tag{2.87b}$$

$$J_X = \fint_{-\infty}^{\infty} \tau_{4X}\,dY. \tag{2.87c}$$

Unfortunately the expressions found are not in a practical form and hence a numerical approach was necessary, which is outlined in section 2.5. As the method introduces several new terms it is advantageous here to normalise the above equations. We may remove the b_1 terms by letting $\check{Y} = b_1^{-1}Y$ and we set $w = W_4$ and $\tau = b_1\tau_4$. As the flow is assumed steady within the critical layer, for convenience, we will drop the T from the function specification of the pressure, i.e. $\tilde{p}(z,X) = \tilde{p}(z,X,T)$. Hence,

$$\check{Y} w_X - \tilde{p}_X w_{\check{Y}} = -\tilde{p}_z, \tag{2.88a}$$

$$\check{Y}\tau_X - \tilde{p}_X\tau_{\check{Y}} = w_z, \tag{2.88b}$$

$$J_X = \fint_{-\infty}^{\infty} \tau_X\,d\check{Y}. \tag{2.88c}$$

For clarity we will drop the dashes from Y. The boundary equations are $w = \tau = 0$ as $X \to \infty$ and $Y < 0$. The method used to solve (2.88a), (2.88b) is again the method of characteristics and hence a new variable, χ is introduced such that $\chi = \frac{Y^2}{2} + \tilde{p}(z, X)$ as before. This change of variable leads to the following relations,

$$\frac{\partial}{\partial Y} \to Y \frac{\partial}{\partial \chi}, \tag{2.89a}$$

$$\frac{\partial}{\partial X} \to \frac{\partial}{\partial X} + \tilde{p}_X \frac{\partial}{\partial \chi}, \tag{2.89b}$$

$$\frac{\partial}{\partial z} \to \frac{\partial}{\partial z} + \tilde{p}_z \frac{\partial}{\partial \chi}. \tag{2.89c}$$

These imply,

$$\frac{\partial w}{\partial X} = -\mathrm{sgn}(Y) \frac{\tilde{p}_z(z, X)}{\sqrt{2}\sqrt{\chi - \tilde{p}(z, X)}}, \tag{2.90a}$$

$$\frac{\partial \tau}{\partial X} = \mathrm{sgn}(Y) \frac{w_z + \tilde{p}_z(z, X) w_\chi}{\sqrt{2}\sqrt{\chi - \tilde{p}(z, X)}}. \tag{2.90b}$$

In this section we solve, in turn, for w, τ and the jump term. It will be shown that this yields a triple repeated integral for J_X. This section concludes with a derivation of an important condition for our analysis, on the spanwise behaviour of the pressure, namely,

$$\int_{-\infty}^{\infty} \tilde{p}_z(z, X)\, dX = 0. \tag{2.91}$$

We will show that this is a direct consequence of the asymptotic behaviour of w, τ and J_X.

We introduce the following notation,

$$\eta_a = \sqrt{2}\left(\chi - \tilde{p}(z, a)\right)^{1/2}, \tag{2.92}$$

and the operator,

$$Q_a(f) = \left[\frac{\partial}{\partial z} + \tilde{p}_z(z, a) \frac{\partial}{\partial \chi}\right]. \tag{2.93}$$

The expression, η_a is the denominator and Q_a is the z derivative in the characteristic variable. The a does not refer to a derivative but it is included to express clearly

the variable, which is useful when studying triple or double integrals. Using (2.92) and (2.93), allows us to rewrite (2.90) as,

$$\frac{\partial w}{\partial X} = -\frac{\tilde{p}_z}{\eta_X}\mathrm{sgn}(Y), \tag{2.94a}$$

$$\frac{\partial \tau}{\partial X} = \frac{1}{\eta_X} Q_X[w]\,\mathrm{sgn}(Y), \tag{2.94b}$$

which are the equations of interest. We also note that $X_0(z,\chi)$ is the solution of $\tilde{p}(z, X_0(z,\chi)) = \chi$. This implies that,

$$\frac{\partial X_0}{\partial \chi} = \frac{-1}{\tilde{p}_X}\bigg|_{z,X_0} \quad \text{and} \quad \frac{\partial X_0}{\partial z} = \frac{\tilde{p}_z}{\tilde{p}_X}\bigg|_{z,X_0}.$$

These expressions will be useful later (in (2.99) for example) as they force the contributions from the ends of the integrals to equal zero.

Finding w

The boundary condition at $X = \infty$, $Y < 0$ is $w = 0$ corresponding to no spanwise velocity on incoming streamlines. This is equivalent to having no three-dimensional disturbances up or downstream. The solution for w, from (2.94), is,

$$w(z,X,\chi) = -\left\{\mathrm{sgn}(Y)\int_{X_0}^{X} \frac{\tilde{p}_z(z,t)dt}{\eta_t} + \int_{X_0}^{\infty} \frac{\tilde{p}_z(z,t)dt}{\eta_t}\right\}. \tag{2.95}$$

The second term above is to ensure that the boundary condition is satisfied. The integrals can be integrated using integration by parts if they are rewritten using,

$$\frac{\tilde{p}_z}{\tilde{p}_t}\frac{\tilde{p}_t}{\eta_t} = -\frac{\tilde{p}_z}{\tilde{p}_t}\frac{\partial}{\partial t}\eta_t,$$

since,

$$\int_a^b \frac{\tilde{p}_z}{\eta_t}\,dt = -\left[\frac{\tilde{p}_z(z,t)}{\tilde{p}_t(z,t)}\eta_t\right]_a^b + \int_a^b \left(\frac{\tilde{p}_z}{\tilde{p}_t}\right)_t \eta_t\,dt,$$

so that,

$$w = -\left\{-\mathrm{sgn}(Y)\left[\frac{\tilde{p}_z}{\tilde{p}_t}\eta_t\right]_{X_0}^{X} + \mathrm{sgn}(Y)\int_{X_0}^{X}\left(\frac{\tilde{p}_z}{\tilde{p}_t}\right)_t \eta_t\,dt - \left[\frac{\tilde{p}_z}{\tilde{p}_t}\eta_t\right]_{X_0}^{\infty} + \int_{X_0}^{\infty}\left(\frac{\tilde{p}_z}{\tilde{p}_t}\right)_t \eta_t\,dt\right\}.$$

We can simplify using $\eta|_{t=X_0} = 0$, $\eta|_{t=X} = \eta_X$ and assuming $\tilde{p}_z \to 0$ as $X \to \infty$. The latter assumption is equivalent to assuming the spanwise disturbance is constrained in X. Hence we find,

$$w = -\left\{\mathrm{sgn}(Y)\left(-\frac{\tilde{p}_z(z,X)}{\tilde{p}_X(z,X)}\eta_X + \int_{X_0}^{X}\left(\frac{\tilde{p}_z(z,t)}{\tilde{p}_t(z,t)}\right)_t \eta_t\,dt\right) + \left(\int_{X_0}^{\infty}\left(\frac{\tilde{p}_z(z,t)}{\tilde{p}_t(z,t)}\right)_t \eta_t\,dt\right)\right\}. \tag{2.96}$$

This is an expression for w, which is not solvable analytically. We continue with this analysis as it may be possible to integrate with a change in the order of integration. We also introduce the following notation, R_a where,

$$R_a = \frac{\tilde{p}_z(z,a)}{\tilde{p}_a(z,a)}. \tag{2.97}$$

Hence we write w as,

$$w = -\left\{\mathrm{sgn}(Y)\left(-R_X\eta_X + \int_{X_0}^{X}\frac{\partial R_t}{\partial t}\eta_t\,dt\right) + \int_{X_0}^{\infty}\left(\frac{\partial R_t}{\partial t}\eta_t\,dt\right)\right\}. \tag{2.98}$$

Finding τ

The next step in the analysis is to find τ. The main forcing for τ is $Q_X[w]$ and so initially we concentrate on this term. We substitute the expression for w in (2.98) into (2.93) so that,

$$\begin{aligned} Q_X[w] = &- \left\{\mathrm{sgn}(Y)\left(-\frac{\partial R_X}{\partial z}\eta_X - \frac{R_X\tilde{p}_z(z,X)}{\eta_X} + \frac{R_X\tilde{p}_z(z,X)}{\eta_X}\right)\right. \\ &+ \mathrm{sgn}(Y)\int_{X_0}^{X}\left(\eta_t\frac{\partial^2 R_t}{\partial t\partial z} - \frac{1}{\eta_t}\frac{\partial R_t}{\partial t}\tilde{p}_z(z,t) + \frac{1}{\eta_t}\frac{\partial R_t}{\partial t}\tilde{p}_z(z,X)\right)dt \\ &+ \left.\int_{X_0}^{\infty}\left(\eta_t\frac{\partial^2 R_t}{\partial t\partial z} - \frac{1}{\eta_t}\frac{\partial R_t}{\partial t}\tilde{p}_z(z,t) + \frac{1}{\eta_t}\frac{\partial R_t}{\partial t}\tilde{p}_z(z,X)\right)dt\right\}. \end{aligned} \tag{2.99}$$

We may integrate one of the integrals using integration by parts, which leads to some cancellation as we now show. Consider,

$$\begin{aligned} \int_{X_0}^{X}\left(\eta_t\frac{\partial^2 R_t}{\partial t\partial z}\right)dt &= \left[\eta_t\frac{\partial R_t}{\partial z}\right]_{t=X_0}^{t=X} + \int_{X_0}^{X}\frac{1}{\eta_t}\frac{\partial\tilde{p}(z,t)}{\partial t}\frac{\partial R_t}{\partial z}\,dt \\ &= \eta_X\frac{\partial R_X}{\partial z} + \int_{X_0}^{X}\frac{1}{\eta_t}\frac{\partial\tilde{p}(z,t)}{\partial t}\frac{\partial R_t}{\partial z}\,dt, \end{aligned} \tag{2.100}$$

since $\eta_{X_0} = \sqrt{2}\sqrt{\chi - \tilde{p}(X_0, z)} = 0$, as $\tilde{p}(X_0(\chi), z) = \chi$. Similarly,

$$\int_{X_0}^{\infty} \left(\eta_t \frac{\partial^2 R_t}{\partial t \partial z} \right) dt = \int_{X_0}^{\infty} \frac{1}{\eta_t} \frac{\partial \tilde{p}(z,t)}{\partial t} \frac{\partial R_t}{\partial z} \, dt, \tag{2.101}$$

as we again assume $R_\infty \to 0$. Hence by defining,

$$H(X, z, t) = \frac{\partial \tilde{p}(z,t)}{\partial t} \frac{\partial R_t}{\partial z} + \frac{\partial R_t}{\partial t} \tilde{p}_z(z, X) - \frac{\partial R_t}{\partial t} \tilde{p}_z(z, t), \tag{2.102}$$

we may write $Q_X[w]$ as,

$$Q_X[w] = -\left\{ \operatorname{sgn}(Y) \int_{X_0}^{X} \frac{1}{\eta_t} H(X, z, t) \, dt + \int_{X_0}^{\infty} \frac{1}{\eta_t} H(X, z, t) \, dt \right\}. \tag{2.103}$$

Therefore,

$$\frac{\partial \tau}{\partial X} = \frac{1}{\eta_X} \int_{X_0}^{X} \frac{H(X, z, t)}{\eta_t} \, dt + \frac{\operatorname{sgn}(Y)}{\eta_X} \int_{X_0}^{\infty} \frac{H(X, z, t)}{\eta_t} \, dt.$$

We integrate with respect to X to find,

$$\tau(z, X, \chi) = \left(\int_{X_0}^{X} \left\{ \frac{1}{\eta_s} \int_{X_0}^{s} \frac{H(s, z, t)}{\eta_t} \, dt + \frac{\operatorname{sgn}(Y)}{\eta_s} \int_{X_0}^{\infty} \frac{H(s, z, t)}{\eta_t} \, dt \right\} ds \right) + C. \tag{2.104}$$

The constant, C is found in the same way as earlier for w by assuming that $\tau = 0$ as $X \to \infty$ and $Y < 0$. Therefore,

$$\begin{aligned} \tau(z, X, \chi) = &\left(\int_{X_0}^{X} \left\{ \frac{1}{\eta_s} \int_{X_0}^{s} \frac{H(s, z, t)}{\eta_t} \, dt + \frac{\operatorname{sgn}(Y)}{\eta_s} \int_{X_0}^{\infty} \frac{H(s, z, t)}{\eta_t} \, dt \right\} ds \right) \\ &- \left(\int_{X_0}^{\infty} \left\{ \frac{1}{\eta_s} \int_{X_0}^{s} \frac{H(s, z, t)}{\eta_t} \, dt - \frac{1}{\eta_s} \int_{X_0}^{\infty} \frac{H(s, z, t)}{\eta_t} \, dt \right\} ds \right). \end{aligned} \tag{2.105}$$

Integrating to find the Jump Term

The third and fourth integrals in (2.105) can be combined since $\int_{X_0}^{\infty} - \int_{X_0}^{s} = \int_{s}^{\infty}$. Therefore integrating the even part of τ to find the jump term leaves us with,

$$J = 2 \int_{\tilde{p}(z,X)}^{\infty} \int_{X_0}^{X} \int_{X_0}^{s} \frac{H(s, z, t)}{\eta_X \eta_s \eta_t} \, dt \, ds \, d\chi + 2 \int_{\tilde{p}(z,X)}^{\infty} \int_{X_0}^{\infty} \int_{s}^{\infty} \frac{H(s, z, t)}{\eta_X \eta_s \eta_t} \, dt \, ds \, d\chi. \tag{2.106}$$

The third integral in (2.105) has an even part equal to zero. It is evident that one way to proceed is to change the order of integration as in Li *et al* (1998) so that the χ integration could be attempted. In the three-dimensional case the χ integration is only possible using elliptic integrals. There are two changes of integration necessary as we need to "move" the $d\chi$ to the inside of the integral. We demonstrate the changes of integration in detail here as there are several occasions in the thesis where we change the order of integration and hence it is important to explain the method clearly.

We consider the integrals separately. We begin with the first integral in (2.106) and the first change of integral is to swap the $d\chi$ and ds. Hence we are studying,

$$\int_{\tilde{p}(z,X)}^{\infty}\int_{X_0}^{X} ds\, d\chi. \tag{2.107}$$

The ranges of integration are shown in figure 2.3 and we note that the plot shown is that of $X_0 = \tilde{p}^{-1}(\chi)$, which is equivalent to $\tilde{p}(s)$. From figure 2.3 it is clear that,

$$\int_{\tilde{p}(z,X)}^{\infty}\int_{X_0}^{X} ds\, d\chi \to \int_{-\infty}^{X}\int_{\tilde{p}(z,s)}^{\infty} d\chi\, ds. \tag{2.108}$$

The second swap is between dt and $d\chi$, making integration with respect to χ the inner integral. The second diagram in figure 2.3 shows the change of integration schematically and so,

$$\int_{\tilde{p}(z,s)}^{\infty}\int_{X_0}^{s} dt\, d\chi \to \int_{-\infty}^{s}\int_{\tilde{p}(z,t)}^{\infty} d\chi\, dt. \tag{2.109}$$

Changing the order of integration in the second integral in (2.106) is similar as we now show. The first swap of $d\chi$ and ds leads to two integrals as shown in figure 2.4, so that

$$\int_{\tilde{p}(z,X)}^{\infty}\int_{X_0}^{\infty} ds\, d\chi \to \int_{-\infty}^{X}\int_{\tilde{p}(z,s)}^{\infty} d\chi\, ds + \int_{X}^{\infty}\int_{\tilde{p}(z,X)}^{\infty} d\chi\, ds. \tag{2.110}$$

The last change takes $d\chi$ to the inner integral and is much simpler as the limits do not depend on the variables of integration, so following figure 2.4 we obtain,

$$\int_{\tilde{p}(z,s)}^{\infty}\int_{s}^{\infty} dt\, d\chi \to \int_{s}^{\infty}\int_{\tilde{p}(z,s)}^{\infty} d\chi\, ds, \tag{2.111}$$

and,

$$\int_{\tilde{p}(z,X)}^{\infty}\int_{s}^{\infty} dt\, d\chi \to \int_{s}^{\infty}\int_{\tilde{p}(z,X)}^{\infty} d\chi\, ds. \tag{2.112}$$

Combining the above results allows us to write the following expression for J,

$$J = 2\Bigg\{ \int_{-\infty}^{X}\int_{-\infty}^{s} H(s,z,t) I_{\tilde{p}(z,t)}\, dt\, ds + \int_{-\infty}^{X}\int_{s}^{\infty} H(s,z,t) I_{\tilde{p}(z,s)}\, dt\, ds + \int_{X}^{\infty}\int_{s}^{\infty} H(s,z,t) I_{\tilde{p}(z,X)}\, dt\, ds \Bigg\}, \tag{2.113}$$

where the elliptic integral I_ν is given by,

$$I_\nu = \frac{1}{2^{3/2}} \int_{\nu}^{\infty} \frac{d\chi}{\sqrt{(\chi - \tilde{p}(z,X))(\chi - \tilde{p}(z,s))(\chi - \tilde{p}(z,t))}}. \tag{2.114}$$

These elliptic integrals do not bring us closer to an usable expression for J as they are still too complicated. Thus a numerical approach is required to solve the system of equations, (2.88). The chosen numerical method is explained in section 2.5. In section 2.3.1 a linear pressure is considered. In this model situation of $\tilde{p} = -X$ to first order, we find that the jump term is zero. This leads us to consider, in section 2.3.3 a more complicated, yet still relatively simple, pressure forcing in order to verify that the jump term is not always equal to zero.

A Condition on the pressure

A result of the asymptotic form of the spanwise velocity and vorticity, which we show here, is an integral condition on the form of the spanwise pressure, which is,

$$\int_{-\infty}^{\infty} \tilde{p}_z(z,s)\, ds = 0. \tag{2.115}$$

If we consider $X \to \infty$, then for $Y \sim 1$ this is equivalent to large χ, hence we may rewrite our expression for w as,

$$w \sim \frac{1}{(2\chi)^{1/2}} \int_{-\infty}^{\infty} \tilde{p}_z\, dt + \ldots, \tag{2.116}$$

$$\sim \frac{1}{(2\chi)^{1/2}} \Theta. \tag{2.117}$$

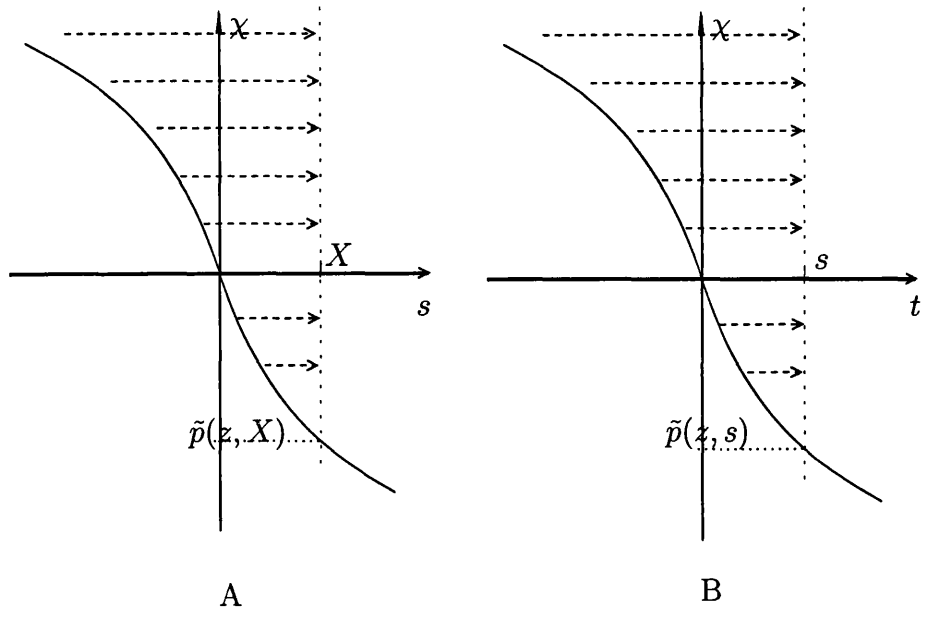

Figure 2.3: The Changes in Order of Integration of the First Integral.

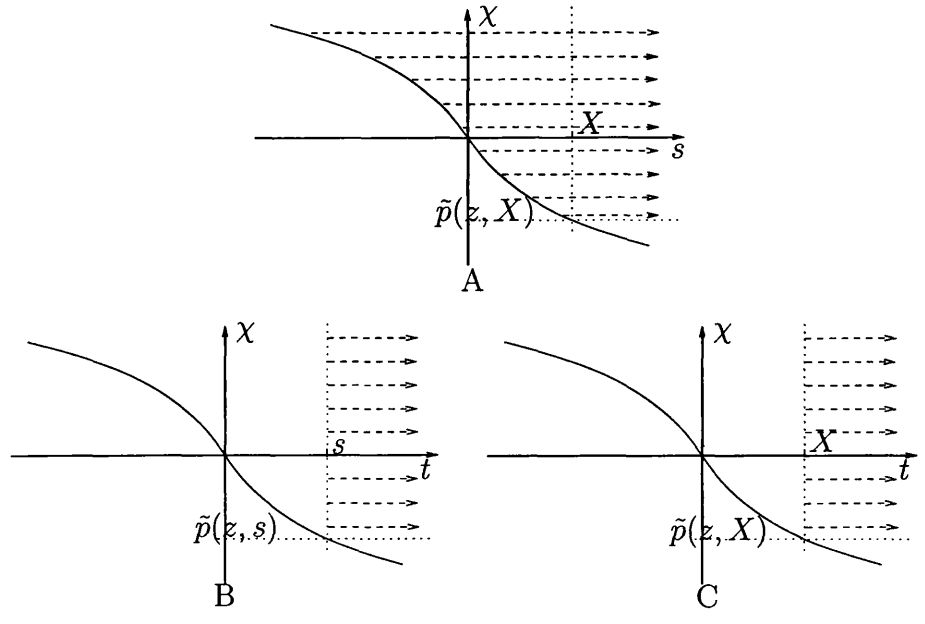

Figure 2.4: The Changes in Order of Integration of the Second Integral.

This feeds into the equation for τ so that,

$$\tau \sim \frac{1}{(2\chi)^{1/2}} \int_{X_0}^{\infty} \frac{1}{(2\chi)^{1/2}} \Theta_z \, ds, \tag{2.118}$$

$$\sim \frac{1}{(2\chi)} X_0 \Theta_z. \tag{2.119}$$

The expression above implies $\tau \sim \chi^2 \Theta_z$ since $X_0 \sim \chi^3$ for large negative X_0. Hence,

$$J \sim \int_0^{\infty} \chi^2 \Theta_z \, dY, \tag{2.120}$$

$$= \int_{\tilde{p}}^{\infty} \frac{\chi^2 \Theta_z}{\sqrt{2(\chi - \tilde{p})}} \, d\chi \sim \Theta_z \tilde{p}^{5/2}. \tag{2.121}$$

Now if $J \sim \Theta_z \tilde{p}^{5/2}$ then $J_X \sim \Theta_z \tilde{p}^{3/2} \tilde{p}_X$, which is larger than the $\tilde{p}\tilde{p}_X$ term in the Benjamin-Ono equation. This implies that $\Theta_z = 0$ or $\Theta = 0$. The former case forces a two-dimensional pressure and so we must take $\Theta = 0$. The effect of this condition is to reduce the forcing by a factor of χ, which corresponds to reducing the jump term by $\tilde{p}$, leading to $J_X \sim \tilde{p}^{1/2} \tilde{p}_X$, which is consistent with the Benjamin-Ono equation.

We now show that if this result is true then it is true for all times. To prove this we consider,

$$\frac{\partial}{\partial T} \int_{-\infty}^{\infty} \tilde{p}_z(z, s) \, ds. \tag{2.122}$$

We may rewrite using the Benjamin-Ono equation since,

$$\frac{\partial}{\partial T} \int_{-\infty}^{\infty} \tilde{p}_z(z, X) \, dX = \int_{-\infty}^{\infty} \tilde{p}_{zT}(z, X) \, dX, \tag{2.123}$$

$$= \int_{-\infty}^{\infty} \frac{\partial}{\partial z} \left\{ -\tilde{p}\tilde{p}_X + \frac{1}{\pi} \int_{-\infty}^{\infty} \frac{\tilde{p}_{ss}}{X - s} \, ds + j \right\} dX \tag{2.124}$$

We consider each term in turn and show that each is equal to zero. The first term is,

$$\frac{\partial}{\partial z} \int_{-\infty}^{\infty} \tilde{p}\tilde{p}_X \, dX = \frac{\partial}{\partial z} \left[\tilde{p}^2 \right]_{-\infty}^{\infty} = 0. \tag{2.125}$$

The second term in (2.124) is more difficult. Here,

$$\frac{\partial}{\partial z}\fint_{-\infty}^{\infty}\int_{-\infty}^{\infty}\frac{\tilde{p}_{ss}}{X-s}\,ds\,dX=\fint_{-\infty}^{\infty}\int_{-\infty}^{\infty}\frac{\tilde{p}_{zss}}{X-s}\,ds\,dX. \tag{2.126}$$

Now if we write,

$$\frac{\partial F}{\partial X}=\fint_{-\infty}^{\infty}\frac{\tilde{p}_{zss}}{X-s}\,ds, \tag{2.127}$$

then we must show that $F \to 0$ as $X \to \pm\infty$. Integrating the above with respect to X leads to,

$$F=\fint_{-\infty}^{\infty}\tilde{p}_{zss}\ln|X-s|ds. \tag{2.128}$$

We integrate by parts so that,

$$F=\left[\tilde{p}_{zs}\ln|X-s|\right]_{-\infty}^{\infty}-\fint_{-\infty}^{\infty}\frac{\tilde{p}_{zs}}{X-s}\,ds. \tag{2.129}$$

As $s \to \pm\infty$ we have $\tilde{p}_{zs} \to 0$ and so the first term above is zero. Furthermore, as $X \to \pm\infty$,

$$\fint_{-\infty}^{\infty}\frac{\tilde{p}_{zs}}{X-s}\,ds \to \frac{1}{X}\int_{-\infty}^{\infty}\tilde{p}_{zs}\,ds. \tag{2.130}$$

The spanwise disturbance is constrained in X and so the integral is a constant and hence this will also be zero as $X \to \pm\infty$.

The final term in (2.123) is also zero. Here, $j = J_X$ and so we require $J = 0$ as $X \to \pm\infty$. This is true in the three-dimensional case since the spanwise disturbance is constrained in X. Hence we may conclude that this condition on the spanwise derivative of the pressure is true and holds true for all time.

2.3 Approximations for the Jump Term

In the following three sections we consider approximate solutions to the Benjamin-Ono equation for the pressures in the critical layer equations. There are two motivations for this. The first is to check that there exist regions where the jump term is non-zero. Secondly the numerical method implemented solves for the jump term independently of the pressure and so the numerical problem can be considered as a critical layer solver and a Benjamin-Ono solver. We find that a constant derivative of the pressure doesn't generate a jump term but if the derivative of the pressure is not constant in X then a non-zero jump term is generated.

2.3.1 The jump is zero for a linear pressure forcing

As a first approximation we consider a linear pressure forcing in X. This is found to drive a zero jump term. This may seem to be an irrelevant simplification but if we consider the pressure initially (as $T \to -\infty$) then we find that this approximation does have some relevance. As $T \to -\infty$ then the pressure almost has a linear profile with a near constant gradient. Therefore at early times $\tilde{p}_{XX} \ll 1$. This compares favourably with the present setting where $\tilde{p} = -X$, $\tilde{p}_X = -1$ and $\tilde{p}_{XX} = 0$. We also assume that the three-dimensional disturbance is small.

We will broadly follow the method of the last section but having found an expression for the even part of the vorticity, τ, we will take, $\tilde{p}_X \equiv -1$ and $\tilde{p}_z \ll 1$. We will again use the method of characteristics and the notation, $\eta_a = \sqrt{2}(\chi - \tilde{p}(z,a))^{1/2}$ and $Q_X = \frac{\partial}{\partial z} + \tilde{p}_z(z,X)\frac{\partial}{\partial \chi}$ as the spanwise derivative in the new χ, Y variable space. We again obtain for w,

$$w(z,X,\chi) = \left\{ \mathrm{sgn}(Y) \int_X^{X_0} \frac{\tilde{p}_z(z,t)dt}{\eta_t} + \int_\infty^{X_0} \frac{\tilde{p}_z(z,t)dt}{\eta_t} \right\}, \tag{2.131}$$

as in (2.95) but with a change in the limits of integration to remove the negative

sign, and similarly we have,

$$\begin{aligned}\tau &= \int_{X_0}^{X} \frac{1}{\eta_s} Q_s \left[\int_{s}^{X_0} \frac{\tilde{p}_z(z,t)dt}{\eta_t}\right] ds + \mathrm{sgn}(Y) \int_{X_0}^{X} \frac{1}{\eta_s} Q_s \left[\int_{\infty}^{X_0} \frac{\tilde{p}_z(z,t)dt}{\eta_t}\right] ds \\ &- \int_{X_0}^{\infty} \frac{1}{\eta_s} Q_s \left[\int_{s}^{X_0} \frac{\tilde{p}_z(z,t)dt}{\eta_t}\right] ds + \int_{X_0}^{\infty} \frac{1}{\eta_s} Q_s \left[\int_{\infty}^{X_0} \frac{\tilde{p}_z(z,t)dt}{\eta_t}\right] ds. \quad (2.132)\end{aligned}$$

Hence it is relatively straightforward to calculate the even part of τ, given by $\tau_E = \frac{1}{2}(\tau(Y) + \tau(-Y))$ and with a combining of two of the integrals the following expression is found,

$$\tau_E = \int_{X_0}^{\infty} \frac{1}{\eta_s} Q_s \left[\int_{\infty}^{X_0} \frac{\tilde{p}_z(z,t)}{\eta_t}\, dt\right] ds + \int_{\infty}^{X} \frac{1}{\eta_s} Q_s \left[\int_{s}^{X_0} \frac{\tilde{p}_z(z,t)}{\eta_t}\, dt\right] ds. \quad (2.133)$$

We now use the approximation and linearise using $\tilde{p}_X \equiv -1$ and $\tilde{p}_z \ll 1$. The latter assumption of the form of the spanwise derivative implies a simplification of the spanwise derivative and this is indeed the case with $Q_s \to \frac{\partial}{\partial z}$. Then,

$$\begin{aligned}\tau_E &= \int_{X_0}^{\infty} \frac{1}{\eta_s} \int_{\infty}^{X_0} \frac{\tilde{p}_{zz}(z,t)}{\eta_t}\, dt\, ds + \int_{\infty}^{X} \frac{1}{\eta_s} \int_{s}^{X_0} \frac{\tilde{p}_{zz}(z,t)}{\eta_t}\, dt\, ds, \quad (2.134) \\ &= -\left\{\int_{X_0}^{X} \frac{\tilde{p}_{zz}(z,t)}{\eta_t} \int_{t}^{X} \frac{1}{\eta_s}\, ds\, dt + \int_{X_0}^{\infty} \frac{\tilde{p}_{zz}(z,t)}{\eta_t} \int_{X_0}^{t} \frac{1}{\eta_s}\, ds\, dt\right\}. \quad (2.135)\end{aligned}$$

with (2.135) found through a change in the order of integration. The s integration is simple since with the approximations implemented earlier, $\eta_X = \sqrt{2}\sqrt{\chi + X}$, which yields,

$$\tau_E = -\left\{\int_{X_0}^{X} \frac{\tilde{p}_{zz}(z,t)\eta_X}{\eta_t}\, dt + \int_{X}^{\infty} \tilde{p}_{zz}(z,t)\, dt\right\}. \quad (2.136)$$

The jump term is given by,

$$\begin{aligned}J &= 2\int_0^{\infty} \tau_E\, dY, \\ &= -2\int_{-X}^{L}\int_{X_0}^{X} \frac{\tilde{p}_{zz}(z,t)}{\eta_t}\, dt\, d\chi - 2\int_{-X}^{L} \frac{1}{\eta_X} \int_{X}^{\infty} \tilde{p}_{zz}(z,t)\, dt\, d\chi, \quad (2.137)\end{aligned}$$

with $L \gg 1$. Another change of integration allows us to carry out the integration with respect to χ. We have,

$$J = -2\int_{-L}^{X} \tilde{p}_{zz}(z,t) \int_{-t}^{L} \frac{1}{\eta_t}\, d\chi\, dt - 2\int_{X}^{\infty} \tilde{p}_{zz}(z,t) \int_{-X}^{L} \frac{1}{\eta_X}\, d\chi\, dt. \quad (2.138)$$

Integrating with respect to χ leads to,

$$J = -2\int_{-L}^{X} \tilde{p}_{zz}(z,t)\sqrt{2}\sqrt{L+t}\,dt - 2\int_{X}^{\infty} \tilde{p}_{zz}(z,t)\sqrt{2}\sqrt{L+X}\,dt. \tag{2.139}$$

The first integral can be integrated by parts so that,

$$J = -2\sqrt{2}\sqrt{L+X}\big[g(t)\big]_{-L}^{X} + \int_{-L}^{X} \frac{2\sqrt{2}}{\sqrt{L+t}} g(t)\,dt - 2\sqrt{2}\sqrt{L+X}\int_{X}^{\infty} \tilde{p}_{zz}(z,t)\,dt, \tag{2.140}$$

with $g'(t) = \tilde{p}_{zz}(z,t)$. If we consider $L \to \infty$ and combine the first and third terms above, since $\big[g(t)\big]_{-L}^{X} = \int_{-L}^{X} \tilde{p}_{zz}(z,t)\,dt$, then $J \to 0$ and $J_X \to 0$ since,

$$\int_{-\infty}^{\infty} \tilde{p}_{zz}(z,t)\,dt = \frac{\partial}{\partial z}\int_{-\infty}^{\infty} \tilde{p}_{z}(z,t)\,dt = 0, \tag{2.141}$$

from the condition found on page 50. Hence we can conclude that the critical layer is passive for a constant streamwise pressure gradient and a small spanwise pressure perturbation. This implies that for early times the jump term is very small.

2.3.2 Short-Scale 3D Perturbations

In the following analysis we take three-dimensional perturbations and hence confirm the previous result. The derived equations allow us to continue in the next section with a study where there exists some curvature in the streamwise pressure. A first approximation is to look for relatively short-scale three-dimensional perturbations to the otherwise two-dimensional flow described in Li *et al.* (1998). If an early time is considered, where the global equation has not had enough time to affect the pressure development and if the local pressure gradient is constant, it is shown here that the perturbations have no feedback as the critical layer jump term is zero. The three-dimensional perturbations are introduced at an early time in the development of the pressure so that the Cauchy-Hilbert term has little global influence. The perturbations in the spanwise direction are introduced, with $\delta \ll 1$ by writing,

$$\tilde{p} = XP_0 + \delta P_1(X)\cos(\beta z), \tag{2.142a}$$

$$w = \delta\tilde{w}(X,Y)\beta\sin(\beta z), \tag{2.142b}$$

$$\tau = \tau_0 + \delta\tilde{\tau}(X,Y)\beta^2\cos(\beta z), \tag{2.142c}$$

$$J = \delta\tilde{J}\beta^2\cos(\beta z). \tag{2.142d}$$

We then find,

$$Y\tilde{w}_X - P_0\tilde{w}_Y = P_1(X), \tag{2.143}$$

$$Y\tilde{\tau}_{0X} - P_0\tilde{\tau}_{0Y} = m(X,T), \tag{2.144}$$

$$Y\tilde{\tau}_{1X} - P_0\tilde{\tau}_{1Y} = \tilde{w} + \frac{1}{\beta^2}\tau_{0Y}P_{1X}. \tag{2.145}$$

The assumption of early times implies that $m(X,T) \sim 0$ in (2.144) and hence $\tau_0 = 0$. We now solve (2.143) and (2.145) with $\tilde{w}$ and $\tilde{\tau}$ zero on incoming streamlines. The solutions can be found using the method of characteristics with $\chi = \frac{Y^2}{2} + P_0X$. Then $Y\tilde{w}_X = P_1(X)$, which implies,

$$\tilde{w} = \mathrm{sgn}(Y)\int_{X_0}^{X}\frac{P_1(t)}{\eta_t}\,dt + \int_{X_0}^{\infty}\frac{P_1(t)}{\eta_t}\,dt,$$

with $\eta_a = \sqrt{2}\sqrt{\chi - P_0 a}$ and $X_0 = -\frac{X}{P_0}$. Similarly, $Y\tilde{\tau}_X = \tilde{w}$ and hence,

$$\tilde{\tau} = \int_{X_0}^{X} \frac{1}{\eta_s} \int_{X_0}^{s} \frac{P_1(t)}{\eta_t}\, dt\, ds + \int_{X_0}^{X} \frac{\mathrm{sgn}(Y)}{\eta_s} \int_{X_0}^{\infty} \frac{P_1(t)}{\eta_t}\, dt\, ds - \int_{X_0}^{\infty} \frac{1}{\eta_s} \int_{X_0}^{s} \frac{P_1(t)}{\eta_t}\, dt\, ds - \int_{X_0}^{\infty} \frac{1}{\eta_s} \int_{X_0}^{\infty} \frac{P_1(t)}{\eta_t}\, dt\, ds.$$

The important even part, which contributes to the jump after a change in the order of integration is,

$$\begin{aligned}
\tilde{\tau}_{\text{even}} &= \int_{X_0}^{X} \frac{P_1}{\eta_t} \int_{t}^{X} \frac{1}{\eta_s}\, ds\, dt + \int_{X_0}^{\infty} \frac{P_1}{\eta_t} \int_{X_0}^{t} \frac{1}{\eta_s}\, ds\, dt, \\
&= \frac{1}{P_{01}} \left(\eta_X \int_{X_0}^{X} \frac{P_1(t)}{\eta_t}\, dt - \int_{X_0}^{X} P_1(t)\, dt + \int_{X_0}^{\infty} P_1(t)\, dt \right), \\
\Rightarrow P_0 \tilde{\tau}_{\text{even}} &= \eta_X \int_{X_0}^{X} \frac{P_1(t)}{\eta_t}\, dt + \int_{X}^{\infty} P_1(t)\, dt.
\end{aligned}$$

This gives,

$$\begin{aligned}
\tilde{J} &= 2 \int_0^{\infty} \tilde{\tau}_{\text{even}}\, dY, \\
&= \frac{2}{P_0} \int_{P_0 X}^{\infty} \frac{1}{\eta_X} \left(\eta_X \int_{\chi/P_0}^{X} \frac{P_1(t)}{\eta_t}\, dt + \int_{X}^{\infty} P_1(t)\, dt \right) d\chi, \\
&= \lim_{L \to \infty} \frac{2}{P_0} \left(\int_{-\infty}^{X} P_1(t) \int_{P_0 t}^{L} \frac{1}{\eta_t}\, d\chi\, dt + \int_{X}^{\infty} P_1(t) \int_{P_0 X}^{L} \frac{1}{\eta_t}\, d\chi\, dt \right), \\
&= 0.
\end{aligned}$$

This expression is equal to zero using a similar argument to that on page 53 since the expression of the jump term is similar to that in (2.138), with $P_0 = -1$. Therefore short-scale three-dimensional perturbations are neutral. However perturbations that see some curvature in the basic pressure may provoke a jump.

This implies that in order to obtain a non-zero jump term some variation in $\tilde{p}_X$ is required. It is therefore necessary to use accurate pressure values from the results obtained solving the Benjamin-Ono equation numerically.

2.3.3 The Case of two different Slopes

In this section we consider the equations derived for the spanwise velocity, vorticity and the jump term in the previous section for short scale three-dimensional disturbances. In the previous section we took the first order pressure forcing to be a linear function, (P_0X, with P_0 a constant) but here we consider the use of two different linear pressures with different constant values of the streamwise derivative. The purpose of the analysis is to illustrate the possibility of generating a non-zero jump term by considering a simple model pressure. In the example that follows we take, $P_0 = -\bar{\gamma}X$, where $\bar{\gamma} = 1$ for positive X and $\bar{\gamma} = \gamma$, a constant for negative X. Hence the pressure distribution is as shown in figure 2.5 and $P_{0X} = -\bar{\gamma}$.

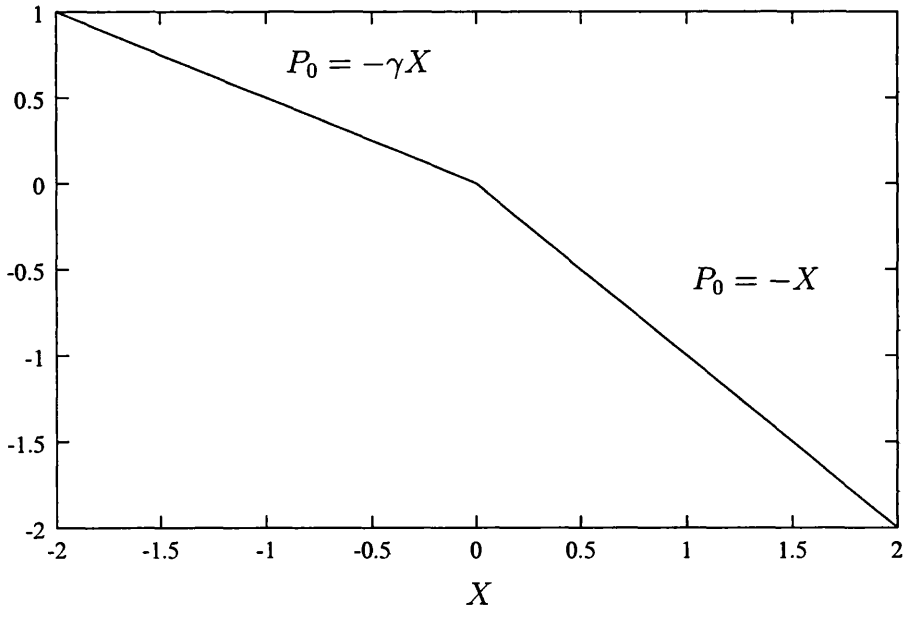

Figure 2.5: The Pressure Distribution.

The linearised equations found in the previous section, with this pressure forcing are,

$$Yw_X + \bar{\gamma}w_Y = P_1(X), \tag{2.146}$$

$$Y\tau_X + \bar{\gamma}\tau_Y = w, \tag{2.147}$$

and using the same notation as earlier allows us to write $\eta_t = \sqrt{2}\sqrt{\chi + \bar{\gamma}t}$ with $\chi = \frac{Y^2}{2} - \bar{\gamma}X$ in this case. We introduce the following notation for the analysis that follows,

$$\eta_X = \sqrt{2}\sqrt{\chi + X}, \qquad \text{and,} \qquad \bar{\eta}_X = \sqrt{2}\sqrt{\chi + \gamma X}. \tag{2.148}$$

The first applies to the region with $X > 0$ and the second applies to $X < 0$.

This analysis requires us to consider 2 main regions with the behaviour of the integrals differing in each one due to the structure of the pressure forcing. The reason is shown clearly in figure 2.6 with different behaviour for positive and negative χ. For negative χ only the behaviour for positive X is relevant but for positive χ the characteristics pass through the regions $X < 0$ and $X > 0$, with the trajectory being exposed to the two different pressure distributions. The path of the characteristic as it passes through each region must be considered carefully to ensure the correct evaluation of each integral in each sector.

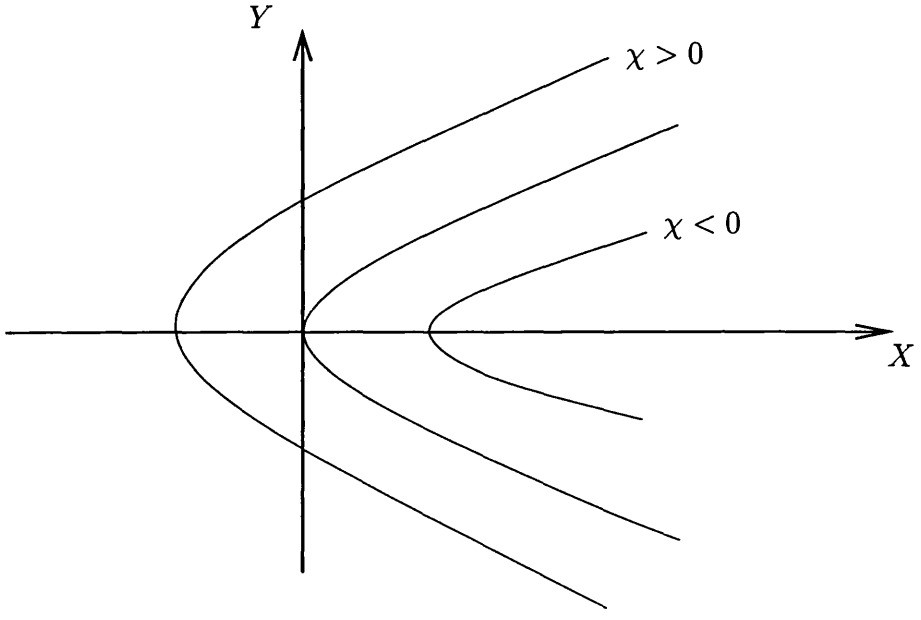

Figure 2.6: The Characteristic trajectories.

Characteristics with $\chi < 0$

Our study commences with the simplest region to consider, the region where the characteristics are defined by negative χ and so X is always positive. Here $\bar{\gamma} = 1$ and $X_0 = -\chi$ and as in the previous sections,

$$w = \left\{ \mathrm{sgn}(Y) \int_X^{X_0} \frac{P_1(t)dt}{\eta_t} + \int_\infty^{X_0} \frac{P_1(t)dt}{\eta_t} \right\}, \tag{2.149}$$

and,

$$\begin{aligned} \tau &= \int_{X_0}^{X} \frac{1}{\eta_s} \int_{X_0}^{s} \frac{P_1(t)}{\eta_t}\, dt\, ds + \mathrm{sgn}(Y) \int_{X_0}^{X} \frac{1}{\eta_s} \int_{X_0}^{\infty} \frac{P_1(t)}{\eta_t}\, dt\, ds \\ &- \int_{X_0}^{\infty} \frac{1}{\eta_s} \int_{X_0}^{s} \frac{P_1(t)}{\eta_t}\, dt\, ds + \int_{X_0}^{\infty} \frac{1}{\eta_s} \int_{X_0}^{\infty} \frac{P_1(t)}{\eta_t}\, dt\, ds. \end{aligned} \tag{2.150}$$

The even part of τ is obtained as in earlier sections with $\tau_E = \frac{1}{2}(\tau(Y) + \tau(-Y))$. Hence,

$$\tau_E = \int_{\infty}^{X} \int_{X_0}^{s} \frac{P_1(t)}{\eta_s \eta_t}\, dt\, ds + \int_{X_0}^{\infty} \int_{X_0}^{\infty} \frac{P_1(t)}{\eta_s \eta_t}\, dt\, ds, \tag{2.151}$$

$$= \eta_X \int_{X_0}^{X} \frac{P_1(t)}{\eta_t}\, dt + \int_{X}^{\infty} P_1(t)\, dt, \tag{2.152}$$

after a change of integration and an integration with respect to s following the method in section 2.3.1. The integrals do exist since we assume that the three-dimensional perturbation, P_1 tends to zero as $t \to \pm\infty$.

The contribution to the jump for negative χ, defined as J^- is obtained with the change of variable, $\chi = \frac{Y^2}{2} - X$. Here χ is the characteristic for $\chi < 0$ (i.e. $X > 0$) and hence $\bar{\gamma} = 1$. We need only integrate between $Y = 0$ to $Y = \sqrt{2X}$ (i.e. from $\chi = -X$ to $\chi = 0$) since we integrate up to the $\chi = 0$ characteristic. Therefore,

$$J^- = 2 \int_{-X}^{0} \int_{X_0}^{X} \frac{P_1(t)}{\eta_t}\, dt\, d\chi + 2 \int_{-X}^{0} \frac{1}{\eta_X} \int_{X}^{\infty} P_1(t)\, dt\, d\chi. \tag{2.153}$$

A change the order of integration followed by an integration with respect to χ leads

to an expression for the jump term,

$$J^- = 2\left\{\int_0^X P_1(t)\int_{X_0}^0 \frac{1}{\eta_t}\,d\chi\,dt + \int_X^\infty P_1(t)\int_{-X}^0 \frac{1}{\eta_X}\,d\chi\,dt\right\}, \quad (2.154)$$

$$= 2\left\{\int_0^X P_1(t)\sqrt{2t}\,dt + \int_X^\infty P_1(t)\sqrt{2X}\,dt\right\}. \quad (2.155)$$

Characteristics with $\chi > 0$

The next step is to study the case, $\chi > 0$. This is more demanding as it requires the careful consideration of four sections of a characteristic's trajectory. These are shown in figure 2.7. The value of the integral for the spanwise velocity and vorticity at the end of each sector is the initial value for the next sector. For example the spanwise velocity found in sector 1 evaluated at $X = 0$ is the initial value of the spanwise velocity to be found in sector 2. For the spanwise velocity we therefore follow the trajectory around starting with sector 1,

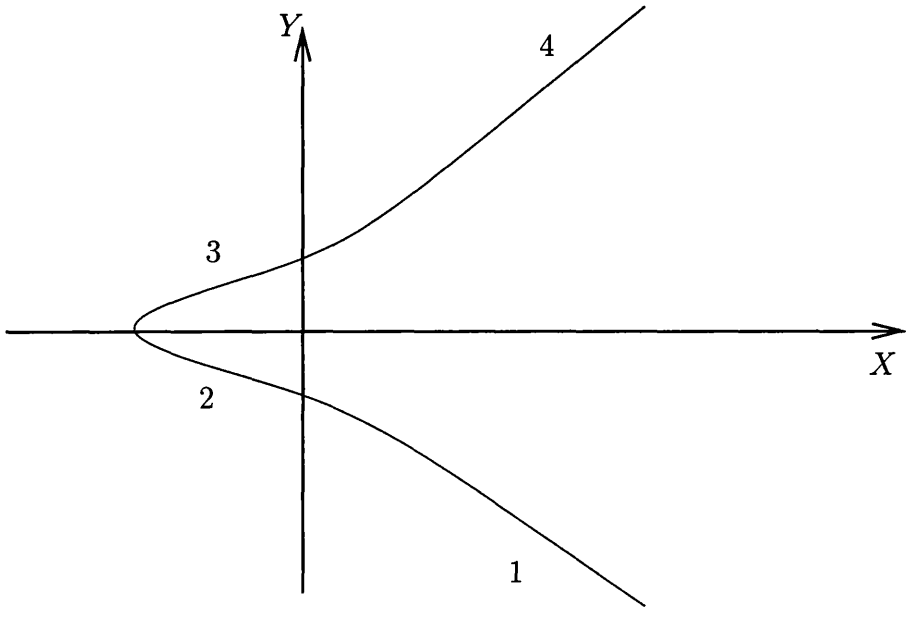

Figure 2.7: The Characteristic Trajectory for $\chi > 0$.

$$w^{(1)}(X) = \int_X^\infty \frac{P_1(t)}{\eta_t}\, dt, \tag{2.156}$$

and for the other 3 sectors, with (2.156) at $X = 0$, the initial value for sector 2,

$$w^{(2)}(X) = w^{(1)}(0) - \int_0^X \frac{P_1(t)}{\eta_t}\, dt, \tag{2.157}$$

$$w^{(3)}(X) = w^{(2)}(\bar{X}_0) + \int_{\bar{X}_0}^X \frac{P_1(t)}{\eta_t}\, dt, \tag{2.158}$$

$$w^{(4)}(X) = w^{(3)}(0) + \int_0^X \frac{P_1(t)}{\eta_t}\, dt. \tag{2.159}$$

The vorticity is found similarly and hence,

$$\tau^{(1)}(X) = -\int_\infty^X \frac{w^{(1)}(s)}{\eta_s}\, ds, \tag{2.160}$$

$$\tau^{(2)}(X) = \tau^{(1)}(0) - \int_0^X \frac{w^{(2)}(s)}{\bar{\eta}_s}\, ds, \tag{2.161}$$

$$\tau^{(3)}(X) = \tau^{(2)}(\bar{X}_0) + \int_{\bar{X}_0}^X \frac{w^{(3)}(s)}{\bar{\eta}_s}\, ds, \tag{2.162}$$

$$\tau^{(4)}(X) = \tau^{(3)}(0) + \int_0^X \frac{w^{(4)}(s)}{\eta_s}\, ds. \tag{2.163}$$

We have τ for each sector and the jump term is now studied by taking positive and negative X separately and finding the even part of the vorticity in each case.

For negative X, it is sector 2 and 3 that are of interest. Therefore,

$$\tau_{\mathrm{E}} = \int_0^\infty \frac{1}{\eta_s} \int_s^\infty \frac{P_1(t)}{\eta_t}\, dt\, ds + \int_{\bar{X}_0}^0 \frac{1}{\bar{\eta}_s} \left(\int_{\bar{X}_0}^0 \frac{P_1(t)}{\bar{\eta}_t}\, dt + \int_0^\infty \frac{P_1(t)}{\eta_t}\, dt \right) ds + \int_0^X \frac{1}{\bar{\eta}_s} \int_{\bar{X}_0}^s \frac{P_1(t)}{\bar{\eta}_t}\, dt\, ds. \tag{2.164}$$

As an aside we note that by putting $\gamma = 1$ we obtain the same regions as for the $P = -X$ case as expected. We consider each integral in turn, changing the order of integration and integrating. A change of integration in the first integral and integrating leads to,

$$\int_0^\infty \frac{1}{\eta_s} \int_s^\infty \frac{P_1(t)}{\eta_t}\, dt\, ds = \int_0^\infty \frac{P_1(t)}{\eta_t} \int_0^t \frac{1}{\eta_s}\, ds\, dt, \tag{2.165}$$

$$= \int_0^\infty \frac{P_1(t)}{\eta_t} \left(\eta_t - \sqrt{2\chi} \right) dt. \tag{2.166}$$

Similarly for the second integral,

$$\int_{\bar{X}_0}^{0} \frac{1}{\bar{\eta}_s} \int_{\bar{X}_0}^{0} \frac{P_1(t)}{\bar{\eta}_t}\, dt\, ds = \int_{\bar{X}_0}^{0} \frac{P_1(t)}{\bar{\eta}_t} \int_{\bar{X}_0}^{t} \frac{1}{\bar{\eta}_s}\, ds\, dt, \tag{2.167}$$

$$= \int_{\bar{X}_0}^{0} \frac{P_1(t)}{\bar{\eta}_t} \left(\frac{\bar{\eta}_t}{\gamma}\right) dt, \tag{2.168}$$

as $\bar{\eta}_{\bar{X}_0} = 0$. The third integral is,

$$\int_{\bar{X}_0}^{0} \frac{1}{\bar{\eta}_s} \int_{0}^{\infty} \frac{P_1(t)}{\eta_t}\, dt\, ds = \int_{0}^{\infty} \frac{P_1(t)}{\eta_t} \int_{\bar{X}_0}^{0} \frac{1}{\bar{\eta}_s}\, ds\, dt, \tag{2.169}$$

$$= \int_{0}^{\infty} \frac{P_1(t)}{\eta_t} \left(\frac{\sqrt{2\chi}}{\gamma}\right) dt. \tag{2.170}$$

Finally the fourth integral is,

$$\int_{0}^{X} \frac{1}{\bar{\eta}_s} \int_{\bar{X}_0}^{s} \frac{P_1(t)}{\bar{\eta}_t}\, dt\, ds = \int_{\bar{X}_0}^{X} \frac{P_1(t)}{\bar{\eta}_t} \int_{t}^{X} \frac{1}{\bar{\eta}_s}\, ds\, dt, \tag{2.171}$$

$$= \int_{\bar{X}_0}^{X} \frac{P_1(t)}{\bar{\eta}_t} \left(\frac{\bar{\eta}_X}{\gamma} - \frac{\bar{\eta}_t}{\gamma}\right) dt. \tag{2.172}$$

These are combined so that,

$$\tau_E = \int_0^{\infty} P_1(t)\, dt + \int_X^0 \frac{P_1(t)}{\gamma}\, dt + \sqrt{2\chi}\left(\frac{1-\gamma}{\gamma}\right) \int_0^{\infty} \frac{P_1(t)}{\eta_t}\, dt + \frac{\bar{\eta}_X}{\gamma} \int_{\bar{X}_0}^{X} \frac{P_1(t)}{\bar{\eta}_t}\, dt. \tag{2.173}$$

Integration to find the jump term is completed using a change of variable as before with $\chi = \frac{Y^2}{2} - \gamma X$ and then integrating in χ from $\chi = -\gamma X$ to $\chi = \infty$,

$$J^{(1+)} = 2\Bigg\{ \int_{-\gamma X}^{L} \frac{1}{\bar{\eta}_X} \int_0^{\infty} P_1(t)\, dt\, d\chi + \frac{1}{\gamma} \int_{-\gamma X}^{L} \frac{1}{\bar{\eta}_X} \int_X^0 P_1(t)\, dt\, d\chi$$
$$+ \left(\frac{1-\gamma}{\gamma}\right) \int_{-\gamma X}^{L} \frac{\sqrt{2\chi}}{\bar{\eta}_X} \int_0^{\infty} \frac{P_1(t)}{\bar{\eta}_t}\, dt\, d\chi + \frac{1}{\gamma} \int_{-\gamma X}^{L} \int_{\bar{X}_0}^{X} \frac{P_1(t)}{\bar{\eta}_t}\, dt\, d\chi \Bigg\}. \tag{2.174}$$

We are able to change the order of integration again to find,

$$J^{(1+)} = 2\Bigg\{ \int_0^{\infty} P_1(t) \int_{-\gamma X}^{L} \frac{1}{\bar{\eta}_X}\, d\chi\, dt + \frac{1}{\gamma} \int_X^0 P_1(t) \int_{-\gamma X}^{L} \frac{1}{\bar{\eta}_X}\, d\chi\, dt +$$
$$\left(\frac{1-\gamma}{\gamma}\right) \int_0^{\infty} P_1(t) \int_{-\gamma X}^{L} \frac{\sqrt{2\chi}}{\bar{\eta}_t \bar{\eta}_X}\, d\chi\, dt + \frac{1}{\gamma} \int_{-\infty}^{X} P_1(t) \int_{-\gamma t}^{L} \frac{1}{\bar{\eta}_X} d\chi dt \Bigg\}. \tag{2.175}$$

Integrating with respect to χ leads to,

$$J^{(1+)} = 2\Bigg\{ \int_0^\infty P_1(t)\sqrt{2}\sqrt{L+\gamma X}\,dt + \frac{1}{\gamma}\int_X^0 P_1(t)\sqrt{2}\sqrt{L+\gamma X}\,dt + \left(\frac{1-\gamma}{\gamma}\right)\int_0^\infty P_1(t)I_1(X,t)\,dt + \frac{1}{\gamma}\int_{-\infty}^X P_1(t)\sqrt{2}\left(\sqrt{L+\gamma t}\right)\,dt\Bigg\}, \quad (2.176)$$

with,

$$\begin{aligned} I_1(X,t) &= \int_{-\gamma X}^L \frac{\sqrt{2\chi}}{\bar{\eta}_X\bar{\eta}_t}\,d\chi, & (2.177)\\ &= \int_{-\gamma X}^L \frac{1}{\bar{\eta}_X}\,d\chi + \int_{-\gamma X}^L \frac{\sqrt{2\chi}-\bar{\eta}_X}{\bar{\eta}_X\bar{\eta}_t}\,d\chi, & (2.178)\\ &= \sqrt{2}\sqrt{L+\gamma X} + I_2(X,t). & (2.179)\end{aligned}$$

Therefore,

$$J^{(1+)} = 2\Bigg\{\frac{1}{\gamma}\int_X^\infty P_1(t)\sqrt{2}\sqrt{L+\gamma X}\,dt + \left(\frac{1-\gamma}{\gamma}\right)\int_0^\infty P_1(t)I_2(X,t)\,dt + \frac{1}{\gamma}\int_\infty^X P_1(t)\sqrt{2}\left(\sqrt{L+\gamma t}\right)\,dt\Bigg\}. \quad (2.180)$$

The third case is for $\chi > 0$ and $X > 0$. Here,

$$\begin{aligned}\tau_E = &\int_0^\infty \frac{1}{\eta_s}\left\{\int_{\bar{X}_0}^0 \frac{P_1(t)}{\bar{\eta}_t}\,dt + \int_0^\infty \frac{P_1(t)}{\eta_t}\,dt\right\}\,ds\\ &-\int_X^\infty \frac{1}{\eta_s}\left\{\int_{\bar{X}_0}^0 \frac{P_1(t)}{\bar{\eta}_t}\,dt + \int_0^s \frac{P_1(t)}{\eta_t}\,dt\right\}\,ds\\ &+\int_{\bar{X}_0}^0 \frac{1}{\bar{\eta}_s}\left\{\int_{\bar{X}_0}^0 \frac{P_1(t)}{\bar{\eta}_t}\,dt + \int_0^\infty \frac{P_1(t)}{\eta_t}\,dt\right\}\,ds. \quad (2.181)\end{aligned}$$

There are six integrals and therefore six changes of integration. Fortunately most of the changes of integration are trivial. The only concern is for the fourth integral but we find,

$$\int_X^\infty\int_0^s \frac{P_1(t)}{\eta_t\eta_s}\,dt\,ds = \int_0^\infty\int_X^\infty \frac{P_1(t)}{\eta_t\eta_s}\,ds\,dt + \int_X^\infty\int_t^\infty \frac{P_1(t)}{\eta_t\eta_s}\,ds\,dt. \quad (2.182)$$

The first and third integrals in (2.181) may be combined and so after carrying out the changes in order of integration we obtain,

$$\begin{aligned}\tau_{\mathrm{E}} = &\int_{\bar{X}_0}^{0} \frac{P_1(t)}{\bar{\eta}_t} \int_0^X \frac{1}{\eta_s}\, ds\, dt + \int_0^\infty \frac{P_1(t)}{\eta_t} \int_0^\infty \frac{1}{\eta_s}\, ds\, dt \\ &- \int_0^\infty \frac{P_1(t)}{\eta_t} \int_X^\infty \frac{1}{\eta_s}\, ds\, dt - \int_X^\infty \frac{P_1(t)}{\eta_t} \int_t^\infty \frac{1}{\eta_s}\, ds\, dt \\ &+ \int_{\bar{X}_0}^{0} \frac{P_1(t)}{\bar{\eta}_t} \int_{\bar{X}_0}^{0} \frac{1}{\bar{\eta}_s}\, ds\, dt - \int_0^\infty \frac{P_1(t)}{\eta_t} \int_0^{\bar{X}_0} \frac{1}{\bar{\eta}_s}\, ds\, dt. \end{aligned} \tag{2.183}$$

We begin by considering the second, third and fourth integrals together as these all have $\eta_t\eta_s$ in the denominator. Hence we may combine and simplify,

$$\left\{\int_0^\infty \int_0^\infty - \int_0^\infty \int_X^\infty - \int_X^\infty \int_t^\infty \right\} \frac{P_1(t)}{\eta_t\eta_s}\, ds\, dt = \int_0^X \frac{\eta_X P_1(t)}{\eta_t}\, dt - \int_0^\infty \frac{\sqrt{2\chi} P_1(t)}{\eta_t}\, dt + \int_X^\infty P_1(t)\, dt.$$

We now consider the other integrals in turn and integrate with respect to s. The first integral becomes,

$$\int_{\bar{X}_0}^{0} \frac{P_1(t)}{\bar{\eta}_t} \int_0^X \frac{1}{\eta_s}\, ds\, dt = \int_{\bar{X}_0}^{0} \frac{P_1(t)}{\bar{\eta}_t} \left(\eta_X - \sqrt{2\chi}\right) dt. \tag{2.184}$$

while the fifth is,

$$\int_{\bar{X}_0}^{0} \frac{P_1(t)}{\bar{\eta}_t} \int_{\bar{X}_0}^{0} \frac{1}{\bar{\eta}_s}\, ds\, dt = \int_{\bar{X}_0}^{0} \frac{P_1(t)}{\bar{\eta}_t} \frac{\sqrt{2\chi}}{\gamma}\, dt. \tag{2.185}$$

Finally the sixth integral integrates so that,

$$\int_0^\infty \frac{P_1(t)}{\eta_t} \int_0^{\bar{X}_0} \frac{1}{\bar{\eta}_s}\, ds\, dt = -\int_0^\infty \frac{P_1(t)}{\eta_t} \frac{\sqrt{2\chi}}{\gamma}\, dt. \tag{2.186}$$

The sum of the six integrals is therefore,

$$\begin{aligned}\tau_{\mathrm{E}} = &\int_{\bar{X}_0}^{0} \frac{P_1(t)\eta_X}{\bar{\eta}_t}\, dt + \int_0^X \frac{P_1(t)\eta_X}{\eta_t}\, dt + \int_X^\infty P_1(t)\, dt \\ &+ \left(\frac{1-\gamma}{\gamma}\right) \int_{\bar{X}_0}^{0} \frac{P_1(t)\sqrt{2\chi}}{\bar{\eta}_t}\, dt + \left(\frac{1-\gamma}{\gamma}\right) \int_0^\infty \frac{P_1(t)\sqrt{2\chi}}{\eta_t}\, dt. \end{aligned} \tag{2.187}$$

We integrate to find the jump term,

$$\begin{aligned} J^{(2+)} &= 2\int_0^L \int_{\bar{X}_0}^0 \frac{P_1(t)}{\bar{\eta}_t}\, dt\, d\chi + 2\int_0^L \int_0^X \frac{P_1(t)}{\eta_t}\, dt\, d\chi + 2\int_0^L \int_X^\infty \frac{P_1(t)}{\eta_X}\, dt\, d\chi \\ &+ 2\left(\frac{1-\gamma}{\gamma}\right)\int_0^L \int_{\bar{X}_0}^0 \frac{P_1(t)\sqrt{2\chi}}{\bar{\eta}_t \eta_X}\, dt\, d\chi + 2\left(\frac{1-\gamma}{\gamma}\right)\int_0^L \int_0^\infty \frac{P_1(t)\sqrt{2\chi}}{\eta_t \eta_X}\, dt\, d\chi. \end{aligned}$$

Simplification is achieved through a change in the order of integration,

$$\begin{aligned} J^{(2+)} &= 2\int_{-\infty}^0 \int_{-\gamma t}^L \frac{P_1(t)}{\bar{\eta}_t}\, d\chi\, dt + 2\int_0^X \int_0^L \frac{P_1(t)}{\eta_t}\, d\chi\, dt + 2\int_X^\infty \int_0^L \frac{P_1(t)}{\eta_X}\, d\chi\, dt \\ &+ 2\left(\frac{1-\gamma}{\gamma}\right)\int_{-\infty}^0 \int_{-\gamma t}^L \frac{P_1(t)\sqrt{2\chi}}{\bar{\eta}_t \eta_X}\, d\chi\, dt + 2\left(\frac{1-\gamma}{\gamma}\right)\int_0^\infty \int_0^L \frac{P_1(t)\sqrt{2\chi}}{\eta_t \eta_X}\, d\chi\, dt. \end{aligned}$$

Integrating with respect to χ gives,

$$\begin{aligned} J^{(2+)} &= 2\int_{-\infty}^0 P_1(t)\sqrt{2}\frac{\sqrt{L+\gamma X}}{\gamma}\, dt + 2\int_0^X \sqrt{2}P_1(t)\left(\sqrt{L+t}-\sqrt{t}\right)\, dt \\ &+ \int_X^\infty \sqrt{2}P_1(t)\left(\sqrt{L+X}-\sqrt{X}\right) + 2\left(\frac{1-\gamma}{\gamma}\right)\int_{-\infty}^0 P_1(t)I_3(X,t)\, dt \\ &+ 2\left(\frac{1-\gamma}{\gamma}\right)\int_0^\infty P_1(t)I_4(X,t)\, dt. \end{aligned}$$

Here we have defined,

$$I_3(X,t) = \int_{-\gamma t}^L \frac{\sqrt{2\chi}}{\bar{\eta}_t \eta_X}\, d\chi, \tag{2.188}$$

and,

$$I_4(X,t) = \int_0^L \frac{\sqrt{2\chi}}{\eta_t \eta_X}\, d\chi. \tag{2.189}$$

Thus we have found an expression for the jump term, which is non-zero. We note that if $\gamma = 1$ then we are left with the same terms as those for the linear pressure in the previous section as expected. We can be sure that the jump term is not zero in the present study due to the I_2, I_3 and I_4 terms generated in the expressions for the jump term in the $\chi > 0$ cases. This confirms the possibility of a jump term being generated at a later time in the development of the pressure.

2.4 Properties of the Flow Leaving the Critical Layer

We now return to the study of the full pressure system derived in sections 2.1 and 2.2. In the numerical plots for the vorticity shown in section 2.5.1 a large non-zero growing feature is visible as $Y \to \infty$ with $\chi \sim 1$. This is different to the other growing vorticity feature, which exists for large χ (as a result of the effects at large negative X). The plot of w in figure 2.16 on page 91 shows a strong non-zero region for $Y \to \infty$, $\chi \sim 1$ but in the case of w the region does not grow in magnitude as $Y \to \infty$. However τ in figure 2.17 on page 96 does seem to grow as $Y \to \infty$ for $\chi \sim 1$. This could be problematic since we need to integrate τ with respect to Y in order to find the jump term. If τ continues to grow as $Y \to \infty$ then the integration to find the jump term will not converge since we integrate with respect to Y to find the jump term. The numerics suggest that the vorticity integrates to zero, giving no net jumps in velocity gradient and no influence on the local flow development. However it could still potentially influence the bulk of the flow with the jump term dominating and cause a breakdown in the assumptions used to derive the governing equations. Here we consider this possibility, tracing the vorticity's development downstream and we additionally verify that the jump in velocity, J_X is zero. The characteristics follow a path, given by $\chi = \tilde{p} + \frac{Y^2}{2}$, from $Y < 0$ and $X = \infty$ to $Y > 0$ and $X = \infty$. The characteristics given by $\chi \sim 1$ pick up non-zero particles near $X \sim 1$ before exiting to $X = \infty$. The characteristics defined by $|\chi| \gg 1$ pick up very little forcing and so should remain very small although we shall show in both the numerical results of section 2.5.1 and in the further analysis of section 2.6 that these small values spend so much time in the critical layer that they do have a strong influence on the vorticity and hence the jump term.

In this section it is shown through an order of magnitude argument leading to a theoretical understanding that any influence of this growing vorticity, or "jet" of vorticity, occurs at later times and so the numerical results obtained do hold. We

will begin by considering the behaviour as $X \to \infty$. This shows that the integral of this jet of vorticity at large X is zero. The region of interest is $X \to \infty$ with $\chi = O(1)$. As before, $\chi = \frac{1}{2}Y^2 + \tilde{p}(z, X)$, and from Li *et al.* (1998), $\tilde{p}(X) \sim X^{1/3}$ as $X \to \infty$. Therefore, $Y \sim X^{1/6}$. The solutions we have for w and τ are,

$$\begin{aligned} w &= -\left\{ \mathrm{sgn}(Y) \int_{X_0}^{X} \frac{\tilde{p}_z(z,t)dt}{\sqrt{2}\sqrt{\chi - \tilde{p}(z,t)}} + \int_{X_0}^{\infty} \frac{\tilde{p}_z(z,t)dt}{\sqrt{2}\sqrt{\chi - \tilde{p}(z,t)}} \right\}, \\ &= -2\int_{X_0(\chi)}^{\infty} \frac{\tilde{p}_z(z,t)\,dt}{\sqrt{2}\sqrt{\chi - \tilde{p}(z,t)}}, \\ &= \bar{w}(\chi, z), \end{aligned} \tag{2.190}$$

where the $\bar{w}$ does not grow downstream. However the vorticity keeps growing, governed in streamline coordinates by,

$$\frac{\partial \tau}{\partial X} = \frac{1}{\eta_X}[\bar{w}_z + \tilde{p}_z \bar{w}_\chi], \tag{2.191}$$

where again $\eta_X = \sqrt{2}\sqrt{\chi - \tilde{p}(z, X)}$. Since $\tilde{p}_z \to 0$ as $X \to \infty$,

$$\frac{\partial \tau}{\partial X} \sim \frac{\bar{w}_z}{\sqrt{2}\sqrt{\chi - \tilde{p}(X)}}. \tag{2.192}$$

Far downstream, $|\tilde{p}(X)| \gg \chi \sim O(1)$ so that,

$$\tau \sim \frac{\bar{w}_z}{\sqrt{2}} \int^{X} \frac{ds}{\sqrt{-\tilde{p}(s)}}, \tag{2.193}$$

$$\sim \frac{6}{5\sqrt{2}} \bar{w}_z X^{5/6}, \tag{2.194}$$

$$= X^{5/6} \bar{\tau}(\chi, z), \tag{2.195}$$

defining $\bar{\tau}(\chi, z)$. From $\chi = \frac{1}{2}Y^2 - X^{1/3}$ we can see that as $X \to \infty$, the Y-range over which $\chi \sim 1$, to which the growing vorticity is confined, shrinks such that,

$$Y \sim \sqrt{2}X^{1/6}\left(1 + \frac{\chi}{X^{1/3}}\right), \tag{2.196}$$

$$\sim \sqrt{2}X^{1/6} + \frac{\chi}{\sqrt{2}X^{1/6}} + \ldots, \tag{2.197}$$

which implies $J \sim X^{5/6}\frac{1}{X^{1/6}} \sim X^{2/3}$ and $J_X \sim X^{-1/3}$. This is the same size as $\tilde{p}\tilde{p}_X$. This is problematic suggesting the jet's influence extends downstream except that,

$$\int_{-\infty}^{\infty} \bar{\tau}(\chi, z)\, d\chi = 0, \tag{2.198}$$

since we now show that,

$$\int_{-\infty}^{\infty} \bar{w}_z \, d\chi = 0. \tag{2.199}$$

We may verify this by considering (2.190) such that,

$$\begin{aligned}
\int_{-\infty}^{\infty} \bar{w}_z \, d\chi &= \int_{-\infty}^{\infty} \frac{\partial}{\partial z} \int_{-X_0(\chi)}^{\infty} \frac{\tilde{p}_z(z,t)}{\sqrt{2}\sqrt{\chi - \tilde{p}(z,t)}} \, dt \, d\chi, && (2.200)\\
&= \int_{-\infty}^{\infty} \frac{\partial}{\partial z} \int_{\tilde{p}(t)}^{\infty} \frac{\tilde{p}_z(z,t)}{\sqrt{2}\sqrt{\chi - \tilde{p}(z,t)}} \, d\chi \, dt, && (2.201)\\
&= \int_{-\infty}^{\infty} \frac{\partial}{\partial z} \frac{2}{\sqrt{2}} \tilde{p}_z(z,t) \left[\sqrt{\chi - \tilde{p}(z,t)}\right] \, dt, && (2.202)\\
&= \lim_{\chi \to \infty} \int_{-\infty}^{\infty} \frac{\partial}{\partial z} \frac{2}{\sqrt{2}} \tilde{p}_z(z,t) \left(\chi^{1/2} - \frac{\tilde{p}}{\chi^{1/2}} - \frac{\tilde{p}^2}{\chi^{3/2}} + \ldots \right) \, dt.
\end{aligned}$$

This tends to zero since the first term is,

$$\int_{-\infty}^{\infty} \chi^{1/2} \tilde{p}_z(z,t) \, dt = \chi^{1/2} \int_{-\infty}^{\infty} \tilde{p}_z(z,t) \, dt = 0. \tag{2.203}$$

Thus $J_X \to 0$ and the large X asymptotics is governed by the inertial nonlinear wave-breaking balance $\tilde{p}_T + \tilde{p}\tilde{p}_X = 0$.

In order to proceed with the study of the possibility of the growing vorticity feeding back into the bulk of the flow as it emerges downstream of our region of concern, we need to consider the relative sizes of the viscous and unsteady terms in the momentum equations. This introduces new scalings and a study of a new set of equations. The unsteady terms are an order $\epsilon^{1/4}$ smaller than the convective inertial terms in the momentum equation, whilst the viscous terms are an order $\epsilon^{3/4}$ smaller. Hence the governing equations are,

$$\epsilon^{1/4} w_T + Y w_X - \tilde{p}_X w_Y = -\tilde{p}_z + \epsilon^{3/4} w_{YY}, \tag{2.204}$$

and,

$$\epsilon^{1/4} \tau_T + Y \tau_X - \tilde{p}_X \tau_Y = w_z + \epsilon^{3/4} \tau_{YY}. \tag{2.205}$$

These are obtained with the same expansions in the critical layer as in the original derivation (section 1.2),

$$\bar{u} = \epsilon \left[c + \epsilon^{1/4} U_1 + \epsilon^{1/2} U_2 + \epsilon^{3/4} U_2 + \epsilon U_2 + \dots \right], \tag{2.206}$$

and $U_1 = b_1 Y$, $U_2 = a_{11}\tilde{p}$, $U_3 = b_3 Y^3 + 2a_{12}\tilde{p}Y$ and $U_4 = b_4 Y^4 + 3a_{13}Y^2\tilde{p} + U_4^*$, with $\tau = U_{4Y}^*$.

The Unsteady Vorticity

Now we look inside the region of growing vorticity to ascertain its behaviour and derive scales that can be used to further our understanding of the role it has on the bulk of the flow. Inside the jet, $Y \sim \sqrt{2}X^{1/6} + \frac{\chi}{\sqrt{2}X^{1/6}} + \dots$ and hence $\frac{\partial}{\partial Y} \sim \sqrt{2}X^{1/6}\frac{\partial}{\partial \chi}$. We also have, $\tilde{p}_X \sim \frac{1}{6}X^{-2/3}$ and therefore substituting into (2.204) gives,

$$\epsilon^{1/4} w_T + (\sqrt{2}X^{1/6} + \frac{\chi}{\sqrt{2}X^{1/6}} + \dots) w_X - \frac{\sqrt{2}}{3} X^{-2/3} X^{1/6} w_\chi = 0 + \epsilon^{3/4} 2X^{1/3} w_{\chi\chi}. \tag{2.207}$$

Hence if $X^{-5/6} \sim \epsilon^{1/4}$, i.e. $X \sim \epsilon^{-3/10}$ the critical layer becomes unsteady, with the momentum equation becoming,

$$\epsilon^{1/4}(w_T + \sqrt{2}X^{1/6} w_X) = \epsilon^{3/4}\epsilon^{-1/10} 2 w_{\chi\chi} X^{1/3}, \tag{2.208}$$

and so the viscous terms can be neglected with a relative error of $\epsilon^{2/5}$. A similar argument generates the τ-equation. The new scalings within the region of growing vorticity are summarised in figure 2.8.

We have now found the governing equations for the local behaviour of the region of growing vorticity for large X, downstream of the original region of interest. These must be solved to trace the subsequent development. The equations are,

$$w_T + \sqrt{2}\hat{X}^{1/6} w_{\hat{X}} = 0, \tag{2.209}$$

$$\tau_T + \sqrt{2}\hat{X}^{1/6} \tau_{\hat{X}} = w_z, \tag{2.210}$$

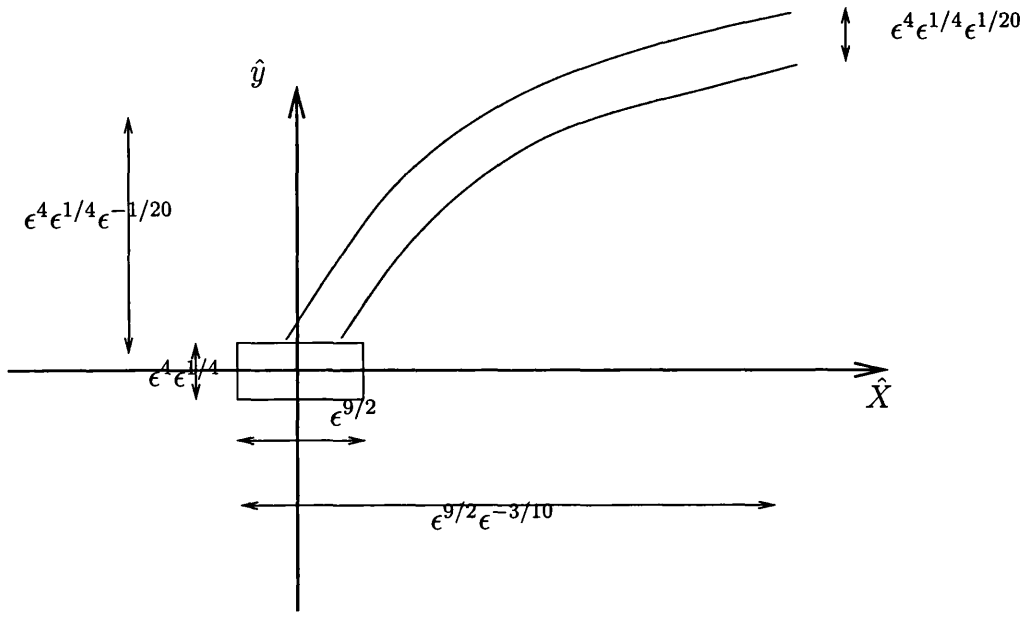

Figure 2.8: Scalings for the jet.

where $X = \epsilon^{-3/10}\hat{X}$. The values of w and τ as $\hat{X} \to 0$ inside the jet, i.e. the boundary conditions, are equivalent to the asymptotic values of w and τ as $X \to \infty$ in the critical layer analysis earlier (in (2.190) and (2.195)), and hence, as $\hat{X} \to 0$,

$$w = \bar{w}(\chi, z, T), \tag{2.211}$$

$$\tau = \hat{X}^{5/6}\bar{\tau}(\chi, z, T). \tag{2.212}$$

The equations given by (2.209) and (2.210) for the behaviour inside the region of growing vorticity can be solved using the method of characteristics so that,

$$\frac{dT}{ds} = 1, \qquad \frac{d\hat{X}}{ds} = \sqrt{2}\hat{X}^{1/6}, \qquad \frac{dw}{ds} = 0, \qquad \frac{d\tau}{ds} = w_z. \tag{2.213}$$

The initial conditions are, $s = 0$ at $X = 0$ and t_0 is the entry time of a fluid particle at $X = 0$. Solving the four ordinary differential equations in (2.213) leads to the following solutions, $T = s + t_0$,

$$\frac{1}{\sqrt{2}}\int \frac{1}{\hat{X}^{1/6}} d\hat{X} = s \qquad \Rightarrow \qquad s = \frac{6}{5\sqrt{2}}\hat{X}^{5/6}, \tag{2.214}$$

$w = \bar{w}(\chi, z, t_0)$ and $\tau = s\bar{w}_z(\chi, z, t_0)$. Equation (2.214) implies $t_0 = T - \frac{6}{5\sqrt{2}}\hat{X}^{5/6}$ and so we obtain the following results for the spanwise velocity,

$$w = \bar{w}\left(\chi, z, T - \frac{6}{5\sqrt{2}}\hat{X}^{5/6}\right), \tag{2.215}$$

and the vorticity,

$$\tau = \left(T - \frac{6}{5\sqrt{2}}\hat{X}^{5/6}\right)\bar{w}_z(\chi, z, T - \frac{6}{5\sqrt{2}}\hat{X}^{5/6}). \tag{2.216}$$

Now, as $\hat{X} \to \infty$ with T fixed, then $\tau \to 0$ if $\bar{w}_z(\chi, z, T) \to 0$ faster than $\frac{1}{|T|}$ as $T \to -\infty$. This depends on the initial conditions since if there is little three-dimensionality as $T \to -\infty$ then there is no jet far downstream. As $T \to \infty$ with $\hat{X} \sim T^{6/5}$ fixed then τ does persist to $\hat{X} \to \infty$ but this corresponds to very large times, which are of no interest to the present study.

Hence the numerical results should be valid as the jet does not influence the bulk of the flow at order 1 times.

2.5 Numerical Method

As anticipated earlier the system of equations (2.70), (2.52), (2.57) and (2.59) must be solved numerically. This is a computationally demanding task as errors can enter in several ways. The system of equations we solve is,

$$a_1\tilde{p}_T + a_2\tilde{p}\tilde{p}_X = \mu J_X + \frac{1}{\pi}\int_{-\infty}^{\infty} \tilde{p}_{ss}\frac{ds}{X-s}, \tag{2.217}$$

$$Yw_X - \tilde{p}_X w_Y = -\tilde{p}_z, \tag{2.218}$$

$$Y\tau_X - \tilde{p}_X\tau_Y = w_z + m(X,T), \tag{2.219}$$

where $m(X,T) = -6b_1^{-3}\left(b_3 b_1 \tilde{p}_T - 2b_4\tilde{p}\tilde{p}_X\right)$, with b_1, b_3, b_4 constants, and,

$$J = \int_{-\infty}^{\infty} \tau\, dY. \tag{2.220}$$

The boundary conditions on (2.217) are $\tilde{p} \sim |X|^{1/3}$ as $X \to \pm\infty$ as explained on page 36. The initial condition on (2.217) is,

$$\tilde{p} \sim |T|^{1/2} f(\xi) \qquad \text{as} \qquad T \to -\infty, \tag{2.221}$$

with $f(\xi) = p_1(\xi)$. This was stated on page 36 and is necessary so that the pressure is compatible with the flow solution in Smith (1988). The boundary conditions on w and τ can be stated as, there is no forcing on a particle entering the critical layer. This is equivalent to $w = \tau = 0$ as $X \to \infty$ and $Y < 0$. We consider solutions of w and τ on characteristic trajectories travelling from $X \sim \infty$ and $Y < 0$, along the characteristic trajectory given by $\chi = \frac{Y^2}{2} + \tilde{p}$. For the purposes of the numerical method and the results given in section 2.5.1, the function $m(X,T)$ in (2.219) is defined as the two-dimensional part of the forcing for τ whilst the w_z is defined as three-dimensional part of the forcing for τ. In our plots of the critical layer solutions in section 2.5.1 we will consider these separately. We use the method of Li (1998) to solve (2.217) and we provide a summary of the method below. We then move on to consider the method for finding the critical layer jump term.

The Benjamin-Ono Solver

The method for solving (2.217) is the numerical method supplied by Dr Linzhong Li of the Mathematics Department at University College London and it is explained fully in Li (1997). For the moment we will not consider the jump term leaving,

$$a_1\tilde{p}_T + a_2\tilde{p}\tilde{p}_X = \frac{1}{\pi}\int_{-\infty}^{\infty} \tilde{p}_{ss}\frac{ds}{X-s}. \tag{2.222}$$

The numerical method uses compact differencing. There are special considerations in Li (1997) given to the three complicated phenomena with (2.222). They are: the complicated boundary and initial conditions; the short scale features of the solution, which demands grid stretching; and the extra computational resources required to solve the Cauchy-Hilbert integral (the right hand side of (2.222)) as it exhibits vastly different behaviour from that of the pressure. These will be discussed below. The Benjamin-Ono equation is solved using a fourth-order implicit compact differencing technique. Compact differencing avoids difficulties with the treatment of boundary conditions common with usual finite differencing techniques. For example a fourth-order accurate approximation with finite differencing may involve five local grid points. The disadvantage of compact differencing is that it introduces new variables (eg. derivatives of the principal function) forming a coupled system but the advantages outweigh this due to the removal of the need for an increase in points and hence a simplification in the algebraic system, which leads to a tridiagonal matrix instead of, for example, a pentadiagonal matrix.

The boundary conditions on (2.222) were given on page 36 in section 2.1 and are,

$$\tilde{p} \propto |X|^{\frac{1}{3}} \text{ as } X \to \pm\infty, \tag{2.223}$$

at finite times, chosen so that the solution matches with the rest of the flowfield. The initial condition,

$$\tilde{p} \sim |T|^{\frac{1}{2}} f(\xi) \text{ as } T \to -\infty, \quad \text{for} \quad \xi = \frac{X}{|T|^{\frac{3}{2}}} \text{ of } O(1), \tag{2.224}$$

with $f(\xi) = p_1(\xi)$, is chosen so that the flow solution matches with the behaviour at the end of step 1. We will shortly consider an explicit form for $f(\xi)$, which is used in the numerical method. Equation (2.222) can be solved using compact difference schemes but before they can be applied the initial and boundary conditions must be dealt with. The initial condition is imposed by taking at very large negative time, $T = -\Gamma$,

$$\tilde{p} \to a_1 a_2^{-1} \Gamma^{\frac{1}{2}} \tilde{p}, \tag{2.225a}$$

$$X \to \Gamma^{\frac{3}{2}} X, \tag{2.225b}$$

$$T \to \Gamma T, \tag{2.225c}$$

which also normalises the governing equations and the initial conditions to give,

$$\tilde{p}_T + \tilde{p}\tilde{p}_X = \frac{a_5}{\pi} \int_{-\infty}^{\infty} \frac{\tilde{p}_{ss}}{X - s}\, ds, \tag{2.226}$$

$$\tilde{p} \sim |T|^{\frac{1}{2}} \frac{f(\xi)}{2\hat{b}} \quad \text{as} \quad T \to -1, \tag{2.227}$$

with $a_5 = \frac{a_2}{a_1^2 \Gamma}$. Note here that $a_5 \sim \Gamma^{-1}$ and so is small. The initial condition used in the numerical method is,

$$f = \frac{2}{\sqrt{3}} \sinh\left[\frac{1}{3}\sinh^{-1}\left(\frac{3^{\frac{3}{2}}X}{2}\right)\right], \tag{2.228}$$

which is a solution of $\tilde{p}_1 \tilde{p}_1' = \hat{b}(\tilde{p}_1 - 3\xi\tilde{p}_1')$, the equation for $\tilde{p}_1$ at the end of step 1 (as noted in Li 1997 and Li *et al.* 1998).

The boundary conditions, $\tilde{p} \propto |X|^{\frac{1}{3}}$ as $X \to \pm\infty$ are imposed by considering asymptotic expansions for large $|X|$, which shorten the effective X integration range. The numerical method uses a coordinate transform to improve the efficiency of the computation, which concentrates the computations in the region where most solution activity occurs. In regions where the solution varies slowly the grid is stretched so that not much computational time is wasted in unnecessary calculations. The actual

transform used is found using the initial condition as the transformation function, g, where $X = g(\tilde{X})$, so that,

$$g = -f^{-1} = \frac{2}{3\sqrt{3}}\sinh\left[3\sinh^{-1}\left(\frac{\sqrt{3}}{2}\bar{X}\right)\right]. \tag{2.229}$$

Therefore the initial condition becomes,

$$\tilde{p}(\bar{X}, -1) = f(X) = -\bar{X}. \tag{2.230}$$

The Cauchy-Hilbert integral term is treated implicitly and it is iterated to ensure the governing equation is closely satisfied. The integral is discretised using Taylor expansions.

The Algorithm

The Benjamin-Ono solver uses a fourth-order compact difference scheme to solve,

$$\tilde{p}_T + \tilde{p}\tilde{p}_X = I, \tag{2.231}$$

where $I = \frac{a_5}{\pi}\int_{-\infty}^{\infty}\tilde{p}_{ss}\frac{ds}{X-s}$. The integral, I is dealt with by using a semi-implicit method. Thus the equation is solved assuming that I is known, to find $\tilde{p}$. Its derivatives are then found and used to calculate I. The solution is then iterated in order to give accurate results for the equation. Since the algorithm iterates for $\tilde{p}$, $\tilde{p}_X$ and also I, it contains two iterate procedures. The solution is calculated at the half time step and extrapolated to give the solution at the full time step. From Li (1997) we obtain the following outline of the algorithm. At each time step, $T = T_n + \frac{1}{2}\triangle t$,

step 1 Using initial values of I $(= I^{(0)})$, solve to find $\tilde{p}^{(0)}$, $\tilde{p}_X^{(0)}$ using compact difference schemes.

step 2 Evaluate derivatives of $\tilde{p}$ to be used in calculation of I in the next step.

step 3 Substitute the values of $\tilde{p}^{(0)}$ and its derivatives into formula for I, to find $I^{(1)}$.

step 4 Consider the errors between $I^{(1)}$ and $I^{(0)}$. If they are smaller than some defined error then continue to the next step, otherwise replace $I^{(0)}$ by $I^{(1)}$ and return to step 1.

step 5 Extrapolate for $\tilde{p}$ to give $\tilde{p}$ at $T = T_n + \triangle t$.

For further details of the method of solving for $\tilde{p}$ and I, see Li (1997).

Modifications to Benjamin-Ono solver

Thus the above outlined method solves,

$$\tilde{p}_T + \tilde{p}\tilde{p}_X = \frac{a_5}{\pi}\int_{-\infty}^{\infty} \frac{\tilde{p}_{ss}\, ds}{X - s},$$

accurately. Modification of this numerical procedure so that the critical layer influence on the bulk flow can be investigated is now considered. Ultimately the major changes made to the Benjamin-Ono solver are the calculation of the jump term, which is considered in the next section, the introduction of spanwise disturbances into the pressure and the extra iteration needed to successfully calculate all the variables correctly although we are unable to do this as we will discover later that the vorticity becomes very large for large negative X. This is problematic as we need to integrate the vorticity in order to find the jump term.

The three dimensionality is introduced using a model spanwise disturbance of the pressure,

$$\tilde{p} = \tilde{p}_0 + 0.1Xe^{-X^2}e^{-z^2},$$

where $\tilde{p}_0$ is the initial two-dimensional pressure. $\tilde{p}_0$ is the initial pressure provided by the initial condition given on page 74. The initial condition is perturbed and allowed to propagate through the numerical solution. This is the value of the two-dimensional pressure at the end of step 1 of Li *et al.* (1998) described in section 2.1. Hence,

$$\tilde{p}_X = \tilde{p}_{0X} + 0.1e^{-X^2}e^{-z^2} - 0.2X^2e^{-X^2}e^{-z^2},$$

$$\tilde{p}_z = 0.2zXe^{-X^2}e^{-z^2}.$$

The jump term, when found, will of course influence the pressure, which in turn influences the jump term again. It is found, when this interaction is implemented, that the jump term becomes very large as $X \to -\infty$. This causes the numerical iterative procedure to diverge. The reasons for this will be considered in section 2.6. Here we concentrate purely on the method to calculate the critical layer jump term and then study the results for the vorticity. This is not ideal but the results are still of great interest as they show the behaviour of the spanwise velocity and the vorticity within the critical layer before vortex generation.

Finding the Jump Term

Two numerical approaches were attempted to solve the critical layer equations. The first method described here, when implemented to solve the critical layer problem was too demanding on computational resources and hence the method described towards the end of this page was used. We give a brief outline of this first method and its limitations here. The first numerical method adopted for the solution of the critical layer problem was found by rewriting (2.218) and (2.219) into their characteristic forms,

$$\frac{dX}{ds} = Y, \qquad \frac{dY}{ds} = -\tilde{p}_X, \tag{2.232}$$

$$\frac{dw}{ds} = -\tilde{p}_z, \qquad \frac{d\tau}{ds} = w_z + \tilde{p}_z w_\chi + m(X,T). \tag{2.233}$$

The solution is then found on a (s,χ) grid with each differential equation solved using an adaptive Runge-Kutta method (explained on page 82). For each χ, or characteristic, s runs from 0 to ∞ and we solve for each s along each χ in turn. The initial conditions for each χ are, $X(s=0) = X_0$, $Y(s=0) = \sqrt{2}\sqrt{\chi - \tilde{p}(X_0)}$, $w(s=0) = \tau(s=0) = 0$. X_0 is chosen so that it is large enough to capture the behaviour of the jump term, whilst w and τ are zero on incoming streamlines. The jump term is then found by integrating τ to find J, before differentiating with respect to X to find

the jump term, J_X. This method gives accurate representations of w and τ, which agree with the method finally chosen but does not accurately predict the behaviour of the jump unless a very small gridsize is chosen. Unfortunately this results in the need for a storage of a large number of huge arrays, which are beyond the computational resources presently available. This method with very small gridsizes is also very slow, which, given that the calculations are performed for each spanwise point at each time step means that this method is currently computationally prohibitively expensive and hence a revised method was undertaken.

This led us to consider a different numerical approach, which we now explain. The numerical solution of the critical layer jump term is achieved by a rearrangement of the critical layer equations so that the equations are solved on a (χ, Y) grid. The characteristics in the X, Y plane are shown in figure 2.9. The present method finds the jump term and the forcing spanwise velocity and vorticity on a χ, Y grid, which avoids the need for several changes of grids and storage of large arrays. The effect of changing the grids is that the solution space is now as shown in figure 2.9 with the characteristic trajectories running parallel to the Y axis. The line of constant X is drawn to show the relative behaviour of the two solution spaces. The line of $X = 0$ is important for the choice of values for the size of the solution spaces as if the Y range is too small then this line crosses the Y_∞ line, which causes a problem as in this case the initial value conditions for w and τ at Y_0 are not zero. We begin as always with the full three-dimensional critical layer equations,

$$Yw_X - \tilde{p}_X w_Y = -\tilde{p}_z, \tag{2.234}$$

$$Y\tau_X - \tilde{p}_X \tau_Y = w_z + m(X,T), \tag{2.235}$$

where $m(X,T) = -6b_1^{-3}\left(b_3 b_1 \tilde{p}_T - 2b_4 \tilde{p}\tilde{p}_X\right)$ and,

$$J = \int_{-\infty}^{\infty} \tau \, dY. \tag{2.236}$$

As found earlier in section 2.2 the characteristics for (2.234) and (2.235) are the curves $\chi = \frac{1}{2}Y^2 + \tilde{p}$, where each χ gives a different characteristic. From (2.234) or

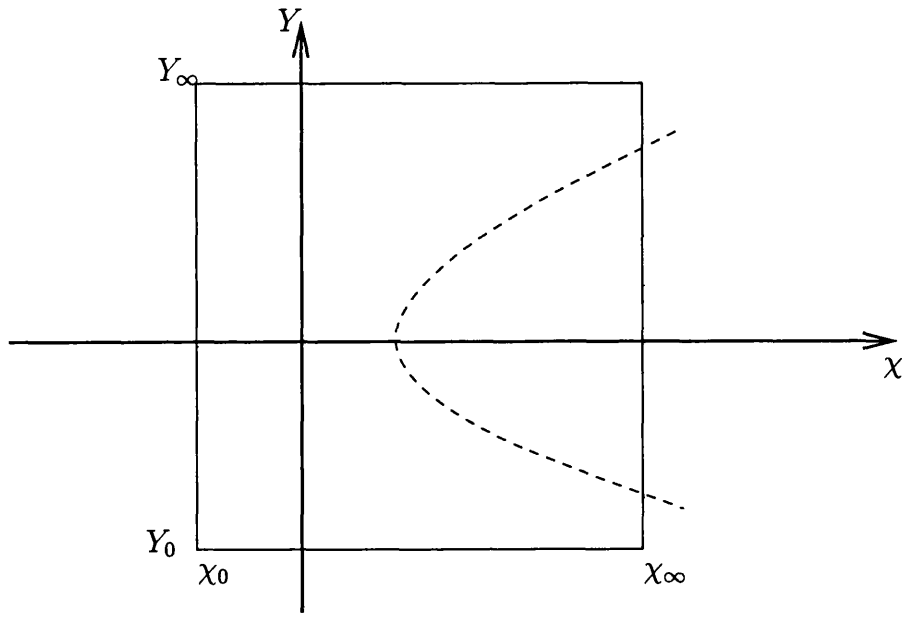

Figure 2.9: Grids for numerical method.

(2.235) it is found that,

$$\frac{dX}{dY} = -\frac{Y}{\tilde{p}_X(X)}. \tag{2.237}$$

Equations (2.234) and (2.235) may be rewritten as,

$$Y\frac{\partial \mathbf{v}}{\partial X} - \tilde{p}_X\frac{\partial \mathbf{v}}{\partial Y} = \tilde{\mathbf{R}}, \tag{2.238}$$

where,

$$\mathbf{v} = \begin{pmatrix} w \\ \tau \end{pmatrix}, \qquad \tilde{\mathbf{R}} = \begin{pmatrix} -\tilde{p}_z \\ w_z + m(X,T) \end{pmatrix}. \tag{2.239}$$

Alternatively, dividing by Y and substituting for $\frac{Y}{\tilde{p}_X}$ using (2.237) gives,

$$\frac{\partial \mathbf{v}}{\partial X} - \frac{dY}{dX}\frac{\partial \mathbf{v}}{\partial Y} = \frac{\tilde{\mathbf{R}}}{Y}, \tag{2.240}$$

and noting,

$$\frac{\tilde{\mathbf{R}}}{Y} = \frac{-\tilde{\mathbf{R}}}{\tilde{p}_X}\frac{dY}{dX}, \tag{2.241}$$

leads to,

$$d\mathbf{v} = \mathbf{R}dY, \qquad \text{with,} \qquad \mathbf{R} = \frac{-\tilde{\mathbf{R}}}{\tilde{p}_X}. \tag{2.242}$$

Thus the coupled equation system (2.234) and (2.235) may be simplified to,

$$\frac{d\mathbf{v}}{dY} = \mathbf{R}, \tag{2.243}$$

with $\mathbf{v}$ as before and,

$$\mathbf{R} = \begin{pmatrix} \frac{\tilde{p}_z}{\tilde{p}_X} \\ -\frac{w_z}{\tilde{p}_X} - \frac{m(X,T)}{\tilde{p}_X} \end{pmatrix}. \tag{2.244}$$

In the numerics that follow $\mathbf{v}$ is stored on an uniform grid in χ and Y, and so we write $\mathbf{v}(X,Y,z) = \tilde{\mathbf{v}}(\chi,\hat{Y},\hat{z})$ with $Y = \hat{Y}$ and $z = \hat{z}$. In these coordinates,

$$\mathbf{R} = \begin{pmatrix} \frac{\tilde{p}_{\hat{z}}}{\tilde{p}_X} \\ -\frac{w_{\hat{z}}}{\tilde{p}_X} - \frac{\tilde{p}_{\hat{z}}}{\tilde{p}_X} w_\chi - \frac{m(X,T)}{\tilde{p}_X} \end{pmatrix}. \tag{2.245}$$

We note here that these equations, as expected, are singular as $\tilde{p}_X \to 0$ and this signifies the generation of a vortex (chapter 3). The value of $\tilde{p}$ can be found, given χ and $\hat{Y}$ from $\chi = \frac{1}{2}\hat{Y}^2 + \tilde{p}(X,\hat{z})$. Having found τ, it is now possible to find the jump term. As the above gives τ on a $(\chi,\hat{Y})$ grid it seems sensible to try to compute the jump term using the values found on this grid. From (2.236) we obtain,

$$J_X = \int_{-\infty}^{\infty} \tau_X \, dY, \tag{2.246}$$

and using,

$$\tau_X = \tau_\chi \tilde{p}_X, \tag{2.247}$$

we derive an expression for the jump term,

$$J_X = \int_0^{\infty} \tilde{p}_X(\tau_\chi(\tilde{p} + \frac{1}{2}\hat{Y}^2, \hat{Y}) + \tau_\chi(\tilde{p} + \frac{1}{2}\hat{Y}^2, -\hat{Y}))\, dY. \tag{2.248}$$

Numerical Solution of the Jump Term

The system of equations given by (2.243), (2.245) and (2.248) are solved numerically to find the critical layer jump term. The values of the pressure and its derivatives that are required for the calculation of the critical layer jump term are found using Li's Benjamin-Ono solver (Li 1997), a summary of which has been given above. The jump term is calculated in two stages. The first stage is to calculate the vorticity and spanwise velocity in the critical layer. These equations are coupled and can be solved simultaneously although the spanwise derivative of the spanwise velocity (w_z) is lagged from the previous iterative step. The integration is completed using an adaptive fifth-order Runge-Kutta method, which includes an error check and so errors are kept very small. A simple trapezoidal method although very quick did not produce results of sufficient accuracy because of the fast changing forcing for $\chi \sim 1$ and some of the very small features of the equations, which can only be captured with an adaptive stepping method. The second stage is to integrate, again using an adaptive fifth-order Runge-Kutta method, the χ derivative of the vorticity in order to find the critical layer jump term.

The preliminary consideration is choosing the size of the grids for χ, z, X, Y. In practice it is impossible to avoid the use of asymptotics for the pressure as any plausible choice of χ and Y will give large values of pressure (through $\tilde{p} = -\frac{Y^2}{2} + \chi$). Therefore there are two considerations when choosing the ranges, Y_0, Y_∞, χ_0 and χ_∞. The first is to choose the Y_∞ large enough to capture the behaviour of the jump term, J_X. The jump term is found by solving the following ordinary differential equation,

$$\frac{\partial J_X}{\partial Y} = \tilde{p}_X \tau_\chi, \tag{2.249}$$

with $J_X(0) = 0$ and the jump term given by $J_X(\infty)$. Numerically this is given by $J_X(Y_\infty)$ and hence Y_∞ must be chosen to be large enough. The second consideration is to make sure the line of constant X does not cross $Y = Y_0$ before reaching $\chi = \chi_\infty$. Therefore it is this condition that is the most significant as Y_∞ must be increased

so that this requirement is satisfied. This condition is necessary in solving for w and τ as otherwise there exists complicated initial values for w and τ at $Y = Y_0$ as shown in the solution for w for a fixed z on a χ, Y grid in figure 2.16, where the initial value of w is zero. The choice is implemented using the relationship for the trajectories $\chi = \frac{Y^2}{2} + \tilde{p}$ and confirming, $\frac{Y_0^2}{2} > \chi_\infty$. These are considered in figure 2.9. The grid sizes (step sizes) are chosen small enough to maintain the accuracy of the solution. It is also worth considering the effect of changing the grid sizes. It is found that it is the stepping grid size in the Y direction that is important in maintaining the accuracy of the solution although as we use an adaptive solver to solve the differential equations this problem is not relevant.

The pressure and its derivatives found from the Benjamin-Ono solver are known on a stretched grid in X. This does not prove to be a problem when it comes to solving for the jump term as the integration interpolates with the pressure to find the pressure derivatives and hence no reference is made to the X grid. Integrating the equations (2.243) with (2.245) to find w and τ is completed using an adaptive Runge-Kutta method.

The Runge-Kutta method is a more complicated and more accurate version of the simple Euler method for advancing a solution to an ordinary differential equation over an interval. It works by combining information from several first order Euler style steps and then using the information obtained to match a Taylor series expansion up to a higher order (Acton 1970, Press *et al.* 1986). The adaptivity of the Runge-Kutta method is introduced using the techniques explained in Press *et al.* (1986) and uses a step doubling approach. This takes each step twice, once as a full step, then as two half steps. The values can be compared and the stepsize varied to attain the required accuracy of the solution. The algorithm is supplied by Press *et al.* (1986) and it is a fifth-order Cash-Karp Runge-Kutta method.

Boundary conditions are needed for w and τ. From the limits of the integrals w and τ in equations (2.98) and (2.105) respectively we assume that the values of w and τ are very small at Y_0. The integration proceeds by taking Y from Y_0 to Y_∞ for

each χ, with the pressure at a specific χ, Y given by $\tilde{p} = -\frac{Y^2}{2} + \chi$. This value of the pressure is used with polynomial interpolation of fourth order to find the necessary derivatives of pressure. This relation for the pressure forces the use of asymptotics to find the values of $\tilde{p}_X$, $\tilde{p}_z$ and $\tilde{p}_T$ as if χ and Y are large then the pressure is greater than the earlier calculated pressures.

The spanwise derivative of pressure is zero at this large X position since the spanwise disturbance is localised near $X = 0$. The asymptotic values for the derivatives are found if we consider,

$$\tilde{p}_T + \tilde{p}\tilde{p}_X = 0. \tag{2.250}$$

We assume that the Cauchy Hilbert integral and the jump term are small for large X, which is reasonable as they are confined in X. We look for a similarity solution of the form,

$$\tilde{p} = |T|^{1/2} f\left(\frac{X}{|T|^{3/2}}\right). \tag{2.251}$$

There are two cases to consider, positive and negative T. We will show the derivation for $T < 0$ as the derivation for $T > 0$ is similar and the resulting asymptotic form of $\tilde{p}_X$ is identical. On substitution into 2.250 we have,

$$-\frac{1}{2}f + \frac{3}{2}\eta f' + ff' = 0, \qquad \text{where,} \qquad \eta = \frac{X}{|T|^{3/2}}. \tag{2.252}$$

The pressure satisfies, $X = \tilde{p}^3 + \tilde{p}$ for large X and hence $\eta = -(f^3 + f)$ and $1 = -(3f^2 + 1)f'$ after differentiating. Hence,

$$\tilde{p}_X = \frac{1}{T}f' = \frac{-1}{T}\frac{1}{3f^2 + 1} = \frac{-1}{3\tilde{p}^2 + T}, \tag{2.253}$$

which gives the result, $\tilde{p}_X = \frac{-1}{3\tilde{p}^2 + |T|}$ for general T. Also $\tilde{p}_T = -\tilde{p}\tilde{p}_X = \frac{\tilde{p}}{3\tilde{p}^2 + |T|}$. At the points where these asymptotes are implemented, $\tilde{p}^2 \gg |T|$ and so the influence of time is not significant.

For the calculation of τ; w_χ and w_z have all been calculated on an uniform χ, Y grid and hence are known at the required (χ, Y) calculation points with the implication

that there is no interpolation necessary. The value of w_z is lagged from the previous iterative step. The result for τ (and τ_χ) (in figure 2.17 in section 2.5.1) shows a large jet at $\chi \sim 1$ and $Y \to \infty$. This jet seems to grow for both. This jet could be a cause of major complications but it was found in the previous section that the jet integrates to zero.

The values of w and τ at each integration step are saved in preparation for the next stage in the calculation, which is to find τ_χ. The τ_χ is then integrated to find the jump term as the theory shown earlier states. τ_χ (and w_z, w_χ) are calculated using a four point difference equation,

if $j = 1$ then,

$$\tau_\chi^{j,k} = \frac{1}{6d\chi}\left\{11\tau^{j,k} + 18\tau^{j+1,k} - 9\tau^{j+2,k} + 2\tau^{j+3,k}\right\}, \tag{2.254a}$$

if $j = 2$ then,

$$\tau_\chi^{j,k} = \frac{1}{6d\chi}\left\{-2\tau^{j,k} - 3\tau^{j+1,k} + 6\tau^{j+2,k} - \tau^{j+3,k}\right\}, \tag{2.254b}$$

if $2 < j < N$ then,

$$\tau_\chi^{j,k} = \frac{1}{6d\chi}\left\{\tau^{j-2,k} - 6\tau^{j-1,k} + 3\tau^{j,k} + 2\tau^{j+1,k}\right\}, \tag{2.254c}$$

if $j = N$ then,

$$\tau_\chi^{j,k} = \frac{1}{6d\chi}\left\{-2\tau^{j-3,k} + 9\tau^{j-2,k} - 18\tau^{j-1,k} + 11\tau^{j,k}\right\}. \tag{2.254d}$$

This is supplied by Abramowitz & Stegun (1964 *page 914*) where N is the number of χ points and $d\chi = \frac{1}{N}(\chi_\infty - \chi_0)$. The solution of the differential equation to find the jump term (2.249) is computed using a simple trapezium method, which we have verified gives sufficient accuracy. The initial value of the jump term $J_X(0)$ is 0 and the method propagates to find $J_X(Y_\infty)$, the value of interest.

2.5.1 Plots of the critical layer solution

As described in section 2.1.1 the three-dimensionality is introduced with an initial disturbance for the pressure given by,

$$\tilde{p} = \tilde{p}_0 + 0.1Xe^{-X^2}e^{-z^2}, \tag{2.255}$$

$$\tilde{p}_X = \tilde{p}_{0X} + 0.1e^{-X^2}e^{-z^2} - 0.2X^2e^{-X^2}e^{-z^2}, \tag{2.256}$$

where $\tilde{p}_0$ is the initial two-dimensional pressure and is given by the initial condition on page 74. The numerical code perturbs the initial two-dimensional pressure with a three-dimensional disturbance, which is allowed to vary as time progresses. This disturbance satisfies the condition that,

$$\int_{-\infty}^{\infty} \tilde{p}_z(z, X)\, dX = 0, \tag{2.257}$$

which is necessary as otherwise the size of the jump term would be much greater than the other terms in the Benjamin-Ono equation as shown in section 2.2. In the results that follow the spanwise disturbance is small. This relative weakness is clearly shown in the plot of pressure in figures 2.10 and 2.11, which show very little difference between the different spanwise pressures or the pressure streamwise derivative. The existence of a three-dimensional disturbance is verified by figure 2.12, which shows the initial spanwise derivative, $\tilde{p}_z$. The choice of spanwise disturbance given by (2.255) is such that the value of $\tilde{p}_z$ reaches a peak as it moves out with increasing z before diminishing as z increases further. This facet features predominantly in the plots of the spanwise velocity and vorticity. This is expected, of course, since $\tilde{p}_z$ is the main contributor to the spanwise velocity. Before we turn our attention to the three-dimensional critical layer problem we consider, briefly, the two-dimensional problem but with the three-dimensional disturbance described by (2.255). It is worth looking at these so that comparisons can be made with the three-dimensional plots shown later. We note that all plots refer to the first time step since the large values of τ for large χ do not allow us to solve the jump term in the general case.

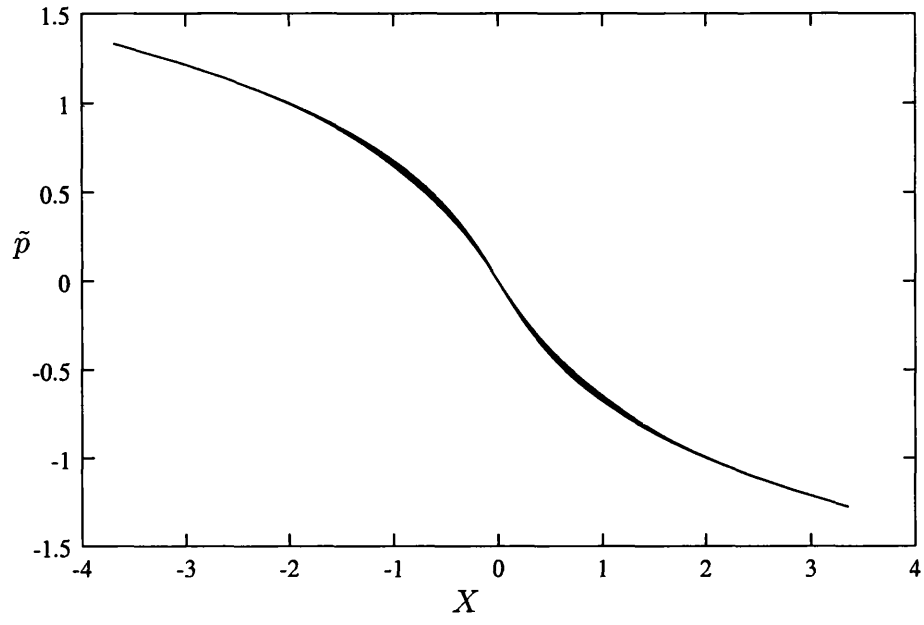

Figure 2.10: Initial pressure distribution plotted for all z.

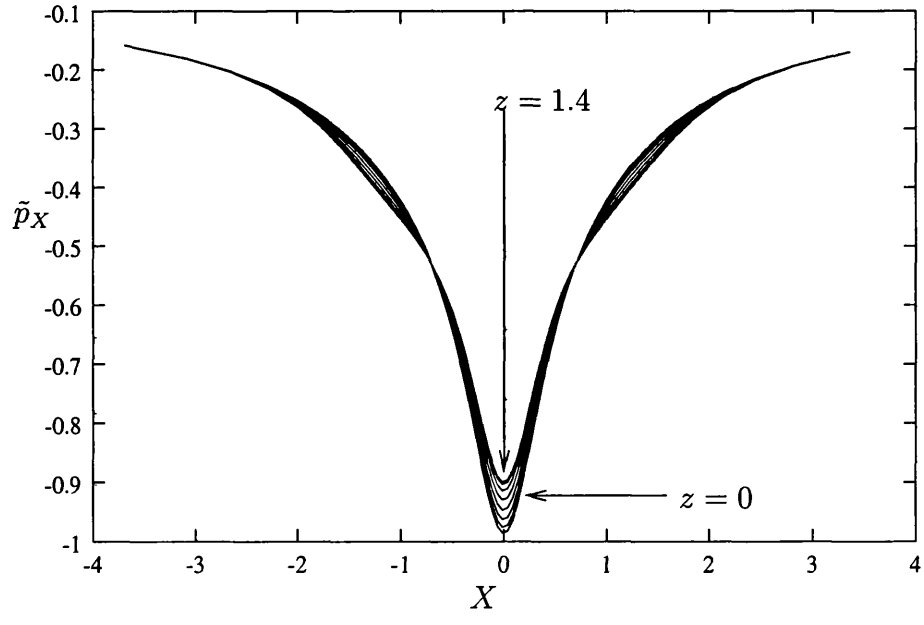

Figure 2.11: Initial streamwise derivative of the pressure plotted for all z.

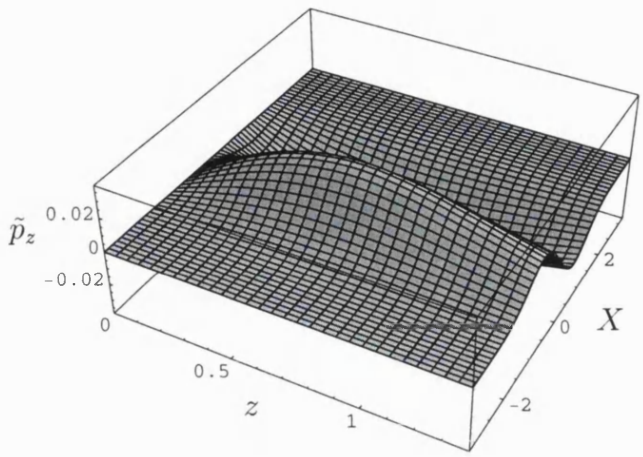

Figure 2.12: Initial spanwise derivative of the pressure.

The two-dimensional critical layer solution

We present three plots in figures 2.13 - 2.15 for the two-dimensional case at the first time step, which show the vorticity on (X, Y) and (χ, Y) grids and the jump term. These plots are solutions of the following sets of equations,

$$Y\tau_X - \tilde{p}_X\tau_Y = 0.1(\tilde{p}_T + \tilde{p}\tilde{p}_X), \tag{2.258}$$

and,

$$J_X = 2\int_0^\infty \tau_X \, dY. \tag{2.259}$$

Our boundary conditions are that $\tau \to 0$ as $X \to \infty$ when $Y < 0$. The choice of constants for the forcing in (2.258) is not important for our present study. The pressure is as described in (2.255). The jump term is shown in figure 2.13. The most notable feature is how little influence the three-dimensional perturbation has had on the jump term. The jump term is similar to the plots of the jump term found in Li (1997). In figures 2.14 and 2.15, the plots of τ on both grids show the significant contribution occurs for characteristics with $\chi \sim 1$. The characteristic follows a path, given by $\frac{Y^2}{2} = \chi - \tilde{p}(X)$ from $X = \infty$, $Y < 0$ to $X = \infty$, $Y > 0$. Figure 2.15 shows

that this characteristic only picks up vorticity after passing through the region with $X \approx 0$. An important feature of this plot is that there is none of the divergent behaviour for large χ, which we see in the plots of the three-dimensional vorticity in figure 2.21. The region of large χ, which causes problems in the three-dimensional case corresponds to large X and large positive Y which are characteristics that have completed large trajectories as we will explain in section 2.6.

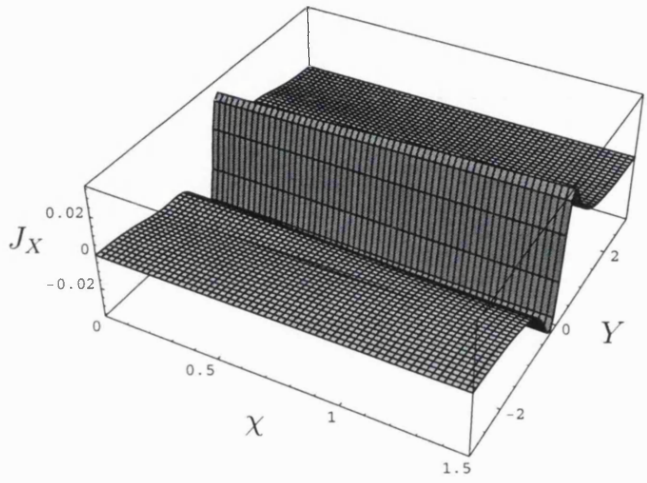

Figure 2.13: The two-dimensional jump term at the first time step.

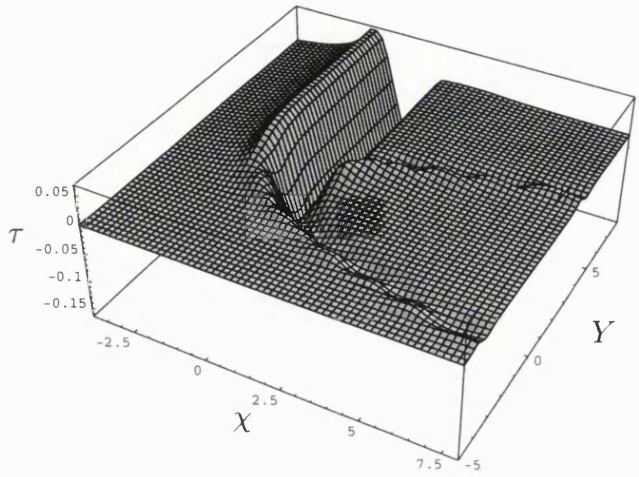

Figure 2.14: The two-dimensional vorticity at the first time step on a (χ, Y) grid.

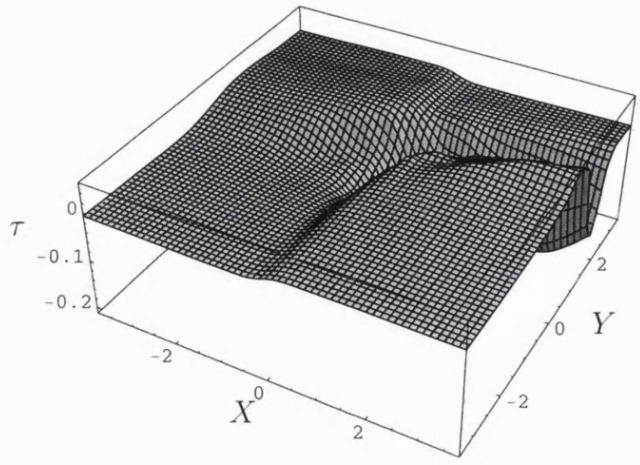

Figure 2.15: The two-dimensional vorticity at the first time step on a (X, Y) grid.

The Three-dimensional critical layer

We now move on to the behaviour of the critical layer at the first time step with the inclusion of a spanwise influence. Here we present the results of the numerical method, which solves,

$$Yw_X - \tilde{p}_X w_Y = -\tilde{p}_z, \tag{2.260}$$

$$Y\tau_X - \tilde{p}_X \tau_Y = w_z, \tag{2.261}$$

$$J_X = 2\int_0^\infty \tau_X dY, \tag{2.262}$$

with $w = 0$, $\tau = 0$ for $X \to \infty$ with $Y < 0$. As described on pages 78 - 80, the method solves for w and τ on a (χ, Y) grid. We therefore begin the description of the results with plots of w and τ printed on a (χ, Y) grid in figures 2.16 - 2.18. As we explain in this section the significant features of the spanwise velocity and vorticity are the regions where $\chi \sim 1$ (the bulk of the flow studied in 2.4) and the very large values of the vorticity for large χ. In section 2.4 we confirmed that the bulk of the flow does not cause a problem in solving for the jump term. However in section 2.6 we confirm that the large values of τ for large χ do adversely impact the jump term leading to a breakdown in the derived governing equations.

In figures 2.19 - 2.22 we show results for w and τ on a (X, Y) grid, which show the features of the critical layer solutions in a more intuitive way. In figures 2.23 - 2.25 we show plots of w and τ on a (z, Y) grid for a fixed X, which shows the influence of the spanwise variation. Towards the end of this section, on page 93, we study the critical layer equations for a model pressure. This analysis leads to an asymptotic expansion for the jump term, which together with the plots in figures 2.26 - 2.29 confirms the accuracy of the numerical method. This also verifies the result of section 2.3.1 that the jump term is zero for linear pressure.

Figure 2.16 shows a significant region for $-1 < \chi < 1$, $Y > 0$ where the bulk of the non-zero spanwise velocity exists. This is the non-zero bulk of the flow region

studied in section 2.4. The region near $X \approx 0$ is where the spanwise disturbance of the pressure (i.e. $\tilde{p}_z$) is greatest and so it is the integration of $\tilde{p}_z$ that causes this non-zero region. We should also note that $\tilde{p}_X$'s behaviour near $X \approx 0$ is at its most significant, which explains a similar non-zero region near $X \approx 0$ for all Y in the two-dimensional equivalent in figure 2.15. The plot in figure 2.17 on a (χ, Y) grid clearly show the worry with the strong jet as $Y \to \infty$ with $\chi \sim 1$ but the earlier study in section 2.4 confirms that this jet does not impact on the critical layer jump term. Another facet of the τ, not visible in figure 2.17 but shown by capping the large jet in figure 2.18 is the decrease in the value for $\chi \gg 1$ and $Y \gg 1$. Although not obvious here the feature shows itself very clearly in the figures of τ on a (X, Y) grid and additionally we show later that this feature leads to the breakdown of the proposed theory.

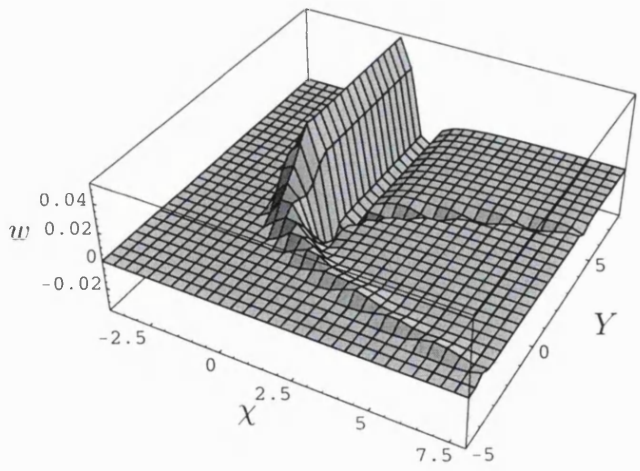

Figure 2.16: The spanwise velocity on a χ, Y grid at the first time step for a fixed $z = 0.2$.

We next show a set of figures (in 2.19 - 2.22) showing w, w_z, w_χ, τ and τ_χ at one spanwise point, $(z = 0.2)$ which is near the centre of the vortex. We consider the important features of these plots in turn beginning with w. The spanwise velocity in figure 2.19 is in agreement with analysis as it is non-zero for the jet described earlier. The main characteristics contributing to w are those with $\chi \sim 1$. The

characteristic picks up the forcing on w as it passes through $X = O(1)$. This occurs when $\chi - \frac{Y^2}{2} = \tilde{p}$ is small. If $|\chi - \frac{y^2}{2}|$ is large then the pressure is large, which implies $\tilde{p}_z = 0$ and hence w should equal zero. The other non-zero region appears for all Y with $X \approx 0$. This does not refer to one characteristic in particular but to several characteristics that pick up and then lose forcing as they pass through the region $X \approx 0$. The forcing on w is non-zero since here,

$$\left|\chi - \frac{Y^2}{2}\right| \sim 1,$$

even though Y and χ are large. The characteristics in this region return to almost zero after they leave this region. In practice they do not return to zero, which numerically, contributes to the large values of τ for large χ.

We also note that the jet of w is not growing as $X \to \infty$, in agreement with the analysis of section 2.4. The main forcing for τ is w_z, shown in figure 2.20, and w_z does not show any of the potential problems associated with τ.

In the plot of τ in figure 2.21 there are two clear features. There is the growing jet, which we have shown does not influence the jump term and the unexpectedly large values as $\chi \to \infty$, which we explain in section 2.6. The plot of τ_χ in figure 2.22 does not have the divergent feature and hence it was thought that it might be possible to calculate the jump term. The analysis in section 2.6.1 will confirm that this is not the case.

The set of figures (2.23 - 2.25) of w, w_z and τ on a (z, Y) grid highlights the significance of the chosen three-dimensional pressure perturbation. Several of the features of $\tilde{p}_z$, shown earlier in figure 2.12, are clear in these sets of data. The peak near $z = 0.6$ is shown in w in figure 2.23. In figures 2.24 and 2.25 we see that it is the influence of $\tilde{p}_{zz}$ that dominates. This is due to the importance of w_z in the solution of τ.

Model Pressure

The following section uses simple analysis to confirm the accuracy of the numerical method. In section 2.3.1 we showed that if the two-dimensional pressure is linear ($\tilde{p}_X \approx -1$) and the three-dimensional perturbation is small then the jump term is zero. We find agreement between our numerical results and the result of section 2.3.1 by considering asymptotic values of the jump term. We can also evaluate w analytically so that we can verify the intermediate steps of the numerical method.

We use a model pressure for the pressure forcing in which we may find some results analytically and compare these with results found numerically. In this case we consider a model three-dimensional pressure forcing implemented using,

$$\tilde{p} = -X + \lambda X e^{-X^2} e^{-z^2}, \tag{2.263}$$

with $\lambda \ll 1$. The solution for w at $Y = 0$ is,

$$w = \frac{1}{\sqrt{2}} \int_{\infty}^{X} \frac{\tilde{p}_z(z,s)}{\sqrt{\tilde{p}(z,X) - \tilde{p}(z,s)}}\, ds. \tag{2.264}$$

This is obtained directly from the integrals given in (2.95) on page 44, with $\mathrm{sgn}(Y) = -1$ and the order of the limits swapped so that we can remove the negative sign. On substitution of the model pressure into this expression for w at $Y = 0$ we find, at leading order,

$$w \sim \frac{2\lambda z e^{-z^2}}{\sqrt{2}} \int_{\infty}^{X} \frac{s e^{-s^2}}{\sqrt{s - X}}\, ds. \tag{2.265}$$

We then compare values of w from the above with the w found numerically using the model pressure and we find good agreement. For example at $(z, X, Y) = (0.2, 0, 0)$ the numerical value for w is 0.01665, which is identical to the analytical value of w to five decimal places. Likewise good agreement is found with w_z although there is some decline in accuracy. For example at $(z, X, Y) = (0.2, 0, 0)$, the numerically found value of w_z is 0.07666 to five decimal places where as the analytical form predicts a value of 0.07659. We can justify the accuracy for τ by arguing as follows.

The numerical calculations for w and τ are similar and given an accurate forcing for $\tilde{p}_z$, the numerical method finds an accurate expression for w. Using this argument we may assume that τ is calculated correctly since we have verified that w_z is accurate.

The analysis of section 2.3.1 shows that the jump term, J_X should equal zero for this model pressure. As explained earlier the jump term is found by integrating the even part of the shear, τ between zero and infinity. Hence we may write J as,

$$\begin{aligned} J &= \int_0^L \tau_E \, dY + \int_L^\infty \tau_E \, dY \\ &= J^L + J^a \end{aligned} \tag{2.266}$$

with the first integral found numerically. The second integral we find analytically as follows. The linearised expression for the even part of τ is,

$$\tau_E = -\left\{ \int_{X_0}^{X} \frac{\tilde{p}_{zz}(z,t)\eta_X}{\eta_t} \, dt + \int_X^\infty \tilde{p}_{zz}(z,t) \, dt \right\}. \tag{2.267}$$

from equation (2.136) in section 2.3.1 with $\eta_X = \sqrt{2}\sqrt{\chi + X}$. Hence the asymptotic form of J is given by,

$$J^a = -\int_L^\infty \left\{ \int_{X_0}^{X} \frac{\tilde{p}_{zz}(z,t)\eta_X}{\eta_t} \, dt + \int_X^\infty \tilde{p}_{zz}(z,t) \, dt \right\} dY. \tag{2.268}$$

We introduce a change of variable with, $\frac{Y^2}{2} = \chi + X$ so that,

$$J^a = -\int_{\frac{L^2}{2}-X}^\infty \frac{1}{\eta_X} \left\{ \int_{X_0}^{X} \frac{\tilde{p}_{zz}(z,t)\eta_X}{\eta_t} \, dt + \int_X^\infty \tilde{p}_{zz}(z,t) \, dt \right\} d\chi. \tag{2.269}$$

A change in the order of integration leads to,

$$\begin{aligned} J^a = \int_{X-\frac{L^2}{2}}^{X} \int_{\frac{L^2}{2}-X}^\infty \frac{\tilde{p}_{zz}(z,t)}{\eta_t} \, d\chi \, dt + \int_{-\infty}^{X-\frac{L^2}{2}} \int_{-t}^\infty \frac{\tilde{p}_{zz}(z,t)}{\eta_t} \, d\chi \, dt \\ + \int_X^\infty \int_{\frac{L^2}{2}-X}^\infty \frac{\tilde{p}_{zz}(z,t)}{\eta_X} \, d\chi \, dt. \end{aligned} \tag{2.270}$$

The infinite ends of the integrals tend to zero as $\tilde{p}_{zz}(z,t)$ is very small for large t and so we find,

$$J^a = \sqrt{2} \int_{X-\frac{L^2}{2}}^{X} \tilde{p}_{zz}(z,t) \sqrt{\frac{L^2}{2} - X + t} \, dt + \sqrt{2} \int_X^\infty \tilde{p}_{zz}(z,t) \sqrt{\frac{L^2}{2}} \, dt. \tag{2.271}$$

This expression for J^a can be rewritten into the following form,

$$J^a = \int_{-\infty}^{X} \tilde{p}_{zz}(z,t) \left\{ \sqrt{\frac{L^2}{2} - X + t} - \sqrt{\frac{L^2}{2}} \right\} dt + \int_{-\infty}^{X-\frac{L^2}{2}} \tilde{p}_{zz}(z,t) \sqrt{\frac{L^2}{2} - X + t}\, dt. \tag{2.272}$$

The second term above is small since L is large and $\tilde{p}_{zz}(z,t)$ is exponentially small for large absolute values of t. Hence we concentrate on the first term and expand the square root with L assumed large. Differentiating with respect to X leads to,

$$J_X^a = 2 \int_{-\infty}^{X} \left\{ -\frac{\tilde{p}_{zz}(z,t)}{L} + \frac{(t-X)\tilde{p}_{zz}(z,t)}{L^3} - \frac{3(t-X)^2 \tilde{p}_{zz}(z,t)}{L^5} + \ldots \right\} dt. \tag{2.273}$$

The expression in (2.273) is an approximation for the asymptotic values of the jump term. We have split the jump term, J_X into two parts, J_X^a and J_X^L. J_X^L is found using the numerical method, which we show in figure 2.26. We have used $L = 7.5$. This is non-zero, which implies that we do need to use the asymptotic expression for J_X^a in order to obtain an accurate result for the jump term. The plot in figure 2.27 shows the influence of including the term of order L^{-1} from (2.273). This has the required effect of substantially reducing the size of the jump term. Further addition of the terms of order L^{-3} and L^{-5} reduces the size of the jump term. We show the influence of adding further terms in the expansion of J_X^a. In figure 2.28 terms of order up to and including L^{-3} have been included. In figure 2.29 we show the plot of $J_X^a + J_X^L$, with J_X^a as given in (2.273) and here we are left with numerical noise only, which confirms the strong accuracy of the numerical method.

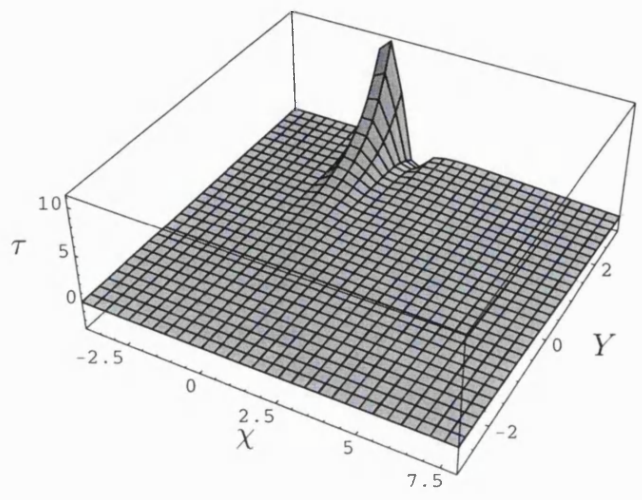

Figure 2.17: The spanwise vorticity on a χ, Y grid at the first time step for a fixed $z = 0.2$.

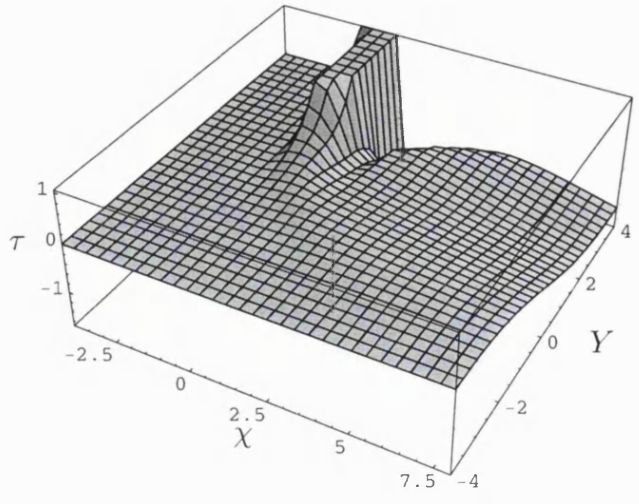

Figure 2.18: The spanwise vorticity on a χ, Y grid at the first time step for a fixed $z = 0.2$ showing problem with large χ.

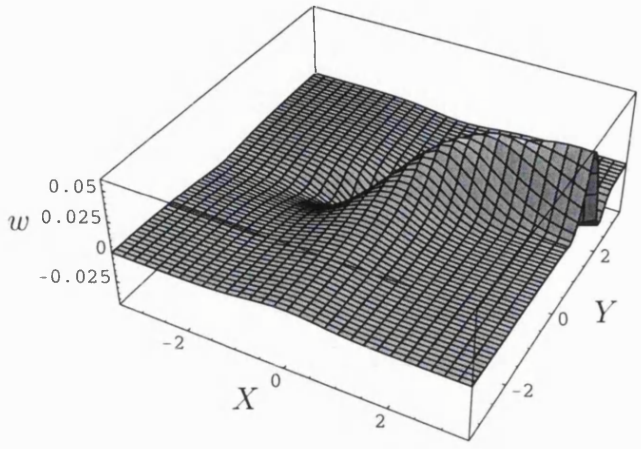

Figure 2.19: The spanwise velocity on a X, Y grid at the first time step for a fixed $z = 0.2$.

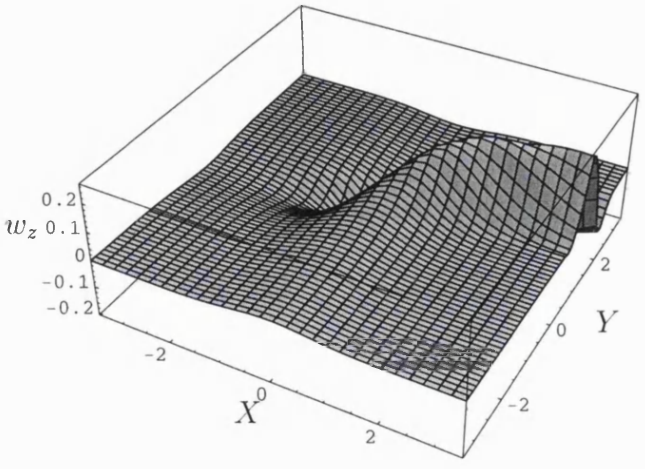

Figure 2.20: The spanwise derivative of the spanwise velocity on a X, Y grid at the first time step for a fixed $z = 0.2$.

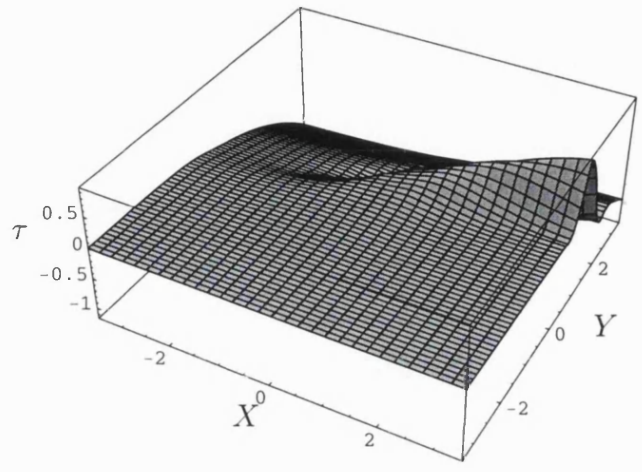

Figure 2.21: The spanwise vorticity on a X, Y grid at the first time step for a fixed $z = 0.2$.

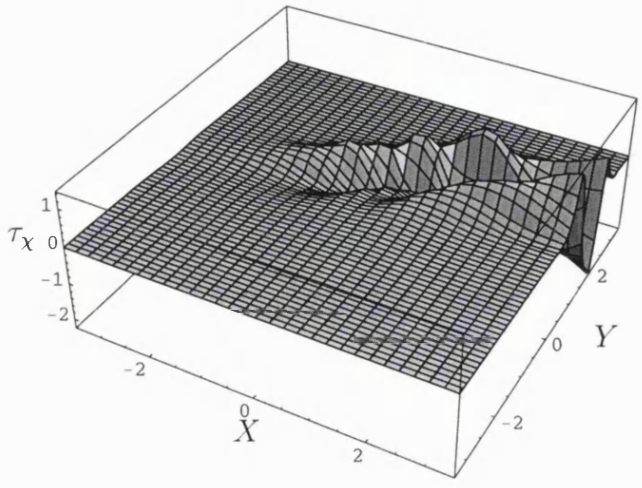

Figure 2.22: The χ derivative of the spanwise vorticity at the first time step on a X, Y grid for a fixed $z = 0.2$.

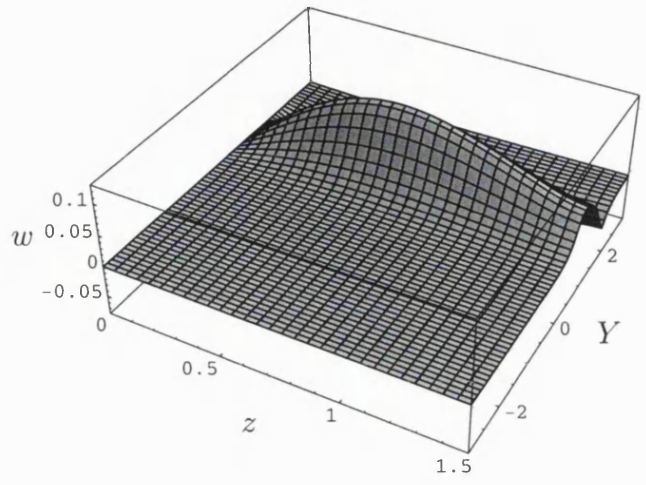

Figure 2.23: The spanwise velocity on a z, Y grid at the first time step with the streamwise point fixed ($X = 1.8$).

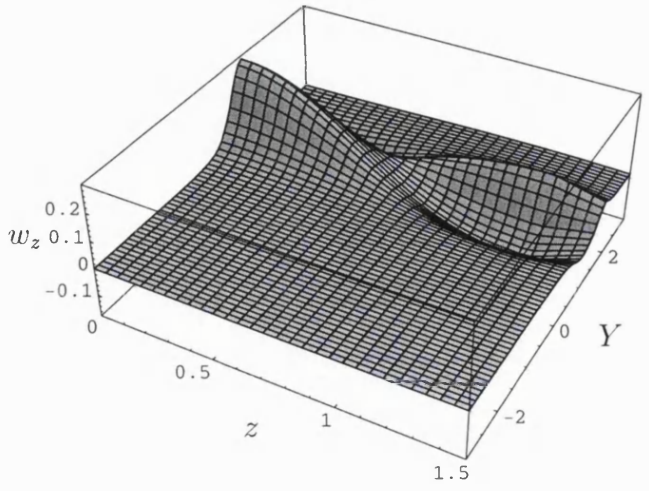

Figure 2.24: The spanwise derivative of the spanwise velocity on a z, Y grid at the first time step with the streamwise point fixed ($X = 1.8$).

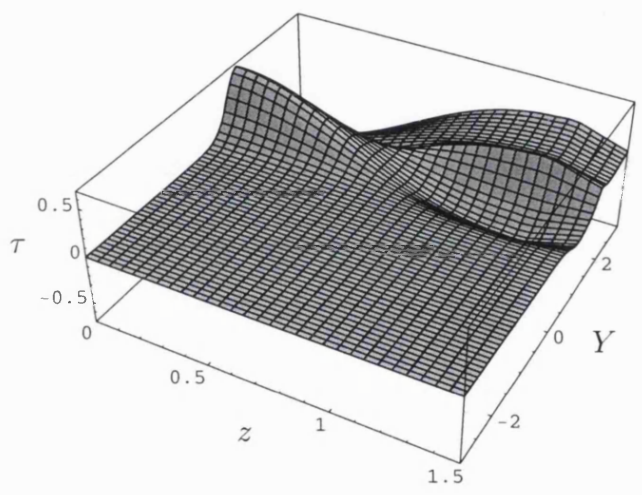

Figure 2.25: The spanwise vorticity on a z, Y grid at the first time step with the streamwise point fixed ($X = 1.8$).

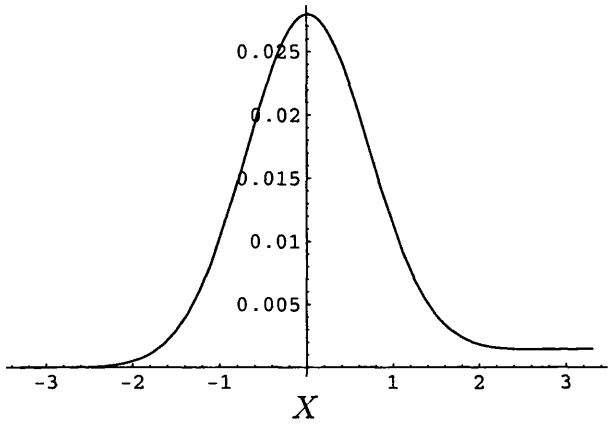

Figure 2.26: J_X^L for $z = 0.2$ with $L = 7.5$. J_X^L is defined on page 94.

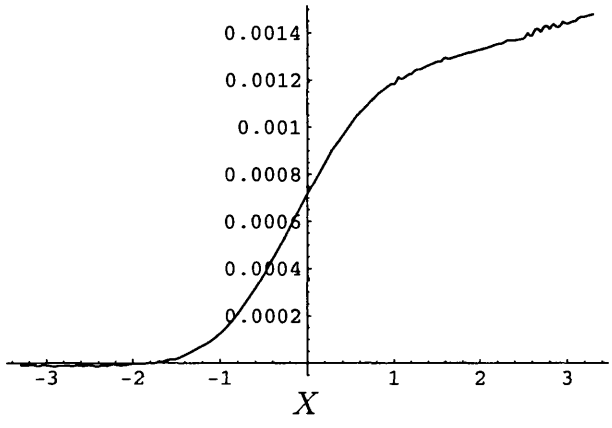

Figure 2.27: $J_X^L + (O(L^{-1})$ term of $J_X^a)$ for $z = 0.2$ with $L = 7.5$. A full description is given on page 95.

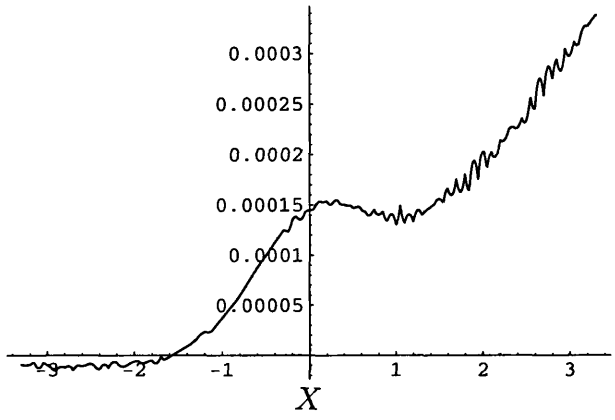

Figure 2.28: $J_X^L + (O(L^{-1})$ and $O(L^{-3})$ terms of $J_X^a)$ for $z = 0.2$ with $L = 7.5$. A full description is given on page 95.

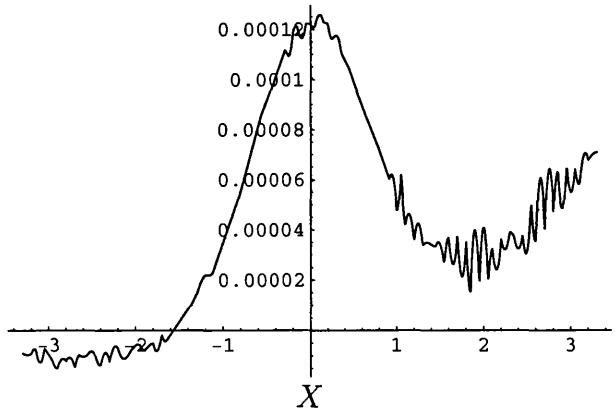

Figure 2.29: $J_X^L + (O(L^{-1})$, $O(L^{-3})$ and $O(L^{-5})$ terms of $J_X^a)$ for $z = 0.2$ with $L = 7.5$. A full description is given on page 95.

2.6 The Jump Term for large negative X

We attempted to introduce interaction from the jump term into the Benjamin-Ono solver. The result of allowing the jump term to interact with the pressure terms was after only a few iterations a large value of the jump term was encountered for large negative X. It is not the interaction that causes the problem but it is only when interaction is allowed do we see the problems in the numerical plots of the jump term. The cause of the divergence for large negative X can be seen in the plots of τ in figures 2.18 and 2.21. One of the contributions to this feature is the form of the boundary condition on the pressure. In the two sections that follow we consider the possible reasons and come to the conclusion that unsteady terms must be considered as they work to dissipate the large growth as $X \to -\infty$. Initially we show the feature predicted by the numerics to be true by studying the behaviour of w, τ and the jump term, J_X as $X \to -\infty$ for large χ before showing a derivation of the unsteady equations for large negative X.

2.6.1 Analysis for large χ

In the asymptotic analysis below it is the second order term in the expansion for $\frac{1}{\eta_X}$ that forces the large growth and so we focus on this term here. The significance of the analysis is to show that the numerical approach is accurate in predicting this divergent behaviour and that it is not due to instability in the numerical regime. It also shows the effect of different choices of the pressure boundary conditions and we find a condition on the form of this boundary condition.

The solution for w from (2.95) is,

$$w(z,X,\chi) = -\left\{\mathrm{sgn}(Y)\int_{X_0}^{X}\frac{\tilde{p}_z(z,t)}{\eta_t}\,dt + \int_{X_0}^{\infty}\frac{\tilde{p}_z(z,t)}{\eta_t}\,dt\right\}, \tag{2.274}$$

as before with $\eta_X = \sqrt{2}\left(\chi - \tilde{p}(z,X)\right)^{1/2}$. Here we are interested in the region where X is large and negative. This corresponds to large, positive χ and we assume that

$\chi \gg \tilde{p}$ in those regions, as it is here that w and τ are generated, as indicated in the plots of w in figure 2.19. In other words $\tilde{p}$ must be of order 1 for the forcing on w to be non-zero. This assumption is equivalent to assuming that where $\chi \sim \tilde{p}$ the spanwise derivative of the pressure is very small ($\tilde{p}_z \ll 1$), which is true as the spanwise disturbance is localised near $X = 0$. This is consistent since very little w is generated if the forcing on w is very small. As χ is large we can write,

$$\frac{1}{\eta_X} = \frac{1}{(2\chi)^{1/2}}\left(1 + \frac{\tilde{p}}{2\chi} + \ldots\right), \tag{2.275}$$

so that,

$$\begin{aligned} w &= \frac{1}{(2\chi)^{1/2}}\left\{\int_{\infty}^{X_0} \tilde{p}_z\, dt + \mathrm{sgn}(Y)\int_{X}^{X_0} \tilde{p}_z\, dt\right\} \\ &+ \frac{1}{(2\chi)^{3/2}}\left\{\int_{\infty}^{X_0} \tilde{p}\tilde{p}_z\, dt + \mathrm{sgn}(Y)\int_{X}^{X_0} \tilde{p}\tilde{p}_z\, dt\right\} + \ldots . \end{aligned} \tag{2.276}$$

If we take $X_0 \to -\infty$ and the condition that controls the size of the jump term, $\int_{-\infty}^{\infty} \tilde{p}_z dx = 0$ (derived on page 48), then,

$$\begin{aligned} w &= \frac{1}{(2\chi)^{1/2}}\left\{\mathrm{sgn}(Y)\int_{X}^{-\infty} \tilde{p}_z\, dt\right\} \\ &+ \frac{1}{(2\chi)^{3/2}}\left\{\int_{\infty}^{-\infty} \tilde{p}\tilde{p}_z\, dt + \mathrm{sgn}(Y)\int_{X}^{-\infty} \tilde{p}\tilde{p}_z\, dt\right\} + \ldots . \end{aligned} \tag{2.277}$$

A further assumption that $X \to -\infty$ then forces the term of order $\frac{1}{(2\chi)^{1/2}}$ to be zero. Hence,

$$w = \frac{1}{(2\chi)^{3/2}} I, \qquad \text{where,} \qquad I = \int_{\infty}^{-\infty} \tilde{p}\tilde{p}_z\, dt. \tag{2.278}$$

The vorticity τ is given by,

$$\frac{\partial \tau}{\partial X} = \mathrm{sgn}(Y)\frac{1}{\eta_X}\left\{\frac{\partial w}{\partial z} + \tilde{p}_z\frac{\partial w}{\partial \chi}\right\}, \tag{2.279}$$

which becomes $\frac{\partial \tau}{\partial X} = \mathrm{sgn}(Y)\frac{1}{\eta_X}\frac{\partial w}{\partial z}$, assuming a small $\tilde{p}_z$. We consider $\frac{\partial \tau}{\partial X}$ for a fixed χ,

$$\left.\frac{\partial \tau}{\partial X}\right|_{\chi} = \frac{1}{(2\chi)^{3/2}}\frac{1}{\eta_X}\mathrm{sgn}(Y) I_z. \tag{2.280}$$

For $Y \sim 1$, $\chi \sim \tilde{p}$ we integrate to find,

$$\tau = -\int_0^{X_0} \frac{1}{\sqrt{2}\sqrt{\chi-\tilde{p}}} \frac{1}{(2\chi)^{3/2}} I_z \, dt, \tag{2.281}$$

$$= \frac{1}{(2\chi)^{3/2}} I_z \int_0^{X_0} \frac{1}{\sqrt{2}\sqrt{\chi+t^{1/3}}} \, dt. \tag{2.282}$$

This is the contribution to τ from large χ characteristics as they pass through the negative Y region between 0 and X, corresponding to the region in which the divergence in τ is generated. Furthermore $X_0 \sim \chi^3$ as $\chi = \tilde{p}(X_0)$ and $\tilde{p}(X_0) \sim X_0^{1/3}$. Therefore,

$$\tau = \frac{4}{5}\chi I_z. \tag{2.283}$$

This implies $\tau \sim \chi$, which agrees with a result that we will find on page 110 in the next section. Hence with L large,

$$\begin{aligned} J(X) &= \frac{4}{5} I_z \int_{\tilde{p}(X)}^{L} \frac{\chi}{\sqrt{2}\sqrt{\chi-\tilde{p}}} \, d\chi, \\ &= \frac{4}{\sqrt{25}} I_z \left[\frac{2}{3}\sqrt{\chi-\tilde{p}}(\chi+2\tilde{p}) \right]_{\tilde{p}(X)}^{L}, \\ &= \frac{2}{3} L^{3/2} \left(1+\frac{2\tilde{p}}{L}\right)\left(1-\frac{\tilde{p}}{2L}+\ldots\right). \end{aligned} \tag{2.284}$$

This yields a jump term, J_X of order $\tilde{p}_X L^{1/2}$, which is divergent as $L \to \infty$. This confirms that the numerical results for the interacting jump term are correct.

We may consider the pressure, $\tilde{p}$ to be equal to some unknown power of X as $|X| \to \infty$ by writing $\tilde{p} \sim X^n$. In this case a study of (2.281) as $|X| \to \infty$ shows a possible way further progress could be made. If $\tilde{p} \sim X^n$ as $|X| \to \infty$ so that

$X_0 \sim \chi^{1/n}$ into (2.281),

$$\begin{aligned}
\tau &\sim \frac{1}{(2\chi)^{3/2}} \int_0^{\chi^{1/n}} \frac{I_z}{\sqrt{2}\sqrt{\chi - |X|^n}} dX, \\
&\sim \frac{1}{(2\chi)^{3/2}} \int_0^{\chi^{1/n}} \frac{1}{\sqrt{2\chi}} \frac{dX}{\sqrt{1 - (|X|^n/\chi)}}, && (2.285) \\
&\sim \frac{1}{(2\chi)^2} \int_0^{\chi^{1/n}} \left(1 + \frac{|X|^n}{\chi} + \ldots\right) dX, && (2.286) \\
&\sim \frac{1}{\chi^2} \chi^{1/n}. && (2.287)
\end{aligned}$$

Hence a convergent jump term exists for $n > \frac{1}{2}$. This suggests further numerical work could be pursued by taking a pressure with boundary conditions such that $\tilde{p} \sim X^n$ and $n > \frac{1}{2}$. The work on a linear pressure forcing (i.e. $n = 1$) in section 2.3.1 taking $X \to -\infty$ ($\chi \to \infty$) yields $\tau \sim \chi^{-1}$, in agreement with this analysis.

The reason why the large values of the jump term only appear in the interacting case is because $\tilde{p}_X$ is small for large X but not zero and so this divergence will only show itself when the jump term is allowed to interact with the pressure in the Benjamin-Ono equation. The data shows that the convergent part is nudging the pressure, which itself nudges the jump term to show its true behaviour. The analysis above allows us to disregard the possibility that it is unstable errors causing the growth for $X \sim -\infty$.

2.6.2 The Interaction Upstream

Having confirmed the results of our numerical method to be correct regarding the prediction of a divergent jump term as $X \to -\infty$, we now consider the reasons behind this phenomena and attempt to identify the features of the flow that we have neglected, which could dissipate any divergent integrals. It will be found below that for large negative X there is a region where unsteady influences should not be neglected. We will show that this occurs when the ratio of the normal distance within the critical layer, M and the streamwise distance, assumed large, designated by L, is roughly equal to the ratio of the square root of a defined short time scale factor, σ and the critical layer thickness, ϖ, that is $\frac{M}{L} \sim \frac{\sigma^{1/2}}{\varpi}$. Within this region the unsteady equations are solved to find that unsteady effects do resolve the problems found within the numerical results.

This section is written in two sections. In the first part of this section we rederive the scalings for the governing equations in order to establish the region where unsteady effects are important. We consider the relative sizes of the terms in the bulk of the flow and then consider the equations as the critical layer is approached. It is here we find a condition for the unsteady effects by taking the solutions for large Y, which gives a scaling for Y. The unsteady equations found can then be solved, which we achieve in the second part of this analysis.

Scalings and identifying the unsteady region

Our approach in providing a deeper understanding of the flow solution for large χ is to reconsider the scalings and expansions used at the beginning of chapter 2 in section 2.1. We may reconsider the scalings through a study of the scalings that are in effect in between those of chapter 2 (step 2 in Li *et al.* 1998) and those of step 1 (Smith 1988 and summarised at the beginning of section 2.1). We introduce, σ where $\sigma = 1$ corresponds to step 1 and $\sigma = \epsilon$ corresponds to the scalings of step 2. We also introduce $\triangle$ and l, which allow a variation in the scalings for the spanwise

velocity and spanwise length scale respectively. We have the expansions in the bulk of the flow given by,

$$\bar{u} = \epsilon[u_0 + \sigma^{1/2}\tilde{u}_1 + \sigma\tilde{u}_2 + ...], \tag{2.288}$$

$$\bar{v} = \frac{\epsilon^3}{\sigma^{3/2}}[\sigma^{1/2}\tilde{v}_1 + ...], \tag{2.289}$$

$$\bar{p} = \epsilon^2[p_0 + \sigma^{1/2}\tilde{p}_1 + ...], \tag{2.290}$$

$$\bar{w} = \frac{\epsilon l}{\sigma}[\triangle\tilde{w} + ...]. \tag{2.291}$$

We are in a frame of reference moving with speed c and the variables in the streamwise, normal and spanwise directions are,

$$t = \text{constant} + \epsilon^2\sigma T, \tag{2.292}$$

$$y = \epsilon^5 Y, \tag{2.293}$$

$$x = c\epsilon^4 T + \epsilon^3\sigma^{3/2}X, \tag{2.294}$$

$$z = \epsilon^3 l Z. \tag{2.295}$$

Our aim in the analysis that follows is to fix $\triangle$. We will then use σ to derive new scalings that allow us to include the influence of the unsteady terms. For reference the Navier-Stokes equations are,

$$\bar{u}_x + \bar{v}_y + \bar{w}_z = 0, \tag{2.296}$$

$$\bar{u}_t + \bar{u}\bar{u}_x + \bar{v}\bar{u}_y + \bar{w}\bar{u}_z = -\bar{p}_x + \epsilon^8\left(\bar{u}_{yy} + \bar{v}_{yy} + \bar{w}_{zz}\right), \tag{2.297}$$

$$\bar{v}_t + \bar{u}\bar{v}_x + \bar{v}\bar{v}_y + \bar{w}\bar{v}_z = -\bar{p}_y + \epsilon^8\left(\bar{u}_{yy} + \bar{v}_{yy} + \bar{w}_{zz}\right), \tag{2.298}$$

$$\bar{w}_t + \bar{u}\bar{w}_x + \bar{v}\bar{w}_y + \bar{w}\bar{w}_z = -\bar{p}_z + \epsilon^8\left(\bar{u}_{yy} + \bar{v}_{yy} + \bar{w}_{zz}\right). \tag{2.299}$$

The requirement that the spanwise velocity is generated through the spanwise variation in $\tilde{p}_1$ (i.e. $u_0\tilde{w}_X \sim \tilde{p}_{1Z}$) implies that $l^2\triangle \sim \sigma^3$. Substituting the expansions ((2.288) - (2.291)) into (2.297) leads to,

$$\begin{aligned}(u_0 - c)\tilde{u}_{1X} + \tilde{v}_1 u_{0Y} &+ \sigma^{1/2}\left(\tilde{u}_{1T} + \tilde{u}_1\tilde{u}_{1X} + \tilde{v}_1\tilde{u}_{1Y}\right) \\ &+ \triangle\sigma^{1/2}\tilde{w}\tilde{u}_Z + \ldots = -\tilde{p}_{1X} + \sigma^{3/2}\tilde{u}_{1YY}.\end{aligned} \tag{2.300}$$

This equation holds in the bulk of the flow. We now consider the flow solution as the critical layer is approached. We introduce, ϖ, to denote the thickness of the critical layer. We may fix this by considering the relative sizes of the $u_0\tilde{u}_{1X}$ and $\tilde{v}_1\tilde{u}_{1Y}$ terms in (2.300) as the critical layer is approached and forcing the terms to be of the same size. Thus $\varpi^2 \sim \sigma^{1/2}$. Differentiating (2.300) with respect to Y leads to,

$$\begin{aligned} u_{0Y}\tilde{u}_{1Y} &+ (u_0 - c)\tilde{u}_{1XY} + \tilde{v}_{1Y}u_{0Y} + \tilde{v}_1 u_{0YY} \\ &+ \sigma^{1/2}\left(\tilde{u}_{1TY} + \tilde{u}_{1Y}\tilde{u}_{1X} + \tilde{u}_1\tilde{u}_{1XY} + \tilde{v}_{1Y}\tilde{u}_{1Y} + \tilde{v}_1\tilde{u}_{1YY}\right) \\ &+ \sigma^{1/2}\triangle(\tilde{w}\tilde{u}_z)_Y + \ldots = 0 + \sigma^{3/2}\tilde{u}_{1YYY}. \end{aligned} \tag{2.301}$$

We now write $\tau = \tilde{u}_{1Y}$ and use continuity to include w_z so that,

$$\begin{aligned} -\triangle\tilde{w}_z u_{0Y} + (u_0 - c)\tau_X &+ \tilde{v}_1 u_{0YY} + \sigma^{1/2}\left(\tau_T - \triangle\tilde{w}_z\tilde{u}_{1Y} + \tilde{u}\tau_X + \tilde{v}\tau_Y\right) \\ &+ \sigma^{1/2}\triangle(\tilde{w}\tilde{u}_z)_Y + \ldots = 0 + \sigma^{3/2}\tau_{YY}. \end{aligned} \tag{2.302}$$

In order to find the relative size of $\triangle$ in terms of σ we consider the balance between the first two terms in (2.302). We want the spanwise velocity to influence the jump term through the vorticity, τ. The jump term matches with $\tilde{u}_2$ outside the critical layer. Thus the τ that generates a jump, which we will define as τ^*, is of the same size as $\tilde{u}_{2Y}$ as the critical layer is approached. Therefore $\tau^* \sim \epsilon\sigma^{3/4}$. Hence a consideration of the balance between the first and second terms in (2.302) as the critical layer is approached leads to,

$$\frac{-\triangle}{\varpi} \sim \varpi\sigma^{3/4} \qquad \Rightarrow \qquad \triangle \sim \sigma^{5/4}. \tag{2.303}$$

We now have enough information to consider the behaviour for large Y and X. We use the expression for large Y found in (2.278) and write in terms of Y so that,

$$w_X \sim \frac{1}{Y^3}, \tag{2.304}$$

and we also have,

$$Y\tau_X \sim \frac{1}{Y^3}. \tag{2.305}$$

We fix the X scale as it is large X that is of most interest and so we assume $X = O(L)$, with L large and we write $Y = O(M)$. Therefore for large X,

$$\tau \sim \frac{L}{M^4}, \tag{2.306}$$

and,

$$J \sim \frac{L}{M^3}\varpi, \quad \text{and,} \quad J_X \sim \frac{1}{M^3} \tag{2.307}$$

The jump term is therefore convergent. There is still a problem with τ, if $L \gg M^4$, in which case unsteadiness affects τ when,

$$\frac{M}{L} \sim \frac{\sigma^{1/2}}{\varpi} \sim \sigma^{1/4}. \tag{2.308}$$

The above condition is found by considering the second and fourth term in (2.302) and fixing so that both terms are of the same size. In summary we have found the following, $\triangle \sim \sigma^{5/4}$, $\varpi \sim \sigma^{1/4}$ and therefore, $\frac{\triangle}{\varpi} \sim \sigma$.

As an aside we note that we may verify our derived scalings. On page 105 we found that $\tau \sim \chi$ for large negative X. Using the scalings derived here we find that for large $X \sim L$, we have $\tilde{p} \sim L^{1/3}$, from the boundary conditions on the pressure, and hence $\chi \sim \tilde{p} \sim M^2$ from the expression $\frac{Y^2}{2} = \chi - \tilde{p}$. Therefore $M^4 \sim \tilde{p}^2 \sim L^{2/3}$. Hence we obtain the size of τ to be,

$$\tau \sim L^{1/3}, \tag{2.309}$$

from (2.306). We find $\tau \sim \chi$ since $L^{1/3} \sim \tilde{p} \sim \chi$.

It is relatively straightforward to identify the sizes of the relative terms using the condition for unsteadiness, (2.308) and the condition that X is large, to firstly find, $L \sim \sigma^{-3/10}$ since $M \sim L^{1/6}$ for a fixed χ. Thus, $M \sim \sigma^{-1/20}$ and $\chi \sim \sigma^{-1/10}$. The equations holding for w and τ are unsteady with $X = \sigma^{-3/10}\bar{X}$ and $Y = \sigma^{-1/20}\bar{Y}$ such that,

$$\tilde{w}_T + \bar{Y}\tilde{w}_{\bar{X}} - \tilde{p}_{\bar{X}}\tilde{w}_{\bar{Y}} = 0, \tag{2.310}$$

$$\tilde{\tau}_T + \bar{Y}\tilde{\tau}_{\bar{X}} - \tilde{p}_{\bar{X}}\tilde{\tau}_{\bar{Y}} = \tilde{w}_z. \tag{2.311}$$

We have shown using a scaling argument that an unsteady region needs to be considered in solving the critical layer equations but that this unsteady region is far away from the main forcing for the critical layer jump term. The large χ characteristics here do not pass through the region where the pressure forces the jump term. The only forcing they will pass through is the small $\frac{1}{Y^2}$ near $X = 0$. The small w generated acts over a long X extent as the particle exits the critical layer and therefore generates a large τ.

The Unsteady Flow

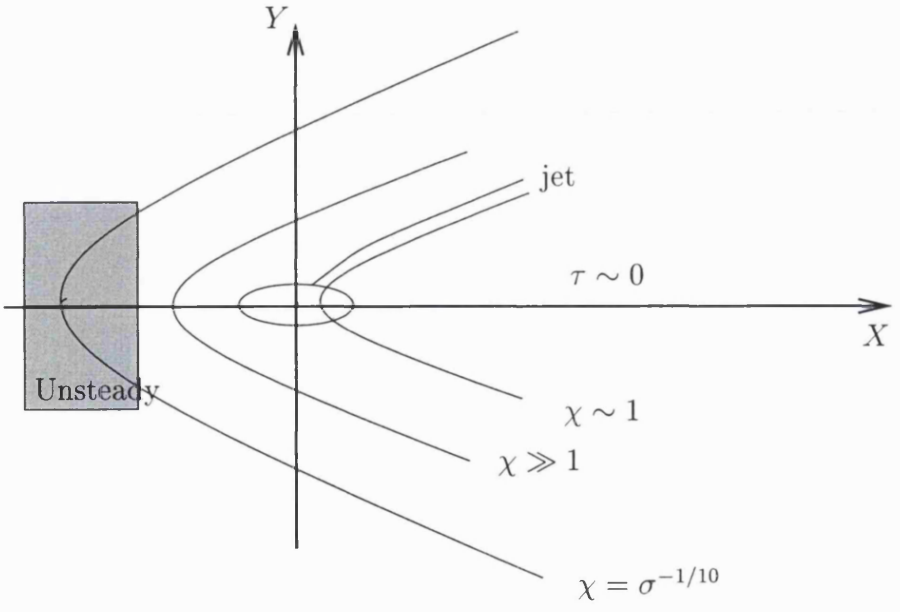

Figure 2.30: The setup for large χ.

By considering a characteristic curve entering the unsteady region we can solve the unsteady equations, (2.310) and (2.311). The boundary condition on w at Y^*, defined as the entry point of the characteristic into the unsteady region with T^* the time at this initial point is,

$$w = \frac{I(T^*)}{\bar{Y}^{*3}}, \tag{2.312}$$

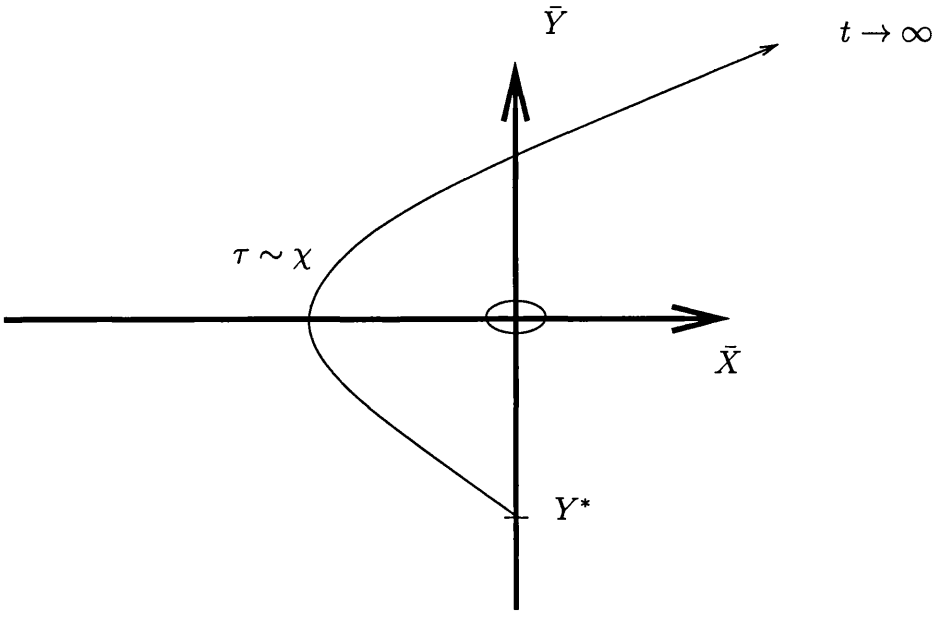

Figure 2.31: A Characteristic with large value of χ.

which is the expression for w for large χ found in section 2.6.1 with $I = \int_{\infty}^{-\infty} \tilde{p}\tilde{p}_z \, dt$ as before. The characteristic equations for large χ of (2.310) and (2.311) are,

$$\frac{d\bar{X}}{dT} = \bar{Y}, \qquad \text{and,} \qquad \frac{d\bar{Y}}{dT} = \frac{1}{3|\bar{X}|^{2/3}}. \tag{2.313}$$

The above also implies $\frac{1}{2}(Y^{*2} - \bar{Y}^2) = |\bar{X}|^{1/3}$, as $|\bar{X}| = 0$ at $Y = Y^*$. We also have $\tau = (T - T^*)\frac{I_z(T^*)}{Y^*}$. We now proceed to solve (2.313), substituting for Y in the second equation so that,

$$T - T^* = \frac{3}{4}\int_{Y^*}^{Y} (Y^{*2} - \bar{Y}^2)^2 \, d\bar{Y}, \tag{2.314}$$

and hence,

$$T - T^* = \frac{1}{20}(Y - Y^*)^3 \left(3Y^2 + 9YY^* + 8Y^{*2}\right). \tag{2.315}$$

Thus,

$$\tau = \frac{1}{20Y^{*3}} I_z(T^*)(Y - Y^*)^3 \left(3Y^2 + 9YY^* + 8Y^{*2}\right). \tag{2.316}$$

Substituting for Y^* gives,

$$\tau = \frac{I_z(T^*)\left(Y-(2\bar{X}^{1/3}+Y^2)\right)^3\left(3Y^2+9Y(2\bar{X}^{1/3}+Y^2)+8(2\bar{X}^{1/3}+Y^2)^3\right)}{20(2\bar{X}^{1/3}+Y^2)^3}, \tag{2.317}$$

and taking $\bar{X} \to 0$ to express τ as,

$$\tau = \frac{-2}{5}I_z Y\left(Y+\sqrt{Y^2}\right) - \frac{4}{5Y}I_z\left(Y+\sqrt{Y^2}\right)\bar{X}^{1/3} \tag{2.318}$$

$$+ \frac{6I_z\left(Y-\sqrt{Y^2}\right)(\bar{X}^{2/3})}{Y^3+(Y^2)^{3/2}} + \frac{4I_z\bar{X}}{Y^2\left(Y+\sqrt{Y^2}\right)^2} + O(\bar{X}^{4/3}). \tag{2.319}$$

Therefore,

$$\tau_{\bar{X}} = \frac{4}{5Y}I_z\left(Y+\sqrt{Y^2}\right)\bar{X}^{-2/3} + O(\bar{X}^{-1/3}), \tag{2.320}$$

which implies that,

$$J_X \sim \bar{X}^{-2/3}. \tag{2.321}$$

This suggests that as $X \to -\infty$ in the earlier analysis in 2.1 that $J_X \sim X^{-2/3}$. Hence we have a convergent jump term as $X \to -\infty$ if we include unsteady effects. However it is still too large to fit into the earlier analysis.

2.7 Conclusions

In chapter 2 we extended the work of Li *et al.* (1998) to three-dimensions, a natural first step in extending the applicability or otherwise of that research. These new scalings derive a deceptively simple set of equations for the three-dimensional problem, which hold in the critical layer. The bulk of the flow outside the critical layer is governed, as in Li *et al.* (1998) by the modified Benjamin-Ono equation,

$$a_1\tilde{p}_T + a_2\tilde{p}\tilde{p}_X = \mu J_X + \frac{1}{\pi}\int_{-\infty}^{\infty} \frac{1}{X-u}\frac{\partial^2\tilde{p}}{\partial u^2}du. \tag{2.322}$$

The three-dimensional critical layer equations are,

$$Yw_X - \tilde{p}_X w_Y = -\tilde{p}_z, \tag{2.323}$$

$$Y\tau_X - \tilde{p}_X\tau_Y = w_z, \tag{2.324}$$

$$J_X = 2\int_0^{\infty} \tau_X\, dY, \tag{2.325}$$

with $\tilde{p}$ governed by (2.322). The spanwise velocity within the critical layer is w, z is the spanwise variable, $\tilde{p}$ is the pressure distribution, τ is the perturbation vorticity within the critical layer and a_1, a_2 and μ are constants. J_X describes the feedback of the critical layer (incipient vortex) dynamics on the pressure development. The critical layer equations capture vorticity intensification through vortex stretching. We established in section 2.2 that a full investigation of these equations would require a numerical study. The solution for the jump term is given by a triple repeated integral.

Further theoretical understanding of the system of equations in the critical layer was developed in several cases:

1. If the pressure is forced so that, $\tilde{p} = -X$ to leading order then it was found that the jump term is zero. This result suggests the critical layer is passive for a linear streamwise pressure gradient.

2. The jump term is non-zero if the streamwise derivative of the pressure is not

constant. This was shown by taking the pressure to have two different constant derivatives for $X < 0$ and $X > 0$.

The numerical results in section 2.5 showed the significant features of the spanwise velocity and vorticity within the critical layer. The results for τ, in figure 2.21 on page 98 showed two strong features of the vorticity, a growing region as $X \to \infty$, with $Y \sim 1$ and another region where there are very large values of τ for large χ. The first feature we considered was the growing feature as $X \to \infty$ for Y of order 1. We showed, in section 2.4 that this was in fact passive and does not adversely effect the jump term. It would only influence the main flow at very large times. However the second feature, which is the large vorticity for large χ is significant. This is shown in section 2.6, where the jump term is found to be divergent as $X \to \infty$. An interesting result of this analysis is that if the boundary conditions on the pressure in the Benjamin-Ono equation satisfy $\tilde{p} \sim X^n$ with $n > \frac{1}{2}$ for $X \to \pm\infty$ then the jump term is not divergent as $X \to -\infty$. There is a possibility of further work using different boundary conditions in the Benjamin-Ono equation. The final section (2.6.2) explained the large χ features comprehensively. For large χ, the characteristics travel through an unsteady region. Therefore unsteady effects must be considered in order to obtain a solution for the jump term although the jump term found is still too large to fit into the analysis of section 2.1. This therefore prohibits a further analysis of the derived equations ((2.323) - (2.325)) as the feedback from the jump term is too strong. However we continue with a delayed critical layer jump term feedback mechanism in chapter 3, where a vortex has been created and our spanwise variation is consigned to the vortex.

Chapter 3

Three-Dimensional Vortex Development

Three-dimensionality has introduced new unexpected scales to the short-scale analysis of Li *et al.* (1998). These new scales could form the basis of a challenging problem. However we continue with a three-dimensional study by considering the development of the boundary layer at a later time and delaying feedback until a vortex has been generated, which corresponds to the vortex-generation stage in Li *et al.* (1998), Smith *et al.* (2000) and Bowles (2000*b*). We concentrate on the small μ study of Bowles (2000*b*), extending this to three-dimensions. The term representing the contribution from the critical layer appearing in the governing equation for the pressure is μJ_X. Thus reducing the size of μ suppresses the influence of the critical layer. It is interesting to note that in Bowles *et al.* (2003) it is this size of the parameter μ that is most relevant for a comparison of the theoretical work with their computational studies. Adapting the approach of Bowles (2000*b*) would seem to be a natural choice for a three-dimensional study, since it constrains the jump term in X and the critical layer is unsteady.

The small μ limit was considered in Smith *et al.* (2000) as a way of investigating the singularity marking the initial vortex generation. It leads to the simplification

that the interaction between the vortex and the pressure is suppressed. In it two timescales were identified and it was shown that under circumstances in which the vortex subsequently grew it became no longer valid to neglect the pressure/vortex interaction. The scaling of μ with Reynolds number adapted in Bowles (2000*b*) is such that this occurs a small time interval after the vortex generation, which is comparable with the slow scale over which the pressure develops, this time affected by the vortex-induced jump term.

Bowles (2000*b*) investigated the properties of the spike development in the later stages of boundary layer transition following on from the work of Li *et al.* (1998). In Li *et al.* (1998) at some finite time local maxima and minima appear in the pressure, which correspond to $\frac{\partial^2 p}{\partial x^2} = \frac{\partial p}{\partial x} = 0$, and so another singularity appears in the solution. Essentially the feedback from the critical layer jump becomes large locally, provoking still shorter time and space scales, which are studied here. These pressure maximum and minimum correspond to incipient vortices in the flow and so by considering the shorter length scales a further understanding of the initial stages of vortex generation is obtained. At each local pressure maximum particles are trapped in the flow on a fast time scale within the critical layer and so create a vortex. In the study here, initially at least, as time marches forward more particles are captured inside the vortex.

We begin the chapter with a derivation of the three-dimensional equations. We again find, in agreement with Bowles (2000*b*) that the area of a particle's orbit is constant with time. The three-dimensionality introduces new derivatives of the area and we then show the spanwise velocity and vorticity within the vortex depend on the ratio of these integrals. These integrals are divergent at one end of the vortex but we show that the ratio of the integrals is finite. A full understanding demands a numerical investigation but this turns out to be a difficult problem in itself due to the divergent integrals noted above and the need for care when dealing with particles newly captured inside the vortex. Hence before attempting a numerical approach much consideration is given to the behaviour of the ratio of the divergent integrals,

careful analysis of the vortex's behaviour near its edges in both the spanwise and streamwise directions, a study to determine whether or not the jump term is continuous and a study of vortices at an early time. These sets of analysis suggest that the derived equations are consistent, producing coherent solutions.

3.1 Derivation and Solution of the equations

The work in Smith *et al.* (2000) looks at the behaviour of the flow as $T \to \infty$ in Li *et al.* (1998), for a finite μ. It is shown that there is a significant difference in behaviour between particles that are captured inside a vortex and those that are ejected along trajectories to $Y = \infty$. It is this that motivates the analysis of the equations with two active time scales. One of which has particles "whizzing" through without being captured or orbiting within closed orbits having been captured inside the vortex and the slower time scale, over which the pressure and so vortex shape develops. The captured particles effect the pressure through the critical layer jump term.

Motivation for the Scalings

Bowles (2000*b*) studies the case of small μ after the generation of a vortex. Despite this, μJ_X is of order 1 since J_X is large. We now demonstrate why this balance requires $\mu \sim Re^{-1/32}$ (equivalently $\mu \sim \epsilon^{1/4}$ with $\epsilon = Re^{-1/8}$). The justification of this choice is achieved by a study of the scalings at the time a vortex is generated (as motivated by Smith *et al.* 2000) at which time μJ_X is still small and then a further analysis at later times where the vortex has grown so that μJ_X is of order 1. We consider the scalings relative to those of Li *et al.* (1998) and section 2.1.

In the two-dimensional case studied in Smith *et al.* (2000) and summarised in Li *et al.* (1998) the stage of the initial vortex generation is considered with $\mu = O(1)$. They study equations describing the initial stages over a short timescale reduced by a factor $\epsilon^{1/10}$ from the scalings of step 2 of Li *et al.* (1998), as we will show below. The derived equations in this case are too difficult to solve but progress is made if $\mu \ll 1$. In this case it is possible to derive equations for the pressure that ignore the jump term as μJ_X is also small. The flow develops without feedback from the critical layer. As a maximum and minimum is generated, typically,

$$P = -X^3 + XT, \tag{3.1}$$

local to the position of the maximum and minimum. Particles in the critical layer follow trajectories governed by,

$$u = \frac{dX}{dT} = Y, \qquad \text{and,} \qquad v = \frac{dY}{dX} = -P_X, \tag{3.2}$$

leading to the equation for the X position of a particle,

$$\frac{d^2X}{dT^2} = -3X^2 + T. \tag{3.3}$$

If a maxima or minima exists then Smith *et al.* (2000) show that the resulting trajectories fall into two groups, those that depart to $X = -\infty$ but with $Y \to \infty$ within a finite time and those that are captured by the vortex, with X, Y remaining finite for all time. From (3.3) the X-extent of the vortex is $X \sim T^{1/2}$. We use $X \sim T^{1/2}$ to express scalings for the other variables in terms of T. From (3.1) we find that $P \sim X^3 \sim T^{3/2}$ and from the equation for the characteristics given by $\frac{Y^2}{2} = \chi - P$ we find that $Y \sim P^{1/2}$ so that $Y \sim T^{3/4}$, giving an estimate for the size of the vortex.

We may find the size of T in terms of ϵ through considering a balance between the terms in the momentum equation with the unsteady term. In equation (2.204) on page 68 we considered the relative sizes of the unsteady terms within the critical layer. Here we wish to include the unsteady terms within the equation and so the required balance is given by,

$$\epsilon^{1/4}\frac{\partial}{\partial T} \sim Y\frac{\partial}{\partial X}. \tag{3.4}$$

Therefore $T \sim \epsilon^{1/5}$ using the scalings for Y, X and P as given in the previous paragraph. At this time, the μJ_X term is still too small to influence the governing Benjamin-Ono equation for the pressure.

The relative error between the right hand side and the left hand side of (3.3) is $T^{-5/4}$ as $T \to \infty$, i.e. for large times after vortex generation. This difference motivates the adoption of two time scales as in Smith *et al.* (2000). We have shown that $T \sim \epsilon^{1/5}$,

which justifies our choice of $\epsilon^{-1/4}$ in equation (3.50) on page 130 where we formally introduce the two active time scales.

In order to find the required value of μ we must consider the size of J_X, which can be found by considering the size of the vorticity, τ. In the two-dimensional case, as particles orbit they develop a τ according to,

$$Y\tau_X - P_X\tau_Y = -b_1^{-3}(b_1b_3P_T - 2b_4PP_X), \tag{3.5}$$

where b_1, b_3 and b_4 are constants from the local expansion of the velocity but they are not relevant here. As the vortex is generated, a maximum and minimum appear in the pressure, giving an estimate for τ from,

$$Y\tau_X \sim P_T. \tag{3.6}$$

The scalings stated earlier and the above equation imply that $\tau \sim T^{1/4}$. We find the size of J through integration as,

$$J = \int_{-\infty}^{\infty} \tau \, dY, \tag{3.7}$$

from chapter 2. We also have that $Y \sim T^{3/2}$ and so $dY \sim T^{1/2}dT$ so that,

$$J \sim T^{7/4}. \tag{3.8}$$

This result agrees with the size of J found in Smith *et al.* (2000). Hence $J_X \sim T^{5/4}$. Although μ is small, μJ_X will enter eventually. This will occur when μJ_X is of the same order as the global contribution from the Cauchy-Hilbert term in the Benjamin-Ono equation (i.e. $O(1)$). Using the size of J_X that we have found above implies that μJ_X is of order 1 when $T \sim \mu^{-4/5}$. At this even later time the length scale of the vortex is of size $T^{1/2}$ larger than at the time of vortex generation measured in shortened scales. This is due to the need to maintain the balance in (3.3) as time tends to infinity. Therefore the length of the vortex at this later time is of size $\epsilon^{1/10}T^{1/2}$ relative to the streamwise length scales in chapter 2. In order that

the vortex has grown to the same size as the length scales of chapter 2 we require, $\epsilon^{1/10}T^{1/2} \sim 1$. Therefore,

$$\epsilon^{1/10}\mu^{-2/5} \sim 1 \tag{3.9}$$

and hence,

$$\mu \sim \epsilon^{1/4} \sim Re^{-1/32}. \tag{3.10}$$

The approach of Bowles (2000*b*) has an obvious application to our problem since it constrains the jump term in X and the critical layer is unsteady. The problem we had earlier was that a large jump term was generated for large negative X. This resolves the problem as the jump term is only non-zero within the vortex.

The derivation

In Bowles (2000*b*) the case of small μ is studied. Here we include weak three-dimensionality inside the vortex. The particles are fixed within each spanwise plane and so in this description the orbits for each spanwise point are independent. The space scalings are the same as those in Li *et al.* (1998) except that within the critical layer there are two active time scales - a fast one over which fluid particles enter and are either ejected or captured and a slower scale over which the pressure and hence the trajectories followed by the particles vary. There are four tiers to consider, which have the same scalings as those in chapter 2. The main differences between chapter 2 and the present case are the existence of two time scales and the velocities are expanded in powers of $\epsilon^{1/4}$, where $\epsilon = Re^{-1/8}$. The velocities are expanded in powers of $\epsilon^{1/4}$ so that we do not neglect any terms as we have introduced an extra time scale of relative size $\epsilon^{1/4}$. The spanwise scalings are found through an order of magnitude argument that introduces the spanwise influence through the vorticity at the slower time scale. We will find that the significant vorticity is generated at third order in the critical layer and we want a $\tilde{W}_3$ to be generated at this order. The order

of magnitude argument matches $\tilde{V}_{3Y}$ with $\epsilon^{1/4}\tilde{W}_{3Z}$ in the continuity equation so that the spanwise influence is introduced at the slower time scale. From the momentum equation we match $\tilde{W}_{3T}$ with $-\epsilon^{1/4}\tilde{p}_{1z}$. This implies that $\tilde{W}_3 \sim \epsilon^{7/4}$ and we have a spanwise scaling of $Z \sim \epsilon^{32/8}$.

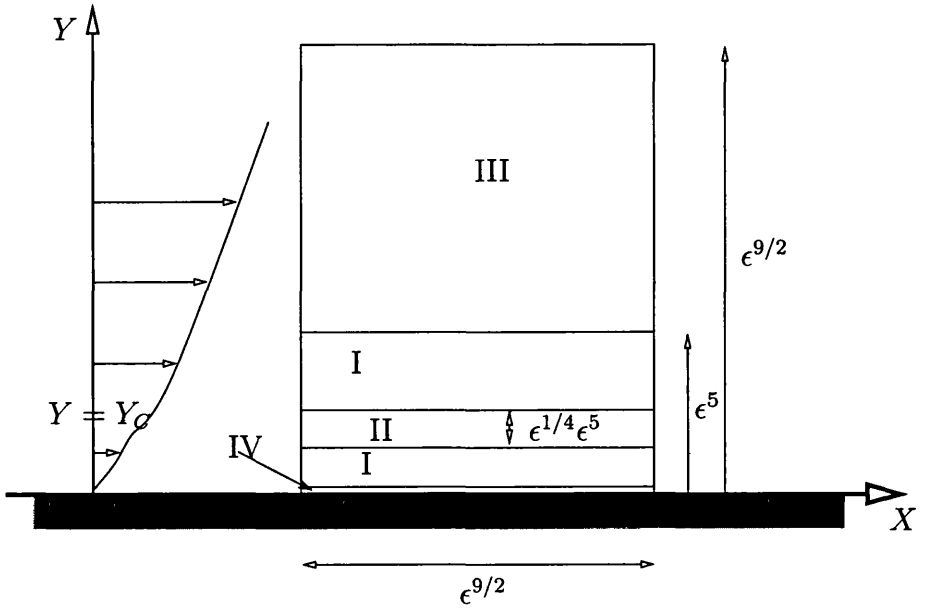

Figure 3.1: The triple-deck structure for small μ.

In the main deck,

$$x^* = x_0^* + \epsilon^4 cT + \epsilon^{9/2}X, \qquad t^* = t_0^* + \epsilon^3 T, \tag{3.11}$$

with x_0^*, t_0^* the position and time respectively of the spiking on the triple-deck scales, with the disturbance travelling with speed ϵc as in Li *et al.* (1998), the velocity of the inflection point in the profile. In the bulk of the flow (region I in figure 3.1) we expand the basic flow velocity, U and the disturbance velocities $(\tilde{u}, \tilde{v})$ in powers of

$\epsilon^{1/4}$. $\bar{U}_1$, $\bar{U}_2$ etc. are included to insist that μ is the right size.

$$\begin{aligned} u^* &= \epsilon\Big\{ \left(\bar{U}_0(y) + \epsilon^{1/4}\bar{U}_1(y) + \epsilon^{1/2}\bar{U}_2(y) + \dots\right) \\ &+ \epsilon^{1/2}\left(\tilde{u}_1(z,X,y,T) + \epsilon^{1/4}\tilde{u}_2(z,X,y,T) + \epsilon^{1/2}\tilde{u}_3(z,X,y,T) + \dots\right)\Big\} \quad (3.12) \\ v^* &= \epsilon^{3/2}\left\{\epsilon^{1/2}\tilde{v}_1(z,X,y,T) + \epsilon^{3/4}\tilde{v}_2(z,X,y,T) + \epsilon\tilde{v}_3(z,X,y,T) + \dots\right\} \quad (3.13) \\ p^* &= \epsilon^2\left\{p_0 + \epsilon^{1/2}\tilde{p}_1(z,X,T) + \epsilon^{3/4}\tilde{p}_2(z,X,T) + \epsilon\tilde{p}_3(z,X,T) + \dots\right\}, \quad (3.14) \\ c &= c_0 + \epsilon^{1/4}c_1 + \epsilon^{1/2}c_2 + \dots, \quad (3.15) \end{aligned}$$

where $y^* = \epsilon^5 y$, $z^* = \epsilon^{32/8} z$ and the spanwise scalings are chosen so that they will influence the critical layer jump term within the vortex. The spanwise velocity is passive in the bulk of the flow. Substitution of these expansions into the Navier-Stokes equations at first order leads to,

$$\tilde{u}_{1X} + \tilde{v}_{1y} = 0, \qquad \text{and,} \qquad (\bar{U}_0 - c_0)\tilde{u}_{1X} + \tilde{v}_1\bar{U}_{0y} = -\tilde{p}_{1X}. \quad (3.16)$$

As in the derivation on page 28 in chapter 2 we have solutions in terms of an unknown pressure, which is found at the third order. Therefore,

$$\tilde{u}_1 = -\tilde{p}_1\Phi'(y), \qquad \text{and,} \qquad \tilde{v}_1 = \tilde{p}_{1X}\Phi(y), \quad (3.17)$$

with Φ defined as,

$$\Phi(y) = (\bar{U}_0(y) - c_0)\int_0^y \frac{d\hat{y}}{(\bar{U}_0(\hat{y}) - c_0)^2}. \quad (3.18)$$

The solution satisfies the boundary condition, $\tilde{v}_1(0) = 0$. As $y \to \infty$ we impose the boundary condition, $\tilde{v}_{1y} = 0$, which suppresses the pressure displacement interaction as on page 29 in chapter 2 and ensures that the large pressure feedback is not generated. This gives the following condition on the velocity profile,

$$\int_0^\infty \frac{d\hat{y}}{(\bar{U}_0(\hat{y}) - c_0)^2} = 0. \quad (3.19)$$

If we take $U_0(y) = \lambda y$ as $y \to \infty$ in (3.16) then we obtain the condition,

$$\tilde{v}_1(y) \to -\frac{\tilde{p}_{1X}}{\lambda} \text{ as } y \to \infty. \quad (3.20)$$

At the next order (reduced by order $\epsilon^{1/4}$) substitution into the Navier-Stokes equations gives,

$$(\bar{U}_0 - c_0)\tilde{u}_{2X} + (\bar{U}_1 - c_1)\tilde{u}_{1X} + \tilde{v}_2\bar{U}_{0y} + \tilde{v}_1\bar{U}_{1y} = -\tilde{p}_{2X}, \tag{3.21}$$

and hence with continuity at the second order and (3.16),

$$-(\bar{U}_0 - c_0)^2\frac{\partial}{\partial y}\left(\frac{\tilde{v}_2}{(\bar{U}_0 - c_0)}\right) = -\tilde{p}_{2X} + (\bar{U}_1 - c_1)\tilde{p}_{1X}\Phi' - \bar{U}_{1y}\tilde{p}_{1X}\Phi. \tag{3.22}$$

This leads to the solutions,

$$\tilde{u}_2 = -\tilde{p}_2\Phi'(y) - \tilde{p}_1\Psi'(y), \qquad \text{and,} \qquad \tilde{v}_2 = \tilde{p}_2\Phi(y) - \tilde{p}_{1X}\Psi(y), \tag{3.23}$$

with Ψ defined as,

$$\Psi(y) = (\bar{U}_0(y) - c_0)\int_0^y \frac{(\Phi(\hat{y}))^2}{(\bar{U}_0(\hat{y}) - c_0)^2}\left(\frac{\bar{U}_1(\hat{y}) - c_1}{\Phi(\hat{y})}\right)' d\hat{y}. \tag{3.24}$$

We take, $\tilde{v}_{2y} \to 0$ as $y \to \infty$. At the next order, we find that $\tilde{u}_3$ and $\tilde{v}_3$ satisfy the following equation,

$$\begin{aligned}\tilde{u}_{1T} + (\bar{U}_0 - c_0)\tilde{u}_{3X} + (\bar{U}_1 - c_1)\tilde{u}_{2X} + (\bar{U}_2 - c_2)\tilde{u}_{1X} + \tilde{u}_1\tilde{u}_{1X} \\ +\tilde{v}_3\bar{U}_{0y} + \tilde{v}_2\bar{U}_{1y} + \tilde{v}_1\bar{U}_{2y} + \tilde{v}_1\tilde{u}_{1y} = -\tilde{p}_{3X}.\end{aligned} \tag{3.25}$$

Hence,

$$\begin{aligned}-(\bar{U}_0 - c_0)^2\frac{\partial}{\partial y}\left(\frac{\tilde{v}_3}{(\bar{U}_0 - c_0)}\right) &= -\tilde{p}_{3X} + \tilde{p}_{1T}\Phi' + \tilde{p}_{2X}\left(-(\bar{U}_1 - c_1)\Phi' + \bar{U}_{1y}\Phi\right) \\ &+ \tilde{p}_{1X}\left((\bar{U}_1 - c_1)\Psi' + (\bar{U}_2 - c_2)\Phi' - \bar{U}_{2y}\Phi - \bar{U}_{1y}\Psi\right) \\ &+ \tilde{p}_1\tilde{p}_{1X}\left(-(\Phi')^2 + \Phi\Phi''\right),\end{aligned} \tag{3.26}$$

and therefore,

$$\left[\frac{\tilde{v}_3}{\bar{U}_0 - c_0}\right]_0^\infty = a_1\tilde{p}_{1T} + a_2\tilde{p}_1\tilde{p}_{1X} + a_3\tilde{p}_{1X} + j_X, \tag{3.27}$$

with,

$$a_1 = -\int_0^\infty \frac{\Phi'}{(\bar{U}_0 - c_0)^2}\, d\hat{y}, \qquad a_2 = \int_0^\infty \frac{(\Phi')^2 - \Phi\Phi''}{(\bar{U}_0 - c_0)^2}\, d\hat{y}, \tag{3.28}$$

and,

$$a_3 = \int_0^\infty \frac{\Phi^2}{(\bar{U}_0 - c_0)^2}\left(\frac{\bar{U}_2 - c_2}{\Phi}\right)' d\hat{y} + \int_0^\infty \frac{\Psi^2}{(\bar{U}_0 - c_0)^2}\left(\frac{\bar{U}_1 - c_1}{\Psi}\right)' d\hat{y}. \tag{3.29}$$

The terms in $\tilde{p}_{2X}$ and $\tilde{p}_{3X}$ do not appear in equation (3.27) since they are both multiplied by an integral that tends to zero as $y \to \infty$. The integral from $y = 0$ to infinity of $(\bar{U}_0 - c_0)^{-2}$ is zero, which justifies removing the term in $\tilde{p}_{3X}$. The term in $\tilde{p}_{2X}$ is multiplied by,

$$\int_0^y \frac{(\bar{U}_{1\hat{y}}\Phi - (\bar{U}_1 - c_1)\Phi')}{(\bar{U}_0 - c_0)^2} d\hat{y} = \int_0^y \frac{(\Phi(\hat{y}))^2}{(\bar{U}_0(\hat{y}) - c_0)^2}\left(\frac{\bar{U}_1(\hat{y}) - c_1}{\Phi(\hat{y})}\right)' d\hat{y}. \tag{3.30}$$

From (3.24) this integral is equal to $(\bar{U}_0 - c_0)^{-1}\Psi(y)$. We have assumed that as $y \to \infty$, then $v_{2y} \to 0$. Thus $\Psi(\infty) = 0$.

The j_X term in (3.27) is found through a consideration of the critical layer. The left hand side of (3.27) is found by considering the solution in the outer region as with the derivation in chapter 2 and here again we find,

$$\left[\frac{\tilde{v}_3}{\bar{U}_0 - c_0}\right]_0^\infty = \frac{1}{\pi}\int_{-\infty}^\infty \frac{1}{X - u}\frac{\partial^2 \tilde{p}_1}{\partial u^2} du. \tag{3.31}$$

Hence the governing equation for the flow is,

$$\frac{1}{\pi}\int_{-\infty}^\infty \frac{\tilde{p}_{1ss}}{X - s} ds = a_1\tilde{p}_{1T} + a_2\tilde{p}_1\tilde{p}_{1X} + a_3\tilde{p}_{1X} + j_X, \tag{3.32}$$

which agrees with Bowles (2000*b*).

The Critical Layer

The critical layer which has $y = y_c$, is defined, as in chapter 2, by $\bar{U}_0''(y_c) = 0$ and $c_0 = \bar{U}_0(y_c)$. As $y \to y_c$ we put,

$$\bar{U}_0(y) = c_0 + b_{01}(y - y_c) + b_{05}(y - y_c)^5 + \dots, \tag{3.33}$$

$$\bar{U}_1(y) = b_{10} + b_{11}(y - y_c) + b_{13}(y - y_c)^3 + b_{14}(y - y_c)^4 + \dots, \tag{3.34}$$

$$\bar{U}_2(y) = b_{20} + b_{21}(y - y_c) + \dots, \tag{3.35}$$

and we expand, $c = c_0 + \epsilon^{1/4}c_1 + \epsilon^{1/2}c_2 + \ldots$, where $c_1 = b_{10}$ and $c_2 = b_{20}$ etc.

Here the critical layer time is again reduced by $\epsilon^{1/4}$ since we are considering a delayed feedback mechanism with the only feedback occuring from particles within the vortex. Hence,

$$t^* = \epsilon^3\epsilon^{1/4}\tilde{T}. \tag{3.36}$$

In the critical layer we have the expansions,

$$u^* = \epsilon\left\{c_0 + \epsilon^{1/4}\tilde{U}_1 + \epsilon^{1/2}\tilde{U}_2 + \epsilon^{3/4}\tilde{U}_3 + \ldots\right\}, \tag{3.37}$$

$$v^* = \epsilon^{3/2}\left\{\epsilon^{1/2}\tilde{V}_1 + \epsilon^{3/4}\tilde{V}_2 + \epsilon\tilde{V}_3 + \epsilon^{5/4}\tilde{V}_4 + \ldots\right\}, \tag{3.38}$$

$$w^* = \epsilon^{7/4}\tilde{W}_3 + \ldots, \tag{3.39}$$

with the spanwise velocity's scaling chosen so that its influence is felt on the slow time scale (i.e. it only has an influence on the particles that are trapped inside the vortex). This implies a spanwise momentum balance of,

$$\tilde{W}_{3\tilde{T}} + \tilde{U}_1\tilde{W}_{3X} + \tilde{V}_1\tilde{W}_{3Y} = -\epsilon^{1/4}\tilde{p}_{1z}, \tag{3.40}$$

with the right hand side's influence felt on the spanwise velocity at the slow time step only. Continuity at this order is,

$$\tilde{U}_{3X} + \tilde{V}_{3Y} + \epsilon^{1/4}\tilde{W}_{3z} = 0. \tag{3.41}$$

If we now consider the solutions in region I and take $y \to y_c$ by writing $y - y_c = \epsilon^{1/4}Y$ the flow velocity expansions become,

$$u^* = \epsilon\left\{c_0 + \epsilon^{1/4}b_{01}Y + \epsilon^{1/2}b_{11}Y + \epsilon^{3/4}(\tilde{p}_1 b_{01}I_{1c}+) + \ldots\right\}, \tag{3.42}$$

$$v^* = \epsilon^{3/2}\left\{\epsilon^{1/2}\tilde{p}_{1X}b_{01}^{-1} + \epsilon^{3/4}\tilde{p}_{1X}b_{01}I_{1c}Y + \ldots\right\}, \tag{3.43}$$

where $I_{1c} = \int_0^{y_c}\left(\bar{U}_0(\hat{y}) - c_0\right)^{-2}\,d\hat{y}$. We follow the method of the derivation in chapter 2 and here obtain the governing equation for the vorticity at the third order. This differs from chapter 2, where the critical layer jump term was found by considering

the equation within the critical layer at the fourth order. This difference is due to the difference in scalings for the length and time scales interacting. Therefore,

$$\tilde{U}_{3\tilde{T}} + \tilde{U}_1\tilde{U}_{3X} + \tilde{U}_2\tilde{U}_{2X} + \tilde{U}_3\tilde{U}_{1X} + \tilde{V}_1\tilde{U}_{3Y} + \tilde{V}_2\tilde{U}_{2Y} + \tilde{V}_3\tilde{U}_{1Y} = -\tilde{p}_{3X}. \tag{3.44}$$

Again we take the Y derivative, write $\tau = \tilde{U}_{3Y}$ and use continuity (3.41) so that,

$$\tau_{\tilde{T}} + b_{01}Y\tau_X - \tilde{p}_{1X}b_{01}^{-1}\tau_Y = \epsilon^{1/4}b_{01}\tilde{W}_{3z}, \tag{3.45}$$

and hence we may write the equations within the critical layer after normalising to remove b_{01} as,

$$\frac{d\tau}{d\tilde{T}} = \epsilon^{1/4}\tilde{W}_{3z}, \quad \text{and,} \quad \frac{d\tilde{W}_3}{d\tilde{T}} = -\epsilon^{1/4}\tilde{p}_{1z}. \tag{3.46}$$

Here, analogous to the derivation in chapter 2,

$$j_X = \frac{1}{b_{01}}\frac{\partial}{\partial X}\left[\tilde{u}_3\right]_{y_{c-}}^{y_{c+}}. \tag{3.47}$$

Area of an orbit is constant

We will return to the study of equations (3.46) on page 132, so that we may study the generation of τ and $\tilde{W}_3$ on the slow scales. Prior to this we consider characteristic equations inside the critical layer, which allow us to show that the area of a particle's orbit is fixed as time progresses. The characteristic equations are,

$$\frac{dX}{d\tilde{T}} = Y, \qquad \text{and,} \qquad \frac{dY}{d\tilde{T}} = \tilde{p}_{1X}. \tag{3.48}$$

These are found by considering, for example (3.45) and using the method of characteristics to derive four equations. For our analysis we need only consider the two equations in (3.48). These characteristic equations also give us the characteristic given by $\chi = \frac{Y^2}{2} + \tilde{p}_1$. In the case we are considering here, for a particle to have been captured requires, $\chi_{min} < \chi < \chi_{max}$, where χ_{min} and χ_{max} are the local pressure maximum and minimum respectively. If $\chi > \chi_{max}$ then these represent trajectories that have not been captured by the vortex and hence will not be influenced by the

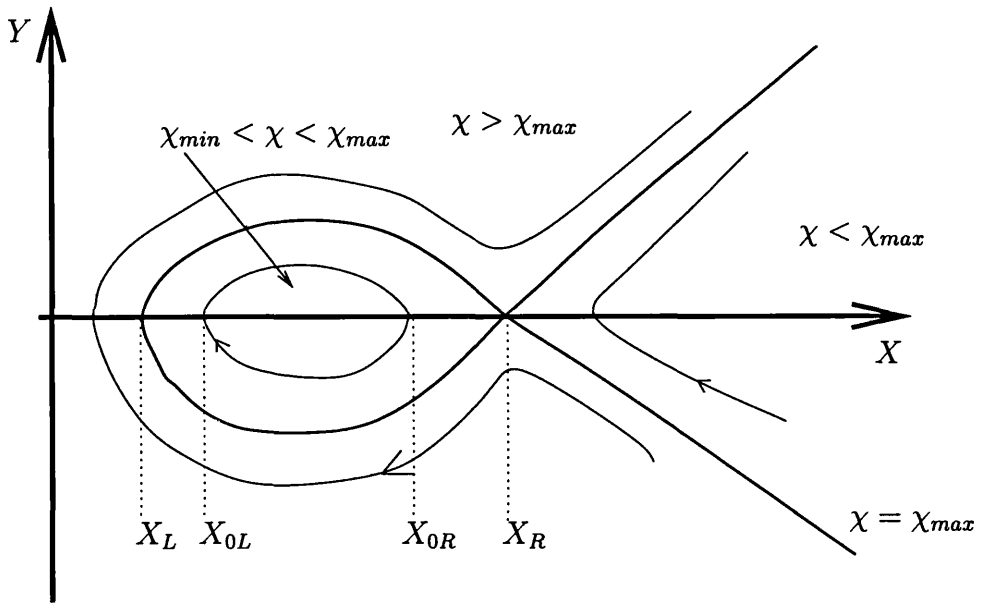

Figure 3.2: The Vortex Structure.

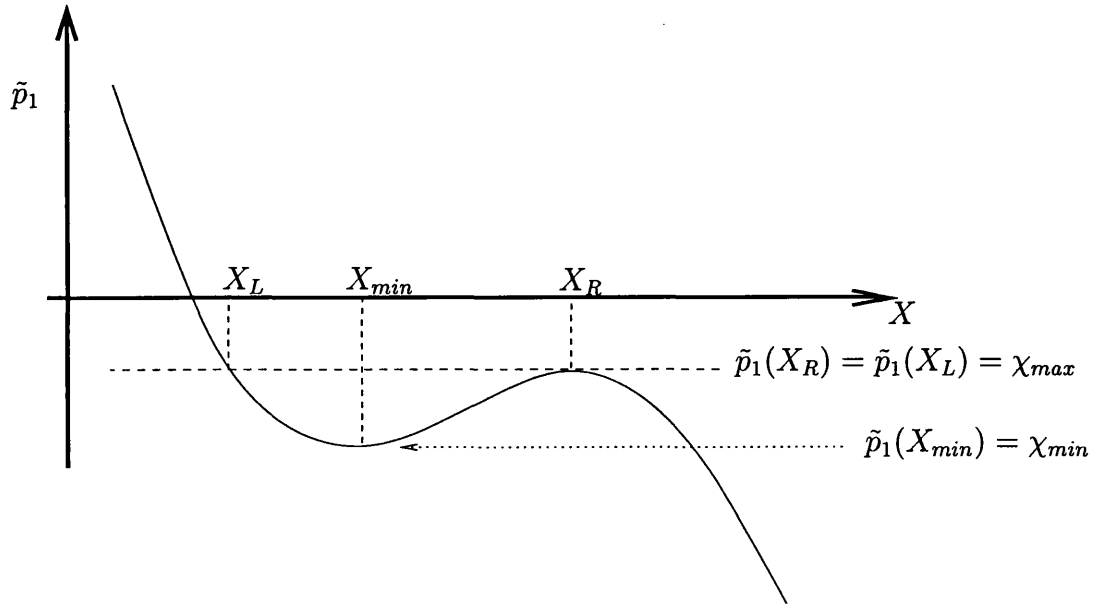

Figure 3.3: The local pressure.

spanwise influences. We also define, for convenience, the points X_L, X_R and X_{min}. X_R is the right streamwise end point of the vortex with $\tilde{p}_1(X_R)$ a local maximum. X_L is the vortex's left streamwise end point with $\tilde{p}_1(X_L) = \tilde{p}_1(X_R) = \chi_{max}$ and X_{min} is the point where $\tilde{p}_1(X_{min}) = \chi_{min}$ is a local minimum. Each χ_1 ($\chi_{min} < \chi_1 < \chi_{max}$) corresponds to a particle's orbit within the vortex, thus we may define X_{0L} and X_{0R} as the local streamwise end points for the trajectory defined by χ_1. Thus $\tilde{p}_1(X_{0L}) = \tilde{p}_1(X_{0R}) = \chi_1$. This is summarised in figure 3.2 and figure 3.3. From (3.48) the characteristics are given by,

$$\frac{d^2X}{d\tilde{T}^2} = -\tilde{p}_{1X}, \tag{3.49}$$

and we expand $X = x_0 + \epsilon^{1/4}x_1$, $\tilde{p}_1(X) = P(X) + \epsilon^{1/4}P_1(X)$ and so $P(x_0 + \epsilon^{1/4}x_1) = P(x_0) + \epsilon^{1/4}x_1P_{x_0}(x_0)$. For clarity we have omitted the $\tilde{T}$ dependence in the expressions for the pressure but it is important to remember that the time dependence does remain. This is different from chapter 2 where we considered a steady flow within the critical layer. We introduce the study of the two time scales; a fast scale, $\bar{t}$, such that particles are either captured or ejected and a slow scale, $\bar{T}$, where the particles are trapped inside the vortex and over which the pressure and hence the trajectories vary. The following analysis will show that the area of an orbit is constant with respect to time. This is found below by considering (3.49) with two time scales. This analysis follows that of Bowles (2000*b*). We write,

$$\tilde{T} = \bar{t}, \quad \text{and,} \quad \tilde{T} = \epsilon^{-1/4}\bar{T}, \tag{3.50}$$

and hence,

$$\frac{\partial}{\partial t} = \frac{\partial}{\partial \bar{t}} + \epsilon^{1/4}\frac{\partial}{\partial \bar{T}}. \tag{3.51}$$

The study of the characteristics given by (3.49) with the two time scales that follows leads to the conclusion that the area of an orbit for a fixed particle's trajectory is constant. Equation (3.49) implies,

$$x_{0\bar{t}\bar{t}} + \epsilon^{1/4}(2x_{0\bar{t}\bar{T}} + x_{1\bar{t}\bar{t}}) = -P_{x_0} - \epsilon^{1/4}(P_{1x_0} + x_1P_{x_0x_0}). \tag{3.52}$$

We thus have,

$$x_{0\bar{t}\bar{t}} = -P_{x_0}(x_0), \tag{3.53}$$

and,

$$2x_{0\bar{t}\bar{T}} + x_{1\bar{t}\bar{t}} = -(P_{1x_0} + x_1 P_{x_0x_0}), \tag{3.54}$$

to first and second order respectively. Multiplying (3.54) by $x_{0\bar{t}}$ and integrating over a period, Π gives,

$$2\int_\Pi x_{0\bar{t}}x_{0\bar{t}\bar{T}}d\bar{t} + \int_\Pi x_{0\bar{t}}x_{1\bar{t}\bar{t}}d\bar{t} = -\int_\Pi x_{0\bar{t}}P_{1x_0}d\bar{t} - \int_\Pi x_1 x_{0\bar{t}}P_{x_0x_0}d\bar{t}. \tag{3.55}$$

This expression may be simplified and we achieve this by considering each term separately. We begin with the first term,

$$\begin{aligned}\int_\Pi x_{0\bar{t}}x_{0\bar{t}\bar{T}}d\bar{t} &= \frac{1}{2}\int_\Pi \frac{\partial}{\partial\bar{T}}(x_{0\bar{t}})^2 d\bar{t}, \\ &= \frac{1}{2}\frac{\partial}{\partial\bar{T}}\int_\Pi (x_{0\bar{t}})^2 d\bar{t} + \frac{\partial\Pi}{\partial\bar{T}}(x_{0\bar{t}})^2|_{\bar{t}_2} - \frac{\partial\Pi}{\partial\bar{T}}(x_{0\bar{t}})^2|_{\bar{t}_1}, \\ &= \frac{1}{2}\frac{\partial}{\partial\bar{T}}\int_\Pi (x_{0t})^2 d\bar{t},\end{aligned} \tag{3.56}$$

where $\bar{t}_1$ and $\bar{t}_2$ are the start and end values of the orbit, which without loss of generality correspond to $x_{0\bar{t}} = 0$ as $x_{0\bar{t}} \sim Y$. The second term in (3.55) may be rewritten using integration by parts as,

$$\int_\Pi x_{0\bar{t}}x_{1\bar{t}\bar{t}}d\bar{t} = [x_{0\bar{t}}x_{1\bar{t}}]_\Pi - \int_\Pi x_{1\bar{t}}x_{0\bar{t}\bar{t}}d\bar{t} = [x_{0\bar{t}}x_{1\bar{t}}]_\Pi + [x_{0\bar{t}\bar{t}}x_1]_\Pi + \int_\Pi x_1 x_{0\bar{t}\bar{t}\bar{t}}d\bar{t}, \tag{3.57}$$

and $[x_{0\bar{t}}x_{1\bar{t}}]_\Pi = [x_{0\bar{t}\bar{t}}x_1]_\Pi = 0$, since their values at the start and end of a period are the same. Using (3.53) and the chain rule,

$$x_{0\bar{t}\bar{t}\bar{t}} = -\frac{\partial}{\partial\bar{t}}P_{x_0} = -\frac{\partial x_0}{\partial\bar{t}}\frac{\partial P_{x_0}}{\partial x_0}, \tag{3.58}$$

gives the following expression for the second term in (3.55),

$$\int_\Pi x_{0\bar{t}}x_{1\bar{t}\bar{t}}d\bar{t} = \int_\Pi x_1 x_{0\bar{t}\bar{t}\bar{t}}d\bar{t} = -\int_\Pi x_{0\bar{t}}x_1 P_{x_0x_0}d\bar{t}, \tag{3.59}$$

which is the same as the fourth term in (3.55). The third term in (3.55) is zero since,

$$\int_{\Pi} x_{0\bar{t}} P_{1x_0} d\bar{t} = \int_{\Pi} P_{1x_0} \frac{dx_0}{d\bar{t}} d\bar{t} = \int_{\Pi} P_{1x_0} dx_0 = 0. \tag{3.60}$$

Hence we may rewrite (3.55) as,

$$\frac{\partial}{\partial \bar{T}} \int_{\Pi} (x_{0\bar{t}})^2 d\bar{t} - \int_{\Pi} x_{0\bar{t}} x_1 P_{x_0 x_0} d\bar{t} = - \int_{\Pi} x_{0\bar{t}} x_1 P_{x_0 x_0} d\bar{t}, \tag{3.61}$$

and so,

$$\frac{\partial}{\partial \bar{T}} \int_{\Pi} (x_{0\bar{t}})^2 d\bar{t} = 0. \tag{3.62}$$

Therefore, $\int_{\Pi} (x_{0\bar{t}})^2 d\bar{t}$ = constant and $\int_{\Pi} (x_{0\bar{t}})^2 d\bar{t} = \int_{x_L}^{x_R} x_{0\bar{t}} dx = \int_{x_L}^{x_R} |Y| dx = A$, where A is the area of a particle's orbit. The interpretation of this is that the area of the closed trajectories remains constant as they develop after capture (Bowles 2000*b*).

The governing three-dimensional equations for the jump term

In the three dimensional case we have the following equation for $\tilde{W}_3$ (second equation of (3.46)), the component of velocity in the spanwise direction,

$$\frac{d\tilde{W}_3}{d\bar{T}} = -\epsilon^{1/4} P_z. \tag{3.63}$$

We will expand this equation using $\tilde{W}_3 = w_0 + \epsilon^{1/4} w_1$. This equation was found earlier by considering the equations found for the extension to three dimensions case of Li *et al.* (1998) and fixing the $\epsilon^{1/4}$ so that its effect is felt at the slow time scale. It is at this time scale where the particles (and hence the trajectories of the particles) within the vortex feel the influence of the pressure distribution. In this case the three-dimensional stretching is only affecting particles trapped within the vortex for extended periods. Therefore,

$$w_{0\bar{t}} = 0, \tag{3.64}$$

and,

$$w_{0\bar{T}} + w_{1\bar{t}} = -P_z(x_0). \tag{3.65}$$

Integrating this over a period of an orbit gives,

$$\int_\Pi w_{0\bar{T}} d\bar{t} + \int_\Pi w_{1\bar{t}} d\bar{t} = -\int_\Pi P_z(x_0) d\bar{t}, \tag{3.66}$$

where Π = period of the orbit. It is straightforward to see that $\int_\Pi w_{1\bar{t}} d\bar{t} = 0$ since it is the integral of a derivative over a period. We also have that $w_{0\bar{T}}$ is constant over an orbit since w_0 is independent of $\bar{t}$ from (3.64) and hence $\int_\Pi w_{0\bar{T}} d\bar{t} = w_{0\bar{T}} \int_\Pi d\bar{t}$. Therefore,

$$\Pi w_{0\bar{T}} = -\int_\Pi P_z(x_0) d\bar{t}. \tag{3.67}$$

We define the characteristic curve, $Y = \sqrt{2}\sqrt{\chi - P}$ with χ and z describing the position of a particle inside the vortex and hence $A(z, \chi)$. This is constant for each orbit. Equation (3.67) can be simplified by considering,

$$\Pi = \int_\Pi d\bar{t} = \int_\Pi \frac{dx}{Y}. \tag{3.68}$$

It is clear that the period is infinite, when $Y = 0$. We also have $A = \int_\Pi Y dx$ and $\frac{\partial Y}{\partial \chi} = \frac{1}{Y}$. We have defined X_L and X_R as the streamwise extremes of the vortex and so we may use these to describe the period of a vortex. Therefore,

$$\int_{X_L}^{X_R} \frac{dx}{Y} = \int_{X_L}^{X_R} \frac{\partial Y}{\partial \chi} dx = \frac{\partial}{\partial \chi} \int_{X_L}^{X_R} Y dx - \frac{\partial X_R}{\partial \chi} Y(X_R) + \frac{\partial X_L}{\partial \chi} Y(X_L), \tag{3.69}$$

$$= \frac{\partial}{\partial \chi} \int_{X_L}^{X_R} Y dx, \tag{3.70}$$

$$= \frac{\partial A}{\partial \chi}, \tag{3.71}$$

as $Y(X_R) = Y(X_L) = 0$. Hence,

$$\Pi = \int \frac{dx}{Y} = \frac{\partial A}{\partial \chi}, \tag{3.72}$$

with A_χ the change in area with respect to χ with z fixed. Similarly,

$$-\int_\Pi P_z d\bar{t} = \int_\Pi P_z \frac{dx}{Y} = \frac{\partial A}{\partial z}, \tag{3.73}$$

with A_z the change in area with respect to z with χ fixed. Substituting into (3.67) gives,

$$\frac{dw_0}{d\bar{T}} = \frac{A_z(z,\chi)}{A_\chi(z,\chi)}, \tag{3.74}$$

an expression for w_0 in terms of derivatives of the area. Now we consider the expression for the spanwise vorticity and derive an expression for the vorticity in terms of the derivatives of the area and spanwise velocity. From (3.46),

$$\frac{\partial \tau}{\partial \tilde{T}} = \epsilon^{1/4} w_{0z}. \tag{3.75}$$

We expand $\tau = \tau_0 + \epsilon^{1/4}\tau_1$. Therefore,

$$\tau_{0\bar{t}} = 0, \quad \text{and,} \quad \tau_{0\bar{T}} + \tau_{1\bar{t}} = w_{0z}, \tag{3.76}$$

and with the introduction of the characteristic variable we have $w(z,\chi)$, implying,

$$\tau_{0\bar{T}} + \tau_{1\bar{t}} = w_{0z} + P_z w_{0\chi}. \tag{3.77}$$

Integrating over an orbit gives,

$$\int_\Pi \tau_{0\bar{T}} d\bar{t} + \int_\Pi \tau_{1\bar{t}} d\bar{t} = \int_\Pi w_{0z} d\bar{t} + \int_\Pi P_z w_{0\chi} d\bar{t}. \tag{3.78}$$

We can take the $\tau_{0\bar{T}}$ outside the integral using the first expression in (3.76) and the second term is zero since τ_1 is the same at the beginning and end of an orbit. Therefore (3.78) becomes,

$$\Pi \frac{\partial \tau_0}{\partial \bar{T}} = \int_\Pi \frac{\partial w_0}{\partial z}|_\chi \, d\bar{t} + \int_\Pi \frac{\partial w_0}{\partial \chi} P_z \, d\bar{t}. \tag{3.79}$$

$w_{0\chi}$ is constant since w_0 is independent of $\bar{t}$, from (3.64), and together with (3.68) and (3.73), we can rewrite the last term in (3.79) as,

$$\int_\Pi \frac{\partial w_0}{\partial \chi} P_z \, d\bar{t} = -\Pi \frac{\partial w_0}{\partial \chi} \frac{A_z}{A_\chi}. \tag{3.80}$$

The first term on the right hand side of (3.79) is more problematic as it seems difficult to immediately clarify whether or not $\frac{\partial w}{\partial z}|_\chi$ remains constant on a trajectory. The obstacle is removed by considering,

$$\frac{\partial}{\partial z}(\Pi w_0) = \frac{\partial}{\partial z}\int_\Pi w_0\, d\bar{t} = w_0\frac{\partial \Pi}{\partial z} + \int_\Pi \frac{\partial w_0}{\partial z}\, d\bar{t}, \tag{3.81}$$

and hence,

$$\begin{aligned}\int_\Pi \frac{\partial w_0}{\partial z}\, d\bar{t} &= -w_0\frac{\partial \Pi}{\partial z} + \frac{\partial}{\partial z}\int_\Pi w_0\, d\bar{t}, &(3.82)\\ &= \frac{\partial}{\partial z}(w_0\Pi) - w_0\frac{\partial \Pi}{\partial z}, &(3.83)\\ &= \Pi\frac{\partial w_0}{\partial z}. &(3.84)\end{aligned}$$

Therefore substitute (3.84) and (3.80) into (3.79),

$$\frac{d\tau_0}{d\bar{T}} = \frac{\partial w_0}{\partial z} - \frac{\partial w_0}{\partial \chi}\frac{A_z}{A_\chi}. \tag{3.85}$$

The jump is given, as in chapter 2, by

$$J_X = 2\frac{\partial}{\partial X}\int_0^{Y_e} \tau_0\, dY, \tag{3.86}$$

except here the upper limit of integration is Y_e, the limit of the Y extent of the vortex and Y_e is a function of X. Changing the variable in (3.86) derives the following expression for the jump term as a function of z and X,

$$\frac{\partial J}{\partial X} = 2\frac{\partial}{\partial X}\int_0^{Y_e} \tau_0\, dY = 2\frac{\partial Y_e}{\partial X}\tau_0(Y_e) + 2\int_0^{Y_e}\frac{\partial \tau_0}{\partial X}\, dY. \tag{3.87}$$

with $\tau_0(Y_e) = 0$. The expression $\tau_0(Y_e)$ represents the three-dimensional vorticity for particles at the edge of the vortex. These particles have no vorticity since they have spent very little time within the vortex and incoming particles have $\tau_0 = 0$. It is only when particles have spent some time within the vortex that their vorticity is non-zero.

Normalisation of the governing Equations

We now have the governing equations within the critical layer in the form of derivatives of the area of the orbit and, in the case of the vorticity, the derivatives of the spanwise velocity. These equations require a numerical approach and this will be considered in section 3.5. We now normalise the governing equation (3.32) in the main tier, which once again will allow us to solve the Benjamin-Ono equation as we can remove the $a_3\tilde{p}_{1X}$ and normalise by taking,

$$\check{p} = \tilde{p}_1 + \frac{a_3}{a_2}, \quad \text{and,} \quad \grave{p} = \frac{a_1}{a_2}\check{p}, \tag{3.88}$$

and hence we obtain,

$$\grave{p}_T + \grave{p}\grave{p}_X = \frac{1}{a_1\pi}\int_{-\infty}^{\infty} \frac{\grave{p}_{1ss}}{X-s}ds + \mu J_X. \tag{3.89}$$

Here $\mu = \frac{a_2}{a_1^2 b_{01}}$, and $J_X = \left([\tilde{u}_3]_{y_c-}^{y_c+}\right)_X$.

In order to continue our study of the critical layer vortex equations (3.74), (3.85) and (3.87), we introduce the following to normalise the equations and this will facilitate the numerical method. The normalisation used in the spanwise direction is,

$$z = z^*\xi, \tag{3.90}$$

with $-1 \leq \xi \leq 1$ and z^* the end point of the vortex in the spanwise direction or equivalently the spanwise point, where the area of the vortex is exactly zero but a vortex does exist at this point. It can be thought of as the point where a vortex has been newly created. The χ variable is normalised by introducing, ϕ, with,

$$\chi = \chi_{min} + \triangle\chi\phi, \tag{3.91}$$

with $0 \leq \phi \leq 1$ and $\triangle\chi = \chi_{max} - \chi_{min}$. These two normalisations have the effect of changing the solution space from an ellipse like shape to a rectangular shape. This acts to change the derivatives using the chain rule so that,

$$\frac{\partial}{\partial\chi} = \frac{1}{\triangle\chi}\frac{\partial}{\partial\phi}, \tag{3.92}$$

and,

$$\frac{\partial}{\partial z} = \frac{1}{z^*}\left(\frac{\partial}{\partial \xi} - \frac{1}{\triangle\chi}\left\{\frac{\partial \chi_{min}}{\partial \xi} + \phi\frac{\partial(\triangle\chi)}{\partial \xi}\right\}\frac{\partial}{\partial \phi}\right). \tag{3.93}$$

For clarity we will write $w_0 = w$ and $\tau_0 = \tau$. We also write, $\bar{T} = T$ as the vortex and the pressure develop at the same time scale. Substitution into (3.74) and (3.85) leads to,

$$\frac{\partial w}{\partial T} = \frac{1}{z^*}\left(\triangle\chi\frac{A_\xi}{A_\phi} - (\frac{\partial \chi_{min}}{\partial \xi} + \phi\frac{\partial \triangle\chi}{\partial \xi})\right), \tag{3.94}$$

and,

$$\frac{\partial \tau}{\partial T} = \frac{1}{z^*}\left(w_\xi - \frac{A_\xi w_\phi}{A_\phi}\right). \tag{3.95}$$

We can go further with (3.87) and derive the jump term in terms of our new variables; ξ and ϕ, since $\frac{\partial \tau}{\partial X} = P_X\frac{\partial \tau}{\partial \chi}$ and $d\chi = \triangle\chi d\phi$,

$$J_X = 2\int_0^{Y_e}\frac{\partial \tau}{\partial X}dY = 2\frac{P_X}{\triangle\chi}\int_{P(z,X)}^{\chi_{max}}\frac{\partial \tau}{\partial \phi}\frac{d\chi}{\sqrt{2(\chi - P)}}, \tag{3.96}$$

$$= 2P_X\int_{F(z,X)}^{1}\frac{\partial \tau}{\partial \phi}\frac{d\phi}{\sqrt{2(\chi_{min} + \phi\triangle\chi - P)}}, \tag{3.97}$$

with $F(z,X) = \frac{(P(z,X) - \chi_{min})}{\triangle\chi}$. We note that the integral converges but the integrand is divergent at the lower limit.

We now consider some special cases for values of ϕ and ξ, which correspond to the behaviour of the vortex at its extremes. We begin with a study for $\phi = 1$, which corresponds to particles that have been newly captured in the vortex and so the area of an orbit here is equal to the area of the vortex itself and there is not much simplification of the equations possible. One problem, which is difficult to overcome within the numerical method is that towards the edge of the vortex (near $\phi = 1$) new particles are entering the vortex as the vortex grows. The continuously growing vortex must be modelled using a discrete numerical method and so we could lose some information about the newly captured particles. In order to overcome this

problem we will derive an analytical approximation for the time a particle has spend inside the vortex. This is explained in section 3.4. Another potential problem in this case but resolved in the next section is that the integrals defining A_ξ and A_ϕ are divergent at $\phi = 1$. At $\phi = 1$,

$$\frac{dw}{dT} = \frac{1}{z^*}\triangle\chi\frac{A_\xi}{A_\phi} - \frac{\partial\chi_{max}}{\partial\xi}. \tag{3.98}$$

At the other extreme, $\phi = 0$ corresponds to the particle that was the first captured particle for that vortex (for a specific spanwise point), and we note that $\frac{\partial\chi_{min}}{\partial\xi} = P_\xi$,

$$\frac{dw}{dT} = -\frac{1}{z^*}\frac{\partial\chi_{min}}{\partial\xi}, \tag{3.99}$$

$$\frac{d\tau}{dT} = \frac{1}{z^*}\frac{\partial w}{\partial\xi}. \tag{3.100}$$

The consideration of the spanwise extremes of the vortex, which corresponds to $\xi = \pm 1$, has $A = 0 \Rightarrow A_\phi = 0$, $w = 0$ and $w_\phi = 0$. Also $\triangle\chi = 0$ at $\xi \pm 1$, therefore,

$$\frac{dw}{dT} = -\frac{1}{z^*}((\chi_{min})_\xi + \phi(\triangle\chi)_\xi), \tag{3.101}$$

$$\frac{d\tau}{dT} = \frac{1}{z^*}\frac{\partial w}{\partial\xi}. \tag{3.102}$$

The only other value of ξ for which we can obtain any useful information analytically is to use symmetry at $\xi = 0$ to find, $A_\xi = 0$ and hence,

$$\frac{dw}{dT} = 0, \tag{3.103}$$

$$\frac{d\tau}{dT} = \frac{1}{z^*}\frac{\partial w}{\partial\xi}. \tag{3.104}$$

These expressions ((3.98) - (3.104)) are useful when we consider the numerical method in section 3.5.

3.2 Behaviour for $\phi \sim 1$

As we have derived the critical layer equations, (3.94) and (3.95), in a normalised form we may now consider some features of these equations. There are three sets of analysis, which are motivated by the numerical method. The three sets of analysis are necessary either to verify that the numerical method will work or alternatively to provide some guidance in our approach to the numerical method. This section and section 3.3 fall into the former category. In this section we will consider the behaviour of particles near $\phi = 1$, so that we may verify that the ratio of the integrals required in our numerical method is not divergent. In section 3.3 we will verify that the jump term is continuous as we move towards the streamwise extremes of the vortex. In effect we verify that $J_X \to 0$ as $X \to X_L, X_R$. In section 3.4 we consider particles that have been newly captured inside the vortex. We will explain in section 3.4 that we must consider these particles as it is necessary to find the time a particle has spent inside a vortex for use in the numerical method, which is explained in section 3.5.

The integrals defining A_z and A_χ are divergent at $\phi = 1$ but we find here that their ratio is finite and additionally the ratio tends to the streamwise derivative of the pressure at the right end of the vortex. We consider χ near χ_{max}. Therefore, $\chi = \bar{P} - \epsilon$, where $\bar{P} = P(X_R) = P(X_L)$ and $\epsilon = 0$ corresponds to the vortex edge. There is a difference in behaviour of the pressure at X_R and X_L. At X_R, $P_X(X_R) = 0$ but at X_L, $P_X(X_L) \neq 0$. We consider the following integral,

$$I_f(\chi) = \int_{x_1}^{x_2} \frac{f(X)}{\sqrt{\chi - P(X)}}\, dX, \tag{3.105}$$

and study the behaviour as $\epsilon \to 0$. We find, $x_1 = X_L + b\epsilon$, where $b = |P_X(X_L)|^{-1}$ and $x_2 = X_R - a\epsilon^{1/2}$, where $a = \sqrt{\frac{2}{|P_{XX}(X_R)|}}$. The difference in the expansions for X_L and X_R is due to the streamwise derivative of the pressure being equal to zero at X_R. Near the left end of the vortex $\sqrt{\chi - P} = O(\epsilon^{1/2})$, $X - X_L = O(\epsilon)$. This gives, assuming $f = O(1)$, a contribution to I_f of order $\epsilon^{1/2}$. In the middle of the vortex,

$\sqrt{\chi - P} = O(1)$, $X - X_L = O(1)$, $X_R - X = O(1)$ and therefore a contribution to I_f of order 1. Towards the right end of the vortex, $X_R - X = O(\epsilon^{1/2})$ and the integrand is of order $\epsilon^{-1/2}$ giving a contribution of order 1 again. However the integrand in the right-most region behaves like $\frac{1}{X_r - X}$ as we move left towards the centre of the vortex. This effect boosts the contribution at the right end by a factor $\log(\epsilon)$ as we now show.

We follow the method outlined in Hinch (1991) and split the range of integration into two. The first covering the bulk of the flow and the left end of the vortex and the second integral range covers only the right end of the vortex. We introduce δ, where $0 < \epsilon^{1/2} \ll \delta \ll 1$ and rewrite (3.105) so that,

$$I_f(\chi) = \int_{X_L}^{X_R - \delta - a\epsilon^{1/2}} \frac{f(X)}{\sqrt{\chi - P(X)}}\, dX + \int_{X_R - \delta - a\epsilon^{1/2}}^{X_R - a\epsilon^{1/2}} \frac{f(X)}{\sqrt{\chi - P(X)}}\, dX. \tag{3.106}$$

We concentrate on the second integral as the first integral's only effect is to cancel the δ from the second integral for the solution for I_f since I_f should be independent of δ. Expanding using a Taylor series and using $\chi = \bar{P} - \epsilon$ gives,

$$J_f(\bar{P} - \epsilon) = \int_{X_R - \delta - a\epsilon^{1/2}}^{X_R - a\epsilon^{1/2}} \frac{f(X_R) + \ldots}{\sqrt{\bar{P} - \epsilon - \left\{\bar{P} - \frac{P_{XX}(X_R)}{2}(X_R - X)^2 + \ldots\right\}}}\, dX, \tag{3.107}$$

and write, $X = X_R - \epsilon^{1/2}a - \epsilon^{1/2}s$ so that,

$$\begin{aligned} J_f(\bar{P} - \epsilon) &= \int_{\delta/\epsilon^{1/2}}^{0} -\frac{f(X_R)\epsilon^{1/2}}{\sqrt{\epsilon\left((a+s)^2\frac{P_{XX}}{2} - 1\right)}}\, ds, && (3.108) \\ &= f(X_R)a \int_0^{\delta/\epsilon^{1/2}} \frac{ds}{\sqrt{s^2 + 2as}}, && (3.109) \\ &= f(X_R)a \int_0^{\delta/\epsilon^{1/2}} \frac{ds}{\sqrt{(s+a)^2 - a^2}}, && (3.110) \end{aligned}$$

where again $a = \sqrt{\frac{2}{|P_{XX}(X_R)|}}$. We may solve this to find,

$$J_f(\bar{P}-\epsilon) = f(X_R)a\sqrt{\frac{2}{-P_{XX}(X_R)}}\cosh^{-1}\left(\frac{\delta}{\epsilon^{1/2}a}\right), \tag{3.111}$$

$$\sim f(X_R)a\sqrt{\frac{2}{-P_{XX}(X_R)}}\log\left(\frac{2\delta}{\epsilon^{1/2}a}\right). \tag{3.112}$$

This logarithm gives a contribution of size $\log\delta$ as well as a term in $\log\epsilon$. The term in $\log\delta$ is cancelled by a similar term that arises in an analysis of the first integral in (3.106) as $\delta \to 0$, and this occurs since the total integral is independent of δ. Thus,

$$I_f(\bar{P}-\epsilon) \sim \frac{af(X_R)}{2}\log\left(\frac{1}{\epsilon}\right). \tag{3.113}$$

We have that $A_z = I_f(\chi)$ with $f(X) = -P_z(X)$ from (3.73) and we also have that $A_\chi = I_f(\chi)$ with $f(X) = 1$ from (3.72). Hence,

$$\frac{A_z}{A_\chi} \sim -P_z(X_R) \qquad \text{as } \chi \to \chi_{max}. \tag{3.114}$$

The result is important for the numerical method and for the analysis that follows. It also confirms the spanwise velocity and vorticity to be finite at the edge of the vortex.

3.3 The Jump Term at X_R and X_L

The vortex jump term generated by the critical layer vortex equations for each spanwise point is only non-zero in the streamwise direction for a small X range corresponding to the streamwise size of the vortex ($X_L \leq X \leq X_R$). For the streamwise region where no vortex exists we assume the jump term to be zero. It is therefore important that the jump term decays to zero at both ends of the vortex (within $X_L \leq X \leq X_R$). We will show that this is the case. The influence this jump term has on the left hand side of the governing Benjamin-Ono equation is also considered and we are able to deduce at the end of this section that the vortex jump does not generate a divergent pressure. Thus it is safe to continue with the derived critical layer vortex equations. This analysis uses the result that $\frac{A_z}{A_\chi} \sim -P_z(X_R)$ near the edge of the vortex (for $\chi \sim \chi_{max}$ or equivalently $\phi \sim 1$) and we start by finding $d\chi$ and dT using our expression for the area, defined on page 132,

$$A = \int_{X_L}^{X_R} \sqrt{\chi - P(z,X,T)}\, dX. \tag{3.115}$$

Therefore,

$$dA = \int_{X_L}^{X_R} \frac{d\chi - P_T dT}{\sqrt{\chi - P(z,X,T)}}\, dX, \tag{3.116}$$

using the chain rule. By taking the area as fixed (i.e. $dA = 0$), we obtain,

$$dT = d\chi \left(\frac{\int_{X_L}^{X_R} \frac{dX}{\sqrt{\chi - P(z,X,T)}}}{\int_{X_L}^{X_R} \frac{P_T\, dX}{\sqrt{\chi - P(z,X,T)}}} \right). \tag{3.117}$$

The dT is the time in orbit and we may rewrite the above to yield,

$$\text{time in orbit} \sim d\chi \frac{1}{P_T(X_R)}, \tag{3.118}$$

for χ near χ_{max}. This analytic form for the time in orbit of a particle confirms that the time in orbit is not infinite near X_R although the period is infinite. This form also suggests that a linear approximation to the exact time in orbit is sufficient.

The spanwise velocity is given by,

$$w \sim \int \frac{A_z}{A_\chi}\, dT, \tag{3.119}$$

$$\sim -\int \frac{P_z(X_R)}{P_T(X_R)}\, d\chi, \tag{3.120}$$

using the result in (3.118) and the result from the previous section. Therefore,

$$w \sim -\frac{P_z(X_R)}{P_T(X_R)}\left(\chi - P(X_R)\right). \tag{3.121}$$

Differentiation gives,

$$w_\chi \sim -\frac{P_z(X_R)}{P_T(X_R)}, \quad \text{and,} \quad w_z \sim \frac{(P_z(X_R))^2}{P_T(X_R)} - \left(\frac{P_z(X_R)}{P_T(X_R)}\right)_z \left(\chi - P(X_R)\right),$$

so that,

$$\frac{d\tau}{dT} = w_z - w_\chi \frac{A_z}{A_\chi}, \tag{3.122}$$

$$\sim w_z + w_\chi P_z(X_R), \tag{3.123}$$

$$\sim -\left(\frac{P_z(X_R)}{P_T(X_R)}\right)_z \left(\chi - P(X_R)\right). \tag{3.124}$$

Hence,

$$\tau \sim -\frac{1}{2}(P(X_R) - \chi)^2 \left(\frac{P_z(X_R)}{P_T(X_R)}\right)_z \frac{1}{P_T(X_R)}. \tag{3.125}$$

Again we use $\tau_X = P_X \tau_\chi$ so that in this special case of $\chi \sim \chi_{max}$,

$$\tau_X = P_X(P(X_R) - \chi)\Upsilon, \qquad \text{where,} \qquad \Upsilon = \left(\frac{P_z(X_R)}{P_T(X_R)}\right)_z \frac{1}{P_T(X_R)}. \tag{3.126}$$

The jump term is then,

$$J_X = 2\Upsilon P_X(X) \int_0^{Y_e} P(X_R) - (\frac{Y^2}{2} + P(X))\, dY, \tag{3.127}$$

$$= 2\Upsilon P_X(X) \left[-\frac{1}{6}Y^3 + (P(X_R) - P(X))\, Y\right]_0^{Y_e}. \tag{3.128}$$

It is important to note that the $P(X)$ and $P_X(X)$ above are local variables and not fixed at X_R. Equation (3.128) is an expression for the jump term for $\chi \sim \chi_{max}$

or $\phi \sim 1$. To study the behaviour at the streamwise end points we consider the behaviour of the pressure near X_R and X_L. We begin with X_R. Here, $\chi = P(X_R)$, $P(X) = P(X_R) + (X - X_R)^2 P_{XX}(X_R)$ and $P_X(X) = (X - X_R)P_{XX}(X_R)$. Therefore $\frac{Y^2}{2} = \chi - P$ becomes,

$$\frac{Y_e^2}{2} + \frac{P_{XX}(X_R)}{2}(X - X_R)^2 = 0, \tag{3.129}$$

and so $Y_e \sim (X - X_R)\sqrt{-P_{XX}(X_R)}$, as $P_{XX}(X_R) < 0$. Therefore,

$$\begin{aligned} J_X &\sim 2\Upsilon P_X(X)(X - X_R)^3 \left(-P_{XX}(X_R)\right)^{3/2}, & (3.130)\\ &= 2\Upsilon (X - X_R)^4 \left(-P_{XX}(X_R)\right)^{5/2}. & (3.131) \end{aligned}$$

This tends to zero very quickly as $X \to X_R$ and so the jump term is continuous at the right hand end.

At X_L, $\chi = P(X_L)$, $P(X) = P(X_L) + (X - X_L)P_X(X_L)$ and $P_X(X) = P_X(X_L) + (X - X_L)P_{XX}(X_L)$. Therefore $Y_e \sim \sqrt{(X - X_L)}\sqrt{-P_X(X_L)}$, as $P_X(X_L) < 0$ and,

$$\begin{aligned} J_X &\sim 2\Upsilon P_X(X)(X - X_L)^{3/2} \left(-P_X(X_L)\right)^{3/2}, & (3.132)\\ &= 2\Upsilon \left(-P_X(X_L)\right)^{5/2} (X - X_L)^{3/2}. & (3.133) \end{aligned}$$

Now this also tends to zero but more slowly. Here the dependence of X_L on time is critical. In the Benjamin-Ono equation the terms must balance and so, $P_T \sim J_X \sim (X - X_L)^{3/2}$. Thus if X_L were independent of time then we would also have $P \sim J_X \sim T(X - X_L)^{3/2}$ at X_L. This implies that $P_{XX} \sim (X - X_L)^{-1/2}$, which diverges as $X \to X_L$. We can therefore deduce that if the vortex stops growing in the streamwise direction then yet another singularity appears into the equations possibly leading to a new set of equations at still shorter length scales.

3.4 Analysis at vortex generation

As part of the numerical method it is important to consider the initial conditions for the vortex carefully due to the use of the Benjamin Ono solver at discrete time steps and hence a situation arises where at a time step, $n-1$, say, there is no vortex but then one does exist at time step n. Some of the particles in the vortex could have been trapped for almost the entire time step, where as others could have been newly captured. If the time spent in the vortex of each particle were not considered then each particle would have an equal weighting for the initial condition and it would be as though all the particles were instantaneously created at time step, $n-1$, with zero velocity and vorticity and had the entire time interval in which to grow. For example, near $|\xi| = 1$ the particle has only just been captured and has been in the vortex for a time less than δT, the size of the time step. In this section we consider an approximation for the pressure and use this to find an expression for the time a particle has spent in the vortex, which we use as part of the numerical method. We also find an expression for the spanwise velocity but it is a complicated expression involving elliptic integrals.

We look at a similarity form for the initial vortex generation, assuming,

$$P = -X^3 + X(T - z^2) + a + bz^2, \tag{3.134}$$

with $z^* = \sqrt{T}$ to study the behaviour of a newly created vortex. The form of (3.134) is chosen as it is a close approximation to the behaviour of the pressure at the creation of a vortex. We know that the pressure is approximately a cubic polynomial in X and that locally the spanwise dependence is quadratic. a and b are constants. We would like to use ϕ in our analysis and hence we need χ_{min} and χ_{max} since, $\chi = \chi_{min} + \phi\triangle\chi$. We may find X_{min} by minimising the expression in (3.134) and hence,

$$P(X_{min}) = \chi_{min} = a + bz^2 - \frac{2}{3\sqrt{3}}(T - z^2)^{3/2}. \tag{3.135}$$

We may find X_R by maximising P in (3.134), from which we can find $\chi_{max} = P(X_R)$, so that,

$$\triangle\chi = \chi_{max} - \chi_{min} = \frac{4}{3\sqrt{3}}(T - z^2)^{3/2}. \tag{3.136}$$

Therefore,

$$\chi = a + bz^2 + \frac{2}{3\sqrt{3}}(T - z^2)^{3/2}(2\phi - 1). \tag{3.137}$$

From section 3.3 and defining $R = \chi_{min} + \phi\triangle\chi$ with $z = z^*\xi$ we have,

$$\frac{dw}{dT} = \frac{A_z}{A_\chi} = \frac{\triangle\chi A_\xi}{z^* A_\phi} - \frac{R_\xi}{z^*}, \tag{3.138}$$

with an extra term due to the change of variable. We may rewrite R using (3.135) and (3.136) so that, $R = a + b(z^*)^2\xi^2 + \frac{2}{3\sqrt{3}}T^{3/2}(1 - \xi^2)^{3/2}(2\phi - 1)$. We also know that $A = 2\int_{x_{0L}}^{x_{0R}} \sqrt{\chi - P(\xi, s, T)}ds$, which on differentiation and recalling that χ is given by R, a function of ξ in this model case, implies,

$$A_\xi = \int_{x_{0L}}^{x_{0R}} \frac{R_\xi - P_\xi}{\sqrt{\chi - P(\xi, s, T)}}ds,$$

and,

$$A_\phi = \int_{x_{0L}}^{x_{0R}} \frac{\triangle\chi}{\sqrt{\chi - P(\xi, s, T)}}ds.$$

Substituting for the derivatives of area into (3.138) and rearranging leads to,

$$\frac{dw}{dT} = -\frac{\int_{x_{0L}}^{x_{0R}} P_\xi/\sqrt{\chi - P(\xi, s, T)}ds}{z^* \int_{x_{0L}}^{x_{0R}} 1/\sqrt{\chi - P(\xi, s, T)}ds}. \tag{3.139}$$

The pressure is known from (3.134). Therefore, $P_\xi = -2XT\xi + 2b(z^*)^2\xi$ and writing $z^* = \sqrt{T}$ so that,

$$\frac{dw}{dT} = \frac{2\xi}{t^{1/2}} \frac{\int_{x_{0L}}^{x_{0R}} s/\sqrt{\chi - P(\xi, s, T)}ds}{\int_{x_{0L}}^{x_{0R}} 1/\sqrt{\chi - P(\xi, s, T)}ds} - 2bT\xi. \tag{3.140}$$

As we will show, the integrals in (3.140) can be solved using elliptic integrals but first a change of variable is needed. We use $s = rT^{1/2}(1-\xi^2)^{1/2}$, $Q = \varrho(2\phi - 1)$ and $\varrho = \frac{2}{3\sqrt{3}}$ so that,

$$\frac{dw}{dT} = (2\xi(1-\xi^2)^{1/2}T)\frac{\int_{r_L}^{r_R} \frac{r}{\sqrt{Q+r^3-r}}dr}{\int_{r_L}^{r_R} \frac{1}{\sqrt{Q+r^3-r}}dr} - 2bT\xi, \tag{3.141}$$

$$= (2\xi(1-\xi^2)^{1/2}T)\frac{I(\phi)}{J(\phi)} - 2bT\xi, \tag{3.142}$$

by defining $I(\phi) = \int_{r_L}^{r_R} \frac{r\,dr}{\sqrt{Q+r^3-r}}$, $J(\phi) = \int_{r_L}^{r_R} \frac{dr}{\sqrt{Q+r^3-r}}$ and,

$$r_{R,L} = \frac{X_{0R,0L}}{T^{1/2}(1-\xi^2)^{1/2}}. \tag{3.143}$$

The expression for $\frac{dw}{dT}$ will be used later on page 152.

Finding an Expression for the Area of an Orbit

We define the area as $\kappa(\phi)$,

$$\kappa(\phi) = \int_{\beta_3}^{\beta_2} \sqrt{Q + r^3 - r}dr, \tag{3.144}$$

with $Q + r^3 - r = (r-\beta_1)(r-\beta_2)(r-\beta_3)$ and $\beta_1 > \beta_2 > \beta_3$. We are left with an elliptic integral ($\kappa(\phi)$) for the area and a ratio of elliptic integrals for the spanwise velocity (I/J), which are solved using standard substitution techniques. We may rewrite the area, $\kappa(\phi)$ by multiplying by $\frac{\sqrt{Q+r^3-r}}{\sqrt{Q+r^3-r}}$ so that,

$$\kappa(\phi) = \int_{\beta_3}^{\beta_2} \frac{Q + r^3 - r}{\sqrt{Q + r^3 - r}}dr. \tag{3.145}$$

We define $J_n = \int \frac{r^n\,dr}{\sqrt{Q+r^3-r}}$ and therefore,

$$\kappa(\phi) == QJ_0 + J_3 - J_1. \tag{3.146}$$

Erdélyi *et al.* (1953) gives a recurrence relation for integrals of the form, $J_n = \int \frac{r^n}{y}\,dr$ such that,

$$3a_0J_4 + 2.5a_1J_3 + 6.2a_2J_2 + 2.3a_3J_1 + a_4J_0 = ry,$$

with y of the form $y^2 = a_0r^4 + 4a_1r^3 + 6a_2r^2 + 4a_3r + a_4$. In the situation here we have $y = \sqrt{Q + r^3 - r}$. Hence, we have $a_0 = 0$, $a_1 = \frac{1}{4}$, $a_2 = 0$, $a_3 = -\frac{1}{4}$ and $a_4 = Q$. Thus the recurrence relation becomes,

$$\frac{10}{4}J_3 - \frac{6}{4}J_1 + QJ_0 = r\sqrt{Q + r^3 - r}.$$

The right hand side is zero at $r = \beta_2$ and $r = \beta_3$, the ends of the interval of integration. Therefore,

$$J_3 = \frac{4}{10}(\frac{6}{4}J_1 - QJ_0)),$$

implying, from (3.146),

$$\text{Area} = \kappa(\phi) = \frac{1}{5}(3QJ_0 - 2J_1).$$

Therefore, by putting $J_0 = J$ and $J_1 = I$,

$$\text{Area} = \kappa(\phi) = \frac{1}{5}(3QJ - 2I). \tag{3.147}$$

$J(\phi)$ can be dealt with by considering,

$$J(\phi) = \int_{\beta_3}^{\beta_2} \frac{dr}{\sqrt{Q + r^3 - r}} = \int_{\beta_3}^{\beta_2} \frac{dr}{\sqrt{(r - \beta_1)(r - \beta_2)(r - \beta_3)}}.$$

To put the integral into Legendre's normal form we use the transformation, $r = \beta_3 + \beta_{23}\sin^2\theta$, to find,

$$J(\phi) = \frac{2}{\sqrt{\beta_{13}}}\int_0^{\pi/2} \frac{d\theta}{\sqrt{1 - m^2\sin^2\theta}},$$

where $\beta_{ij} = \beta_i - \beta_j$ and $m^2 = \frac{\beta_{23}}{\beta_{13}}$ (Erdélyi *et al.* 1953). The final integral needed is $I(\phi)$, which can be found by rewriting and substituting, $r = \beta_3 + \beta_{23}\sin^2\theta$,

$$I(\phi) = \int_{\beta_3}^{\beta_2} \frac{r\,dr}{\sqrt{(r-\beta_1)(r-\beta_2)(r-\beta_3)}}, \tag{3.148}$$

$$= \int_{\beta_3}^{\beta_2} \frac{(r-\beta_1)\,dr}{\sqrt{(r-\beta_1)(r-\beta_2)(r-\beta_3)}} + \int_{\beta_3}^{\beta_2} \frac{\beta_1\,dr}{\sqrt{(r-\beta_1)(r-\beta_2)(r-\beta_3)}},$$

$$= -2\sqrt{\beta_{13}} \int_0^{\pi/2} \sqrt{1-m^2\sin^2\theta}\,d\theta + \frac{2\beta_1}{\sqrt{\beta_{13}}} \int_0^{\pi/2} \frac{d\theta}{\sqrt{1-m^2\sin^2\theta}}. \tag{3.149}$$

Hence we find,

$$I(\phi) = -2\sqrt{\beta_{13}}E(m) + \frac{2\beta_1}{\sqrt{\beta_{13}}}K(m),$$

where, $E(m) = \int_0^{\pi/2} \sqrt{1-m^2\sin^2\theta}\,d\theta$ and $K(m) = \int_0^{\pi/2} \frac{d\theta}{\sqrt{1-m^2\sin^2\theta}}$. Hence,

$$\frac{I}{J} = -\beta_{13}\frac{E}{K} + \beta_1. \tag{3.150}$$

We have on substitution into (3.147),

$$Area = \kappa(m) = \frac{1}{5}(3QJ - 2I), \tag{3.151}$$

$$= \frac{2}{5}\sqrt{\beta_{13}}\,(3QK + 2\beta_{13}E - 2\beta_1 K)\,. \tag{3.152}$$

Thus we have found an expression for the area of an orbit in terms of the elliptic integrals, E and K.

Expression for the Time In Orbit of a Particle

In order to find an expression for the time in orbit, a particle path through ξ and ϕ with respect to time is needed as they change for each time step but as time progresses the particle is fixed at a specific z coordinate. If at time T a particle has z coordinate, $z = T^{1/2}\xi$ and at an earlier time, t its ξ value was $\bar{\xi}$ then,

$$t^{1/2}\bar{\xi} = T^{1/2}\xi \quad \Rightarrow \quad \bar{\xi} = \frac{T^{1/2}\xi}{t^{1/2}}. \tag{3.153}$$

This particle at this fixed z position entered the vortex at some time, t^*, at which time for this particle, $\xi = 1$ and so,

$$z = (t^*)^{1/2} = T^{1/2}\xi \quad \Rightarrow \quad t^* = T\xi^2. \tag{3.154}$$

To find the value of ϕ the areas of the orbits must be considered. The area of the orbit is conserved for this particular particle as the vortex grows. If a particular orbit was first entrained at $T = \bar{t}$ then,

$$A(\xi, \phi, T) = A(\bar{\xi}, 1, \bar{t}), \tag{3.155}$$

and,

$$\begin{aligned} &\int_{X_{0L}}^{X_{0R}} \sqrt{\varrho(T - z^2)^{3/2}(2\phi - 1) + X^3 - (T - z^2)X}\, dX \\ &\qquad = \int_{X_{0L}}^{X_{0R}} \sqrt{\varrho(\bar{t} - z^2)^{3/2} + X^3 - (\bar{t} - z^2)X}\, dX, \end{aligned} \tag{3.156}$$

which is an expression for $\bar{t}$, the time the orbit corresponding to ϕ was entrained, if it is T now. Making a change of variable gives,

$$\begin{aligned} &(T - z^2)^{5/4} \int_{r_L}^{r_R} \sqrt{\varrho(2\phi - 1) + r^3 - r}\, dr \\ &\qquad = (\bar{t} - z^2)^{5/4} \int_{r_L}^{r_R} \sqrt{\varrho + r^3 - r}\, dr, \end{aligned} \tag{3.157}$$

with ϱ, r_R and r_L defined earlier. Therefore,

$$(T - z^2)^{5/4}\kappa(\phi) = (\bar{t} - z^2)^{5/4}\kappa(1). \tag{3.158}$$

If $z = T^{1/2}\xi$ and $\bar{t} = \bar{\mu}T$, then $\bar{\mu} \in [0, 1]$ and we have,

$$\frac{(1 - \xi^2)}{(\bar{\mu} - \xi^2)} = \left[\frac{\kappa(1)}{\kappa(\phi)}\right]^{4/5}, \quad \text{or,} \quad \bar{\mu} = \xi^2 + (1 - \xi^2)\left[\frac{\kappa(\phi)}{\kappa(1)}\right]^{4/5}. \tag{3.159}$$

So the time in orbit, $\hat{T}$ is,

$$\begin{aligned}
\hat{T} &= (T - \bar{t}), && (3.160)\\
&= T(1 - \bar{\mu}), && (3.161)\\
&= T(1 - \xi^2 - (1 - \xi^2)\left[\frac{\kappa(\phi)}{\kappa(1)}\right]^{4/5}, && (3.162)\\
&= T(1 - \xi^2)\left(1 - \left[\frac{\kappa(\phi)}{\kappa(1)}\right]^{4/5}\right). && (3.163)
\end{aligned}$$

This is the expression for the time a particle has spent within the vortex. This is an important result as we will use it in the numerical method in section 3.5 to gain some understanding of the behaviour of particles entering the vortex between numerical time steps.

Expression for the Spanwise Velocity

We now find an expression for the spanwise velocity but we will find that is too complicated to be incorporated into the numerical method. To relate ϕ now to the value of ϕ, $\tilde{\phi}$ say, of the orbit at earlier time, $t < T$ then we use,

$$\begin{aligned}
&\int_{X_{0L}}^{X_{0R}} \sqrt{\varrho(T - z^2)^{3/2}(2\phi - 1) + X^3 - (T - z^2)X}\, dX\\
&= \int_{X_{0L}}^{X_{0R}} \sqrt{\varrho(t - z^2)^{3/2}(2\tilde{\phi} - 1) + X^3 - (t - z^2)X}\, dX,
\end{aligned} \qquad (3.164)$$

which implies,

$$(T - z^2)^{5/4}\kappa(\phi) = (\bar{t} - z^2)^{5/4}\kappa(\tilde{\phi}), \qquad (3.165)$$

after a change of variable as in (3.158). We also have that if $z = T^{1/2}\xi$ and $t = \lambda T$ with $\lambda \in [0, 1]$, then,

$$\lambda = \xi^2 + (1 - \xi^2)\left[\frac{\kappa(\phi)}{\kappa(\tilde{\phi})}\right]^{4/5}, \quad \text{or,} \quad \kappa(\tilde{\phi}) = \kappa(\phi)\left[\frac{1 - \xi^2}{\lambda - \xi^2}\right]^{5/4}. \qquad (3.166)$$

We now return to the expression for $\frac{dw}{dT}$ given by (3.141) and integrate,

$$w(T,\phi,\xi) = \int_t^T 2\xi(1-\xi^2)^{1/2}\hat{t}\frac{I(\tilde{\phi})}{J(\tilde{\phi})}d\hat{t} - \int_t^T 2b\xi\hat{t}d\hat{t}. \tag{3.167}$$

Therefore, with $\hat{t} = \bar{\lambda}T$,

$$w(T,\phi,\xi) = 2\xi(1-\xi^2)^{1/2}T^2\int_{\lambda(\xi,\phi)}^1 \frac{I(\tilde{\phi})}{J(\tilde{\phi})}\bar{\lambda}d\bar{\lambda} - 2b\xi T^2\int_{\lambda(\xi,\phi)}^1 \bar{\lambda}d\bar{\lambda}, \tag{3.168}$$

but from (3.166),

$$d\bar{\lambda} = -\frac{4}{5}(1-\xi^2)(\kappa(\phi))^{4/5}\frac{1}{(\kappa(\tilde{\phi}))^{9/5}}\frac{\partial\kappa}{\partial\tilde{\phi}}d\tilde{\phi}. \tag{3.169}$$

Hence,

$$\begin{aligned} w(T,\phi,\xi) &= \frac{8}{5}T^2(1-\xi^2)^{3/2}\xi(\kappa(\phi))^{8/5}\int_\phi^1 \frac{I(\tilde{\phi})}{J(\tilde{\phi})}\frac{1}{(\kappa(\tilde{\phi}))^{13/5}}\frac{\partial\kappa}{\partial\tilde{\phi}}d\tilde{\phi} \\ &- b\xi T^2(1-\xi^2)\left(1-\left[\frac{\kappa(\phi)}{\kappa(1)}\right]^{4/5}\right). \end{aligned} \tag{3.170}$$

Finally, since,

$$\frac{\partial\kappa}{\partial\tilde{\phi}} = \frac{2}{3\sqrt{3}}J(\tilde{\phi}), \tag{3.171}$$

then we obtain,

$$w(T,\phi,\xi) = T^2\xi(1-\xi^2)(q(\xi,\phi)+r(\phi)), \tag{3.172}$$

with,

$$q(\xi,\phi) = \frac{16}{15\sqrt{3}}(1-\xi^2)^{1/2}(\kappa(\phi))^{8/5}\int_\phi^1 \frac{I(\tilde{\phi})}{(\kappa(\tilde{\phi}))^{13/5}}d\tilde{\phi}, \tag{3.173}$$

and,

$$r(\phi) = b\left(1-\left[\frac{\kappa(\phi)}{\kappa(1)}\right]^{4/5}\right). \tag{3.174}$$

The important conclusion of this section is that we have found an expression for the time in orbit given by (3.163). We have been able to express the spanwise velocity in terms of functions of time, ϕ and ξ but this expression is too complicated to use in the later numerics.

3.5 Numerical Method

In this section a numerical method for solving the following equations is presented,

$$\frac{\partial w}{\partial T} = \frac{1}{z^*}\left(\triangle\chi\frac{A_\xi}{A_\phi} - (\frac{\partial\chi_{min}}{\partial\xi} + \phi\frac{\partial\triangle\chi}{\partial\xi})\right), \tag{3.175}$$

$$\frac{\partial\tau}{\partial T} = \frac{1}{z^*}\left(w_\xi - \frac{A_\xi w_\phi}{A_\phi}\right), \tag{3.176}$$

and,

$$J_X = 2P_X\int_{F(z,X)}^{1}\frac{\partial\tau}{\partial\phi}\frac{d\phi}{\sqrt{2(\chi_{min}+\phi\triangle\chi-P)}}, \tag{3.177}$$

with $F(z,X) = \frac{(P(z,X)-\chi_{min})}{\triangle\chi}$. In summary the method takes the three-dimensional pressure and its derivatives from the Benjamin-Ono solver of chapter 2, finds the areas of the vortices corresponding to these pressures before finding w, τ and the jump term. The important result, which allows us to implement the numerical method, is that the area of an orbit of a particle is constant as time progresses. Hence we may use area to compare results between different time steps even though the grids, defined by ϕ through $\triangle\chi$ and χ_{min} are different at each time step. The spanwise vortices are considered independent of each other and therefore the three-dimensional problem can almost, apart from the spanwise derivatives, be considered a series of two-dimensional problems. The numerical approach uses the same initial three-dimensional disturbances as chapter 2. Therefore,

$$P = P_0 + 0.1Xe^{-X^2}e^{-z^2}, \tag{3.178}$$

and hence,

$$P_X = P_{0X} + 0.1e^{-X^2}e^{-z^2} - 0.2X^2e^{-X^2}e^{-z^2}. \tag{3.179}$$

As with the numerical method in chapter 2, P_0 is the initial two-dimensional pressure provided by the Benjamin-Ono solver and it is of the form given on page 74.

The numerical method begins at $T = -1$ in the computational approach (corresponding to the beginning of step 2 in chapter 2). It marches forward in time following the algorithm on page 75 until there exists an X such that $P_X(X) = 0$ and hence there exists a vortex. In practice a test that $P_X \geq 0$ is sufficient since leading up to the creation of a vortex, $P_X(X) < 0$. If a vortex exists then we calculate the jump term using the method outlined below.

The description of the numerical method is written in two stages. The first describes how we extract values required for the normalisation of the equations from the Benjamin-Ono solver and find the area of the orbits. In the second stage we describe the method to solve for the spanwise velocity, vorticity and the jump term.

Normalisation and Finding the Area of an Orbit

At the end of section 3.1 we defined ξ and ϕ using,

$$z = z^*\xi \qquad (-1 \leq \xi \leq 1), \tag{3.180}$$

$$\chi = \chi_{min} + (\triangle\chi)\phi \qquad (0 \leq \phi \leq 1). \tag{3.181}$$

If a vortex exists then we must calculate z^*, χ_{min} and $\triangle\chi = \chi_{max} - \chi_{min}$. We commence with the calculation of z^*. This has been defined as the point in the spanwise direction where the area of the vortex is exactly zero or equivalently where $P_X = 0$ at only one X point. It is clear that it is required to find a root of some function but what is perhaps not as clear is how to choose this function. It is known that if $P_X = 0$ at only one X point then this point is a turning point in the X grid (i.e. $P_{XX} = 0$ at this X point). Therefore the spanwise point which gives an X point where $P_{XX} = 0$ and $P_X = 0$ is the required z^*. This is found in practice by using a root finding subroutine described in Press *et al.* (1986), which combines bisection with the secant method to find the root of the function that given a z returns the value of P_X at the X point where $P_{XX} = 0$. In other words we want z, such that, $f(z) = 0$, where $f(z) = P_X(z, X_1(z))$ with $P_{XX}(z, X_1(z)) = 0$. As part

of the implementation a four point polynomial interpolation in z is used to find P, P_X and P_{XX}. It is therefore important to have enough spanwise points in the range $-z^* \leq z \leq z^*$, which is achieved by keeping the spanwise stepsizes small to allow the interpolation routines to produce data that captures the key features inside the vortex with sufficient accuracy, since for early vortices, z^* is small, see figure 3.7.

The calculation of χ_{min} and χ_{max} is completed for each ξ as they are different for each spanwise position. The constants χ_{min} and χ_{max} are the local pressure minimum and maximum respectively and they are marked on figure 3.3 on page 129. It is therefore convenient to find the other necessary data relating to the pressure, the X extremes of the vortex and the area of the vortex at the same time. This process is rather simple, the only practical problem is minimising the errors as the values for the area of each orbit and $\triangle\chi$ found are small, especially in the initial stages of vortex generation. It is the derivatives of these variables that are used later and as calculating derivatives numerically tends to increase the size of the errors it is very important that errors are kept to a minimum. There are several values of interest to be extracted from the pressure data received from the Benjamin-Ono solver. χ_{min} is equal to the local pressure minimum and so a minimisation algorithm taken from Press *et al.* (1986) is used. The algorithm returns the value $P(X_{min})$ and X_{min}. The χ_{max} is found similarly. The notation from the derivation in section 3.1 is used here and hence the local pressure maximum is $P(X_R)$ with the X_R corresponding to the right hand side of the vortex. The left hand point of the vortex, X_L, is found using a root finding (again from Press *et al.* 1986) algorithm to find the root of $g(X) = P(X_R) - P(X)$.

It can be seen from the plots of pressure and its derivative (in figures 3.4 and 3.5) that for early times the vortex is very small. Hence some of the values calculated above will also be very small. Another potential complication is making sure that there are enough gridpoints in the streamwise grid. If the gridsize is too large then a situation arises where there are only a small number of streamwise points within the vortex. In this situation it becomes difficult to find the required normalisation

variables although still possible as the behaviour of the pressure is smooth, without any significant change in behaviour within the vortex.

These new variables were defined earlier where they were said to facilitate the numerical method. Here an argument as to why this is true is given. The introduction of the ξ variable in the spanwise plane allows the numerical method to concentrate on the vortex region only and ignore the spanwise regions where, as yet, no vortex exists. It also removes the need to handle complicated end conditions at the extreme spanwise point of the vortex. The ϕ variable removes complications introduced by the different χ grids for each z and the possibility that these χ grids could then be disjoint for each spanwise point. Storing the data on uniform ξ, χ grids also allows easy differentiation and storing of the data, which is necessary for the success of the numerical method.

It is also convenient to find the area for each ξ and χ such that $\chi_{min} \leq \chi \leq \chi_{max}$ within the same algorithm and before changing from the ξ, χ grid to the ξ, ϕ grid as all the necessary data has been calculated. The area is found numerically for each ξ and time step by using the adaptive Runge-Kutta method described in chapter 2 to integrate,

$$A = 2\sqrt{2} \int_{X_{0L}}^{X_{0R}} (\chi - P(z, s, T))^{1/2} \, ds,$$

i.e.

$$\frac{dA}{dX} = 2\sqrt{2} \, (\chi - P(z, X, T))^{1/2}, \tag{3.182}$$

for each χ to find $A(T, z, \chi)|_{X_{0R}}$ with $A(T, z, \chi)|_{X_{0L}} = 0$. The X_{0L} and X_{0R} are the points where $P(X_{0L}) = P(X_{0R}) = \chi$ (i.e. the left and right extremes of an orbit inside a vortex). At X_{0L} the area is zero and at X_{0R} the area is the area of the orbit. For $\chi = \chi_{max}$, we have $X_{0L} = X_L$ and $X_{0R} = X_R$ and hence the area of the orbit is the area of the whole vortex. In the case of $\chi = \chi_{min}$, then $X_{0L} = X_{0R}$ and so the area of the orbit is zero and this corresponds to the centre of the vortex.

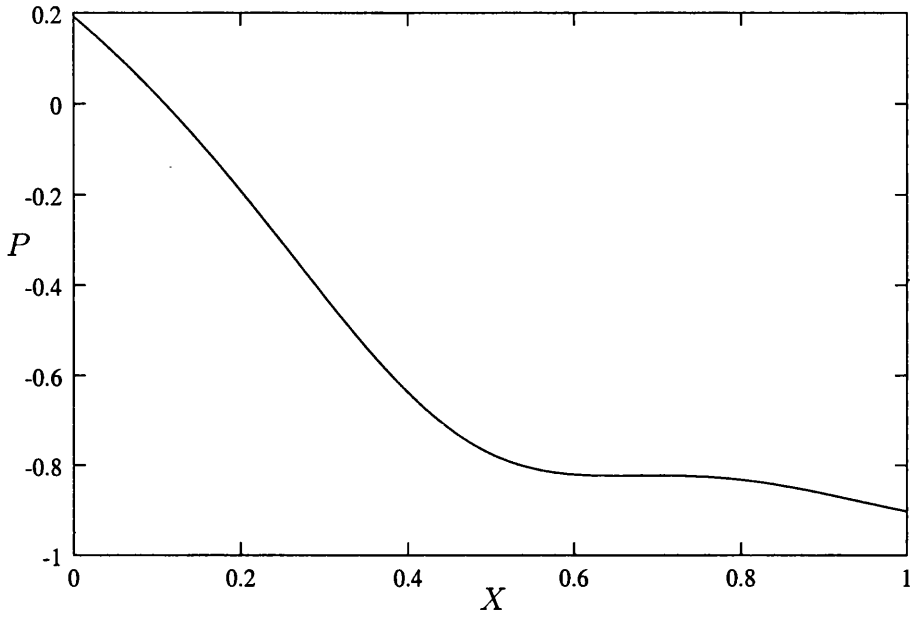

Figure 3.4: P at first vortex step for $\xi = 0$.

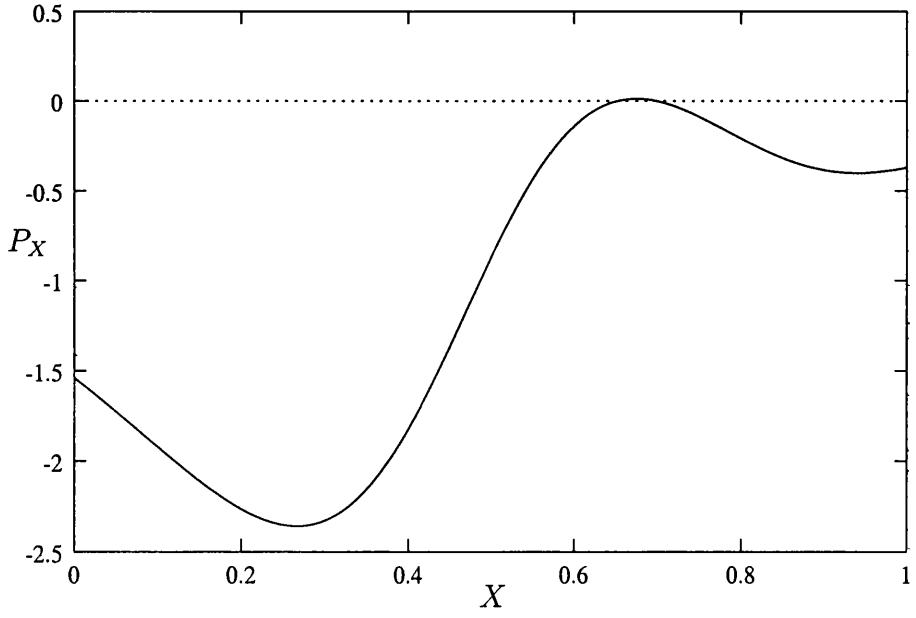

Figure 3.5: P_X at first vortex step for $\xi = 0$.

We now have $A(\xi, \phi)$ and using the difference scheme from Abramowitz & Stegun (1964) described in chapter 2 we find, $\frac{\partial A}{\partial \xi}$, $\frac{\partial A}{\partial \phi}$, $\frac{\partial \chi_{min}}{\partial \xi}$ and $\frac{\partial \triangle \chi}{\partial \xi}$, which are needed to find the spanwise velocity and vorticity. The area, as expected is 0 at $\phi = 0$, for all ξ and is also zero for $\xi = \pm 1$ for all ϕ. These correspond to orbits of zero area, which are the particles that were the first captured particles within the vortex. We find $\frac{\partial A}{\partial \xi}$, $\frac{\partial A}{\partial \phi}$ to be divergent at $\phi \to 1$ as we expect from the form of the integral but in section 3.2 we showed that their ratio is not divergent and so we may continue to use them to find w.

Finding the Spanwise Velocity, Vorticity and Jump Term

It would seem that since we are able to find area and its derivatives accurately we can find the spanwise velocity and vorticity by solving (3.175) and (3.176) using an ordinary differential equation solver. The boundary conditions on w and τ are straightforward, $w = \tau = 0$ on $\xi \pm 1$ as the vortex area here is zero and $w = \tau = 0$ on $\phi = 1$ as these particles have only just been captured. Initially $w = \tau = 0$ but there was some difficulty in implementing the initial condition in the numerical code. As a particle enters the vortex, $w = \tau = 0$, but in order to make use of this we must consider the growth of the vortex between time steps. For this we need the analysis of section 3.4.

The time a particle has spent inside a vortex will affect its velocity and hence its vorticity. This leads to the need for a consideration of the time a particle has spent inside the vortex for those particles newly captured inside a vortex. The time in orbit influence diminishes for those particles captured for a long time within the vortex. The time in orbit consideration and the constant addition of new captured particles into the vortex introduces problems which seem impossible to resolve, namely the introduction of discontinuities in the derivatives of the spanwise velocity and vorticity in the numerical regime at the point where the particles that existed within the vortex for a time greater than the time step, δT, meet particles that have been

captured within a time δT. Much effort has been undertaken to minimise this numerical discontinuity. The method outlined below minimises the discontinuities but due to the delicate nature of numerically calculated derivatives some errors are still introduced.

There are clearly two different circumstances to consider. The first is the behaviour at the first time step where there exists a vortex and the second is later time steps, where the vortex has had time to develop.

The first vortex time step

At this time step all particles have been newly captured (within a time δt) and significantly the analysis of section 3.4 holds since the assumption made for the pressure holds here. Therefore using the trapezium rule as a guide,

$$w = \frac{T}{2}(f^n(A) + f^c(A)), \tag{3.183}$$

$$\tau = \frac{T}{2}(h^n(A) + h^c(A)), \tag{3.184}$$

with $f(A) = \frac{1}{z^*}\left(\triangle\chi\frac{A_\xi}{A_\phi} - \frac{\partial}{\partial\xi}(\chi_{min} + \phi\triangle\chi)\right)$ and $h(A) = \frac{1}{z^*}\left(w_\xi - \frac{A_\xi w_\phi}{A_\phi}\right)$. This assumes the initial value of w and τ to be zero. As we have no previous data for the particles we must approximate the forcing at the time of capture, f^c and g^c. We use the result of section 3.2 to give,

$$f^c = -P_z(X_R), \tag{3.185}$$

and $h^c = 0$ since $w_\phi = w_\xi = 0$ at time of capture. T is the time in orbit, which was found in section 3.4 to be,

$$T = (\text{age of vortex})\,(1-\xi)^2\left(1 - \frac{A}{A_v}\right)^{4/5}. \tag{3.186}$$

This method produces smooth plots of w and τ, which are accurate enough to find the jump term using the method on page 162.

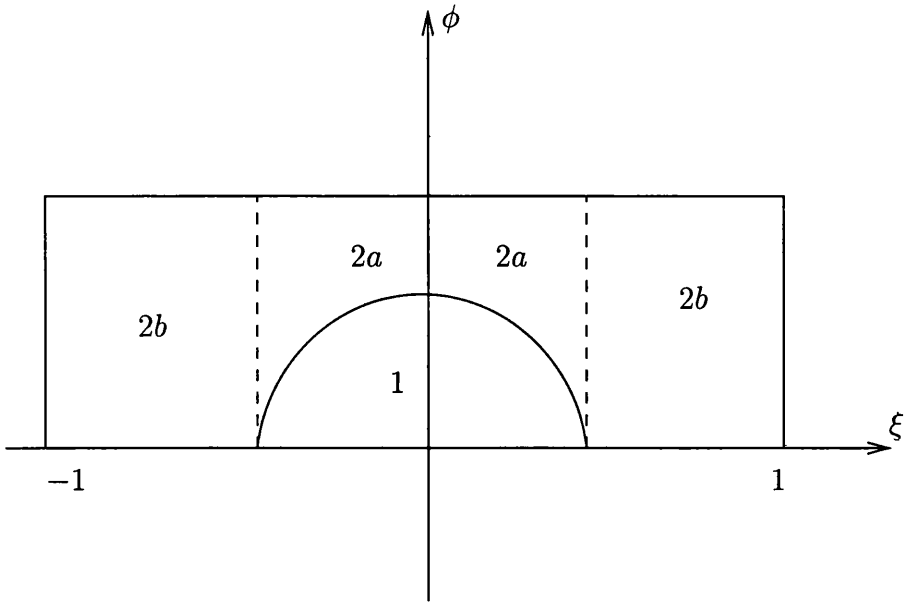

Figure 3.6: The Vortex in Normalised Coordinates showing the different categories of Particles at Later Time Steps.

Later time steps

It is at the later time steps that complications arise. This is due to the difference in behaviour between particles that existed within the vortex at the previous time step (defined here as category 1 particles) and those newly captured (categories 2a and 2b). We shall see that even a small difference in the particles' behaviour found numerically causes a discontinuity in the derivatives of the spanwise velocity, causing large spikes in the plots of τ. The best case is to have a second order trapezium scheme and use interpolation to approximate the data at the time of capture. The area of the orbit of a particle is used to decide into which category a particle should be placed. If the area of a particle's orbit is greater than the area of the vortex at the previous time step then the particle has been newly captured and is defined as a category 2 particle for the work that follows. A summary of the particle categories within the vortex is provided in figure 3.6.

The simplest case is the category 1 particles with orbits whose areas are less than the area of the vortex at the previous time step. For these particles we have all the necessary data: w and τ at the previous time step ($\bar{w}$ and $\bar{\tau}$); the forcing at the current time step (f^n and g^n) and the forcing at the previous time step (f^{n-1} and g^{n-1}). Thus,

$$w = \bar{w} + \frac{\delta T}{2}\left(f^n + f^{n-1}\right), \tag{3.187}$$

$$\tau = \bar{\tau} + \frac{\delta T}{2}\left(g^n + g^{n-1}\right). \tag{3.188}$$

Here we use δt since the particle has been captured within the vortex for a time greater than δt.

The category 2 particles are now considered. This category is itself divided into two since the vortex is growing in a streamwise direction (defined by $\Delta\chi$ and the vortex becomes larger for a fixed spanwise point) and in the spanwise direction (defined by the growth in z^* see figure 3.7). The first type of particles (category 2a) are those for which a vortex did exist at that spanwise point at the previous time step. Hence these are particles that have been captured due to the streamwise growth in the vortex. Category 2b particles are defined as particles whose spanwise extent is beyond the spanwise extent of the vortex at the previous time step. The spanwise velocity and vorticity for the category 2b particles are solved in the same way as the first time step particles since each spanwise vortex can be considered a two-dimensional problem.

The category 2a particles' velocity and vorticity are found by solving,

$$w = \frac{T}{2}\left(f^n(A) + f^c(A)\right), \tag{3.189}$$

$$\tau = \frac{T}{2}\left(g^n(A) + g^c(A)\right), \tag{3.190}$$

where f^c is an interpolated approximation for the forcing at the time of capture. It is given by, $f^c = f^n\theta + \bar{f}^e(1-\theta)$, with $\bar{f}^e$ the forcing at the edge of the vortex at the previous time step.

These methods introduce discontinuities in the derivatives of w and τ, which cause problems with the solution for the jump term.

The jump term

We use the expression (3.97) to find the jump term, with a slight modification as shown below, to avoid using a divergent integrand at the lower limit. The integrand in (3.97) is divergent at the lower limit although the integral is not divergent. In order to solve the integral numerically we must subtract the divergent part and then add it again. Therefore,

$$J_X = 2\int_{F(z,X)}^{1} P_X\left(\frac{\tau_\phi(\phi)-\tau_\phi(\phi=0)}{\sqrt{\chi_{min}+\phi\triangle\chi-P}}\right)d\phi + 2\int_{F(z,X)}^{1} P_X\left(\frac{\tau_\phi(\phi=0)}{\sqrt{\chi_{min}+\phi\triangle\chi-P}}\right)d\phi. \tag{3.191}$$

with $F(z,X) = \frac{(P(z,X)-\chi_{min})}{\triangle\chi}$. The first term must be solved numerically but crucially the integrand is not divergent. The second integral can be solved analytically and hence we need not worry that the integrand is divergent at the lower limit in this case. If the data for τ_ϕ is smooth then we obtain smooth plots for the jump term against ξ and X as shown for the first time step in figure 3.23.

3.6 Results

In this section we present sets of data of similar plots at different times in the vortex development. We also consider the behaviour of the parameters introduced into the numerical regime such as z^* and $\triangle\chi$. We begin with a set of eight figures which underline the rapid growth of the vortex as time progresses. There then follows a study of the behaviour of the spanwise velocity, vorticity and jump terms for two time steps. We end with two plots of the jump term at much later times.

The three figures 3.7, 3.8 and 3.9 underline the rapid growth of the vortex in both a spanwise direction with the z^* growth and in the streamwise and wall normal directions, as shown with the increases in vortex area and $\triangle\chi$. The first plot, showing z^* represents the spanwise growth. The growth is linear, apart from the last section of the graph. This is caused by a feature of the pressure distribution at this time. The pressure distribution implies that there exists a vortex for all z at later times. In other words the vortex expands to cover the entire spanwise domain in this model situation. Changing the initially small three-dimensional disturbance does not influence the time of this occurrence since it decays for large z, leaving the two-dimensional profile unaltered. At this time step the two-dimensional pressure itself implies the existence of a vortex. The influence of the chosen three-dimensional disturbance is to generate a vortex earlier than this.

The second plot, figure 3.8, shows the growth of the vortex's area with time. Again this growth in area is rapid. As this plot is for a fixed $\xi = 0$, corresponding to $z = 0$, the growth is also exhibited by the increases in $\triangle\chi$ shown in figure 3.9 and the increases in the streamwise extent of the vortex given by, $X_R - X_L$. The spanwise influence does not affect this graph. Plots showing the growth of $\triangle\chi$ are given in figures 3.9 and 3.10. Care should be taken when comparing the different plots in figure 3.10 since the ξ grid changes for each time step although $\xi = 0$ always corresponds to the centre of the vortex (at $z = 0$).

The growth in $\triangle\chi$ and $X_R - X_L$ is influenced by P_T. P_T is negative within the

vortex range, see figure 3.13, which results in a decrease in value of the pressure but significantly the pressure is decreased by a greater amount towards X_{min}. This has the effect of reducing $\chi_{min} = P(X_{min})$ more than the reduction in the value of $\chi_{max} = P(X_R)$. This causes an increase in their difference, $\Delta\chi$. The plots in figures 3.11 and 3.12 confirm this development. If we look at χ_{max} near $\xi = 0$, we see that it has reduced from approximately -0.8225 to -0.82, a reduction of approximately 0.0025 in five time steps, whereas χ_{min} has been reduced from -0.823 to -0.86, a difference of almost 0.4. A consideration of the behaviour of P_T also explains the behaviour shown in figures 3.14 and 3.15. The P_T acts to reduce X_L and X_R, corresponding to the vortex travelling upstream. Recall that this upstream movement is itself within a frame travelling downstream with speed c, see section 3.1 and so the overall vortex movement is downstream. This local upstream movement is captured in figures 3.14 and 3.15 for $\xi = 0$ with the X_L moving upstream from $X = 0.63$ to $X = 0.55$ within five time steps.

We are now able to turn our attention to the plots of the area of the orbits and their derivatives. These are important since they comprise the forcing for the spanwise velocity and vorticity. The behaviour of the area is consistent with our understanding of the vortex. There is a maximum at $\xi = 0$, $\phi = 1$ and the area is zero for all ξ at $\phi = 0$ (the streamwise "middle" of the vortex) and for all ϕ at $\xi = \pm 1$ (the spanwise extremes of the vortex). $\phi = 0$ corresponds to point orbits at X_{min}, the size of which is zero. $\phi = 1$ corresponds to orbits whose trajectories are equivalent to the edge of the vortex, thus we expect their areas to be greatest. The peak at $\xi = 0$ is expected as the vortex is largest at the line of symmetry, $\xi = 0$. The rapid vortex growth is demonstrated in figure 3.25 with a maximum area twenty times that of figure 3.16.

The integral representations of A_ξ and A_ϕ are divergent as $\phi \to 1$, see section 3.2. However we calculate A_ξ and A_ϕ using a difference method to differentiate the calculated area numerically. In figure 3.18 the divergence is modelled using the difference method although there is no hint of any divergence in figure 3.17. We

have shown that the ratio $\frac{A_\xi}{A_\phi}$ is not divergent and so we may use this ratio in the numerics. Near $\phi = 1$, the time in orbit is small and hence this feature doesn't dominate the numerical result for w. Its significance is its appearance in the forcing for the previous time step. It is this that introduces errors since the gradients of w and $\bar{w}$ are different causing discontinuities in their derivatives. The discontinuities or errors do not show themselves in the plots here due to the interpolation regimes for contour plotting. At the first time step the areas are very small but smooth plots of A, A_ξ and A_ϕ are still obtained, which suggests the reliability of the numerical method at this stage of the calculation. The plots at the fifth time step ($T = -0.355$) in figures 3.25, 3.26 and 3.27 confirm this durability as, with a significantly larger area, the plots of the derivatives are similar to the first time step calculations. The considerable growth in the area is caused by the two streamwise contributions noted earlier. A_ϕ is 0 at $\xi \pm 1$, which is true since numerically the vortex exists at one point only and hence $\chi_{min} = \chi_{max}$ and $A = 0$ for each ϕ. A_ϕ is consistent since we expect its behaviour to be divergent towards $\phi = 1$. The plot of A_ξ does not capture the divergence hence confirming the need to use an approximation for the forcing on w at the edge of the vortex. The divergence is not shown in A_ξ since relatively, the P_z is small.

In figure 3.19 we show the spanwise velocity, w. The key features are that $w = 0$ at the edge of the vortex ($\phi = 1$) at each spanwise point as expected. These are particles that have been newly captured and hence have not been inside vortex long enough for the pressure to have impacted upon them. Equivalently $w = 0$ at $\xi = \pm 1$, i.e. particles at the spanwise extremes of the vortex. Particles in the spanwise centre ($z = 0$) of the vortex also have zero spanwise velocity. These are particles that were trapped inside the vortex at its creation and have orbits with very small areas. Numerically we see that the spanwise velocity is zero here since A_ξ, $(\chi_{min})_\xi$ and $(\triangle\chi)_\xi$ are all zero at $\xi = 0$ due to symmetry. The two plots in figures 3.20 and 3.21 show the derivatives of the spanwise velocity and these comprise the

main forcing for τ, which is given by,

$$\frac{\partial \tau}{\partial T} = \frac{1}{z^*}\left(w_\xi - \frac{A_\xi w_\phi}{A_\phi}\right). \tag{3.192}$$

The influence of both terms is visible in figure 3.22. The behaviour near $\xi = 0$ is dominated by w_ξ since $w_\phi \approx 0$ near $\xi = 0$, and the small peaks at $\xi \approx \pm 0.5$ are caused by the peaks in w_ϕ. The final plots in the set of figures for the first time step show the jump term, J_X as both a surface and contour plot in figures 3.23 and 3.24 respectively. This is a very interesting plot. Unfortunately as the jump term is very small at this early time the key features are hidden. We therefore turn our attention to the results at a later time step and delay our presentation of an analysis of the jump term.

The most striking feature of this set of data at the fifth time step ($T = -0.355$) in figures 3.25 - 3.33 is the significant increase in values although they are still small. The maximum value of the area has grown considerably. The possible reasons for this rapid growth were covered earlier. Another feature is the qualitative similarities between the vortex time steps. This is due to the relatively smooth progress of pressure with respect to time.

We now turn our attention to the jump term in figures 3.32 and 3.24. The contour plot in figure 3.33 shows the behaviour clearly. Here we consider the influence the jump term has on P_T if $\mu > 0$ and hence on the shape and position of the vortex. We see that towards the spanwise centre of the vortex, J_X is negative for $X_L \leq X \leq X_{min}$ and positive for $X_{min} \leq X \leq X_R$. Thus for $X_L \leq X \leq X_{min}$, J_X increases the negative forcing on P_T. In contrast the jump term works to increase the pressure for $X_{min} \leq X \leq X_R$. Thus increasing this section of the pressure. This influence acts to increase the size of the vortex. Towards the spanwise extremes of the vortex, the opposite seems to be true, with $J_X > 0$ for $X_L \leq X \leq X_{min}$. This acts to increase the pressure in this region and so decreases the vortex size. These particles, as the vortex grows in a spanwise direction, enter the spanwise centre region and hence their behaviour will revert to the spanwise centre vortex

behaviour. The jump term with $\mu < 0$ would have the opposite effect to that explained above.

Figures 3.34 - 3.37 show the jump term at even later times (corresponding to the tenth ($T = -0.305$) and fourteenth ($T = -0.265$) vortex time steps). The shape of the jump term is consistent with the previous time steps. The jump term is growing and this would have an increasingly strong feedback onto the pressure distribution especially inside the vortex. Unfortunately, given the problems at the interface of the vortices at different time steps described in section 3.5 it is not possible to run the numerical regime much further.

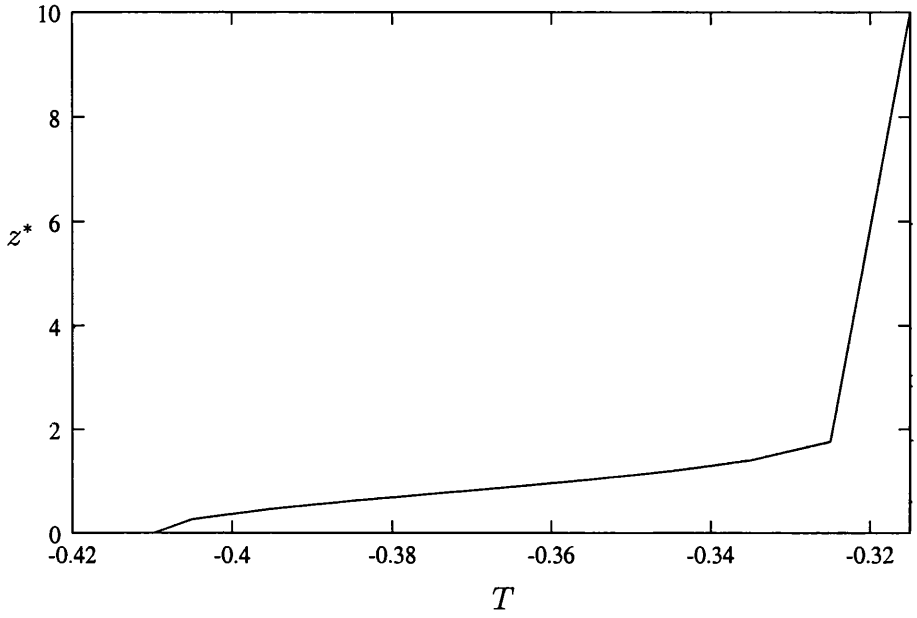

Figure 3.7: z^* plotted against time for $\xi = 0$.

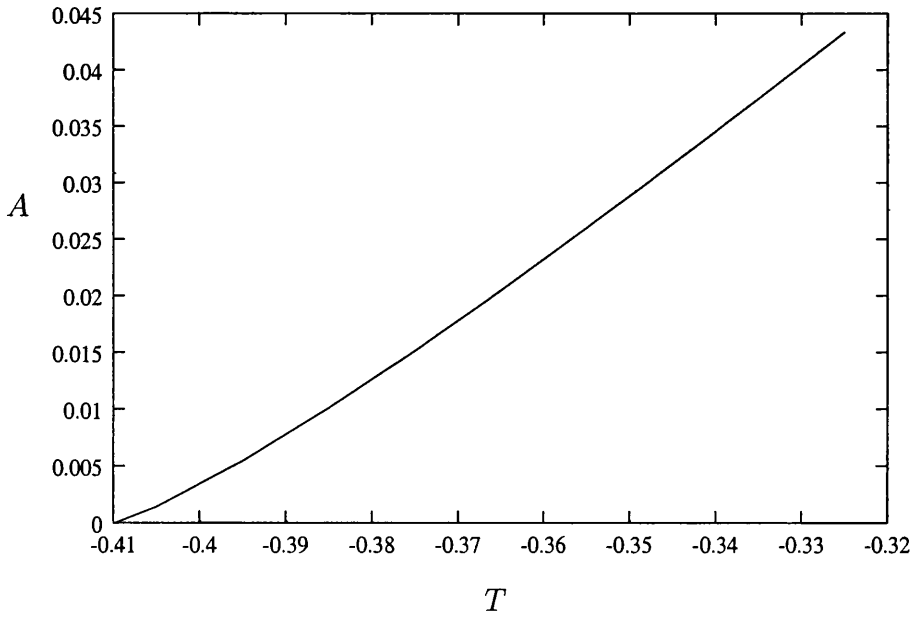

Figure 3.8: Area of the vortex plotted against time for $\xi = 0$.

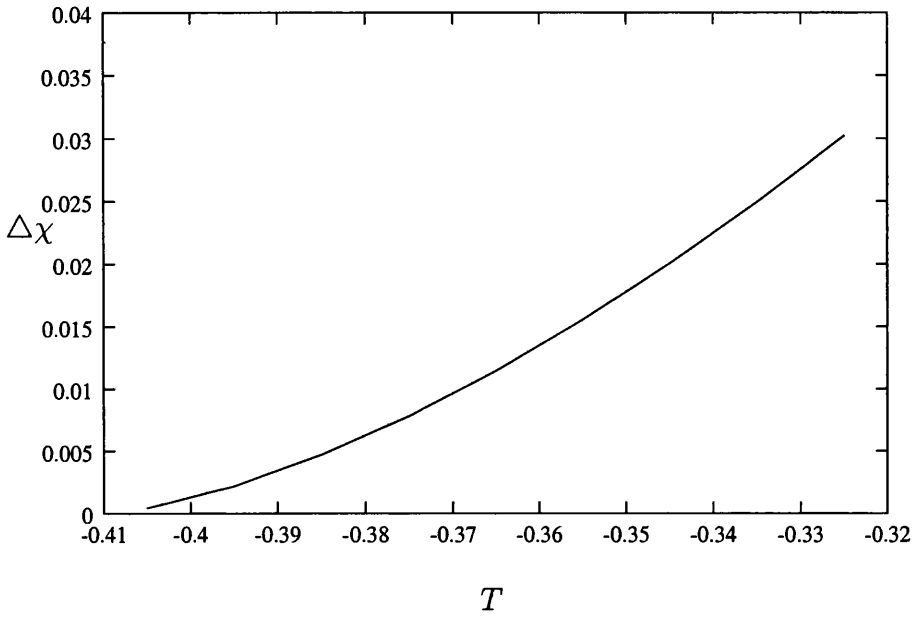

Figure 3.9: $\triangle\chi$ plotted against time for $\xi = 0$.

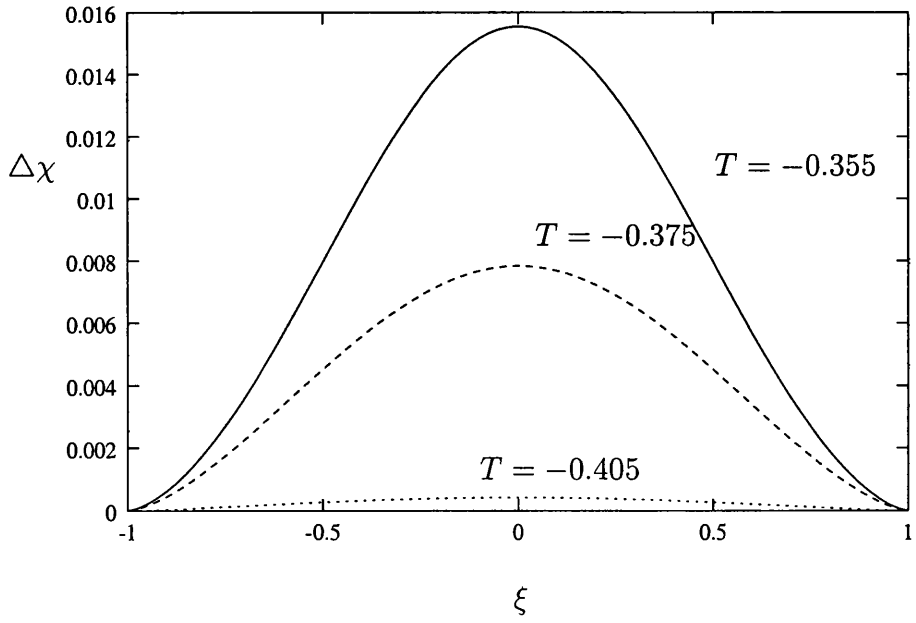

Figure 3.10: $\triangle\chi$ plotted against ξ for selected time steps.

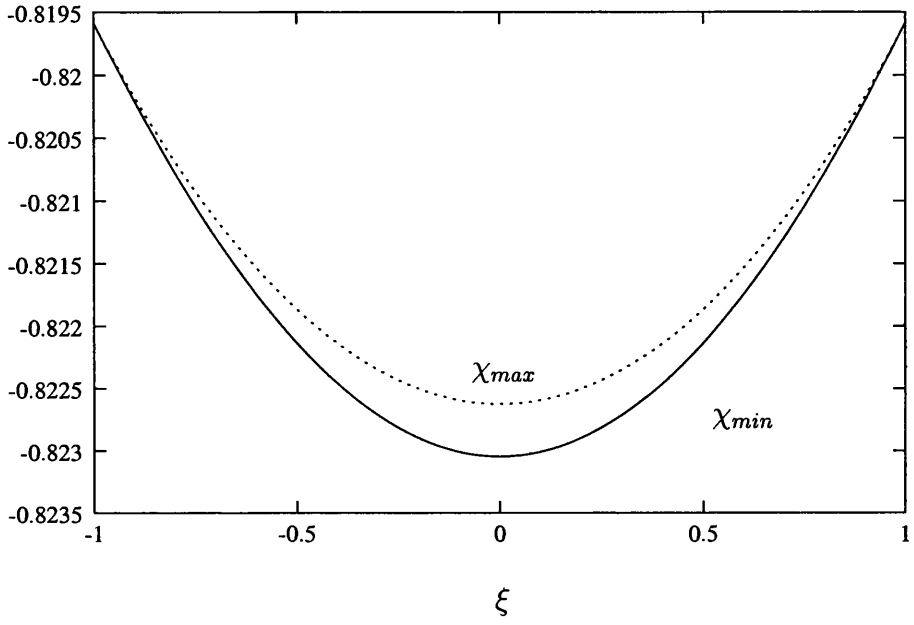

Figure 3.11: χ_{min} and χ_{max} plotted against ξ for $T = -0.405$.

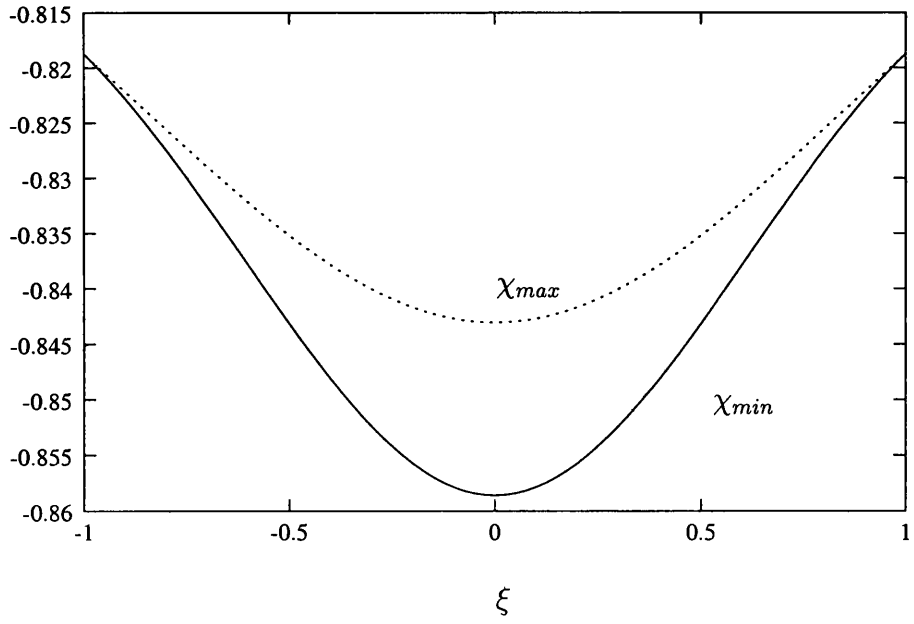

Figure 3.12: χ_{min} and χ_{max} plotted against ξ for $T = -0.355$.

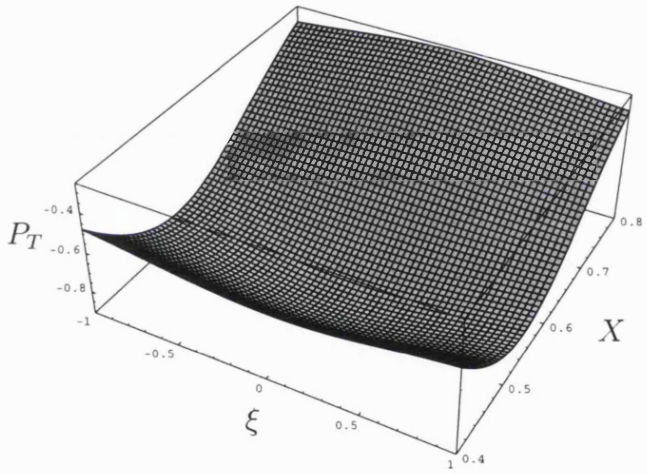

Figure 3.13: P_T at $T = -0.355$.

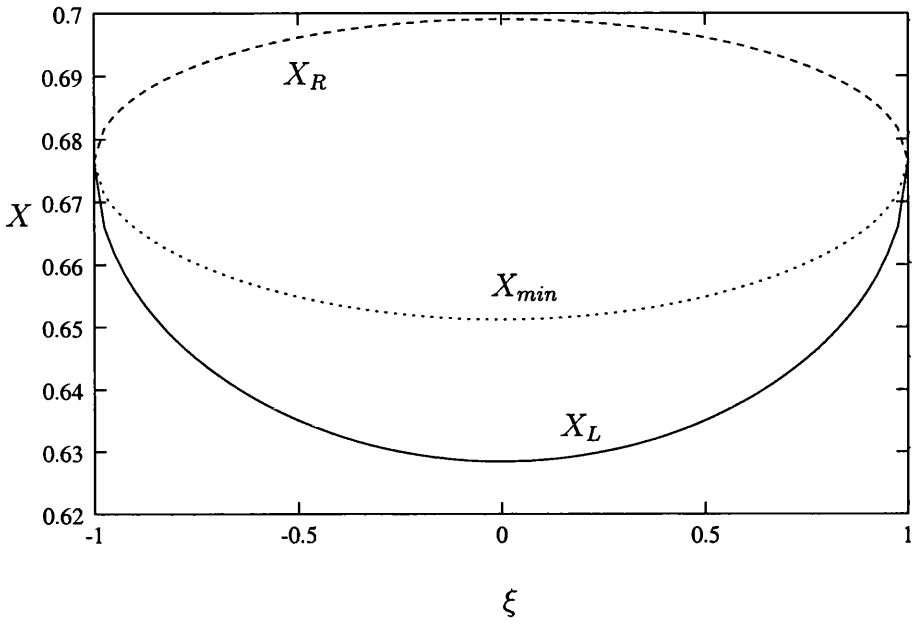

Figure 3.14: X_L, X_{min} and X_R plotted against ξ for $T = -0.405$.

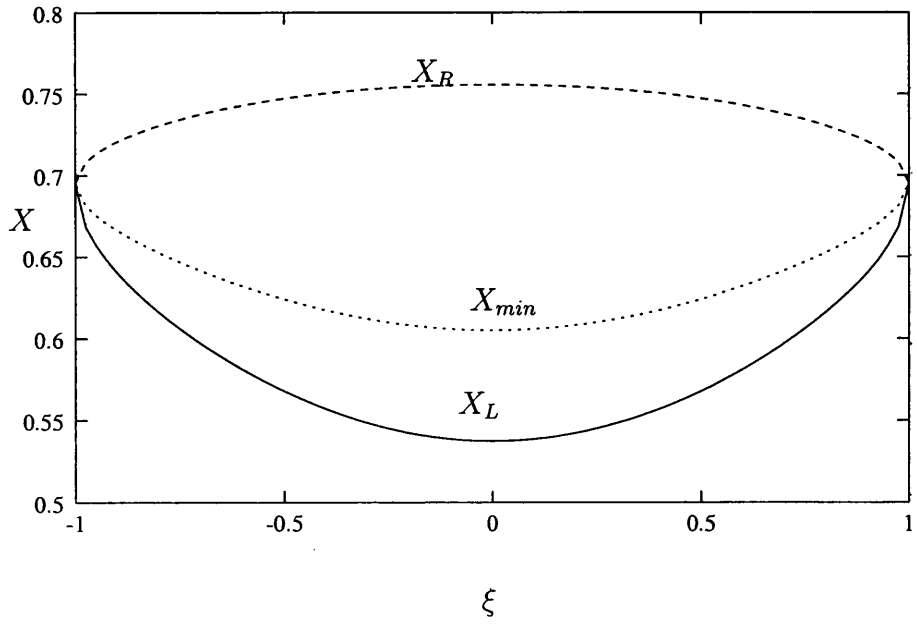

Figure 3.15: X_L, X_{min} and X_R plotted against ξ for $T = -0.355$.

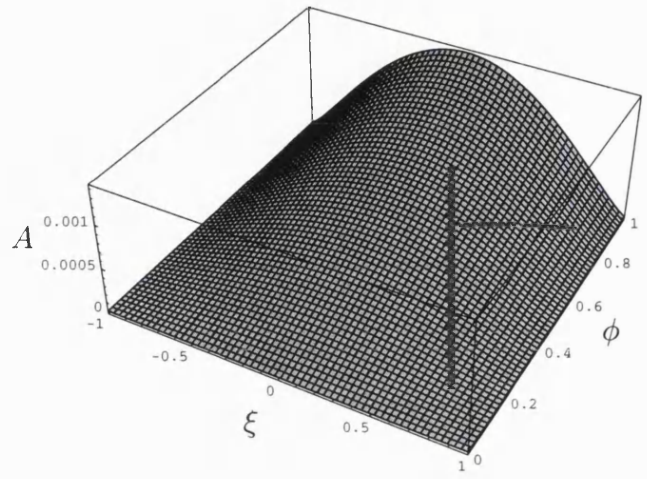

Figure 3.16: Area at $T = -0.405$.

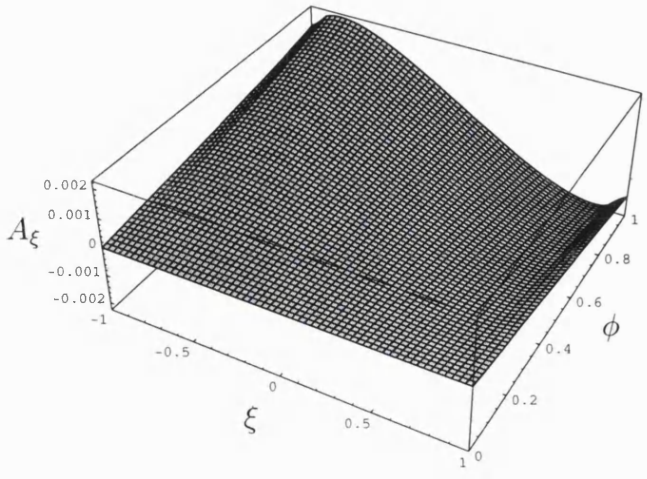

Figure 3.17: A_ξ at $T = -0.405$.

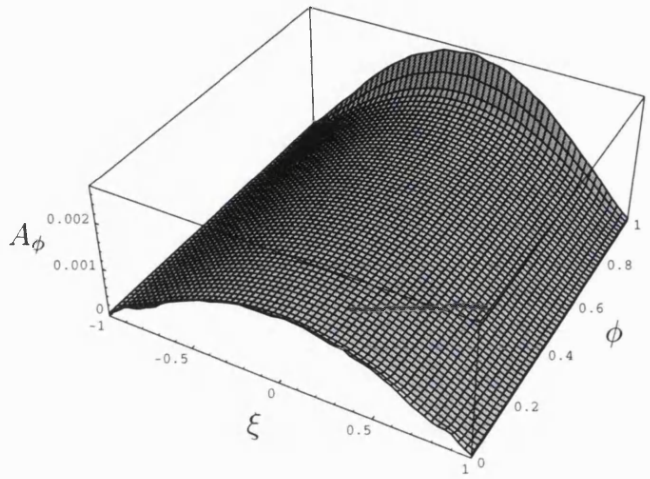

Figure 3.18: A_ϕ at $T = -0.405$.

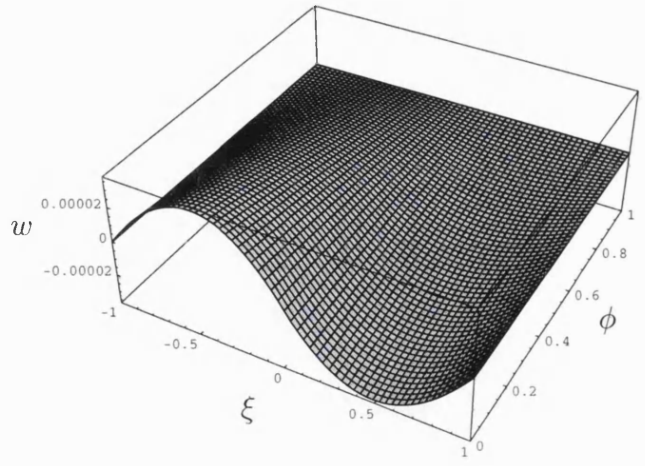

Figure 3.19: The spanwise velocity at $T = -0.405$.

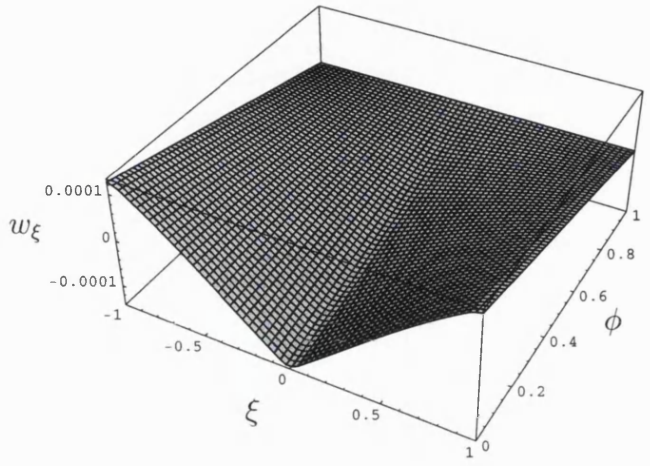

Figure 3.20: The ξ derivative of the spanwise velocity at $T = -0.405$.

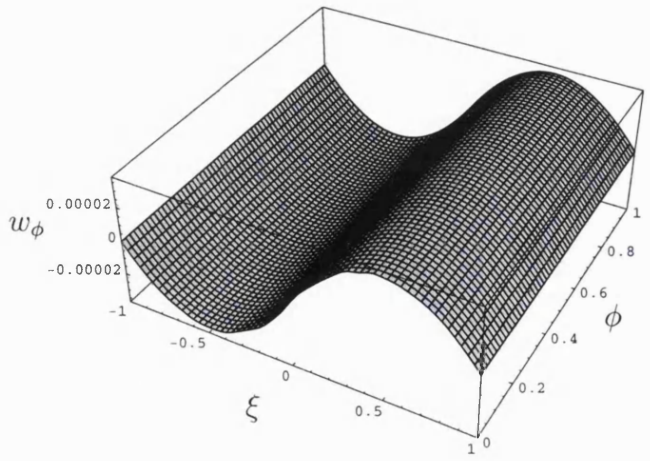

Figure 3.21: The ϕ derivative spanwise velocity at $T = -0.405$.

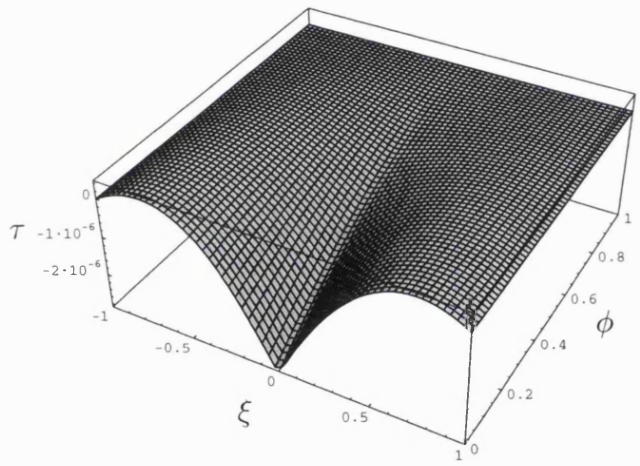

Figure 3.22: The spanwise vorticity at $T = -0.405$.

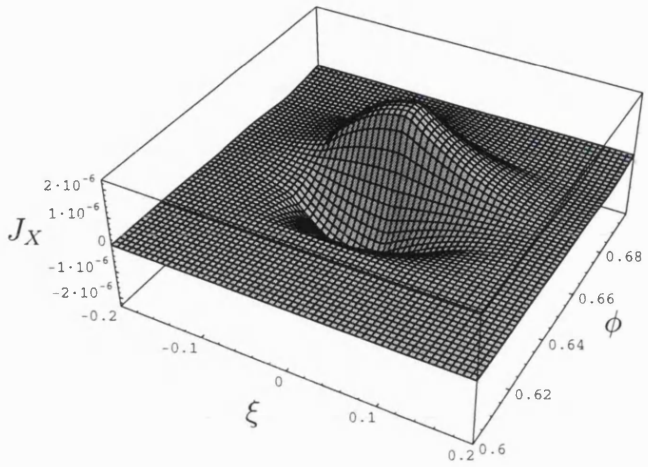

Figure 3.23: Surface plot of the jump term at $T = -0.405$.

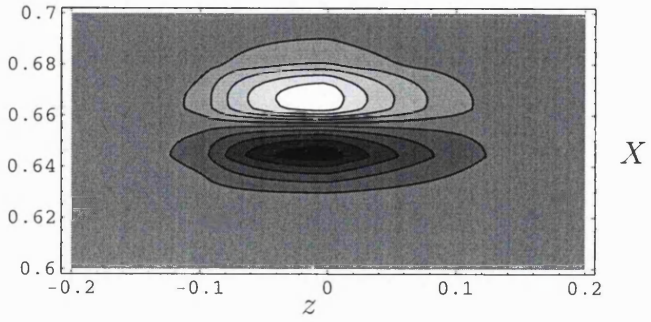

Figure 3.24: Contour plot of the jump term at $T = -0.405$.

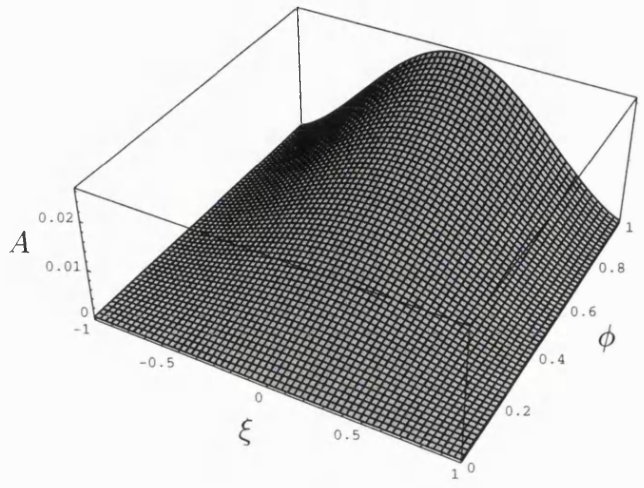

Figure 3.25: Area at $T = -0.355$.

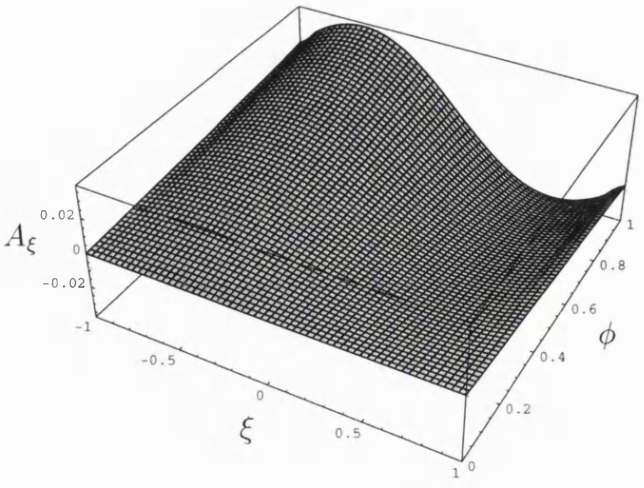

Figure 3.26: A_ξ at $T = -0.355$.

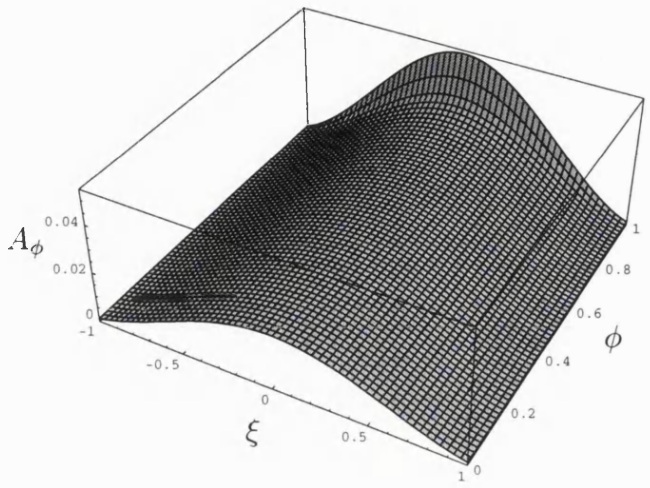

Figure 3.27: A_ϕ at $T = -0.355$.

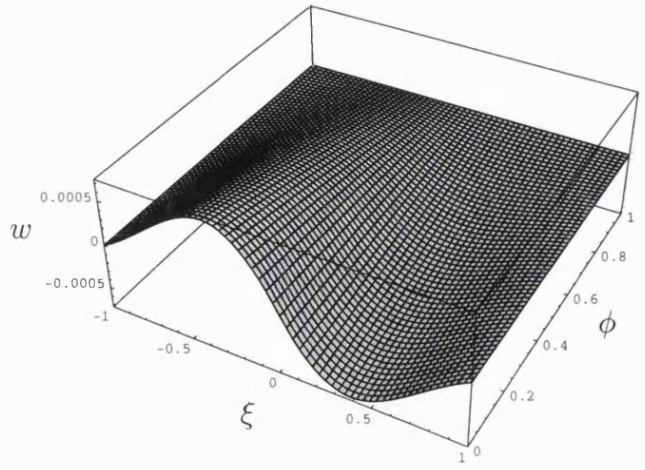

Figure 3.28: The spanwise velocity at $T = -0.355$.

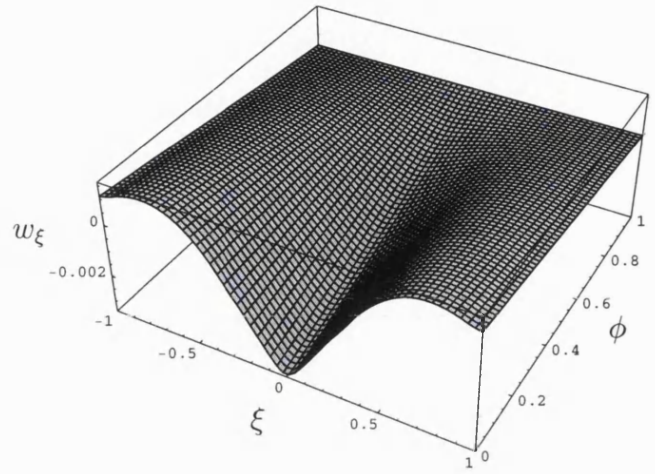

Figure 3.29: The ξ derivative of the spanwise velocity at $T = -0.355$.

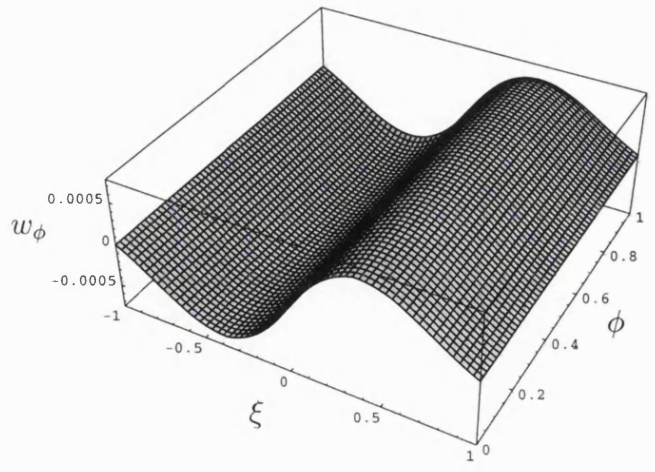

Figure 3.30: The ϕ derivative of the spanwise velocity at $T = -0.355$.

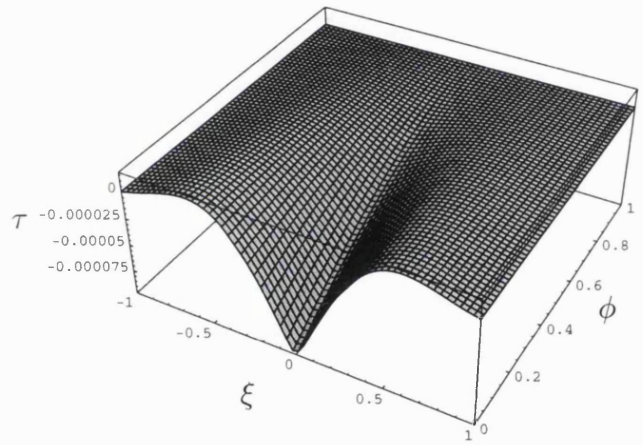

Figure 3.31: The spanwise vorticity at $T = -0.355$.

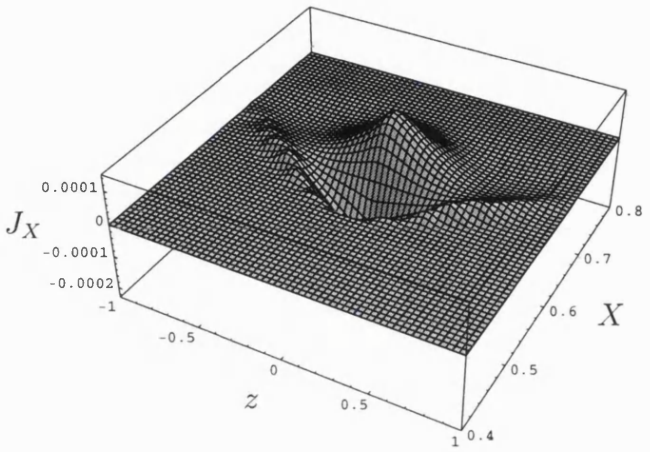

Figure 3.32: Surface plot of the jump term at $T = -0.355$.

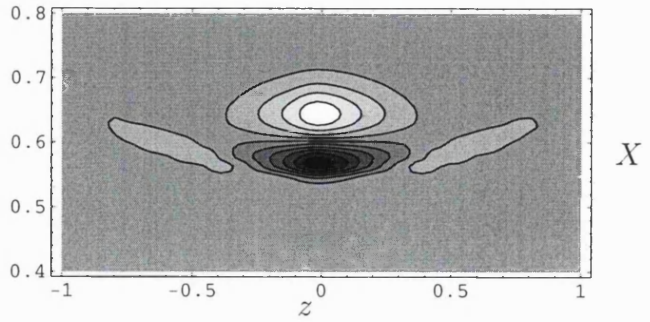

Figure 3.33: Contour plot of the jump term at $T = -0.355$.

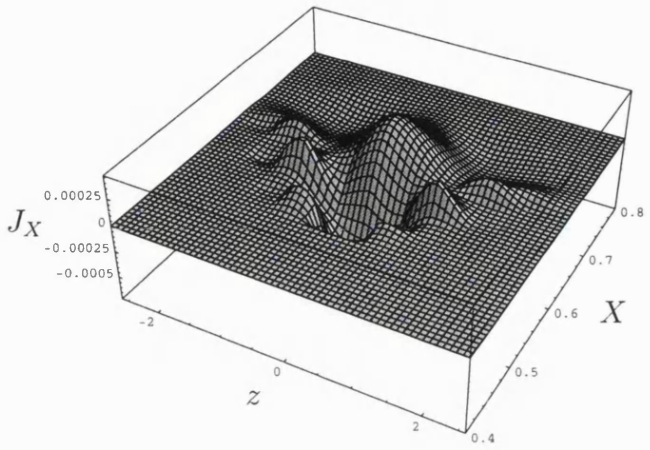

Figure 3.34: Surface plot of the jump term at $T = -0.305$.

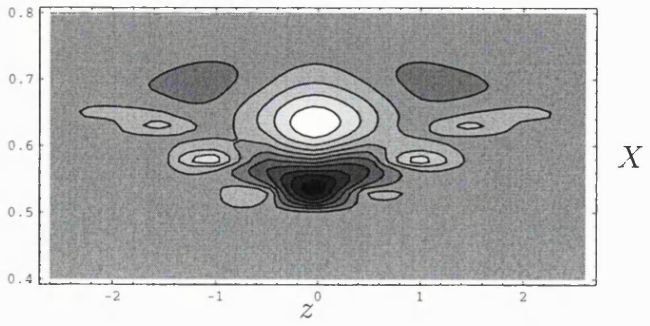

Figure 3.35: Contour plot of the jump term at $T = -0.305$.

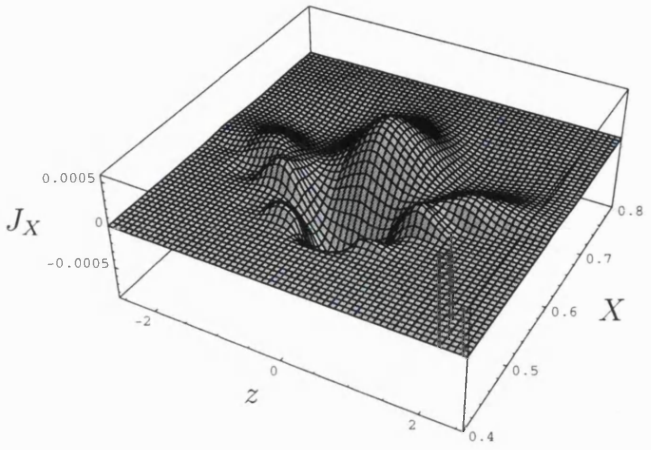

Figure 3.36: Surface plot of the jump term at $T = -0.265$.

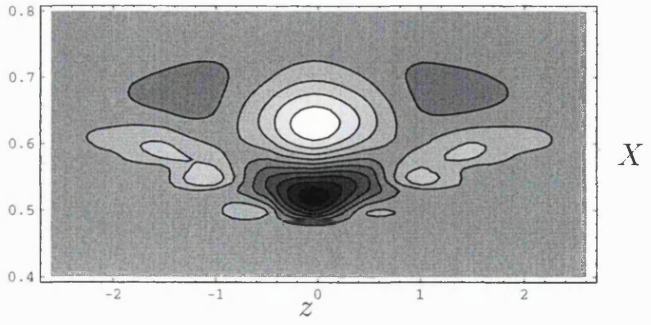

Figure 3.37: Contour plot of the jump term at $T = -0.265$.

3.7 Conclusions

In chapter 3 we have attempted to overcome the problems encountered with the strong feedback mechanism in chapter 2. This has been achieved by delaying the feedback mechanism until a vortex of sufficient size has been created. It was expected that this would simplify the problem but it still produces several challenging problems. Much of the analysis following the derivation was motivated by the numerical method since it was unclear how to deal with the addition of particles into the vortex as time progresses especially in the initial stages where the vortex grows rapidly. The difficulty of understanding the behaviour of the new particles was compounded by the singular behaviour of the integrals used to express the growth rate for the spanwise velocity, w and the spanwise component of vorticity τ within the vortex. This behaviour has well established physical origins but tends to introduce errors that caused differences in gradients in the forcing for w and τ. Therefore generating discontinuities in the derivatives of w and τ. The positive aspect of having to overcome these hurdles is that it directed our analytical study of the problem in varying directions. The addition of three-dimensionality into Bowles (2000*b*) through the critical layer implied,

$$w_T = \frac{A_z}{A_\chi}, \tag{3.193}$$

$$\tau_T = w_z - w_\chi \frac{A_z}{A_\chi}. \tag{3.194}$$

Here A corresponds to the area of an orbit and χ represents a characteristic orbit. These are derived in section 3.1.

The first analytical investigation into the equations, (3.193) and (3.194), in section 3.2, is a study of the integrals at the edge of the vortex, in which we confirm that the ratio of the integrals comprising the forcing for w and τ is not divergent. Significantly the ratio was found to be approximately equal to an easily calculated value of the spanwise derivative of the pressure. The existence of divergent integrals is curious. The period of an orbit is represented by an integral that is divergent at $\phi = 1$, hence

the length of time a particle on the edge of a vortex takes to complete an orbit is infinite. However at the next time step (or even at an infinitesimal small time later) this particle is no longer at the edge of the vortex and hence its period is finite. The particles at the extreme edge of the vortex are related to the structure of a thin region surrounding the vortex edge. Analogous regions are described in Smith *et al.* (2000). In these regions the increased orbital period balances the time taken for the pressure to develop and the multiple time scale assumption breaks down.

Our second analytical study in section 3.3 considered the behaviour of the jump term towards the streamwise ends of the vortex. We found that $J_X \to 0$ at both ends (although at different rates of convergence due to the different pressure gradient in each case). This analysis also produced a possibly interesting criterion. The continuity of pressure generated through the Benjamin-Ono equation with the feedback of the jump term in this model is conditional on the continued growth of the vortex. If X_L's position remains constant then the equations breakdown with yet another singularity leading to new scalings locally.

The third analytical study in section 3.4 concentrated on the time near the generation of a vortex. This analysis implied the need for the time in orbit of a particle to be considered. It also gave an expression for the time in orbit at early times. We were able to obtain a better understanding of the continuous problem thus helping to translate (3.193) and (3.194) to the discrete numerical regime.

The numerical results given in section 3.6 capture several features of the vortex. The vortex grows rapidly in both the streamwise and spanwise directions. There is also a rapid growth in the area of the vortex. The area of the vortex at each time step (on a (ξ, ϕ) grid) is as expected and the accuracy of this aspect of the numerical method is highlighted by the smoothness of the plots of area even when the areas involved are very small. The spanwise velocity and vorticity are initially very small but grow steadily as time progresses. The numerical results show a strong growing jump term towards the spanwise centre of the vortex. This feature was captured by the numerical method even with the very small vortex produced at early times.

An analysis of the jump term shows the influence the jump term has on the pressure. It was shown that at the spanwise centre (i.e. $z = 0$) of the vortex the jump term acts to increase the size of the vortex. In contrast the jump term at the spanwise extremes had the opposite effect although here the jump term is very small suggesting that this influence is negligible.

Chapter 4

Final Comments

This thesis is based on a theoretical inquiry into the three-dimensional study of the end stages of boundary layer transition. The first approach of the thesis is to consider the two-dimensional short scale structure derived in Li *et al.* (1998) and extend to three-dimensions. The second part of the thesis is a study of transition at even later times where a vortex has formed. This delays the feedback from the three-dimensional critical layer. In this chapter we provide a summary of the main results of the thesis.

In chapter 2 we consider the structure of Li *et al.* (1988) and extend to three-dimensions by introducing a spanwise variation within the critical layer, which corresponds to an inflection point in the base flow. We are able to derive a system of steady three-dimensional equations for the perturbation to the base flow that are valid in the critical layer. The three-dimensional equations holding in the critical layer are,

$$Yw_X - \tilde{p}_X w_Y = -\tilde{p}_z, \tag{4.1}$$

$$Y\tau_X - \tilde{p}_X \tau_Y = w_z, \tag{4.2}$$

$$J_X = 2\int_0^\infty \tau_X \, dY. \tag{4.3}$$

The spanwise velocity within the critical layer is w, z is the spanwise variable, $\tilde{p}$

is the pressure distribution and τ is the perturbation vorticity within the critical layer. J_X describes the feedback of the critical layer (incipient vortex) dynamics on the pressure development. The pressure $\tilde{p}$ is governed by a modified Benjamin-Ono equation,

$$a_1\tilde{p}_T + a_2\tilde{p}\tilde{p}_X = \mu J_X + \frac{1}{\pi}\int_{-\infty}^{\infty} \frac{1}{X-u}\frac{\partial^2\tilde{p}}{\partial u^2}du, \tag{4.4}$$

which holds in the bulk of the flow with a_1, a_2 and μ constants. The critical layer equations capture vorticity intensification through vortex stretching. We established in section 2.2 that a full investigation of these equations would require a numerical study. Finding a solution to the critical layer equations is a challenging numerical task since the solution for the jump term is given by a triple repeated integral. We are able to make some analytical progress however. We find that some curvature in the pressure is required to generate a non-zero jump term, which corresponds to the spanwise terms in the critical layer influencing the pressure in the bulk of the flow. This was shown through a consideration of a simplified pressure distribution. If the pressure is linear to first order then the three-dimensional jump term is zero. This pressure distribution provides a reasonable approximation at early times. By introducing some variation into the streamwise derivative of the pressure distribution within the critical layer we find that a non-zero jump is generated.

The numerical results are informative and they show two curious features that differ from the two-dimensional case. The first feature is that the vorticity seems to continue to grow as X and Y increase. We show in section 2.4, through an analytical study that the growing vorticity does not influence the flow at order 1 times. The second feature is significant as it seems to produce a divergent jump term in the numerics. Our analytical analysis shows that there is in fact a large jump term generated but that it is not divergent. However this jump term is too large to fit into our derived equations. The reason for the large jump term is that a large vorticity is generated inside the critical layer in the three-dimensional case. Our analysis in section 2.6.2 shows that one way of resolving the issue is to include unsteady terms

within the critical equations. This motivates the analysis of chapter 3 where we consider an unsteady critical layer and where the jump term is constrained in X.

In chapter 3 we continue our analysis of the three-dimensional flow by considering a delayed critical layer jump term feedback mechanism. Here a vortex has been created within the critical layer and the spanwise variation is consigned to the vortex. This apparent simplification of the model is still able to generate some interesting results. The work is an extension of Smith *et al.* (2000) and Bowles (2000*b*) to three-dimensions. The equations governing vorticity intensifying due to vortex stretching within the vortex are found to be,

$$w_T = \frac{A_z}{A_\chi}, \tag{4.5}$$

$$\tau_T = w_z - w_\chi \frac{A_z}{A_\chi}. \tag{4.6}$$

Here w and τ are the spanwise velocity and vorticity respectively, A corresponds to the area of an orbit and χ represents a characteristic orbit. Much of the analysis in chapter 3 is motivated by the need to find a numerical method to solve the above equations.

The first analysis considers the derivatives of the area. The expressions for A_z and A_χ are divergent at one edge of the vortex. We are able to show that their ratio is not divergent at the edge of the vortex and that this ratio is equal to the spanwise derivative of the pressure. Hence the system of equations is valid inside the vortex.

The second analysis verifies that the jump term does tend to zero at the streamwise extremes of the vortex. We have a zero jump outside the vortex and hence it is required that the jump term does tend to zero at the edge of the vortex for continuity in the streamwise direction. This analysis also implies that the vortex must continue to grow in the streamwise direction as otherwise the equations breakdown.

A difficult problem to overcome is how to model the continuously growing vortex using a discrete numerical regime. We resolve this problem with an analytical study of a newly generated vortex that allows us to accommodate particles as they join

the vortex. The vortex is continually growing and hence more and more particles are being absorbed into the vortex. It is important when considering a discrete numerical method to take into account the continuous capture of new particles inside the vortex by deriving an expression for the time a particle has spent inside the vortex.

The numerical results capture several features of the vortex. The vortex grows rapidly in both the streamwise and spanwise directions. There is also a rapid growth in the area of the vortex. The spanwise velocity and vorticity are initially very small but grow steadily as time progresses. The numerical results show a strong growing jump term towards the spanwise centre of the vortex. This feature was captured by the numerical method even with the very small vortex produced at early times.

In conclusion, an extension to three-dimensions is a difficult problem and care must be taken in deriving the governing equations in three-dimensions. Based on the work in the thesis it would seem that unsteady terms have a stronger influence in a three-dimensional flow than in a purely two-dimensional flow.

4.1 Acknowledgements

I am most grateful to my supervisor, Dr. Robert Bowles for suggesting this line of research and for his invaluable help, guidance and encouragement throughout the course of this work.

Thanks go also to my family for their continued support and patience during the preparation of this thesis.

Financial Support was provided by the Engineering and Physical Sciences Research Council (EPSRC).

Bibliography

[1] Abramowitz, M. & Stegun, I. A. 1964 *Handbook of mathematical functions.* National Bureau of Standards. Applied Mathematics series.

[2] Acton, F. S. 1970 *Numerical Methods that work.* Harper & Row.

[3] Bake, S., Fernholz, H. H. & Kachanov Y. S. 2000 Resemblance of K- and N-regimes of boundary-layer transition at late stages. *Eur. J. Mech. B - Fluids* **19** 1-22.

[4] Bake, S., Ivanov, A. V., Fernholz, H. H. Neemann, K. & Kachanov Y. S. 2002*a* Receptivity of boundary layers to three-dimensional disturbances. *Eur. J. Mech. B - Fluids* **21** 29-48.

[5] Bake, S., Meyer, D. G. W. & Rist, U. 2002*b* Turbulence mechanism in Klebanoff transition: a quantitative comparison of experiment and direct numerical simulation. *J. Fluid Mech.* **459** 217-243.

[6] Borodulin, V. I. & Kachanov, Y. S. 1995 Formation and development of coherent structures in a transitional boundary layer. *J. Applied Mechanics and Technical Physics* **36** 532-564.

[7] Bowles, R. I. 2000*a* Transition to turbulent flow in aerodynamics. *Phil. Trans. R. Soc. Lond.* A **358** 245-260.

[8] Bowles, R.I. 2000*b* On vortex interaction in the latter stages of boundary-layer transition. In *Proc. IUTAM Symp. on Laminar-Turbulent Transition, Sedona, Arizona, USA*, (ed. H. Fasel & W. S. Saric), Springer.

[9] Bowles, R. I., Davies, C. & Smith, F. T. 2003 On the spiking stages in deep transition and unsteady separation. *J. Engineering Mathematics* **45** 227-245.

[10] Breuer, K. S., Cohen, J. & Haritonidis, J. H. 1997 The late stages of transition induced by a low-amplitude wavepacket in a laminar boundary layer. *J. Fluid Mech.* **340** 395-411.

[11] Brotherton-Ratcliffe, R. V. & Smith, F. T. 1987 Complete breakdown of an unsteady interactive boundary layer. *Mathematika* **34** 86-100.

[12] Drazin, P. G. 1989 *Solitons.* Cambridge University Press.

[13] Drazin, P. G. & Johnson, R. S. 1989 *Solitons: an Introduction.* Cambridge University Press.

[14] Drazin, P. G. & Reid, W. H. 1981 *Hydrodynamic Stability.* Cambridge University Press.

[15] Eliahou, S., Tumin, A. & Wygnanski, I. 1998 Laminar-turbulent transition in Poiseuille pipe flow subjected to periodic perturbation emanating from the wall. *J. Fluid Mech.* **361** 333-349.

[16] Erdélyi, A., Magnus, W., Oberhettinger, F. & Tricomi, F. G. 1953 *Higher transcendental functions* McGraw-Hill.

[17] Fasel, H. & Konzelmann, U. 1990 Non-parallel stability of a flat-plate boundary layer using the complete Navier-Stokes equations. *J. Fluid Mech.* **221** 311-347.

[18] Hall, P. & Smith, F. T. 1991 On strongly nonlinear vortex/wave interactions in boundary-layer transition. *J. Fluid Mech.* **227** 641-666.

[19] Han, G., Tumin, A. & Wygnanski, I. 2000 Laminar-turbulent transition in Poiseuille pipe flow subjected to periodic perturbation emanating from the wall. Part 2. Late stages of transition. *J. Fluid Mech.* **419** 1-27.

[20] Healey, J. J. 1995 On the neutral curve of the flat-plate boundary layer: comparison between experiment, Orr-Sommerfeld theory and asymptotic theory. *J. Fluid Mech.* **288** 59-73.

[21] Herbert, T. 1988 Secondary Instability of boundary layers. *A. Rev. Fluid Mech.* **20** 487-526.

[22] Hinch, E. J. 1991 *Perturbation Methods.* Cambridge University Press.

[23] Hoyle, J. M. 1991 PhD Thesis, University of London.

[24] Kachanov, Y. S. 1994 Physical mechanisms of laminar-boundary-layer transition. *A. Rev. Fluid Mech.* **26** 411-482.

[25] Kachanov, Y. S. 2000 Three-dimensional receptivity of boundary layers. *Eur. J. Mech. B - Fluids* **19** 723-744.

[26] Kachanov, Y. S., Ryzhov, O. S. & Smith, F. T. 1993 Formation of solitons in transitional boundary layers: theory and experiments. *J. Fluid Mech.* **251** 273-297.

[27] Klebanoff, P.S., Tidstrom, K. D. & Sargeant, L. M. 1962 The three-dimensional nature of boundary-layer instability. *J. Fluid Mech.* **12** 1-34.

[28] Li, L. 1997 Numerical study of nonlinear evolution equations, using compact differencing. PhD Thesis, University of London.

[29] Li, L., Walker, J.D.A., Bowles, R.I. & Smith, F.T. 1998 Short-scale breakup in unsteady interactive layers: local development of normal pressure gradients and vortex wind-up. *J. Fluid Mech.* **374** 335-378.

[30] Lin, C. C. 1955 *The Theory of Hydrodynamic Stability.* Cambridge University Press.

[31] Meyer, D. G. W., Rist, U., Borodulin, V. I., Gaponenko, V. R., Kachanov, Y. S., Lian, Q. X. & Lee, C. B. 1999 Late-stage transitional boundary-layer structures. Direct numerical simulation and experiment. In *Proc. IUTAM Symp. on Laminar-Turbulent Transition, Sedona, Arizona, USA* (ed. H. Fasel & W. Saric), Springer.

[32] Meyer, D., Rist, U. & Wagner, S. 2003 Direct numerical simulation of the development of asymmetric perturbations at very late stages of the transition process. In *Recent Results in Laminar-Turbulent Transition Selected Numerical and Experimental Contributions from the DFG-Verbundschwerpunktprogramm "Transition" in Germany* (ed. S. Wagner, M. Kloker, U. Rist) NNFM Vol. 86, Springer, Heidelberg.

[33] Moston, J., Stewart, P. A. & Cowley, S. J. 2000 On the nonlinear growth of two-dimensional Tollmien-Schlichting waves in a flat-plate boundary layer. *J. Fluid Mech.* **425** 259-300.

[34] Nishioka, M., Asai, M. & Iida, S. 1979 An experimental investigation of the secondary instability. In *Laminar-turbulent Transition. IUTAM Mtg, Stuttgart.*

[35] Nishioka, M. & Morkovin, M. V. 1986 Boundary-layer receptivity to unsteady pressure gradients: experiments and overview. *J. Fluid Mech.* **171** 219-261.

[36] Press, W. H. Flannery, B. P., Teukolsky, S. A. & Vetterling, W. T. 1987 *Numerical recipes: the art of scientific computing.* Cambridge University Press.

[37] U. Rist 2003 Visualization of Unsteady Flow Structures in a High-Performance Computing Environment. In *Recent Results in Laminar-Turbulent Transition Selected Numerical and Experimental Contributions from the DFG-*

Verbundschwerpunktprogramm "Transition" in Germany (ed. S. Wagner, M. Kloker, U. Rist) NNFM Vol. 86, Springer, Heidelberg.

[38] Rist, U. & Fasel, H. 1995 Direct numerical simulation of controlled transition in a flat-plate boundary layer. *J. Fluid Mech.* **298** 211-248.

[39] Robinson, S. K. 1991 Coherent motions in the turbulent boundary layer. *A. Rev. Fluid Mech.* **23** 601-639.

[40] Rosenhead, L. 1963 *Laminar Boundary Layers.* Oxford University Press.

[41] Sandham, N. D. & Kleiser, L. 1992 The late stages of transition to turbulence in channel flow. *J. Fluid Mech.* **245** 319-348.

[42] Saric, W. S., Reed, H. L. & White, E. B. 2003 Stability and transition of three-dimensional boundary layers. *A. Rev. Fluid Mech.* **35** 413-440.

[43] Schubauer, G. B. & Skramstad, H. K. 1943 Laminar-boundary-layer oscillations on a flat plate. NACA report, no 909.

[44] Shaikh, F. N. 1997 Investigation of transition to turbulence using white-noise excitation and local analysis techniques. *J. Fluid Mech.* **348** 29-83.

[45] Smith, F. T. 1979 On the nonparallel flow stability of the Blasius boundary layer. *Proc. R. Soc. Lond. A* **366** 91-109.

[46] Smith, F. T. 1982 On the high Reynolds number theory of laminar flows. *IMA J. of Applied Mathematics* **28** 207-281.

[47] Smith, F.T. 1988 Finite time break-up can occur in any unsteady interacting boundary-layer. *Mathematika* **35** 256-273.

[48] Smith, F. T. 1996 On transition over surface roughness. *AIAA Paper* 91-1992.

[49] Smith, F.T. 1993 Theoretical aspects of transition and turbulence in boundary layers. *AIAA J.* **31** 2220-2226.

[50] Smith, F.T. & Bodonyi, R. J. 1987 Properties of a time-dependent nonlinear viscous critical layer. *Stud. Appl. Maths* **77** 129-150.

[51] Smith, F.T. & Bowles, R.I. 1992 Transition theory and experimental comparisons on (a) amplification into streets and (b) a strongly nonlinear break-up criterion. *Proc. R. Soc. Lond.* **A439** 163-175.

[52] Smith, F. T. & Walton, A. G. 1989 Nonlinear interaction of near-planar TS waves and longitudinal vortices in boundary-layer transition. *Mathematika* **36** 262-289.

[53] Smith, F. T., Bowles, R. I. & Walker, J. D. A. 2000 Wind-Up of a spanwise vortex in deepening transition and stall. *Theoret. Comp. Fluid Dynamics* **14** 135-165.

[54] Sobey, I. J. 2000 *Introduction to interactive boundary layer theory.* Oxford University Press.

[55] Stewart, P. A. & Smith, F. T. 1987 Three-dimensional instabilities in steady and unsteady non-parallel boundary layers, including efects of Tollmien-Schlichting disturbances and cross flow. *Proc. R. Soc. Lond.* **A409** 229-248.

[56] Stewart, P. A. & Smith, F. T. 1992 Three-dimensional nonlinear blow-up from a nearly planar initial disturbance, in boundary layer transition: theory and experimental comparisons. *J. Fluid Mech.* **244** 79-100.

[57] Stewartson, K. 1981 Marginally stable inviscid flows with critical layers. *IMA J. Appl. Maths* **27** 133-175.

[58] Stuart, J. T. 1965 The production of intense shear layers by vortex stretching and convection. *AGARD Rep.* 514.

[59] Tollmien, W. 1929 Über die Entstehung der Turbulenz. *Nachr. Ges. Wiss. Göttmaen, Math. Phys.* K. L., pp. 21-44. (English Trans. 1931 The production of turbulence. *Tech. Memor. Nat. Adv. Comm. Aero. Wash.*, no. 609).

[60] Williams, D. R., Fasel, H. & Hama, F. R. 1984 Experimental determination of the three-dimensional vorticity field in the boundary-layer transition process. *J. Fluid Mech.* **149** 179-203.

[61] Würz, W., Herr, S., Wörner, A., Rist, U., Wagner, S. & Kachanov, Y. S. 2003 Three-dimensional acoustic-roughness receptivity of a boundary layer on an airfoil: experiment and direct numerical simulations. *J. Fluid Mech.* **478** 135-163.